

DETONATION AND THE HYDRODYNAMICS OF REACTIVE SHOCK WAVES

Roger A. Strehlow

Department of Aeronautical and Astronautical Engineering
University of Illinois, Urbana, Illinois

INTRODUCTION

The contents of this review may be conveniently separated into two rather distinct parts. On the one hand this review covers our current understanding of detonation as a unique natural phenomena, while on the other hand the review discusses the limitations that hydrodynamics places on the utility of the shock tube as a tool for studying high temperature reaction kinetics. Specific reaction kinetic studies are not covered because they are so extensive that it is difficult to do them justice in a short review. The reader is referred to recent more extensive reviews for this purpose¹⁻⁵.

DETONATION

I. Theories Relating to Structure and Stability

The Zel'dovich⁶, von Neumann⁷, Doring⁸ (ZND) model of a one-dimensional steady detonation wave as a shock discontinuity followed by a zone of homogeneous chemical reaction is probably the most useful concept to evolve prior to the mid 1950's. Even though this model must now be modified to accommodate non-steady and three-dimensional effects, its implication that an element of the flow may be treated as containing an exothermic chemical reaction triggered by a strong shock, which may in itself be handled as a discontinuity in the flow, represents a useful tool for understanding the structure and non-steady behavior of detonation waves.

The Chapman⁹-Jouguet¹⁰, (CJ), concept that a minimum steady one-dimensional mass flow exists for any specific exothermic system undergoing reactive shock transition is at present useful only insofar as it allows a rather exact calculation of the velocity and pressure in a detonation wave. Unfortunately, at the present time, this success must be considered to be either fortuitous or at least empirical because recent work has shown that a one-dimensional detonation traveling at the CJ velocity is dynamically unstable.

The first attempt to look at time-dependent stability in a detonation wave was made by Shchelkin¹¹ in 1958. He used a square wave detonation as his model. In this model the chemical reaction is concentrated at the CJ plane and this plane is separated from the shock wave by an induction zone. In his model, he perturbed the position of the CJ plane with time and discussed the consequences of this perturbation. He found that the detonation will be unstable to this type of perturbation if the induction zone reactions have a sufficiently large activation energy. This model is unrealistic because one cannot truly cause the CJ plane to suffer a perturbation, since it is a steady concept. However, Shchelkin was the first to discuss the effect of a time-dependent perturbation on stability.

Since 1963, there have been a number of papers¹²⁻¹⁹ which discuss the stability of the square wave detonation. However, recent work on detonation stability, using models which allow for an extended heat release

zone, show quite definitely that all the interesting amplification mechanisms which lead to instability occur in the region of heat release. Therefore, the square wave model appears to be unsuitable for discussing stability.

Two approaches have been used to investigate the stability of a ZND detonation wave with an extended reaction zone. Erpenbeck²⁰⁻²¹ has examined stability by following the response of the shock discontinuity to a purely transverse harmonic perturbation in the flow downstream of the shock wave (i.e., in the reaction zone). His analysis is applicable to disturbances of arbitrary wave length but requires a model for the heat release reactions throughout the entire reaction zone. He has not formally examined the CJ detonation case, but has always worked with detonations that have some arbitrary overdrive. His analysis, which is performed in Laplace transform space, is very complex and he finds that stability in the general case can be discussed only by resorting to numerical techniques. His results indicate that the occurrence of instability is dependent on the frequency of the disturbance, the activation energy of the first order heat release reaction that he has used in his model and the amount of the overdrive present in the detonation. In a following paper, Erpenbeck²² has extended his analysis to transverse waves of high frequency. In this case, he finds that there are three types of stability regimes which may be present in the reaction zone of the detonation. The type of regime that is present is dependent on the local value of the quantity $d(a^2-u^2)/dx$ where x is measured from the shock and a and u are the sound velocity and flow velocity at a point in the steady flow behind the shock. He observed that this quantity either increases, goes through a maximum, or decreases, in that order, as one passes from the shock wave to the plane where heat addition is terminated. If the quantity simply decreases in the reaction zone he finds that the detonation will be stable to a high frequency transverse wave. If this quantity goes through a maximum or if it increases, he finds that the detonation behaves unstably to a high frequency transverse perturbation. In the limit behavior which he investigated, the ultimate stability is found to be dependent on the activation energy of the first order chemical reaction which was assumed in the analysis. Specifically, systems with a sufficiently low activation energy were found to be stable.

In the other approach to the stability problem, Strehlow and Fernandes²³ and Barthel and Strehlow²⁴ have used a ray tracing technique to discuss the behavior of a high frequency coherent transverse acoustic wave in the reaction zone of a ZND detonation. They also find that the quantity $d(a^2-u^2)/dx$ is important to the behavior of these coherent transverse waves. For a transverse wave propagating in a flowing gas, the direction of propagation of the energy trapped in the acoustic front (i.e., the ray direction) is the direction which is of interest. They find that, in the region where the quantity $d(a^2-u^2)/dx$ is decreasing, an acoustic wave front of any orientation (except for one very specific orientation) subsequently passes through the reaction zone of the detonation at most only twice (due to reflection from the shock front). However a wave front of the proper orientation was found to asymptotically approach the plane where $d(a^2-u^2)/dx$ has a maximum value. Furthermore, this ray was found to subsequently propagate parallel to the shock front for an infinitely long time. Thus, if the detonation did not have a plane where $d(a^2-u^2)/dx$ was maximum, their theory also predicted that the detonation would be dynamically stable to a transverse wave perturbation. They also noted that since the ray propagating at the plane $d(a^2-u^2)/dx = \text{maximum}$ is propagating in a region where a temperature and

density sensitive exothermic chemical reaction is occurring, its rate of amplitude growth is dependent on the details of the chemical reaction. Briefly, they came to the conclusion that any exothermic reaction that has been observed in nature would produce transverse wave amplification under these conditions.

In the region where the quantity $d(a^2-u^2)/dx$ is increasing they found another interesting behavior. In this region, wave fronts which have a particular range of initial orientations convolute with time in such a manner that an element of the wave front propagates some distance away from the shock front, then turns around and returns to the front to reflect and repeat the process. Since this behavior is occurring in a region which contains a temperature-sensitive exothermic reaction, it is also expected that the amplitude of this wave front will grow with time. Interestingly enough they found that this wave front eventually produces multiple shock contacts which asymptotically approach a regular spacing and that this spacing is dependent on the extent and the detailed structure of the reaction zone of the detonation.

Relative to the problem of longitudinal instability in detonation waves, Erpenbeck²¹ has performed an analysis for transverse waves with arbitrarily long wave lengths (which effectively become a longitudinal disturbance in the flow). He once again found values of overdrive above which instability occurs. In a recent paper, Fickett and Wood²⁵ have performed a one-dimensional non-steady method of characteristic analysis on a propagating overdriven detonation produced by a piston motion. They carried their analysis out to very long times and observed a continued large oscillation in the shock velocity for the case that Erpenbeck predicted would be unstable. They also observed no sustained oscillations for one of Erpenbeck's stable cases. In a following paper, Erpenbeck²⁶ has been able to predict the magnitude of these large scale oscillations by extending his analysis to include nonlinear terms.

From the above we see that one should expect hydrodynamic instabilities in many of the flow situations in which a shock wave is closely followed by exothermic chemical reaction. Specifically, these results show that the CJ plane is not important to the occurrence of flow instabilities and therefore that the self sustenance of detonation is not a requirement for instability. In other words, the instabilities observed on self-sustaining detonations are quite certainly a restricted example of a general class of hydrodynamic instabilities which occur in flows containing a heat release zone following a shock transition.

II. Structure

A number of investigators have observed that essentially all detonations propagate with a complex non-steady frontal structure. Early work in this area was performed primarily by Russian investigators and has been summarized in a number of recent Russian texts.^{27, 28, 29, 30} The primary findings of these and subsequent investigators is that the main shock front consists of many sections which are locally convex towards the upstream flow and the intersection of these sections are traveling across the front as waves (see for example the early photographs obtained by White³¹). Both the occurrence and structure of these transverse waves are intimately connected to the chemistry of the reactions occurring in the detonation. In the following sections our current understanding of the nature of this transverse structure and its interaction with the chemistry will be discussed.

a. The Nature of Transverse Waves

The transverse waves that propagate across the front of a detonation have been found to occur at the front as Mach stems or triple shock intersections of finite amplitude^{27,32,33}. The single spin detonation that occurs in a round tube is unique because it was the first non-one-dimensional structure to be observed and because it is the only example of a transverse wave structure which is steady in the proper coordinate system. (In this case, the coordinate system which renders the wave motion steady is one which rotates at the spin frequency with its axis of rotation along the tube axis.) Spinning detonation contains a very complex double Mach stem pattern which has been described by Voitsekhovskii, Mitrofanov and Topchian²⁷ and verified by the careful work of Duff³² and Schott³³. In all other observed transverse structures, there are always opposing transverse waves propagating across the front simultaneously and the structure at the front is necessarily two or three-dimensional non-steady.

At the present time, all the details of this complex structure are not understood. However, as mentioned above, it is known that these transverse waves consist of Mach stem interactions at the front. These have been observed experimentally, both on propagating detonations^{34,35,36} and as an artificially produced reactive Mach stem on the "laminar" detonation which White and Cary³⁷ first produced by expanding an overdriven detonation through a cylindrical nozzle. A spark interferogram of such an artificially produced Mach stem and an analysis of its triple point structure is shown in Figure 1. This structure was observed by White and Cary³⁷ and analyzed by Strehlow.³⁸ Strehlow found that even though the shock triggered a highly exothermic reaction a few microseconds after it passes an element of the gas, the triple point structure is still controlled by an unreactive-unreactive slipstream balance. The observations on propagating detonations have not been analyzed as extensively at the present time. There are still serious questions concerning the disposition of the reflected shock and the manner in which it interacts with the reaction zone.

The triple points propagating on the shock front of the detonation have been found to have the property that they will "write" a line on a smoked surface. This behavior was first observed by Antolik³⁹ in 1875 and was used by E. Mach in conjunction with his studies of spark discharges and the interaction of shock waves produced by bullets fired in the laboratory. The technique lay dormant for over 80 years until in 1958, Denisov and Troshin⁴⁰ started to use it to study detonation structure. Oppenheim and Utriew⁴¹ have recently verified that the triple point is writing the pattern by direct laser schlieren photography looking through the smoked film.

This property has been very helpful in the study of transverse wave phenomena in detonations. To perform an experiment, one simply smokes a surface with either wood, acetylene, kerosine, or any other appropriate smoke and exposes it to the detonation. After exposure the film is "fixed" with a clear lacquer spray. The quality is almost as good as that of a photographic negative. A few examples of smoke track records obtained with detonations propagating in a rectangular tube are shown in Figure 2.

In Figure 3, the results of studying a symmetric interaction using the smoke track technique are summarized⁴². In this case, a number of sand grains were placed on the smoke plate before the detonation

passed over the plate and each grain wrote a wake pattern whose axis is normal to the local orientation of the leading shock wave of the detonation. The intersection geometry is therefore completely determined and one may calculate all shock and flow properties in the neighborhood of the intersection. From this calculation one concludes that the normal shock velocity is discontinuously increased by about 30 to 40% at the center line of the intersection and therefore that all portions of the leading shock are attenuating very rapidly in the detonation. This is very disturbing, because even though the shock is locally propagating at a velocity which varies from 10 to 20% below CJ to 10 to 20% above CJ, the detonation as a whole is still observed to propagate at very close to the CJ velocity. The mechanism which makes this possible is not understood at the present time.

b. Acoustic Coupling and Limits

The transverse waves on the detonation front exhibit a degree of regularity which is dependent on the geometry of the detonation tube and on the chemical system which is supporting the detonation. The effect of detonation tube geometry is primarily caused by the fact that the high pressure regions propagating across the front (immediately behind the Mach stem) produce transverse pressure waves in the gas column following the front and that these transverse waves have a tendency to couple with resonant transverse modes of the gas column downstream of the front. Manson⁴³ and Fay⁴⁴ predicted this behavior for near limit detonations approximately 15 to 20 years ago. It now appears, however, that this coupling is incidental to the occurrence of transverse waves on the front. For example, Duff and Finger⁴⁵ have observed transverse structure on a spherical detonation. However, the occurrence of transverse waves on the front is not incidental to the self-sustenance of the detonation wave. It has been noted repeatedly in the literature that as the initial pressure is lowered or as the detonable mixture is diluted with an inert gas, the characteristic spacing of the structure gets larger. It also has been observed that the last transverse frontal structure that occurs in any specific tube corresponds to the lowest transverse acoustic mode of the hot gas column following the front in that tube. In the case of round tubes, this mode is the single spin mode. It is also now quite certain, that detonations propagating just inside these limits propagate at an average velocity lower than the CJ velocity. This is evidently caused because a significant fraction of the chemical energy released in the reaction zone resides in transverse wave energy for an appreciable length of time in these limit detonations.

In certain chemical systems, the tube geometry has a very marked effect on the regularity of the writing pattern. Figure 4 illustrates that extremely regular patterns can be observed in rectangular and planar (very narrow rectangular) geometries. Incidentally, the planar mode occurs when the preferred transverse spacing of the detonation is at least five times the width of a narrow channel. It is the simplest self-sustaining detonation mode which may be studied, since it is two-dimensional non-steady. In other chemical systems however, it has been observed that the regularity of the transverse structure is poor in all tube geometries. Typical smoke track records are shown in Figure 2 and results for a number of fuel-oxidizer mixtures are summarized in Table 1. The reason for this behavior has not been discovered at the present time. It is, however, quite obviously related to the chemistry of the system which is detonating.

c. Spacing of Transverse Waves and Chemistry

In systems which show a reasonably regular writing pattern in rectangular tubes, it has been observed that the characteristic size of the pattern is dictated by the initial pressure level and the dilution⁴². The transverse wave spacing of regular smoke track patterns is usually defined as the average distance between two successive waves propagating in the same direction measured along a line parallel to the average orientation of the leading shock wave, i.e., along the diameter of the tube.

The most extensive data on spacing has been taken in the hydrogen-oxygen system containing argon as an inert diluent. This data is summarized and compared with the acoustic predictions for the spacing and with average induction zone and recombination zone lengths in Figure 5. Here the recombination zone length has been approximated by normalizing the reciprocal of the maximum rate of recombination and using the flow velocity at the start of recombination. We notice from this figure that the spacing is always larger than the sum of the induction plus recombination zone lengths in this system and therefore that each element of the detonatable mixture is never traversed by more than one transverse wave of the same family before it completes its reaction. We also note from Figure 5 that the spacing predicted from the acoustic theory is considerably less than any of the reaction lengths or than the spacing of the transverse wave at the front of the detonation. Thus it appears that the acoustic theory cannot be used to predict the spacing of the finite amplitude transverse waves that are observed on propagating detonations. This is not surprising, however, since the interaction of opposing waves appears to be the regulating mechanism in a propagating detonation⁴². However, it is interesting that the spacings which are measured and the spacings which are calculated using the acoustic theory are roughly proportional to each other.

d. Spontaneous Growth of Transverse Waves

The acoustic theory of Strehlow and Fernandes²³ predicts that coherent transverse waves should grow in amplitude as they propagate through the reaction zone of the detonation and the Barthel and Strehlow²⁴ theory predicts that a single acoustic front should convolute to produce a number of evenly spaced shock contacts after some time. This contention has been verified experimentally for at least one case, during the homogeneous initiation of detonation behind a reflected shock wave in a hydrogen-oxygen-argon mixture. Figure 6 contains an (x,t) initiation photograph and a smoke track record obtained simultaneously on a side wall of the tube. It is interesting to note that during this nicely one-dimensional initiation experiment, very weak transverse waves appear on the front and then grow in amplitude (as indicated by an increase in the refraction of opposing waves at their intersection). In a recent paper, Strehlow, Liaugminas, Watson and Eyman⁴² have shown that the appearance location on the smoke track records may be used to predict a reasonably constant exponential coefficient for the linear theory of acoustic growth. From these experimental results we may deduce that there is little doubt but that the acoustic theory of amplitude growth offers a viable mechanism for the appearance of the finite amplitude transverse waves that occur on propagating detonations.

III. Initiation and Failure

a. Flame to Detonation Initiation

This subject has been studied extensively in tubes of varying geometry and in many chemical systems. By far the most quantitative study of the subject has been performed by Oppenheim, Urtiew and co-workers⁴⁶⁻⁵² at Berkeley. The phenomena is complex and the process of flame acceleration (eventually leading to detonation) is very dependent on the condition of the tube walls and the presence of obstacles in the flow.

In general the process develops in the following manner. A flame, generated at the closed end of tube produces a compression wave in the gas which steepens into a shock wave some distance from the end of the tube. This flow develops a boundary layer which becomes turbulent and causes the flame to accelerate. The acceleration of the flame then subsequently reinforces the original shock wave. Eventually, the shock preheats the gas sufficiently to cause the onset of detonation. However, the actual occurrence of detonation is sometimes obscured by the proximity of a very turbulent flame in the neighborhood of the initiation point and in general the process is not one-dimensional. The acceleration process depends very strongly on the ratio of the burning velocity to the sound velocity in the combustible mixture. High values of this ratio cause more rapid acceleration in the system and therefore cause a shorter detonation "induction" distance. If the tube has a finite length and is closed at both ends, shock reflection from the far end may occur before ignition. The reflection process will always preferentially trigger detonation and it has the added disadvantage that it produces very high pressures before the detonation occurs. This type of initiation is extremely important to the prediction of possible hazardous detonations in large industrial installations. It appears, from the information now available that one may make quite realistic estimates of the possibility of detonation for any specific apparatus and combustible mixture.

b. Homogeneous Initiation

Homogeneous one-dimensional initiation has been observed behind a reflected shock wave in a conventional shock tube^{54,55,56}. Figure 6 shows an x,t schlieren interferogram of such an initiation process. The gas dynamics of this process have been modeled by Gilbert and Strehlow⁵⁶ using an (x,t) method of characteristics analysis. They assumed that each element of the gas reacts with kinetics which are dependent only on the previous time-temperature pressure history and that the gas dynamics may be modeled in a conventional manner. The results of their analysis agreed with experimental observations of high temperature reflected initiation in every detail and showed that this type of initiation process is directly caused by the interaction of reaction kinetics and inviscid gas dynamics. In short, they found that because shock heating is a wave process it generates a reaction wave which interacts with and accelerates the shock wave in a manner which is completely predictable if the kinetics are well understood. Furthermore they found that for this process thermal conduction and diffusion are unimportant to the wave development process.

In a following work, Strehlow, Crooker, and Cusey⁵⁷ have experimentally and theoretically studied the process of detonation initiation when a step shock wave passes into a slowly converging channel. Once again they observed that the first point of initiation, in real time, in the converging channel could be predicted by simple application of non-steady gas dynamics and the proper reaction kinetics.

c. Hot Spot Initiation

The most extensive studies of initiation have been performed in the hydrogen-oxygen system^{56, 58, 59}. At high temperature and low pressure this system exhibits a strictly homogeneous initiation behavior in simple flow geometries. However at low temperature (900°-1100°K) and high pressure (i.e., at high reactant concentrations) the system shows a very unusual type of initiation which is difficult to categorize. At its first appearance, the initiation occurs as a series of "hot spots" and these propagate in a number of spherically growing flames until the coalescence of these flames leads to the initiation of detonation. An example is shown in Figure 7. This behavior appears to occur in the pressure and temperature region which is roughly above and to the left of a line on a (P,T) explosion limit diagram obtained by extrapolating the second limit line into the "explosion" region. It appears that this behavior occurs under conditions where appreciable quantities of the species HO₂ are able to accumulate in the mixture⁵⁹. More quantitative work on this type of initiation is needed.

d. Detonation Failure

In this reviewer's estimation the problem of detonation failure has not adequately been studied at the present time. It is quite apparent that each frontal element of a self-sustaining detonation is failing at a rate which is quite rapid when compared to the rate of heat release in the reaction zone. It is also true that if the detonation is allowed to propagate into an enlargement of the tube, sections of the detonation are observed to "fail" because opposing transverse waves are not reflected from the wall and momentarily fail to intersect⁶⁰. However there has never been a truly quantitative study of this process. To date there has been only one theoretical study of this problem and this study is relatively incomplete. Strehlow and Hartung⁶¹ constructed a "steady" one-dimensional overdriven detonation and then allowed it to interact with a strong rarefaction fan approaching it from the rear. The kinetics were assumed to be zero order with a constant activation energy. Rapid failure of the detonation was found to occur for activation energies of 18 and 50 kcal. For a third case, when the activation energy was assumed to be zero, the results were inconclusive because the detonation did not decay to below the CJ velocity. As mentioned above, more work is needed on failure of detonation waves.

IV. The Use of Detonations in Reaction Kinetic Studies

There have been two major techniques developed to study reaction kinetics in actual detonations. White and Cary³⁷ have produced "laminar" detonations by passing an ordinary detonation through a convergent-divergent nozzle. While this flow is non-steady it is still useful for rates studies. They have applied it to the study of vibrational relaxation in exothermic systems and to the study of the effect of vibrational relaxation processes on induction zone kinetics. This technique has also been used to study induction zone kinetics by Mullany and co-workers^{62, 63}.

In another technique, a one-dimensional detonation has been stabilized in a wind tunnel and the reaction profile studied by observing the pressure profile downstream of the normal shock⁶⁴. This technique has interesting engineering implications because it measures overall rates of heat release directly in a nicely controlled one-dimensional geometry.

Unfortunately, it appears that all attempts to resolve the reaction zone in ordinary self-sustaining detonations are doomed to failure, because of the presence of transverse waves. Soloukhin in his discussion of what are, in his terminology, "multi-fronted detonations"⁶⁰, has pointed out that either averaging across the transverse structure with optical techniques or using pressure transducers at the wall will always yield results which are incorrect in terms of a one-dimensional theory. Thus the utility of ordinary propagating detonations for kinetic studies is at best marginal.

SHOCK TUBE HYDRODYNAMICS

Since the inception of its use in the early 1950's the chemical shock tube has greatly expanded the temperature range available for quantitative experimental studies of the physico-chemical properties of gases. The success of its application as a research tool may be gauged by the fact that throughout the world the extant chemical shock tube literature consists of over a thousand references^{65,1} and is presently being increased at the rate of approximately 150 references per year.

In the field of reaction kinetics studies, there are two fundamental reasons for this success. In the first place the step shock wave produced during the operation of an ideal shock tube yields an extremely precise and reproducible heating cycle with excellent initial conditions. In the second place the shock tube is particularly suited for studies in systems that are highly diluted with an inert gas and studies in such dilute systems have consistently yielded the best quantitative kinetic data. Therefore, one might say that gas dynamics is the servant which allows one to make relatively precise rate measurements at high temperatures in a chemical shock tube. However, it is also the master of the situation in that, (1) the geometry of the chemical shock tube is dictated primarily by gas dynamics considerations, (2) specific gas dynamics non-idealities limit the utility of the apparatus and (3) the coupling of the chemical reaction and the gas dynamics is always important to the study of reaction kinetics; particularly in exothermic systems.

At the present time sufficient information has been compiled concerning the behavior of shock tubes, so that the design of a shock tube for precise chemical rate studies is possible. This portion of the paper will present a critical discussion of the relative merits of various experimental techniques and in addition will review recent work on non-ideal shock tube behavior and recently acquired knowledge concerning the occurrence of those flow idealities caused by the presence of exothermic reactions.

I. Studies Behind "Steady" Incident Shock Waves

The most precise measurement of a chemical reaction rate constant may be obtained by observing the reaction immediately behind the incident shock wave produced in a conventional shock tube. For the

highest precision it is imperative that these measurements be made at high dilution in a monatomic gas and that both the rate measurement and the shock velocity measurement be extrapolated to the instant the shock uncovered the observation station. In all other cases flow non-idealities will cause difficulties in the interpretation of the data. This type of extrapolation is possible in only certain specific cases, for example, in the study of the initial dissociation rate of a diatomic or more complex molecule. Typical examples of investigations which have yielded results of high precision using this technique are the measurements of the dissociation rate of triatomic molecules by Olschewski, Troe and Wagner^{66,67,68,69}, the measurement of hydrogen dissociation by Myerson, Thompson and Joseph⁷⁰ and the measurement of oxygen atom recombination by Kiefer and Lutz⁷¹.

In cases where the reaction process must be followed for a long time after shock passage the measurement of a correct rate is not really very straightforward. The raw data after being reduced with the help of ideal shock tube theory must still be corrected for the non-ideal flow behavior in the particular tube that is being used in the experiment. Since combustion drivers, heated gas drivers, double diaphragm tubes, detonation drivers, etc., produce notoriously non-ideal flow situations in the test gas, we will discuss correction procedures which must be used for only the simplest driving process: a cold gas driver operating with a simple pressure burst in a conventional constant area shock tube. Even in this case there are three overlapping but relatively independent corrections which must concern the investigator if he is to obtain reasonable rate constants. The first of this concerns the diaphragm material used in the study. Diaphragm opening time is a function of both the inertia and the tearing properties of the diaphragm material^{72,73}. Probably the best material in this respect is cellulose acetate because it disintegrates so thoroughly on bursting. Mylar is quite slow and irregular and has been shown to produce irreproducible late pressure pulses⁷⁴ (probably due to flapping or late tearing) which could lead to scatter in the rate measurements. Metal diaphragms in general appear to open rather slowly but reasonably reproducibly, if scored uniformly.

It has been observed that even when reproducible, the rate of the diaphragm opening process is extremely important in determining the early behavior of the shock tube flow. White⁷² and Alpher and White⁷³ have shown that for a slow diaphragm opening process, the shock velocity increases for a considerable distance and only then exhibits the decay that one would expect from boundary layer growth. It has been shown theoretically that this slow acceleration may easily yield velocities which are slightly above the theoretical velocity for that bursting pressure ratio. Since this is the formative period for the shock wave, it is best to make kinetic measurements outside of this region. This region extends for a distance from the diaphragm clamp which is a function of the diaphragm material, the bursting pressure ratio and the tube diameter. White⁷² reports an accelerating shock 40' from the clamp with a metal diaphragm in a 3 1/4" square tube at $M = 15$ in argon. However at a shock Mach number of 8 he found that the maximum velocity occurred only 12 feet from the diaphragm. If one remains clear of this accelerating region the major problem which may arise from the diaphragm bursting process is the problem of late spurious pressure signals from materials such as mylar.

Other flow non-idealities that occur in a shock tube during the late flow are all connected to the development of the boundary layer behind the incident shock. These effects have been reviewed by Spence and Woods⁷⁵ and by Holbeche and Spence⁷⁶. In addition, Mirels^{77,78,79,80,81}, in a number of papers has discussed the seriousness of this problem. If one assumes an ideal diaphragm burst it has been found that the flow essentially divides itself into two regimes. The first of these is a period when the shock is decaying due to the boundary layer growth. During this period, the length of the hot column of test gas is growing at a reasonably constant rate that is somewhat below the theoretical rate predicted by ideal theory. After this initial period the boundary layer has grown to such an extent that it is accumulating test gas from the main test sample at the same rate as the incident shock is accumulating new test gas. In this situation, the rate of decay in the incident shock velocity becomes less than before and the length of the test gas column becomes relatively constant. This effect was first reported by Duff⁸². Recently Fox, McLaren and Hobson⁸³ have shown that Mirel's theory quite adequately predicts the observed behavior.

There are two distinctly different types of corrections necessary because of these flow non-idealities. In this paper the effects of non-ideal flow will be discussed for only the state property temperature because reaction rates are primarily temperature sensitive. In the first place the shock wave is continually decelerating -- at first rapidly and later slowly -- and this introduces a temperature gradient in the gas sample which can be large. This temperature gradient may be calculated if one assumes that the shock attenuates at a specific rate and that there are two possible limit behaviors for the pressure decay behind the front. These are: 1. Each fluid element retains its shock transition pressure. In this case the gas contains a relatively step pressure gradient due to attenuation and 2. Each element of gas after shock compression, is isentropically expanded to the instantaneous shock transition pressure. The real behavior behind the decaying shock lies somewhere between these two limit behaviors. These two assumptions yield the following equations for the temperature gradient in the gas following the shock wave.

1. With a residual pressure gradient (no pressure change after shock transition)

$$\frac{dT_2}{T_1} = \frac{4(\gamma-1)}{(\gamma+1)^2} \left(\frac{\gamma M_1^4 + 1}{M_1^2} \right) \frac{dM_1}{M_1}$$

2. With isentropic expansion

$$\frac{dT_2}{T_1} = \frac{4(\gamma-1)}{(\gamma+1)^2} \frac{(M_1^2 - 1)^2}{M_1^2} \frac{dM_1}{M_1}$$

Figure 8 is a plot of T_2 /millisecond in the flow behind a shock wave in argon with an attenuation rate of 1% per meter. As this figure shows, the gradients are sizable and very dependent on the testing temperature T_2 .

The second correction has been estimated by Mirels⁸¹ on the basis of a boundary layer development theory. In his theory for the late flow he assumes a constant velocity shock wave propagating down the tube and he calculates the changes in flow properties along the tube axis due to

the boundary layer growth. His results are plotted as a function of the dimensionless distance from the shock wave l/l_m where l_m is the equilibrium length of the hot gas column. In general he finds that all state properties increase in value as one travels away from the shock. Specifically for a $\gamma = 5/3$ gas at $M = 3$ he finds that the temperature rises to about $1.07 T_2$ at a distance $l = 0.2 l_m$ and then remains relatively constant for the remainder of the transit time. However he finds that an even more serious correction than this is the correction to the testing time that must be included for strong shocks. Specifically, the real testing time for a strong shock increases rapidly over the ideal testing time and at a position $l = 0.2 l_m$ the real testing time is $3/2$ of the ideal testing time. This has been verified quantitatively by Fox, McLaren and Hobson⁸³.

The non-ideal temperature drifts caused by the effects of shock velocity attenuation and boundary layer growth are in the same direction (each yielding a temperature increase as one travels away from the shock) and they may be added to a good first approximation. The testing time correction augments both of these temperature gradients and can in itself cause large errors if ideal flow is assumed. It appears as though some of the extant reaction kinetic data obtained in shock tubes should be re-evaluated in the light of these developments. It should be pointed out that these corrections can change the apparent activation energy of the reaction as well as the absolute rate because in all cases the correction becomes more severe as the run temperature increases.

In the previous discussion it was implied that dilution with an inert monatomic gas is desirable for accurate kinetic rate measurements. Modica and La Graff⁸⁴ have recently studied the decomposition of N_2F_4 using both argon and nitrogen as a diluent and their comparative results reinforce the contention that monatomic gas dilution is necessary to reduce the ambiguity of results. In another interesting experiment along these same lines Seery and Britton⁸⁵ have shown that xenon is apparently not a completely inert diluent during the dissociation of fluoroine.

II. Reflected-Shock Time-Resolved Techniques

Rate measurements made behind the reflected shock offer certain advantages over measurements made using the incident technique. In particular, sampling with a time-of-flight or quadrapole mass spectrometer is possible and laboratory time is real time because the gas is relatively quiescent in the neighborhood of the end-wall. Also, for the same initial conditions the reflected technique produces considerably high temperatures than an incident technique.

In this section we will discuss some difficulties exhibited by only the simplest time-resolved reflected techniques, those in which a sample is drawn from the end wall for mass spectrometer analysis or in which an emission or absorption spectroscopic technique is used to observe a gas sample trapped near the back wall. In these cases the initial temperature behind a reflected shock may be calculated quite accurately from the incident shock velocity measured at the moment of impact, assuming that the gas is entirely inert. The shock velocity at impact must be determined by extrapolating upstream measurements and the calculation is only valid for the case where the reactant is highly diluted with a monatomic carrier gas. As in the case of incident measurements, if it is not possible to extrapolate

the rate to the shock, corrections for the flow non-idealities must be included to accurately determine the rates.

Boundary layer corrections are still important in this case. If one operates near the back wall (within approximately 5mm of the back wall) the testing time correction ceases to be important and if one operates with a monatomic carrier gas, bifurcation problems are not serious⁸⁶. However the pressure rise in the gas traveling behind the incident shock does cause a serious perturbation to the pressure-time and temperature-time history of the gas sample trapped near the back wall. As the reflected shock propagates away from the back wall, it encounters this pressure increase and transmits signals to the gas at the back wall. Fortunately the sample near the back wall is compressed isentropically during this process and for a monatomic gas the temperature increase may be estimated rather accurately using the equation:

$$\frac{\Delta T}{T_2} = \frac{\gamma - 1}{\gamma} \frac{\Delta p}{P_2} \approx 0.4 \frac{\Delta P}{P_2}$$

Thus a pressure gauge may be used to monitor the rate of pressure change at the back wall and this rate of change may be used to estimate the equivalent temperature drift near the back wall. Alternately, Mirels' theory may be used in conjunction with Rudinger's simplified method of characteristics analysis⁸⁷ to calculate a pressure and temperature change at the back wall for the particular shock tube and initial conditions of the experiment.

In the case of mass spectrometer analyses sampling techniques are important and the correction for heat transfer to the wall should be considered in any calculation⁸⁸. These corrections are reasonably straightforward, however, since in this time scale convection does not occur. Therefore, only a conduction equation need be solved to determine the necessary correction. Heat transfer can also be important in spectroscopic techniques because absorption in the cold boundary layer gases at the wall can completely dominate the measurement in certain cases⁸⁹. Allen, Textoris and Wilson⁹⁹ have developed an ingenious apparatus to circumvent this difficulty.

In addition to the above, reflected-shock, time-resolved techniques suffer from two unique difficulties related to the chemistry. In the first place, the occurrence of chemical reaction behind the incident shock cannot always be dismissed in an a priori manner but should be examined for each experimental system. This problem is particularly serious for a first order reaction with a relatively low activation energy and could also be serious for a second order reaction with a very low activation. In the second place, the occurrence of a reaction behind the reflected shock leads to a non-steady reflected shock behavior. There are two reasons for this; either the molecular weight or the enthalpy of the gas may change due to the occurrence of the chemical reaction. By far the most important of these two changes under ordinary conditions is the enthalpy change associated with the reaction process. If an endothermic reaction occurs behind the reflected shock, the shock wave will decelerate and this will cause a pressure decrease and an attendant isentropic temperature decrease at the back wall. Johnson and Britton⁹⁰ have discussed the main features of this flow and a detailed method of characteristic calculation of the interaction for the vibrational relaxation of oxygen has been reported by Nafzinger⁹². He found that the shock relaxation process

took approximately $7 \tau_v$ where τ_v is the characteristic relaxation time behind the reflected shock at the back wall. He also observed that this non-steady process led to a substantial residual entropy gradient along the tube axis in the neighborhood of the back wall. The effect of exothermic reactions will be discussed in Section IVb.

III. Single Pulse Techniques

Single pulse techniques⁹³ suffer from a number of relatively distinct problems. In this reviewer's opinion, the sum total of these deficiencies are serious enough to make the technique very difficult for quantitative kinetic studies. It is, however, still a useful systems technique for qualitative and comparative studies for new or complex systems.

Let us first consider those difficulties that are inherent in a single pulse experiment performed with an ideal shock tube. Even in this case, there are five major problems which limit the technique's utility. These are: 1. Analyses are performed after the experiment is completed. Thus only stable products may be identified and, at best, only the systems overall behavior may be studied. Therefore the deduction of responsible individual reactions with a concordant determination of their rates is very difficult. 2. The heating cycle is not the same for the entire gas sample. Therefore, an average processing time must be estimated for the run. 3. Contact surface tailoring is necessary to obtain long test times and thereby reduce the errors caused by the averaging process mentioned in Part 2 above. However off-design tailoring will cause substantial temperature changes during the last (and usually major) part of the testing time and this is serious if the reaction has a high temperature sensitivity. 4. Cooling must necessarily be produced by a rarefaction fan and this introduces yet another uncertainty into the calculated testing time. 5. If the reaction is not thermally neutral, effects of self-heating must be included. These last two problems have been discussed by Palmer, Knox and McHale⁹⁴.

The non-ideality of a real shock tube flow compounds these problems. By far the most serious non-ideality is the growth of the boundary layer behind the incident shock. This leads to three distinct difficulties which cause problems. In the first place the temperature cannot be held constant for the desired testing time because the upward drift is always appreciable on a time scale of 1 to 4 milliseconds. Secondly, tailoring cannot be exact because of the shift-in properties caused by the boundary layer growth. Thirdly, the growing boundary layer can entrain a sizable quantity of the test gas. Therefore the entire reactive sample is not treated by the test pulse. This last difficulty is particularly serious if the entire contents of the tube are being analyzed after the run and may be alleviated to some extent by analyzing only that portion of the test gas that was in the neighborhood of the back wall during the pulse cycle.

The majority of the difficulties mentioned above cause errors in both the activation energy and the actual magnitude of the rate measured with a single pulse tube. This is because the severity of most of these corrections increase as the temperature of the test run increases.

There have been many variations of the single pulse technique introduced in the past few years. Tsang,^{95,96,97,98,99,100} for example, has applied the technique to the study of hydrocarbon decomposition and rearrangement reactions using a mixture that contains a small quantity of "propyl chloride" as a trace reactant. This specie is used to independently

obtain information on the temperature-time pulse so as to increase the accuracy of the experimental decomposition measurement. This type of "trace reaction" technique has utility only if it can be proved in an unambiguous manner that the trace reaction is occurring independently of the unknown reaction. It should have the highest accuracy when the activation energies of the two reactions are approximately equal.

Tschuchikow-Roux^{101,102,103} has proposed a ball valve technique which may be used to isolate a sample either between the ball valve and the end plate of the tube or just in the bore of the ball valve. However, his heating cycle analysis is based on ideal shock tube flow theory and since he proposes to calculate heating time by subtracting two large times which are themselves calculated by using ideal theory, the accuracy of his calculation will be low. However, there is the possibility of improving the accuracy by including the necessary boundary layer growth corrections.

Lifshitz, Bauer and Resler¹⁰⁴ have introduced and used a tube with a side dump tank on the test section leg. In conjunction with this they operate the tube without a tailored interface. Instead they "tune" the length of the driver section by inserting plugs at the end wall so that the strong rarefaction fan in the driver gas, after reflecting from the end of the driver section, will overtake the contact surface at the instant that it is met by the reflected shock wave. Thus, testing time in the sample theoretically ranges from zero to approximately $2 t_{ave}$. The technique suffers, however, from the fact that non-ideal boundary layer growth will always cause the contact surface to intersect the reflected shock earlier than the theoretical time. If this effect is not included in the "tuning" operation the test gas sample will suffer a complex time-temperature heating cycle and the interpretation of the data will be difficult. The presence of a side dump tank modifies the downstream flow in the test section but a reasonable constant shock velocity is still attained near the end plate. The side dump tank is used primarily to prevent multiple high pressure reflections in the gas sample. It is probably adequate for this purpose.

IV. Exothermic System Instabilities

In addition to all the difficulties mentioned above, in exothermic systems the application of the shock tube to reaction kinetic studies is limited by the occurrence of non-steady flow processes which may be triggered by the presence of the exothermic reaction. Specifically, two distinct types of flow instabilities may occur and it has been found that two independent criteria may be used to predict the occurrence of these instabilities on the basis of known flow properties of the particular system which is under investigation. The two criteria will be called the Chapman-Jouguet criterion and the tube diameter criterion.

a. The Chapman-Jouguet Criterion

Consider a gas mixture capable of sustaining a reaction which drives the system toward a state of full chemical equilibrium. With this restriction we define the mixture to be "exothermic" if, in the (P, V) plane, the Rayleigh line through the point (P_1, V_1) which just tangents the equilibrium Hugoniot represents a shock transition whose Mach number, M_{CJ} , is greater than unity. We call the value of this minimum Mach number for steady shock propagation the Chapman-Jouguet criterion for instability. It

may, of course, be calculated quite accurately if thermodynamic properties are available for the system in question.

An example of the application of this criterion may be discussed with the help of Figure 9. The system considered in this figure is a stoichiometric hydrogen-oxygen mixture diluted with various amounts of argon at the initial conditions $T_1 = 300^\circ\text{K}$ and $P_1 = 100$ torr. The unreactive shock temperature for a shock of Mach number $M = M_{CJ}$ is plotted versus the mixture composition in this figure. The vertical lines approximate regions in which studies have been reported, admittedly for different stoichiometrics and pressure levels (the numbers on the lines are reference numbers). The approximation is reasonably good because, however, pressure shifts the curve in Figure 9 only slightly and stoichiometry changes are effectively dilution changes on the basis of a CJ calculation. Region I, above and to the left of the stability line $M = M_{CJ}$, corresponds to the experimental conditions under which steady incident shock waves may be produced and studied in this system, while region II, below and to the right of the stability curve represents initial shock conditions for which a steady shock wave with chemical reaction cannot exist. Note that Belles and Lauver¹⁰⁷ worked with incident shocks just at the edge of region I and that all other extant incident shock studies were performed well inside region I. It is interesting that Belles and Lauver report instability difficulties at low temperatures.

In region II of Figure 1, kinetic studies must necessarily be performed in conjunction with a flow which is longitudinally non-steady. For this reason well controlled and reproducible initial conditions are important to the design of these experiments. For example, the simple fact that the initial flow produced by the diaphragm bursting process is neither one-dimensional nor reproducible obviates the use of a conventional incident shock technique for region II studies. There are, however, four shock tube techniques which either have been used or have a potential use for performing kinetic studies under region II conditions. These will be discussed individually.

The first of these techniques uses the reflected shock region. Reflected shock studies, when performed in a gas mixture with a high heat capacity ratio, yield a reasonably one-dimensional heating cycle with well defined initial conditions⁵⁴. Even though the flow following reflection remains non-steady for an extended period of time (and indeed may yield a detonation wave propagating away from the end wall) the gas near the end wall may be used for kinetic studies since it is quiescent, it suffers no additional shock transitions after reflected shock passage and its pressure-time history during the reaction process may be predicted reasonably well⁵⁵. This technique has been used successfully by numerous investigators^{54, 105, 106} in situations where the steady incident technique would not be applicable in terms of the CJ criterion.

The second technique consists of passing a weak, but well established, step shock wave produced in a conventional constant area shock tube into and through a section of tubing whose cross sectional area is slowly decreasing with distance. If the rate of decrease of area is sufficiently slow (a maximum wall angle to the center line of approximately 1° for example) the flow will become a quasi one-dimensional non-steady flow in which the leading shock wave is

continually accelerating. In this situation a non-steady flow calculation is required to sort the reaction kinetics from the gas dynamics effects. This experiment has been performed and such a calculation has been made for a tube in which $d(\ln A)/dx = -k$ during convergence⁵⁷. Figure 10 contains iso-temperature and iso-pressure plots in an (x,t) coordinate system for a typical theoretical run assuming that the flow is entirely inert. The region which is mapped is bounded by the leading shock wave, the reflected shock wave and the "explosion line". The locus of the "explosion line" in this figure was determined by assuming that the fraction of the delay time to explosion which has been used at each instant along each separate particle path may be calculated using the relation.

$$d\phi = \frac{dt}{\tau(T,P)}$$

where

$$\tau = \frac{A}{[O_2]} \exp(-E/RT)$$

With this model the points at which

$$\int_0^t \frac{dt}{\tau(T,P)} = 1$$

on each particle path describe the locus of the explosion line. This approach assumes that the reaction is thermally neutral during the induction period and therefore that the reaction does not interact with the flow. Furthermore, as presently constructed, the model only allows one to predict the location of the minimum time in the explosion line locus on an (x,t) plot since the effect of heat release during the explosion is not included in the model. Reference 57 contains a more complete discussion of this technique.

To this author's knowledge the third possible non-steady technique has not yet been applied to the study of reaction kinetics in exothermic systems. It is an incident technique which involves the use of a ball valve whose internal bore is exactly equal to the diameter of the shock tube. This type of ball valve shock tube has been used in the study of endothermic systems¹⁰¹ and to prevent premature explosions in reflected shock studies⁵⁴. If the initial pressure were adjusted externally before opening the valve and if the shock tube were operated vertically, density separation of an inert gas near the diaphragm and the explosion mixture downstream could be maintained until a well formed incident shock wave passes the location of the ball valve. Observation at a number of window stations downstream of the valve would then allow reaction kinetic studies to be studied even though the flow was non-steady. This technique has two advantages relative to the converging channel technique in that both the construction of the apparatus and the calculation of the flow would be simpler. A simpler calculation of the flow may be made because one may assume the flow in the reactive mixture to be pseudo steady until an

appreciable amount of chemical reaction has occurred. This technique also has an advantage over the reflected shock technique for those cases where the system to be studied cannot be diluted to repress bifurcation. This is because, in the ball valve technique only simple boundary layer growth can occur to perturb the incident flow.

The fourth possible technique involves direct expansion of an incident shock wave through a suitably instrumented two-dimensional nozzle. This technique has been described by White and Cary³⁷ and has been discussed in Section IVa.

b. The Tube Diameter Criterion

Even in circumstances where incident shock wave studies are allowable on the basis of the CJ criterion, transverse instabilities may appear during an experiment. This type of behavior has been reported by Schott¹¹⁰, Schott and Bird¹¹¹ and Hawthorne¹¹² and is important to the kineticist because it can produce state variable fluctuations across the tube which may be misinterpreted if the usual one-dimensional assumptions are used in reducing the data.

Schott¹¹⁰ has shown that in acetylene-oxygen mixtures diluted with 97.5 percent argon, this type of instability behavior produces soot track writings which are equivalent to those obtained when a self-sustaining detonation propagates over a smoked foil. This experimental evidence implies that the transverse instabilities observed in reaction kinetic studies in the shock tube are of the same type as those observed⁴² on propagating detonations. This is really not very surprising since the theoretical results discussed in Section a show that detonation per se is not necessary for the appearance of transverse instabilities.

It is also known that all self-sustaining detonations exhibit a transverse wave spacing which is roughly proportional to the "thickness" of the detonations reaction zone. Thus, theoretical predictions and experimental observations both lead to the conclusion that the transverse structure associated with an exothermic reaction zone triggered by shock passage should exhibit a characteristic spacing which is roughly proportional to the reaction zone thickness.

One more experimental observation must be mentioned before we may present a criterion for the occurrence of transverse wave instability in a reactive shock wave propagating in a specific channel. Both Manson⁴³ and Fay⁴⁴ have shown that transverse structure fails to couple with transverse acoustic modes of the tube when the preferred transverse spacing at the front becomes somewhat larger than the major transverse dimension of the tube. Thus it appears that this type of resonance must be possible before transverse instabilities will appear.

Unfortunately, at the present time, the relation between the reaction zone thickness and the characteristic cell size of the structure is not known except for a few systems and then only in an empirical manner. Therefore, at the present time, the "tube diameter" criterion for the occurrence of transverse instabilities in a steady incident shock wave experiment must be stated as follows: Transverse instability may occur in a steady shock wave followed by exothermic reaction only if the bulk of the exothermic process occurs as close to the shock wave as the major transverse dimension of the tube.

This criterion correctly predicts the occurrence of the currently observed transverse instabilities during incident shock reaction kinetic studies in a shock tube. More quantitative information on this subject is available in Schott's report in this symposium volume.¹¹³

SUMMARY

Detonations in premixed gases contain a very complex internal wave structure which is related to the exothermic chemical reactions occurring behind the leading waves. This structure negates many of the classical one-dimensional arguments concerning detonation and the full reasons for its existence and form are not understood at the present time. The mechanism of self-sustenance of a propagating detonation is also open to question at the present time. The situation is not hopeless, however, because it appears that the application of the principles of non-steady reactive gas dynamics (in which all shocks are considered to be infinitely thin non-reactive discontinuities in the flow) will eventually allow a complete description of the structure from first principles.

The discussion of shock tube hydrodynamics indicates that while the shock tube is an extremely useful apparatus for high temperature gas phase reaction kinetic studies, it has its limitations. These are primarily caused by gas dynamic non-idealities due to boundary layer growth and to the interaction of the chemistry and the flow. The implication of this section is that a good kinetic rate measurement may be obtained from a shock tube experiment only if the full contribution of these non-idealities are considered.

REFERENCES

1. Bradley, J. N., Shock Waves in Chemistry and Physics, Wiley, New York (1962b).
2. Gaydon, A. G. and Hurle, I. R., The Shock Tube in High-Temperature Chemical Physics, Reinhold, New York (1963).
3. Greene, E. F. and Toennies, J. P., Chemical Reactions in Shock Waves, Academic Press, New York (1964).
4. Bauer, S. H., "Shock Waves", in Annual Review of Physical Chemistry, Vol. 16, Annual Reviews Inc., Palo Alto, Calif. (1965).
5. Strehlow, R. A., Shock Tube Chemistry, a chapter in Vol. II of High Temperature Physics, Chemistry and Technology, Pergamon Press (1967) (In Press).
6. Zel'dovich, Y. B., J. Exptl. Theo. Phys. (USSR) 10, 542, (1940): English Translation NACA TM 1261, (1950).
7. von Neumann, J., "Theory of Detonation Waves", Prog. Rept. No. 238, (April 1942) OSRD Report No. 549, (1942).
8. Doring, W., Ann. Physik, 43, 421 (1943).
9. Chapman, D. L., Phil. Mag. 213, Series A, 47, 90, (1899).
10. Jouguet, M., J. Math. Pure and Appl., 70, Series 6, 1, 347, (1905); 71, Series 6, 2, 1, (1906).
11. Shchelkin, K. I., Soviet Physics, JETP 9 (36), 416, (1959).
12. Erpenbeck, J. J., Ninth Symposium (International) on Combustion, (Academic Press, New York, N. Y.) p. 442, (1963b).
13. Zaidel, R. M. and Zel'dovich, Ya. B., Zh. Prikl. Mekh. i Tekh. Fiz., No. 6, 59, (1963).
14. Pukhnachov, V. V., Zh. Prikl. Mekh. i Tekh. Fiz., No. 4, 79, (1965).
15. Shchelkin, K. I., Dokl. Akad. Nauk, SSSR, 160, 1144, (1965b).
16. Ilkaeva, L. A. and Popov, N. A., Fiz. Gor. i Vzr., No. 3, 20, (1965).
17. Aslanov, S. K., Dokl. Akad. Nauk, SSSR, 163, 667-671, (1965).

18. Aslanov, S. K., Dokl. Akad. Nauk, SSSR, 169, 136-9, (1966a).
19. Kuznetsov, N. M., Dokl. Akad. Nauk, SSSR, 164, 1097, (1965).
20. Erpenbeck, J. J., Phys. Fluids, 7, 684, (1964a).
21. Erpenbeck, J. J., Phys. Fluids, 8, 1192, (1965).
22. Erpenbeck, J. J., Phys. Fluids, 9, 1293, (1966).
23. Strehlow, R. A. and Fernandes, F. D., Comb. and Flame, 9, 109, (1965).
24. Barthel, H. O. and Strehlow, R. A., Phys. Fluids, 9, 1896, (1966).
25. Fickett, W. and Wood, W. W., Phys. Fluids, 9, 903, (1966).
26. Erpenbeck, J. J., Phys. Fluids, 10, 274, (1967).
27. Voitsekhovskii, B. V., Mitrofanov, V. V. and Topchian, M. E., Structure of a Detonation Front in Gases, Izd-vo Sibirsk, Otdel. Akad. Nauk, SSSR, Novosibirsk, (1963); English Translation, Wright-Patterson Air Force Base, Report FTD-MT-64-527, (AD 633-821) February 1966.
28. Soloukhin, R. I., Shock Waves and Detonations in Gases, Mono Book Corp., Baltimore, Maryland, (1966c).
29. Shchelkin, K. I. and Troshin, Ya. K., Gasdynamics of Combustion, Mono Book Corp., Baltimore, Maryland, (1965).
30. Shchetinkov, E. S., Fizika Gorenia Gazov (Physics of Gaseous Combustion) Izdatel'stvo "Nauk" Glavnaa Redaktsia Fiziko-Matematicheskoi Literatury, Moscow, (1965).
31. White, D. R., Phys. Fluids, 4, 465, (1961).
32. Duff, R. E., Phys. Fluids, 4, 1427, (1961).
33. Schott, G. L., Phys. Fluids, 8, 850, (1965).
34. Edwards, D. H., Parry, D. J., and Jones, A. T., J. Fluid Mech., 26, 321, (1966a).
35. Edwards, D. H., Parry, D. J. and Jones, A. T., Brit. J. App. Phys., 17, 1507, (1966b).
36. Oppenheim, A. K., Astron. Acta., 11, 391, (1965).
37. White, D. R. and Cary, K. H., Phys. Fluids, 6, 749, (1963).
38. Strehlow, R. A., Phys. Fluids, 7, 908, (1964b).
39. Antolik, K., Paggendorp Ann. Phys. und Chemie, 230, sec 2, 154, 14, (1875).
40. Denison, Yu. H. and Troshin, Ya. K., Doklady Akad. Nauk, SSSR, 125, 110, (1959); Translation, Phys. Chem. Sect. 125, 217, (1960).
41. Oppenheim, A. K. and Urtiew, P. A. (Private Communication, Summer 1966).
42. Strehlow, R. A., Liaugminas, R., Watson, R. H. and Eyman, J. R., Eleventh Symposium (International) on Combustion, Mono Book Corp., Baltimore, Maryland, p. 177, (1967).
43. Manson, N., Compt. Rend., 222, 46 (1946).
44. Fay, J. A., J. Chem. Phys., 20, 942, (1952).
45. Duff, R. E. and Finger, M., Phys. Fluids, 8, 764, (1965).
46. Oppenheim, A. K., Arch. Mekh. Stosowanej, 216, 405, (1964).
47. Oppenheim, A. K., Urtiew, P. A. and Weinberg, F. J., Proc. Roy. Soc. London, A291, 279, (1966).
48. Urtiew, P. A., Experimental Study of Wave Phenomena Associated with the Onset of Detonation, Report AS-65-1, Univ. of Calif., Berkeley, February 1965, (AD 621-214) (1965).
49. Urtiew, P. A., Laderman, A. J. and Oppenheim, A. K., Tenth Symposium (International) on Combustion, (The Combustion Institute, Pittsburgh, Pa.) 797, (1965).
50. Urtiew, P. A. and Oppenheim, A. K., Comb. and Flame, 9, 405, (1965).
51. Urtiew, P. A. and Oppenheim, A. K., Proc. Roy. Soc., 295, 13, (1966).
52. Urtiew, P. A. and Oppenheim, A. K., Eleventh Symposium (International) on Combustion, Mono Book Corp., Baltimore, Maryland, (1967).
53. Bollinger, L. E., Fong, M. C., Laughrey, J. A. and Edse, R., Experimental and Theoretical Studies on the Formation of Detonation Waves in Variable Geometry Tubes, NASA TN D-1983, June 1963.

54. Strehlow, R. A. and Cohen, A., *Phys. Fluids*, 5, 97, (1962).
55. Gilbert, R. B. and Strehlow, R. A., *AIAA Journal*, 4, 1777, (1966).
56. Soloukhin, R. I., *Zh. Prikl. Mekh. i Tekh. Fiz.*, #4, 42, (1964).
57. Strehlow, R. A., Crooker, A. J. and Cusey, R. E., *Comb. and Flame*, 11, (1967) (In Press).
58. Schott, G. L. and Kinsey, J. L., *J. Chem. Phys.*, 29, 1177, (1958).
59. White, D. R., "A Study of Shock Wave Induced Reactions," ARL Report 66-D177, Office of Aerospace Research, USAF Wright-Patterson AFB, Ohio, (September 1966) (AD 646-559).
60. Soloukhin, R. I., *Comb. and Flame*, 10, 51, (1966a).
61. Strehlow, R. A. and Hartung, W., *Comb. and Flame*, 9, 423, (1965).
62. Mullaney, G. J. and Arave, R., "Determination of Induction Times in One-Dimensional Detonations," Boeing Scientific Laboratory Research Report, DL-82-0324, Boeing Aircraft Corp., Seattle, Washington, (December 1963).
63. Mullaney, G. J., Ku, P. S. and Botch, W. B., *AIAA Journal*, 3, 873, (1965).
64. Rubins, P. M. and Panesci, J. H., "Experimental Standing Wave Shock-Induced Combustion for Determining Reaction Kinetic Histories," AIAA Paper 65-607, (June 1965).
65. Nesterichin, Y. E. and Soloukhin, R. I., "Rapid Instrumentation Methods for Gasdynamics and Plasma Physics," *Novosibirsk Hydrodynamic Institute, Novosibirsk*, (1965); English Translation: *JPRS 39,657 TT 67-30306, CFSTI, Washington, D. C.*, (January 1967).
66. Olschewski, H. A., Troe, J. and Wagner, H. Gg., *Z. Physik. Chem.*, (Frankfurt) 47, 383, (1965c).
67. Olschewski, H. A., Troe, J. and Wagner, H. Gg., *Z. Physik. Chem.*, (Frankfurt) 45, 329, (1965b).
68. Olschewski, H. A., Troe, J. and Wagner, H. Gg., *Ber. Bunsen Ges. Physik. Chem.*, 70, 450, (1966b).
69. Olschewski, H. A., Troe, J. and Wagner, H. Gg., *Eleventh Symposium (International) on Combustion*, Mono Book Corp., Baltimore, Maryland, (1967).
70. Myerson, A. L., Thompson, H. M. and Joseph, P. S., *J. Chem. Phys.*, 42, 3331, (1965).
71. Kiefer, J. H., Lutz, R. W., *J. Chem. Phys.*, 42, 1709, (1965b).
72. White, D. R., *J. Fluid Mech.*, 4, 585, (1958).
73. Alpher, R. A. and White, D. R., *J. Fluid Mech.*, 3, 457, (1958).
74. Dynner, H. B., *Phys. Fluids*, 9, 879, (1966).
75. Holbeche, T. A. and Spence, D. A., *Proc. Roy. Soc.*, A279, 111, (1964).
76. Spence, D. A. and Woods, B. A., *J. Fluid Mech.*, 19, 161, (1964).
77. Mirels, H., *Phys. Fluids*, 6, 1201, (1963).
78. Mirels, H. and Mullen, J. F., *Phys. Fluids*, 7, 1208, (1964).
79. Mirels, H., *AIAA Journal*, 2, 84, (1964).
80. Mirels, H., *Phys. Fluids*, 9, 1265, (1966a).
81. Mirels, H., *Phys. Fluids*, 9, 1907, (1966b).
82. Duff, R. E., *Phys. Fluids*, 2, 207, (1959).
83. Fox, J. N., McLaren, T. I. and Hobson, R. M., *Phys. Fluids*, 9, 2345, (1966).
84. Modica, A. P. and LaGraff, J. E., *J. Chem. Phys.*, 45, 4729, (1966b).
85. Seery, D. J. and Britton, D., *J. Phys. Chem.*, 70, 4074, (1966).
86. Strehlow, R. A. and Cohen, A., *J. Chem. Phys.*, 30, 257, (1959).
87. Rudinger, G., *Phys. Fluids*, 4, 1463, (1961).
88. Modica, A. P., *J. Phys. Chem.*, 69, 2111, (1965).
89. Charatis, G. and Wilkerson, T. D., *Phys. Fluids*, 2, 578, (1959).
90. Allen, R. A., Textoris, A. and Wilson, J., *J. Quant. Spectr. Radiative Transfer*, r, 95, (1965).
91. Johnson, C. D. and Britton, D., *J. Chem. Phys.*, 38, 1455, (1963).

92. Nafzinger, L. E., "Non-Steady Relaxation Phenomena Behind a Reflected Shock Wave," M.S. Thesis, University of Illinois, (August 1966).
93. Glick, H. S., Squire, W. and Hertzberg, A., Fifth Symposium (International) on Combustion, Reinhold, New York, 393, (1955).
94. Palmer, H. B., Knox, B. E. and McHale, E. T., AIAA Journal, 1, 1195, (1963).
95. Tsang, W., J. Chem. Phys., 40, 1171, (1964a).
96. Tsang, W., J. Chem. Phys., 40, 1498, (1964b).
97. Tsang, W., J. Chem. Phys., 41, 2487, (1964c).
98. Tsang, W., J. Chem. Phys., 42, 1805, (1965a).
99. Tsang, W., J. Chem. Phys., 43, 352, (1965b).
100. Tsang, W., J. Chem. Phys., 44, 4283, (1966).
101. Tschuikow-Roux, E. and Marte, J. E., J. Chem. Phys., 42, 2049, (1965); Erratum: 43, 1438.
102. Tschuikow-Roux, E., Phys. Fluids, 8, 821, (1965a).
103. Tschuikow-Roux, E., J. Chem. Phys., 42, 3639, (1965b).
104. Lifshitz, A., Bauer, S. H. and Resler, E. L., J. Chem. Phys., 38, 2056, (1963).
105. Voevodskii, V. V. and Soloukhin, R. I., Tenth Symposium (International) on Combustion, The Combustion Institute, Pittsburgh, Pennsylvania, 279, (1965).
106. Miyama, H. and Takeyama, T., J. Chem. Phys., 41, 2287, (1964).
107. Belles, F. E. and Lauver, M. R., J. Chem. Phys., 40, 415, (1964).
108. Skinner, G. B. and Ringrose, G. H., J. Chem. Phys., 42, 2190, (1965).
109. Schott, G. L., J. Chem. Phys., 32, 710, (1960).
110. Schott, G. L., Los Alamos Scientific Lab., Los Alamos, New Mexico, Private communication, (1963).
111. Schott, G. L. and Bird, P. F., J. Chem. Phys., 41, 2869, (1964).
112. Hawthorne, R. D. and Nixon, A. D., "Shock Tube Ignition Delay Studies of Endothermic Fuels," AIAA Paper, #65-594. Presented at AIAA Joint Propulsion Specialists Meeting, Colorado Springs, Colorado, (June 1965) also Hawthorne, R. D., Shell Development Co., Emeryville, Calif., Private communication, (1965).
113. Schott, G. L., "Detonation Spin in Driven Shock Waves in a Dilute Exothermic Mixture," Division of Fuel Chemistry Preprints for Symposium on Detonations and Reactions in Shock Waves, ACS National Meeting, Chicago, Illinois, (September 1967).

Table I Structure Regularities of Transverse Waves in Detonations

MIXTURE	DILUENT	% DILUTION	REGULARITY
H ₂ — O ₂	—	—	POOR
	1	50	POOR
	1	40	POOR
	1	70	EXCELLENT
	1	60 85	EXCELLENT
	1	60 & 16	EXCELLENT
	1.5	—	POOR
	.5	Ar	GOOD
	1.5	Ar	POOR
	.75	Ar 2.06	GOOD
C ₂ H ₂ — O ₂	—	—	POOR
	1	Ar 75 85	EXCELLENT
C ₂ H ₄ — O ₂	—	—	POOR
	1	Ar 50	GOOD
	1	Ar 75	EXCELLENT
CH ₄ — O ₂	1	Ar 0 80	IRREGULAR
	1	Ar 2.0 50	IRREGULAR
	1	Ar 50 80	POOR
	1.25	—	POOR
	1.25	Ar 80	POOR
CO — O ₂	1	Ar 50	GOOD
	1	—	IRREGULAR
	1	Ar 40	IRREGULAR
NH ₃ — O ₂	1	—	IRREGULAR
	1	Ar 40	IRREGULAR

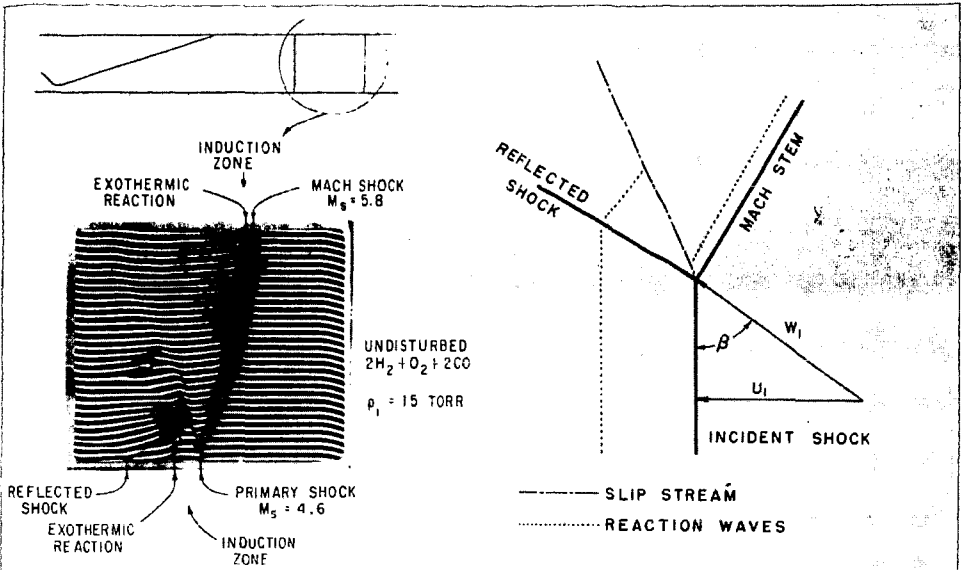
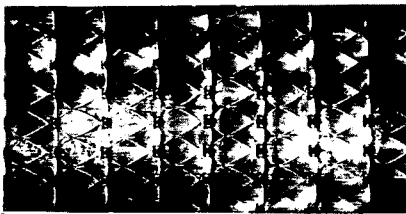
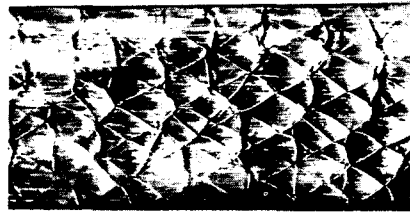


FIGURE 1. ARTIFICIALLY PRODUCED REACTIVE MACH STEM. (COURTESY REF. 37)



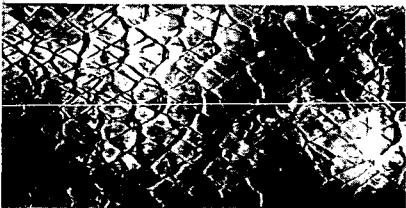
EXCELLENT: $C_2H_4 + 3O_2 + 75\% Ar$
 $P = 100$ mm



GOOD: $1.26 H_2 + O_2 + 40\% Ar + 16\% N_2$
 $P = 150$ mm

PROPAGATION DIRECTION

2 IN



POOR: $2H_2 + O_2$ $P = 125$ mm



IRREGULAR: $CH_4 + 2O_2$ $P = 50$ mm

FIGURE 2. A FEW EXAMPLES OF SMOKE TRACK RECORDS. $3\frac{1}{4} \times 1\frac{1}{2}$ DETONATION TUBE.

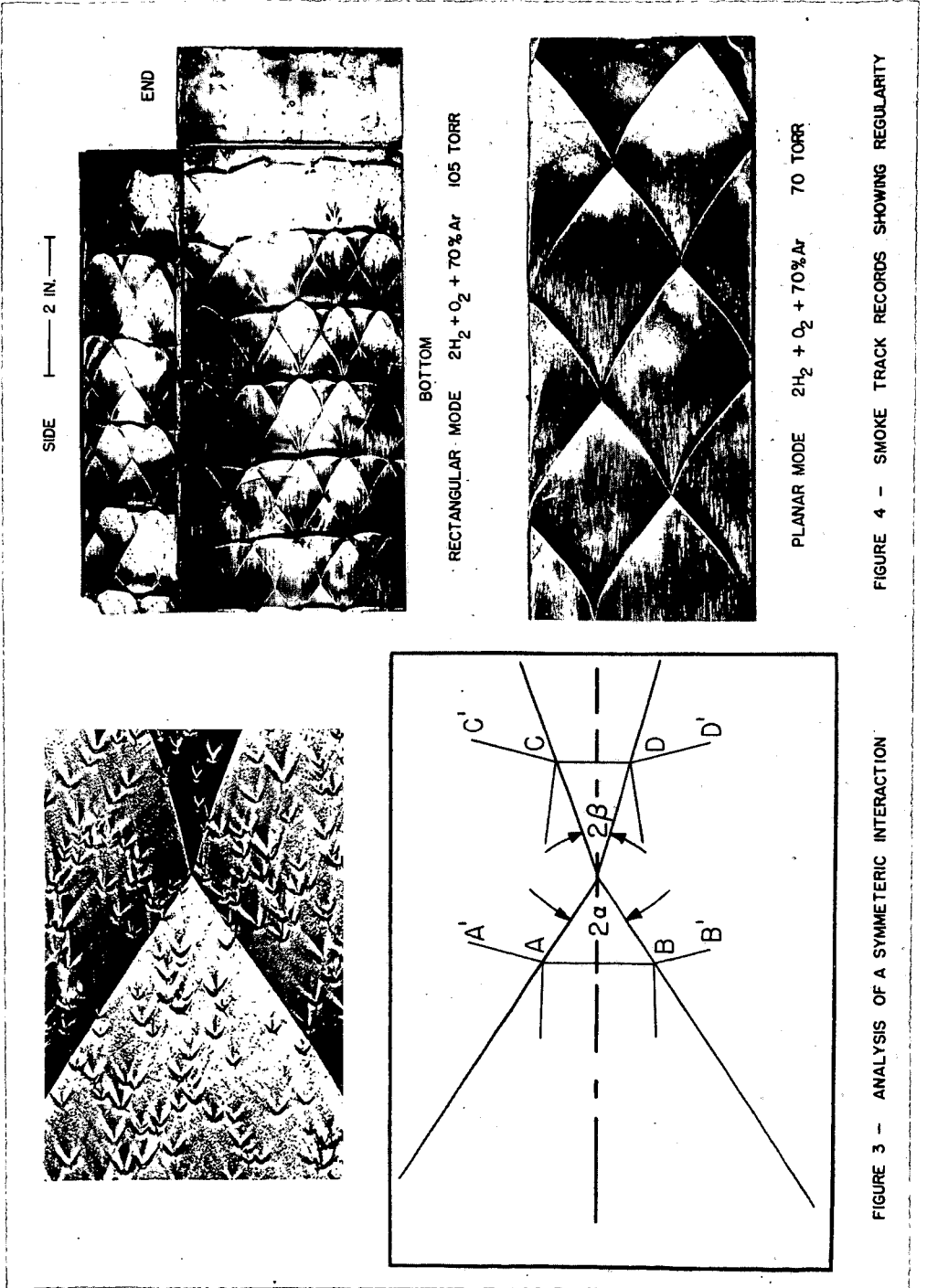


FIGURE 3 - ANALYSIS OF A SYMMETRIC INTERACTION



SIDE |-----| 2 IN. |-----|



END

BOTTOM

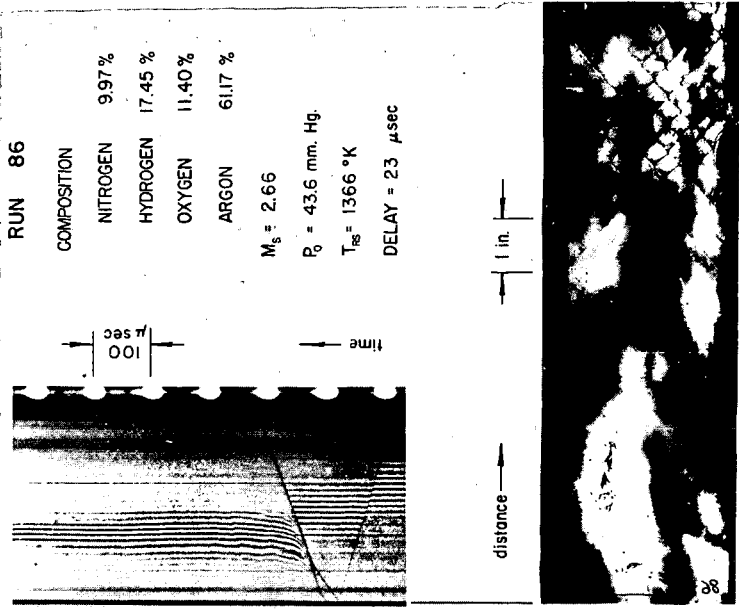
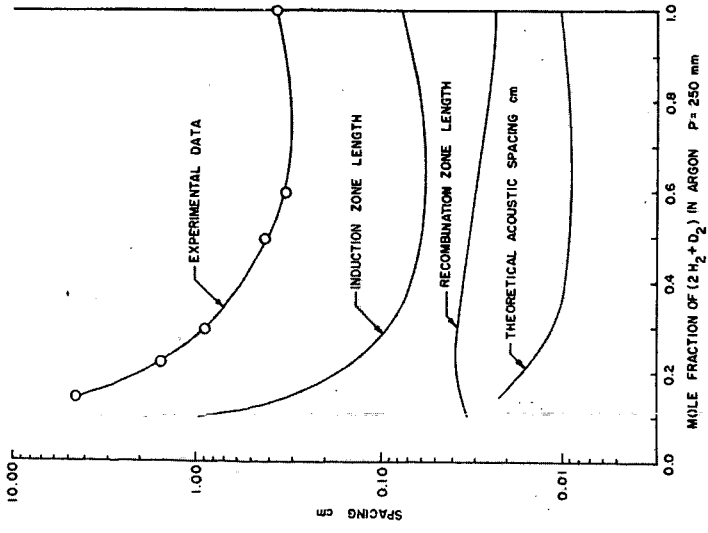
RECTANGULAR MODE $2H_2 + O_2 + 70\%Ar$ 105 TORR

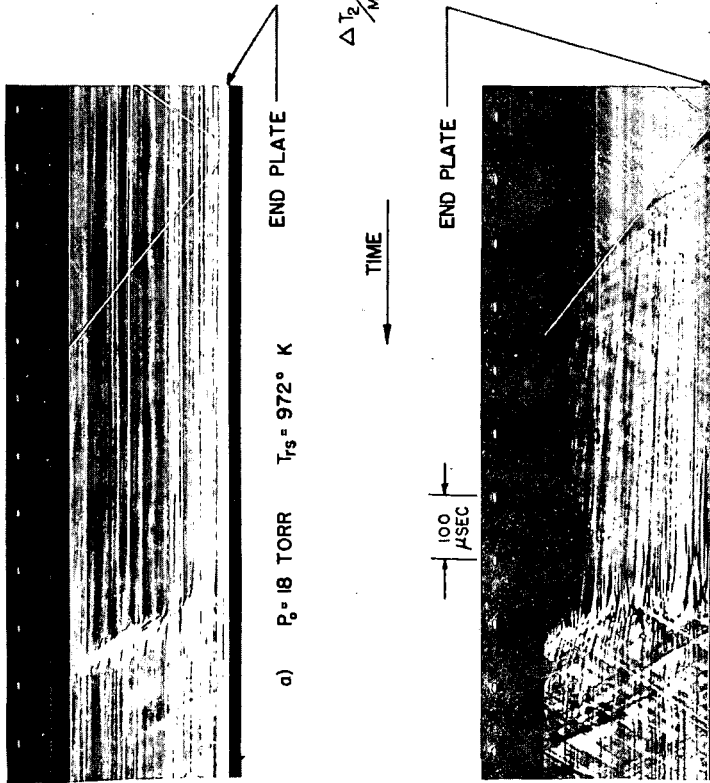


PLANAR MODE $2H_2 + O_2 + 70\%Ar$ 70 TORR

FIGURE 4 - SMOKE TRACK RECORDS SHOWING REGULARITY

FIGURE 5 - TRANSVERSE WAVE SPACINGS IN THE $2H_2 + O_2$ SYSTEM
 FIGURE 6 -- THE APPEARANCE OF TRANSVERSE WAVES DURING INITIATION BEHIND A REFLECTED SHOCK





b) $P_0 = 24.9 \text{ TORR}$ $T_{rS} = 1020^\circ \text{ K}$

FIGURE 7 - HOT SPOT INITIATION IN $0.08\text{H}_2 + 0.02\text{O}_2 + 0.90\text{Ar}$ MIXTURES BEHIND REFLECTED SHOCK
COURTESY A. COHEN, BALLISTIC RESEARCH LABORATORIES.

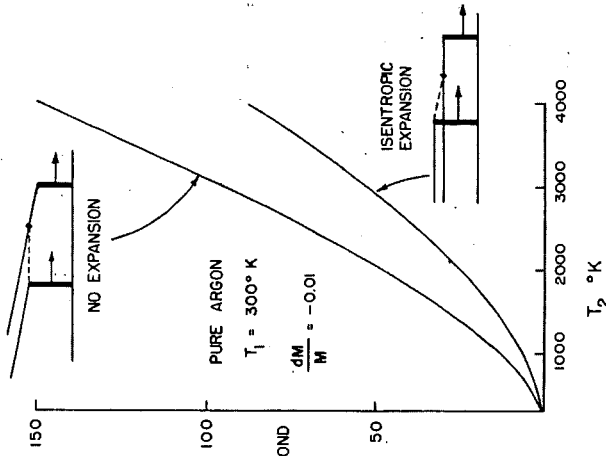


FIGURE 8 - TEMPERATURE CORRECTION FOR SHOCK ATTENUATION

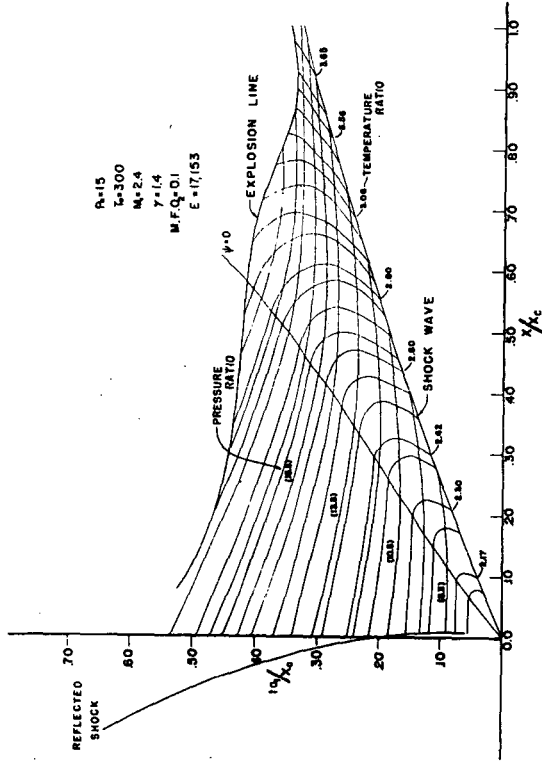


FIGURE 10 - NONSTEADY FLOW BEHIND A STEP SHOCK PROPAGATING INTO A CONVERGING CHANNEL. REF. 57

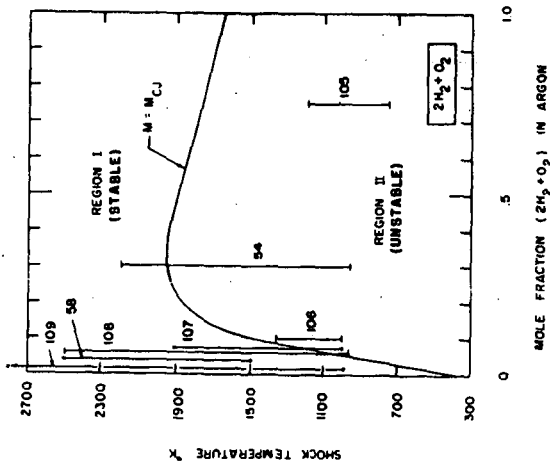


FIGURE 9 - STABILITY REGIONS DEFINED BY THE CJ CRITERION

Detonation Spin in Driven Shock Waves in a Dilute Exothermic Mixture

Garry L. Schott

University of California, Los Alamos Scientific Laboratory,
Los Alamos, New Mexico 87544

There have been many uses of shock waves in diluted mixtures of exothermic reactants for studies of chemical reaction rates. It was once commonly thought, for lack of evidence to the contrary, that one could operate in a regime free of complications from spontaneous "detonation" phenomena arising from the deposition of the reaction energy in the flowing gas by generating shock waves faster and stronger than the Chapman-Jouguet wave for the dilute mixture. Such shock waves are in reality overdriven detonation waves, and the only basis for distinguishing them from strong detonation waves in more concentrated mixtures is the fact that the dilute mixtures, if not supported, may fail to sustain a slower, Chapman-Jouguet velocity wave. This distinction is one of degree rather than of kind, and recent experience with unsupported detonations and overdriven detonations in detonable gas mixtures indicates that three-dimensional structure which characterizes the Chapman-Jouguet velocity waves remains present, on a progressively finer scale, in overdriven waves.^{1,2}

The occurrence of transverse waves or other instabilities in driven shock waves in dilute, only mildly exothermic mixtures has been less completely characterized. Indeed, many successful investigations of kinetics of exothermic reactions have been carried out in shock waves in dilute mixtures without major or even noticeable interference. On the other hand, there have been isolated reports of "instabilities", in the reaction zones in particular, under circumstances where the system was diluted well beyond the limit of detonability and the shock wave was clearly stronger than a Chapman-Jouguet wave. Examples of these occurrences may be found in studies of the hydrogen - bromine reaction,³ ozone decomposition,⁴ and hydrogen-oxygen combustion.⁵ The present paper reports the occurrence of such instabilities in shock waves in a mixture of 1% C₂H₂, 1.5% O₂, 97.5% Ar and the identification of conditions where the phenomena exhibit the recognizable and quasi-reproducible form of single-headed spin.^{6,7}

Experimental

The experiments reported here were carried out in the 10 cm i.d. circular brass shock tube used for several previously reported chemical investigations.⁵ Several different test section configurations were utilized for the various kinds of diagnostic experiments. Either brass shim stock or Mylar sheet diaphragms were used, and the driver gas was hydrogen. The several batches of 1.0% C₂H₂, 1.5% O₂, 97.5% Ar test gas mixture were prepared manometrically from tank argon and a single, homogeneous stock mixture of 40% C₂H₂, 60% O₂ prepared initially from tank supplies. The composition of one batch was checked by mass spectral analysis, and 0.03% N₂ was the only detected departure from the intended composition. Experiments were carried out at initial shock tube pressures, p₀, of 20, 50, and 120 Torr.

Shock wave speeds were monitored by raster oscilloscope recording of the progress of the shock front past five piezoelectric pressure transducers spaced at 30 cm or longer intervals along a 140 cm or longer segment of the tube beginning 200 cm or 350 cm from the diaphragm.

In other experiments, where the departure of the shock front from planarity was under examination, four of the piezoelectric gauges were arranged at 90° intervals around the tube perimeter in a plane perpendicular to the axis, and their responses were displayed on four synchronized oscilloscope traces.

The presence of OH radicals in the combustion zone was monitored in many of the experiments by oscilloscope recording of the absorption of a beam of ultraviolet

OH molecular line radiation⁹ which passed diametrically across the tube through quartz windows.

Mylar foils coated with wood smoke soot² were placed against the interior surface of the shock tube end flange in many of the experiments to record the presence of irregularities in the shock front reaching the tube end. Smoked foils lining the side walls along a 14 cm length of the test section were also used in some experiments. The loci at the tube wall of the abrupt intersections of segments of creased shock waves are recorded as inscriptions in the soot coating.

Finally, open shutter photography in a 60 cm long glass extension of the test section was used to record the luminous trajectory of the spinning reaction zone - shock front complex in shock waves exhibiting the single-headed spin phenomenon.

Results

The initial results which suggested that spin-like irregularities might be present in promptly reactive shock waves in the 97.5% Ar mixture consisted of the occurrence of quasi-periodic undulations in spectrophotometric records of OH radical concentration in the reaction zone, which persisted for several hundred microseconds after passage of the shock wave. These records did not identify the instability definitively, nor have they proven to be even reliable indicators of the presence of instability in all instances. Accordingly, the investigation of the instability phenomena turned to the inclusion of other diagnostic techniques with which we have experience from the study of gaseous detonations.^{2,6}

Positive confirmation of the occurrence of single-headed spin was made with a smoked foil along the inside wall of the tube. After passage of a spinning wave, the smoke layer bears a helical, ribbon-like inscription. The forward edge of the ribbon is the path of the backward pointing crease in the otherwise convex shock front. The trailing edge is the path of the rear terminus of the transverse detonation wave which propagates in the compressed, unreacted gas accumulated behind the weaker region of the primary shock front. This promptly reactive transverse compressional wave couples the revolving crease in the primary shock front to the predominantly circumferential acoustic oscillation of the pressure of the column of burned gas flowing behind the combustion wave system. The phase of the helix in the tube and also the pitch angle, θ , whose tangent is the ratio of the axial to the circumferential velocity component, is recorded by the side wall smoked foil. Good specimens of these single spin records were obtained at initial pressures of 20 and 50 Torr. These differ from the records of single spin in unsupported detonations, however, in that the fine structure found within the transverse wave band in the latter records^{2,6} is absent. Foils placed only on the end wall are more durable and are generally easier to work with. These record the location of radially or circumferentially propagating creases in the shock front anywhere in the tube cross section upon arrival of the wave at the end. Single spinning waves are recognized by the presence of a single, more or less radially oriented mark extending inward from the rim.²

Another prominent characteristic of single spinning waves is severe departure of the shock front from planarity.^{2,6,7} This leads to scatter in the apparent shock wave velocity deduced from the time intervals between arrival of the shock at gauges spaced arbitrarily along the tube. This scatter in apparent velocity was observed to be as great as $\pm 10\%$ over 30 cm intervals in waves where the end foils revealed the presence of single spin. That this scatter is in fact attributable to the revolving, nonplanar shock front which moves at much more nearly constant average axial velocity is confirmed by the differences in arrival times measured by the four pressure gauges placed in a ring around the tube. These differences were as great as 11 usec, corresponding to a 15 mm differential in axial position, in shock waves where the smoked foil confirmed the presence of single-headed spin.

Finally, the occurrence of single-headed spin is demonstrated very graphically in the open shutter photograph reproduced in Fig. 1.

Quantitative examination of the conditions under which spin and related instability phenomena occur is hampered by the uncertainty in the measurement of the axial velocity with the present interval method. Nevertheless, determination of the approximate ranges of conditions under which spin is observed has been pursued. The Chapman-Jouguet velocity of the 1% C_2H_2 , 1.5% O_2 , 97.5% Ar mixture initially at room temperature and ca. 0.1 atm pressure is about 0.9 km/sec, and the velocities of the shock waves studied were between 1.0 and 2.0 km/sec. At each of the three initial pressures studied, there is a range of shock velocities above 1.0 km/sec in which neither single-headed spin nor any other discernible perturbation at the shock wave front was observed. At $p_0 = 20$ and 50 Torr, the occurrence of chemical reaction behind the shock front was indicated at shock velocities above ca. 1.1 km/sec by the growth and subsequent leveling off of absorption of the ultraviolet line radiation of OH. But evidence of spin was not present in smoked foil or open shutter photographic records except at velocities above ca. 1.2 km/sec for $p_0 = 50$ Torr and above ca. 1.33 km/sec for $p_0 = 20$ Torr. At 120 Torr, single-headed spin occurred at velocities as low as ca. 1.10 km/sec, but not at still lower velocities. At these lower velocities, where for normal shock waves the temperature before reaction lies below about 1300°K, OH radical absorption did not provide a good means of detecting the occurrence of reaction, even though other work⁹ has shown that the induction zone, scaled for density of reactants, lies well within the time and space regimes of the present experiments. Evidently, little OH is formed unless the combustion takes place at higher temperatures than this.

When the shock velocity was raised above the threshold range for single spin, spin modes of higher multiplicity were obtained. For example, at $p_0 = 50$ Torr, single-headed spin was obtained fairly reproducibly near 1.3 km/sec, but shock fronts with 2, 3, or 4 visible creases extending to the perimeter of the end plate smoked foils were common near 1.4 km/sec. The ability of smoked and plate foils to record the impingement of highly segmented fronts in the interior of the shock tube, as has been done so successfully in unsupported detonations,^{2,10} was disappointing. At shock velocities above ca. 1.5 km/sec at $p_0 = 50$ Torr, only small, isolated segments of wave intersection tracks were recorded. Thus while the presence of persistent spin-like perturbations is indicated, it was not possible to observe any orderly structure or study variation of structure with shock velocity.

OH absorption oscillograms showed pronounced undulations not only in experiments where single spin was indicated, but also in experiments with coarse multi-headed spin. In still faster shock waves, though, the structure was evidently of sufficiently fine scale and/or low intensity that properties averaged over the tube diameter, as by a photon beam absorption experiment, may become usable for determination of combustion stoichiometry and the course of slow chemical changes that follow behind the induction zone.

Another regime of interesting phenomena was found in reactive shocks at velocities just below those at which single-headed spin was observed. OH absorption oscillograms were not reproducible, sometimes indicating abrupt formation of large quantities of OH and on other occasions, under closely similar conditions, showing scarcely detectable appearance of OH. Raster oscilloscope records of the shock wave progress down the tube showed scatter which was appreciable, with differences in apparent velocity as large as 3% between successive 30 cm intervals. Tests revealed corresponding departures of the shock fronts from planarity, which were only about one-third as large as those found when spin was identifiable. Smoked foil records showed no creases extending to the perimeter of the tube. Instead, end plate foils showed patches of indistinct disturbance in the interior of the tube.

On the basis of this somewhat incomplete characterization of these sub-spinning instabilities, it is hypothesized that they represent irregularities in the reaction zone which are not of sufficient, localized exothermicity to extend their influence in large amplitude form to the shock front or are not of proper wavelength to couple to acoustic oscillations of the burned gas. Attention is here drawn to interferograms of reactive shock waves in dilute exothermic systems,

including an $\text{NH}_3 - \text{O}_2$ system¹¹ and one of the $\text{H}_2 - \text{O}_2 - \text{Ar}$ mixtures¹² previously used for kinetics studies in our Laboratory⁵ in which at initial pressures between 100 and 200 Torr there had been pronounced undulations in OH absorption oscillograms. These interferograms showed that the shock front is quite flat, though slightly tilted in the tube, but the reaction zone is much more significantly disturbed. It also seems appropriate to report that attempts to record smoked foil inscriptions in the $\text{H}_2 - \text{O}_2 - \text{Ar}$ mixture under these same conditions gave negative results.

To relate the present work in acetylene - oxygen mixtures to other work in the same system, we note that most of the kinetics studies,¹³ some of which have used more concentrated mixtures than the present one, have been done in an initial pressure regime an order of magnitude lower. In addition, many of the studies have been done using reflected shock waves and in ways which are not so subject to interference by transverse waves either at the shock front or in the reaction zone.

The occurrence of spin in an environment divorced from marginally propagating detonation would appear to offer a heretofore unrealized opportunity to study the limiting conditions for the occurrence of spin with additional variables at one's command in the hope of elucidating detonation limit phenomena. The lack of sharpness of the limits observed in the present system detracts somewhat from the attractiveness of this approach, but further work may be appropriate.

A brief attempt is made here to relate some parameters of the single spinning waves observed in these driven shock waves to known properties of the chemical mixture. From the admittedly approximate values of the threshold velocities for spin, $B_{\text{threshold}}$, at the three experimental initial pressures, the induction times t_i and axial induction zone lengths x_i for the temperature and density behind the axially normal portions of the convex spinning shock fronts have been evaluated from independent induction period data.⁹ These values are recorded in Table I, where it can be seen that the induction zone lengths for these spinning waves are not constant, but become smaller at lower density, and are all smaller than the 100 mm tube diameter.

The mean pitch angle, θ , from smoked side foils and the mean axial velocity, B , were obtained from separate experiments, done for $p_0 = 20$ and 50 Torr, each at constant tube loading conditions. These data were combined to determine the circumferential velocity component of the single spin under these two conditions. In Table II these are recorded and compared with the perimetral velocity for pure fundamental circumferential oscillation in the reacted gas estimated for a plane shock wave at the axial velocity B with reaction to chemical equilibrium (1.84 times the sound velocity, c).¹⁴ Also tabulated are the Chapman-Jouquet detonation velocities D'_{CJ} for the unsupported detonation of the hot, compressed, unreacted gas behind the primary shock front having velocity D . The circumferential velocity of the transverse spin wave at the tube perimeter is seen to lie between these two characteristic velocities of the system, which are sufficiently different from each other under the present experimental circumstances that the spinning wave cannot be in close resonance with both, as it has been found to be in certain unsupported spinning detonations.^{14,15}

In simplest terms, the experiments described here show that the occurrence of single-headed spin, which may be universally associated with unsupported detonations at the limits of their ability to propagate, is not exclusively a property of unsupported waves or of Chapman-Jouquet flow.

The initial experiments in which the occurrence of spin in this acetylene - oxygen - argon mixture was first identified were carried out in July 1963 by E. P. Eastman and P. F. Bird, and in collaboration with Prof. R. A. Strehlow. J. L. Young and J. G. Williamson carried out most of the subsequent experimental work.

Table I. Normal Shock Induction Zones at Spin Threshold for 1% C₂H₂, 1.5% O₂, 97.5% Ar in 10 cm diameter tube.

P ₀ Torr	D _{threshold} km/sec	T °K	t _i usec	x _i mm
20	1.33	1820	52	20
50	1.20	1518	83	29
120	1.10	1317	122	41

Table II. Circumferential Velocity Considerations for Single-Headed Spins in Driven Shock Waves.

P ₀ Torr	D km/sec	θ	1.84 c km/sec	D cotθ km/sec	D' _{CJ} km/sec
20	1.38	46°	1.59	1.33	1.25
50	1.31	43°	1.53	1.40	1.24

References

1. D. R. White, *Phys. Fluids* 4, 465 (1961).
2. R. E. Duff, *Phys. Fluids* 4, 1427 (1961).
3. D. Britton and R. M. Cole, *J. Phys. Chem.* 65, 1302 (1961); also D. Britton and N. Davidson, *J. Chem. Phys.* 23, 2461 (1955).
4. W. M. Jones and N. Davidson, *J. Am. Chem. Soc.* 84, 2868 (1962).
5. G. L. Schott and P. F. Bird, *J. Chem. Phys.* 41, 2869 (1964).
6. G. L. Schott, *Phys. Fluids* 8, 850 (1965).
7. B. V. Voitsekhovskii, V. V. Mitrofanov, and M. E. Topchian, "The Structure of a Detonation Front in Gases," USSR Academy of Sciences, Siberian Division, Novosibirsk, 1963; (English transl. FTD-MT-64-527, AD 633821, issued by U.S. Air Force, Wright-Patterson AFB, Ohio, 1966.)
8. S. H. Bauer, G. L. Schott, and R. E. Duff, *J. Chem. Phys.* 28, 1089 (1958).
9. R. I. Soloukhin, *Combust. Flame* 9, 51 (1965).
10. R. A. Strehlow, R. Liaugminas, R. Watson, and J. R. Eyman, *Symp. Combust.* 11th, Univ. Calif., Berkeley, Calif., 1966 (1967).
11. R. I. Soloukhin, "Some Shock Tube Methods in Chemical Physics," USSR Academy of Sciences, Siberian Division, Novosibirsk, 1966, Fig. 19, page 38. (Text in Russian and English.)
12. D. R. White, General Electric Research Laboratory, Private Communication, July, 1964.
13. W. C. Gardiner, Jr., W. G. Mallard, K. Morinaga, D. L. Ripley, and B. F. Walker, *Symp. Combust.* 11th, Univ. Calif., Berkeley, Calif., 1966 (1967); and refs. cited therein.
14. J. A. Fay, *J. Chem. Phys.* 20, 942 (1952).
15. B. V. Voitsekhovskii, *Dokl. Akad. Nauk SSSR* 114, 717 (1957). (English transl. *Proc. Acad. Sci. USSR, Appl. Phys. Sect.* 114, 193 (1957).)

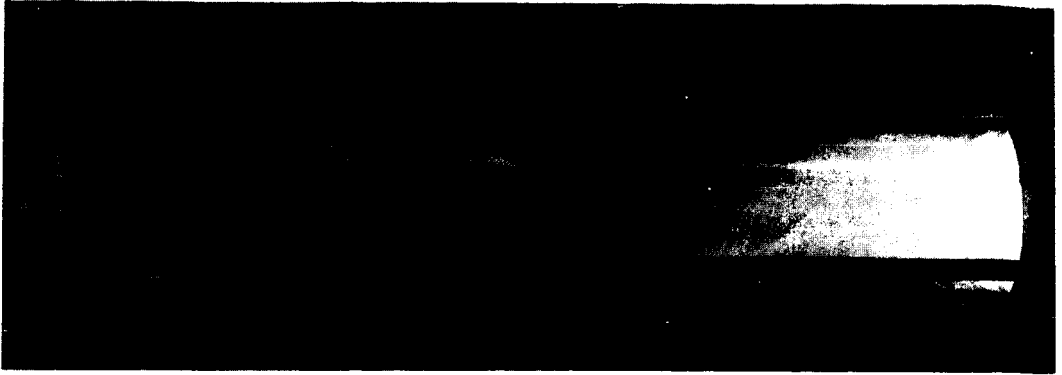


Figure 1.

Still photograph of luminosity of driven shock,
 $D = 1.3 \text{ mm}/\mu\text{sec}$, in 1.0% C_2H_2 , 1.5% O_2 , 97.5% Ar
at 50 torr. in 10 cm diameter glass tube.
Shock motion left to right.

Transition from Branching Chain Kinetics to Partial Equilibrium in the Shock-Induced Combustion of Lean Hydrogen-Oxygen Mixtures

W. C. Gardiner, Jr., K. Morinaga, D. L. Ripley
and T. Takeyama

Department of Chemistry, The University of Texas, Austin, Texas

The chemical kinetics of the high-temperature reaction between hydrogen and oxygen has been the subject of numerous experimental studies. For the case of combustion in shock waves through hydrogen-oxygen mixtures highly diluted with argon, the kinetics may be divided into three regimes: in the initiation regime, small concentrations of atoms and/or radicals are generated by slow, unknown reactions; in the induction regime, bimolecular branching chain reactions lead to exponential increase in the concentrations of H, O and OH; in the recombination regime, termolecular reactions cause evaluation of heat and establishment of chemical equilibrium. The induction regime kinetics are thought to be explicable in terms of the mechanism



When the OH radical concentration is high, the fast reaction



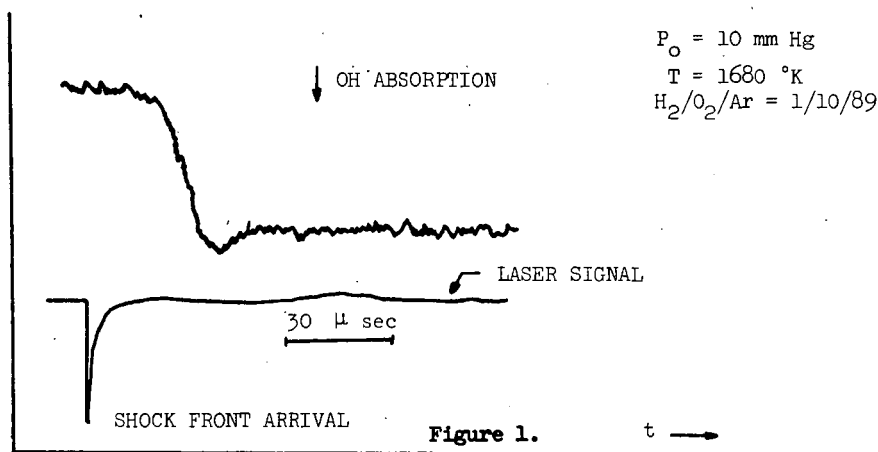
also contributes to interconversion of species. Neglecting the step



which is important for $p > 1$ atm, $T < 1200^\circ\text{K}$, defines the limits of validity of this mechanism. Rate constant expressions for all of these steps, based on a variety of experiments, have been proposed¹. The agreement among the various investigators is good.

The separation between induction and recombination regimes lies essentially in the fact that the termolecular reactions of the latter are far slower than the bimolecular reactions of the former. Steps (1-4) have, as a consequence, almost equal forward and reverse rates during the recombination regime, leading to a condition of partial equilibrium². It was shown recently by Hamilton and Schott³ that in mixtures with $[\text{H}_2]/[\text{O}_2] \equiv R$ either $\gg 1$ or $\ll 1$ the transition between induction regime kinetics, governed by the rates of (1-3) and the partial equilibrium condition, governed by the equilibrium constants of (1-3) could involve transient effects capable of yielding worthwhile information on the rate constants of (1-4). They investigated the situation with $R \gg 1$. They predicted large O-atom spikes, and from the experimental absence of OH spikes, they were able to deduce an upper limit for k_1/k_2 . We have investigated the situation for $R \ll 1$. The OH spikes absent in $R \gg 1$ mixtures are found to be quite pronounced for $R < 1$. Quantitative investigation of incident shocks in $\text{H}_2/\text{O}_2/\text{Ar} = 1/10/89$ mixtures, $p_0 = 10$ torr, $1400 < T < 2500^\circ\text{K}$ is reported here. The experimental technique combined OH concentration measurement by the Bi(3067) method⁴ with conventional shock tube methods.

The OH absorption signal for a run at 1680°K is shown in Fig. 1.



In order to convert the data to graphical form, some approximations are needed. First, the extinction coefficient for the Bi(3067) method fluctuates considerably from run to run. For these experiments each run was used as its own calibration point, and Beer's Law was taken to calculate the ratio $[\text{OH}](\text{spike})/[\text{OH}](\text{partial equilibrium})$, with the level portion of the trace assigned to the partial equilibrium condition, for which $[\text{OH}]$ can be readily computed from the shock speed. To assign error limits to this ratio, the appropriate extreme points were read from the records and likewise substituted into Beer's Law to get the upper and lower limits for the $[\text{OH}](\text{spike})/[\text{OH}](\text{partial equilibrium})$ ratio. Since the full width of the spikes is difficult to determine both on the experimental records and on the computed profiles, we use the apparent full width at half height for the quantitative shape parameter. By apparent half width is meant the width which would be obtained on the accurate computer plotout of the profile by extrapolating the slightly sloped post-spike $[\text{OH}]$ (a small amount of recombination does occur on the time scale of these experiments via Reaction (5)) back to the center of the spike, and then measuring the full width of the spike half way between the back extrapolation and the top. On the records themselves, this means reapplication of Beer's Law to get the correct half height. The results are presented in Figs. 2 and 3.

The first approach to interpret these data is to search for a set of rate constants for the mechanism (1-4) which will predict the correct spike heights and spike durations. This is greatly assisted by the availability of much good data, and a suggestion by Schott that lean mixture maxima would be favored by large values of the ratio k_2/k_3 . We started with the rate constant expression for k_1 given by Baldwin and Melvin^{1b}, the k_2 expression given by Clyne and Thrush^{1c}, and the k_3 and k_4 expressions given by Kaufman and DelGreco^{1a}. A recent experiment by Gutman and Schott^{1f} provides a new value for k_1 which can also be used as input. For the critical k_2 , there are three studies which supercede the consensus of Clyne and Thrush, all giving higher values of k_2 ; these were done by Wong and Potter^{1g}, Westenberg and de Haas^{1e}, and Gutman and Schott^{1f} again. A higher value of k_4 has been reported by Dixon-Lewis, Wilson and Westenberg^{1h}. The hint regarding the k_2/k_3 ratio may be understood in the following way. In order to produce a spike in the OH profile, the induction period reactions must behave in such a way that OH production temporarily exceeds OH destruction as the H_2 concentration suddenly drops from its induction period value to its partial equilibrium value. Reaction (4) unambiguously destroys OH rapidly at this time; Reaction (1) provides reactants for both (2) and (3) at equal rates; this leaves (2) and (3) as the primary generators of the OH profile. Both of them have the same dependence on H_2 , so both will have rates which drop suddenly as the last H_2 is consumed. Overproduction of OH by (2) can then lead to more OH than can be consumed by (3) when H_2 comes into

short supply, and an overshoot occurs. This analysis is rather oversimplified, as our subsequent analysis will show; however, the direction of seeking high values of k_2 is clear. Whether or not it will be fruitful to seek low values of k_3 will depend on the value of k_4 .

First consider the peak heights and half widths which are predicted by numerical integration using the k_1 and k_2 values of Gutman and Schott. (Figs. 2 and 3.) The half widths are approximately correct, but the heights are far lower than the data indicate. Immediately we can conclude that it is unnecessary to investigate further with the k_2 value of Clyne and Thrush, for it is lower than Gutman and Schott's at 1500°K by factor 2. Next, increase the value of k_2 and see what happens. Just as expected, the heights increase; the half widths decrease. By trial and error, a k_2 value 5 times that of Clyne and Thrush, or 2-1/2 times that of Gutman and Schott, is found to give the right height and half width at 1500°K. In subsequent calculation it is found that the right temperature dependence is found also, although the high temperature values are perhaps somewhat high. The influence of k_1 in place of the Gutman and Schott value. It is seen that the difference is minor. Varying k_2 has little effect. When the rates of the reactions are checked, it is found that the lack of effect of k_2 is simply due to the fact that OH is mostly consumed by (4) rather than (3) at the spike time. Therefore, in order to try to reproduce the spike by lowering the OH consumption rate at the time of the spike, k_4 must be reduced. It is indeed possible to increase the heights somewhat by this procedure; however, the predicted half widths are seen to become far too large, and we conclude that it is useless to try to predict the spikes by lowering the OH destruction rate from that predicted by the consensus rate constants.

To summarize this approach to predicting the spikes by numerical integration of the conventional mechanism, we find that reasonably satisfactory agreement is obtained if k_2 is taken as about 2-3 times the value predicted by the expressions of Gutman and Schott, Wong and Potter, or Westenberg and de Haas. Furthermore, this is the only way to predict spikes with this mechanism. The shortcomings of this approach are the disagreement with other values for k_2 and the impossibility of reconciling high values for k_2 with the observed dependence of ignition delays upon R_4 .

There are several other ways in which OH-spikes might be produced. The possibility that the observed oscilloscope traces are due to an inadequacy in the Bi(3067) method arising from its sensitivity to OH($v=0$) may be rejected as a quantitative explanation by noting that at 1500°K only 7% of the OH molecules are in excited vibrational states. The maximum thermal effects of vibrational relaxation are only 3-4% for these mixtures. Trace amounts of impurities could only affect the results by bimolecular catalysis of the recombination reactions or by intervention in the already fast branching mechanism. We see no way to accomplish either of these, although they cannot be rejected on our evidence. Finally, it must be allowed that some combination of causes could be the source of the observed spikes.

We conclude that the observed OH profiles in shock-induced combustion of lean H_2-O_2 -Ar mixtures can be explained on the basis of the conventional mechanism if the rate for $O + H_2 = OH + H$ is assumed to be about twice the current best value from other experiments. Since such an assumption leads to substantial discrepancies in the interpretation of other experiments, we consider this explanation to be suggestive only, and subject to refinement as further experimentation is done on the high-temperature chemistry of the H_2-O_2 reaction.

Acknowledgement

We are indebted to B. F. Walker and C. B. Wakefield for assistance with the computational aspects of this research. Our work was supported by the U. S. Army Research Office - Durham, The Robert A. Welch Foundation and The University of Texas Research Institute.

References

1. (a) F. Kaufman and F. P. DelGreco, Symp. Combust. 9th, Cornell University, Ithaca, New York, 1962, 659 (1963); (b) R. R. Baldwin and A. Melvin, J. Chem. Soc. 1964, 1785; (c) M. A. A. Clyne and B. A. Thrush, Nature 189, 135, 1961; (d) R. W. Getzinger and G. L. Schott, J. Chem. Phys. 43, 3237 (1965); (e) A. A. Westenberg and N. de Haas, J. Chem. Phys. 46, 490 (1967); (f) D. Gutman and G. L. Schott, J. Chem. Phys., to be published, 1967; (g) D. L. Ripley and W. C. Gardiner, Jr., J. Chem. Phys. 44, 2285 (1966); (h) G. Dixon-Lewis, W. E. Wilson and A. A. Westenberg, J. Chem. Phys. 44, 2877 (1966); (i) W. S. Watt and A. L. Myerson, 6th International Shock Tube Symposium, Freiburg, 1967; (j) E. L. Wong and A. E. Potter, J. Chem. Phys. 43, 3371 (1965).
2. G. L. Schott, J. Chem. Phys. 32, 710 (1960).
3. C. W. Hamilton and G. L. Schott, Symp. Combust. 11th, University of California, Berkeley, 1966.
4. D. L. Ripley, dissertation, The University of Texas, January 1967.

Note for Figs. 2 and 3. The solid error bars denote runs made using the Bi(3067) method; the dashed error bars denote runs made using the water lamp method.

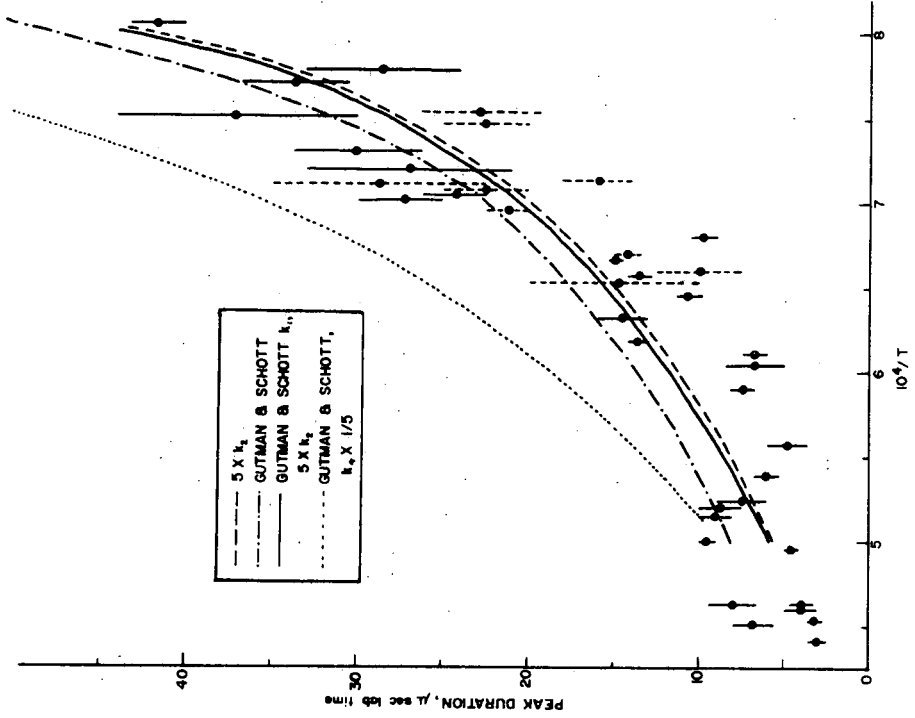


Figure 3.

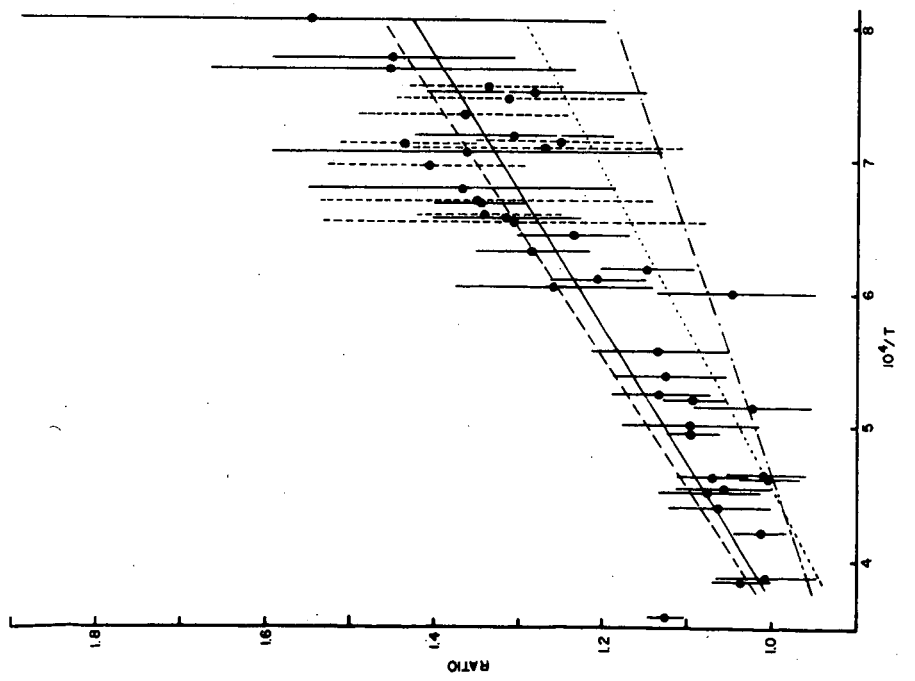


Figure 2.

INITIATION OF DETONATION BY INCIDENT SHOCK WAVES
IN HYDROGEN-OXYGEN-ARGON MIXTURES

G.B. Skinner
Wright State Campus, Dayton, Ohio

G. Mueller, U. Grimm and K. Scheller
Aerospace Research Laboratories, Wright-Patterson Air Force
Base, Ohio

INTRODUCTION

The steps involved in the initiation of detonation by incident shock waves have been outlined by Strehlow and Cohen (1). In their words, "An exothermic reaction occurring in a small region of a flowing gas causes an increase in the local pressure Since this region is subsonic the pressure increase will propagate to the front and increase the velocity of the front, thereby increasing the temperature of the next element of gas heated by shock compression. This process is self-accelerating and in general a steady-state wave will not be obtained until the wave is traveling at or above the Chapman-Jouguet velocity for the mixture."

For dilute hydrogen-oxygen-argon mixtures, ignition induction times ranging from microseconds to milliseconds can be obtained over a range of temperatures (2,3). In a shock tube equipped with several velocity-measuring stations, we have shock-heated such mixtures to temperatures at which induction times are a few milliseconds long, and observed in considerable detail the process by which the reaction wave, initiated several meters behind the shock wave, overtakes and couples with the shock wave.

Earlier measurements (4,5,6) have indicated the increase in shock velocity due to coupling of the reaction to the shock wave, but have not shown many of the details of the process. Strehlow and co-workers (1,7,8) have made extensive studies of initiation of exothermic reactions behind reflected shock waves. Oppenheim, Laderman, and Urtiew (9,10) have reported extensive studies on the initiation of detonations in gaseous mixtures where the ignition source was a spark, a flame, or a hot wire.

EXPERIMENTAL

A square shock tube 7.62 cm. on a side was used. This had a driver gas section 1.83 meters long and a sample gas section 6.10 meters long. Diaphragms were of 1.22 mm. thick aluminum, scribed diagonally so that, when they burst, four triangular sections would fold back, one along each side of the tube. Air was used as driver gas.

When a run was made, the air was added to the driver section at the desired pressure (below the bursting pressure of the diaphragm), then the diaphragm was ruptured by a plunger. This permitted close control (about 0.5%) over the driver gas pressure.

The sample gas section was instrumented with thin-film platinum heat transfer gauges for velocity and heat transfer measurements, and with SLM Model 603 piezoelectric gauges (Kistler Instrument Corporation, Clarence, New York) for pressure measurements. The positions of these gauges with respect to the diaphragm are listed in Table I.

Table I

Positions of Gauges with Respect to Shock-Tube Diaphragm

<u>Gauge</u>	<u>Distance Downstream from Diaphragm, Meters</u>
Heat transfer No. 1	3.2004
Heat transfer No. 2	3.8100
Heat transfer No. 3	4.4196
Heat transfer No. 4	4.6482
SLM No. 1	4.6991
Heat transfer No. 13	4.6991
Heat transfer No. 5	4.8006
Heat transfer No. 6	4.9022
SLM No. 2	4.9530
Heat transfer No. 7	5.0038
Heat transfer No. 8	5.1054
Heat transfer No. 9	5.2070
Heat transfer No. 10	5.3086
Heat transfer No. 11	5.3594
Heat transfer No. 12	5.9690

Heat transfer gauges 1, 2, and 3, and SIM gauge 1 were mounted on the side of the tube; the others were on the top. Heat transfer gauge 13 was used to measure the rate of heat transfer from the gas to the wall. The time base for all velocity measurements was a Tektronix Model 180A time-mark generator. Outputs from the piezoelectric gauges were fed into charge amplifiers, then recorded using a

Tektronix Model 555 oscilloscope. The piezoelectric gauges were calibrated statically against a precision laboratory pressure gauge.

RESULTS

In the temperature range under study, the induction time for ignition of a hydrogen-oxygen-argon mixture varies rapidly with temperature. Accordingly, a good many experiments were necessary to determine the conditions needed to bring about coupling of the reaction and shock waves in the right part of the tube. This point is illustrated by the data of Figure 1, which apply to a gas mixture containing approximately 4% H₂ and 2% O₂ by volume in argon.

With sample pressures above about 0.086 atm., the variation of shock speed with sample pressure is as one would expect when no chemical reaction is occurring. In the sample pressure range of 0.082 to 0.086 atm., the shock speed reaches a high value as the reaction wave catches up to the incident wave. For lower sample pressures, the reaction has coupled to the shock wave before the wave reached the measuring station. The effects of small differences in initial pressure, and of other minor variables such as the speed of diaphragm rupture, are shown by the three different shock speeds measured for presumably identical runs at 0.084 atm. Complete data for these three runs show that in one case the peak shock speed occurred before heat transfer gauge 8, in one case between gauges 8 and 9, and in the other case after gauge 9.

A complete set of data for the run that gave the highest velocity in Figure 1 is shown in Figures 2 and 3. The data of Figure 3 have been redrawn from the original oscilloscope records in order to have the same time scale for all the records, and the same pressure scale for the pressure records.

Similar sets of data were obtained for gas mixtures containing approximately 6% H₂ and 3% O₂, and 8% H₂, and 4% O₂. For these mixtures, of course, the energy release by chemical reaction was greater than for the first mixture studied, and the pressure and velocity effects correspondingly more pronounced. Data for a run with the more concentrated mixture are shown in Figures 4 and 5.

DISCUSSION

The data presented in Figures 2 to 5 can best be related by drawing wave diagrams for each experiment. Sufficient data are available to draw reasonably complete wave diagrams, which are given in Figures 6 and 7.

The procedure for drawing Figure 6 was as follows: From Figures 1 and 2 it can be seen that the first velocity measurement of Figure 2 corresponds to a shock wave unaffected by chemical reaction.

Therefore, the shock velocity from the diaphragm to heat transfer gauge 2 will be constant (neglecting diaphragm opening effects and attenuation) at a velocity of approximately 870 meters/sec. (The shock speed that is calculated from the pressures of sample and driver gas, by means of Markstein's graphical method (11), is 880 meters/sec., in close agreement.) If the diaphragm opening time is taken as 0, the incident shock wave will reach heat transfer gauge 2 in 4.38 milliseconds (point A of Figure 6). From this point on, the times to reach various points on the tube are given directly by the data.

It is evident from the slow rise in shock speed between 3.5 and 4.9 meters (Figure 2) that the chemical reaction first produces a gentle pressure wave that travels through the shock-heated gas with velocity $u + a$, where u is the flow velocity behind the shock wave (551 meters/sec) and a is the speed of sound in the heated gas (557 meters/sec). Accordingly, a characteristic line with $u + a$, of 1108 meters/sec. can be drawn back from Point A, to represent the path of this first pressure wave that communicates energy from the reaction to the shock wave.

The origin of this wave is undoubtedly near the driver-sample interface, at which is located the part of the gas sample that was heated first (point B of Figure 6). It is apparent that the ignition induction time was about 2 milliseconds, or a little less if it is considered that some of the sample next to the diaphragm will be cooled by driver gas and not react. The calculated temperature behind the incident shock wave is 880°K., and the pressure 0.68 atm.

From Point B the reaction front first appears as a line parallel to the incident shock wave. That is, once the gas has been heated for 2 milliseconds, it starts to react. However, as pressure waves from the reaction increase the incident shock speed, they also increase u and a behind the shock wave. This means, first, that the ignition induction times of successive elements of the gas become shorter, so that the velocity of the reaction wave exceeds that of the shock wave, and second, that pressure waves can catch up with waves sent out previously, thereby generating a shock wave. The formation of this second shock wave is shown in Figure 3. It was just beginning to form as it passed SLM gauge 1, and was better formed as it passed SLM gauge 2. The average velocity in the interval, 1340 meters/sec., is just a little greater than $u + a$, as one would expect for a weak shock wave. Once the two waves coalesce, the temperature behind the wave is close to 2000°K., at which temperature the induction time is about 20 microseconds (2,3). By this time, then, the reaction wave is close behind the shock wave, as shown in Figure 6.

The wave diagram for the more concentrated gas mixture, Figure 7, is similar in many ways to Figure 6. One notable difference is that the first evidence of chemical reaction to reach the incident shock wave was a well-developed second shock wave, of velocity

2080 meters/sec., which had overtaken and assimilated weak pressure waves sent out earlier when reaction started. The fact that the shock wave had the same shape at the two pressure measuring stations suggests that this is a detonation wave in the gas which had been preheated to 830°K., compressed to 0.79 atm., and accelerated to 555 meters/sec. by the incident shock wave. A calculation of the detonation properties made by standard methods (12) gave the following data, which are compared to the experimental measurements.

<u>Property</u>	<u>Observed</u>	<u>Calculated</u>
Detonation velocity relative to unreacted gas	1,525 meters/sec.	1,465 meters/sec.
Detonation pressure	4.6 atmospheres	5.7 atmospheres
Temperature after reaction	-	2,700°K

The agreement, while not highly accurate, is sufficiently close to confirm the identity of the wave.

The data for this run do not indicate where the detonation wave started, nor where it caught up with the first pressure wave from the reaction zone. Two extreme cases can be considered.

1. The detonation wave formed as soon as reaction started, so a line drawn back from the intersection of the detonation wave with the incident shock wave (Point C of Figure 7) with a slope corresponding to 2080 meters/sec intersects the driver-sample interface at the point of initial reaction, at a time of 4.9 milliseconds.
2. The detonation wave overtook the first pressure wave from the reaction just before the latter reached SIM gauge 1, so that a characteristic drawn back from the detonation wave at this point, with a slope corresponding to a $u + a$ of 1110 meters/sec., intersects the driver-sample interface at the point of initial reaction, at a time of 3.2 milliseconds. The wave diagram has actually been drawn half-way between these two extremes, on the assumption that the induction time was 4.0 milliseconds.

The fact that the speed of the incident shock wave goes through a maximum value as the reaction wave couples to it, than later decreases somewhat, is to be expected from the mechanism of the process. Since no reaction occurs during the first few milliseconds, the rate of energy release by chemical reaction reaches a transient maximum value significantly above the normal rate as the reaction wave catches up with the shock wave.

More quantitatively, the velocity of a shock wave with heat release can be calculated, and the calculation gives a value lower than the maximum velocity of Figure 2. We have used Markstein's graphical method (11) in these calculations also. With reference to the experimental conditions of Figure 2, if the induction time was zero an ordinary-looking shock wave would be obtained, with a velocity of 1110 meters/sec., a pressure of 0.75 atm., and a temperature of 1460°K (compared to calculate values of 880 meters/sec., 0.71 atm and 890°K when no reaction occurs). The shock velocity of 1110 meters/sec. would be reached eventually in our experiment with an induction time, if the tube were long enough and attenuation could be neglected. Once this steady situation was reached the pressure would be uniform from the shock front to the driver gas expansion region.

When the same type of calculation is made for the gas mixture containing more hydrogen and oxygen, corresponding to Figures 4 and 5, it is found that the air driver is not capable of maintaining sufficient flow velocity to keep the pressure constant behind the incident shock wave when reaction occurs. The final steady state wave would, therefore, have an appearance between a shock and an ordinary detonation wave, with some drop in pressure, temperature and flow velocity behind the shock front.

ACKNOWLEDGEMENT

One of the authors (G.B.S.) wishes to acknowledge that several preliminary experiments were carried out at Monsanto Research Corporation, Dayton, Ohio, while he was employed there. Mr. Donald L. Zanders assisted materially in these preliminary experiments. He also wishes to acknowledge financial assistance from the Aerospace Research Laboratories under Contract AF33(615)-1915 with The Ohio State University Foundation.

REFERENCES

1. R.A. Strehlow and A. Cohen Phys. Fluids 5, 97 (1962).
2. G.L. Schott and J.L. Kinsey. J.Chem. Phys. 29, 1177 (1958).
3. G.B. Skinner and G.H. Ringrose. J.Chem. Phys. 42, 2190 (1965).
4. J.A. Fay, Fourth Symposium (International) on Combustion, 1952, p. 501.
5. M. Steinberg and W.E. Kaskan. Fifth Symposium (International) on Combustion, 1954, p. 664.
6. F.E. Belles and J.G. Ehlers. Am. Rocket Soc. J. 32, 215 (1962).
7. R.A. Strehlow and H.B. Dyner, AIAA Journal 1, 591 (1963).
8. R.B. Gilbert and R.A. Strehlow, AIAA Journal 4, 1777 (1966).
9. A.J. Laderman and A.K. Oppenheim, Proc. Roy. Soc. A268, 153(1962).
10. P.A. Urtiew and A.K. Oppenheim, Proc. Roy. Soc. A295, 13(1966).
11. G.H. Markstein. Am. Rocket Soc. J. 29, 588 (1959).
12. B. Lewis and G. von Elbe. Combustion, Flames, and Explosions of Gases, Second Edition, New York, Academic Press, Inc., 1961, p. 524.

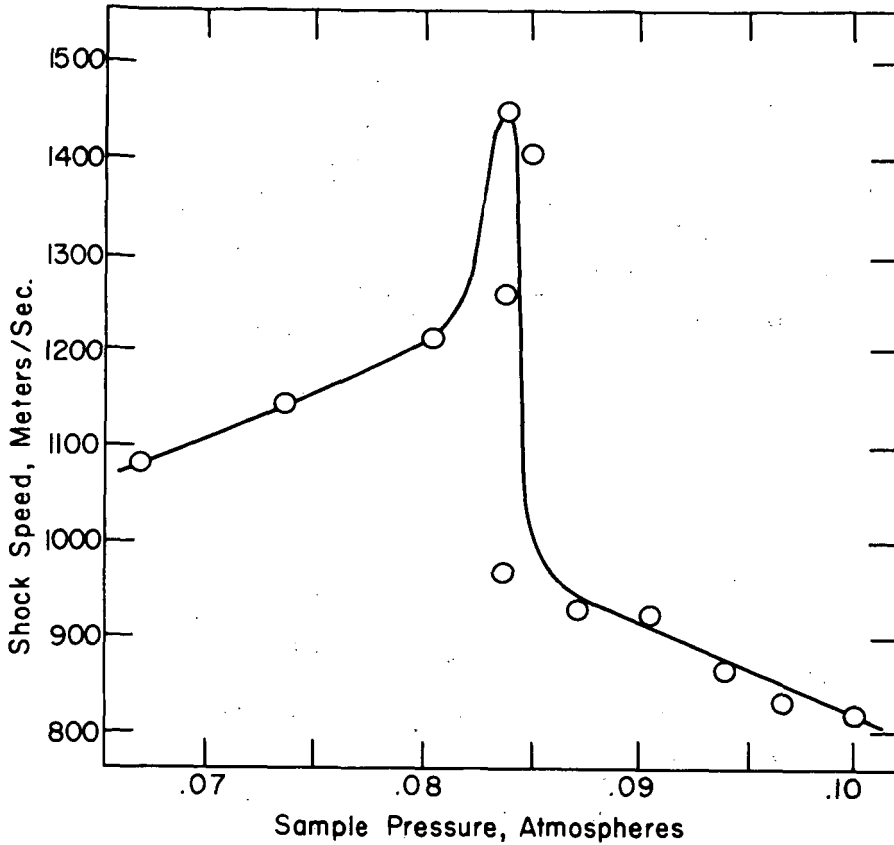


Figure 1. Incident shock speeds measured between heat transfer gauges 8 and 9 for a gas mixture containing 4.33% H_2 and 1.88% O_2 by volume in argon. Driver gas 17.0 atm. of air.

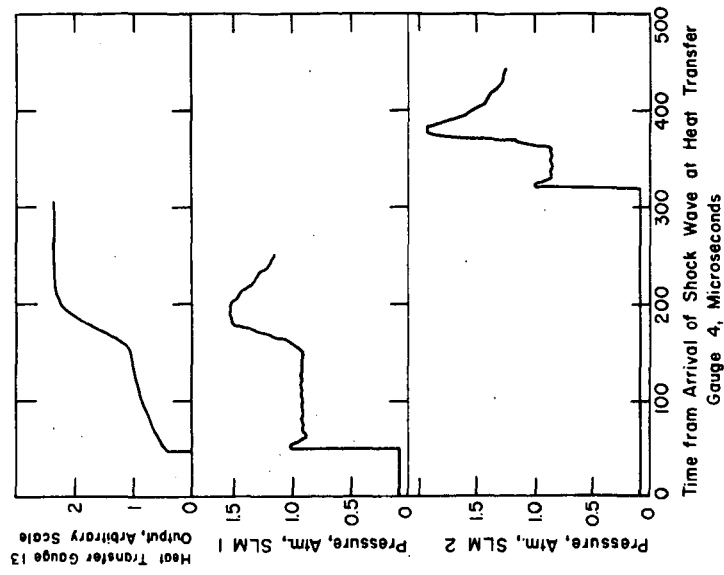


Figure 3. Pressure and heat transfer records for the same experiment as Figure 2 (sample pressure 0.084 atm.).

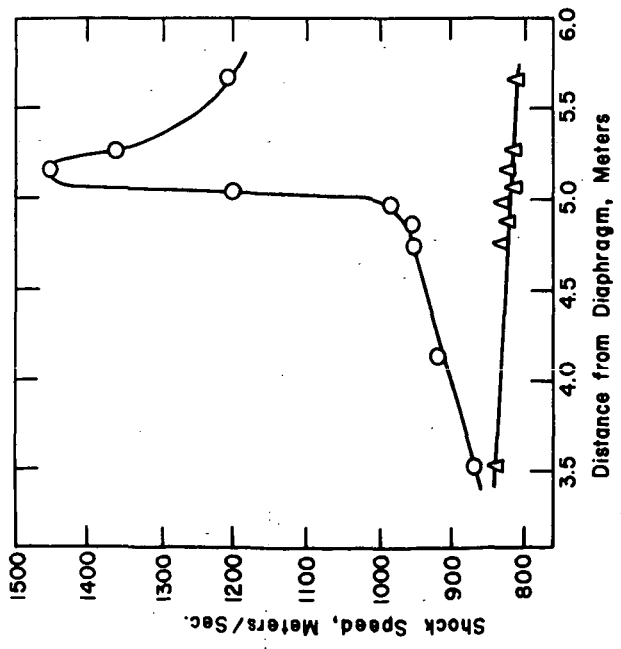


Figure 2. Incident shock speeds measured at different positions along the tube for a gas mixture containing 4.33% H₂ and 1.88% O₂ by volume in argon. Driver gas 17.0 atm. of air. O Sample pressure 0.084 atm.; Δ Sample pressure 0.100 atm., for comparison

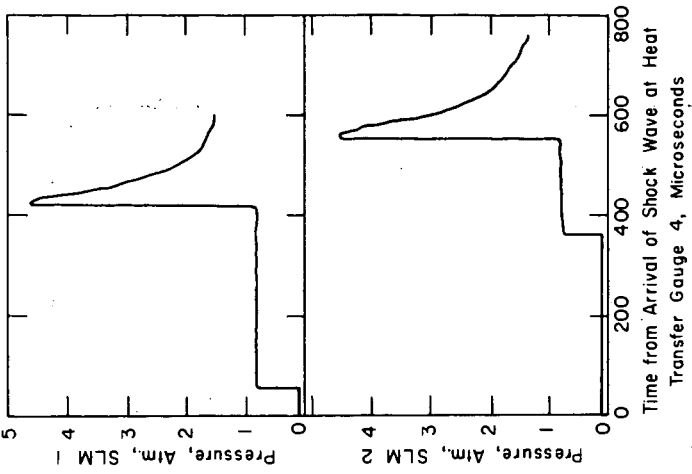


Figure 5. Pressure gauge records for the same experiment as Figure 4.

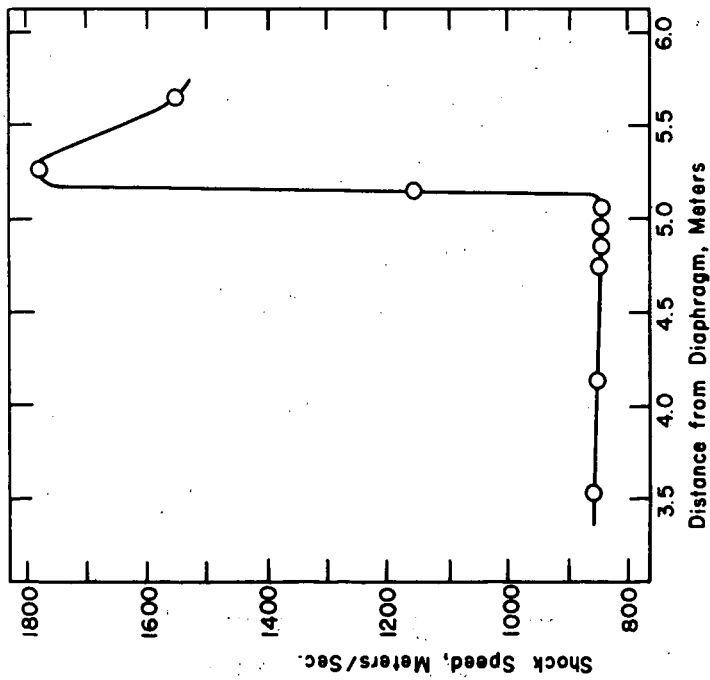


Figure 4. Incident shock speeds measured at different positions along the tube for a gas mixture containing 7.82% H₂ and 4.46% O₂ by volume in argon. Sample pressure 0.100 atm., driver gas 17.0 atm. of air.

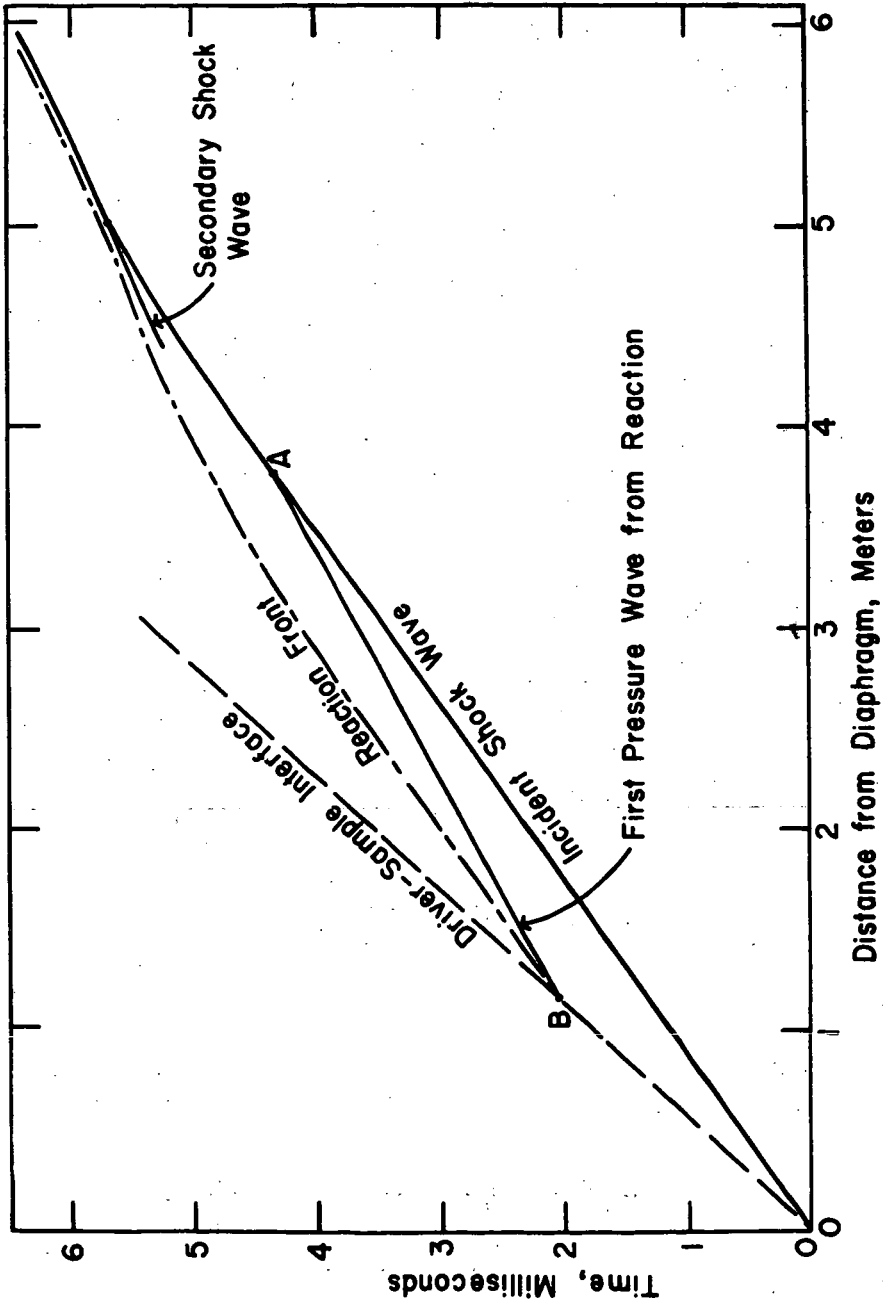


Figure 6. Wave diagram drawn from data of Figures 2 and 3.

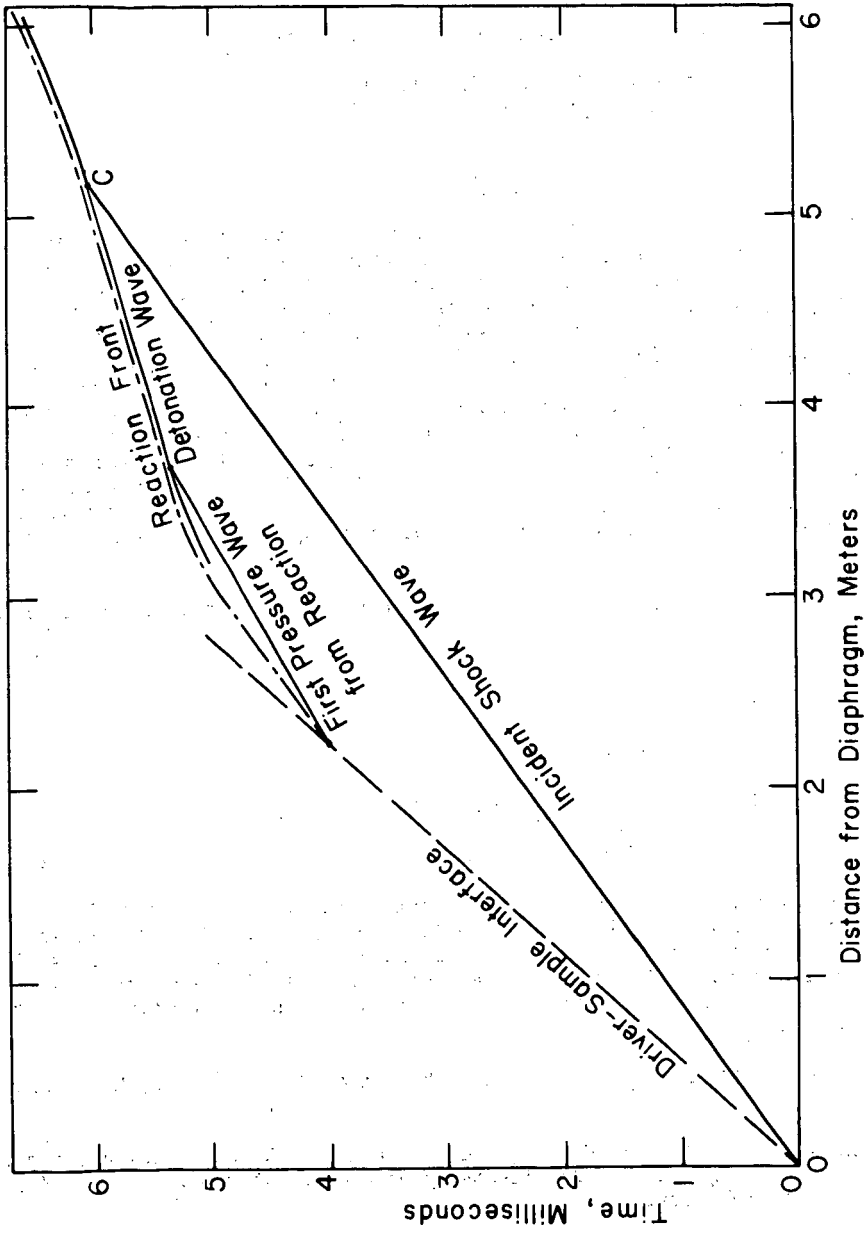


Figure 7. Wave diagram drawn from data of Figures 4 and 5.

SHOCK TUBE STUDY OF THE $\text{H} + \text{O}_2 + \text{Ar} \rightarrow \text{HO}_2 + \text{Ar}$
 REACTION USING A NEW END-ON TECHNIQUE

David Gutman and Edward A. Hardwidge

Department of Chemistry, Illinois Institute
 of Technology, Chicago, Illinois 60616

INTRODUCTION

The reaction $\text{H} + \text{O}_2 + \text{M} \rightarrow \text{HO}_2 + \text{M}$ is an important radical recombination step in many gaseous oxidation reactions and plays a particularly vital role as a chain-terminating process at the second limit of the $\text{H}_2\text{-O}_2$ reaction. In this study we have determined the rate constant of this reaction for $\text{M}=\text{Ar}$ (k_4^{Ar}) in the temperature range 1125-1370°K. The purpose of this study was twofold: first, to obtain accurate values of this constant for use in the analysis of future shock tube studies of combustion reactions (which are most often studied in a high argon dilution) and, second, to assess the potential of the "end-on" shock tube technique for studying recombination reactions. Our experiments consisted of shock-heating $\text{H}_2\text{-O}_2\text{-CO-Ar}$ mixtures and subsequently monitoring the exponential growth of the O-atom concentration during the induction period of this reaction. Values for k_4^{Ar} were obtained from the chain-branching equation using the measured exponential growth constants and known rate constants.

The significant reactions during the induction period of the $\text{H}_2\text{-O}_2$ reaction are:¹



When mixtures of H_2 and O_2 are suddenly heated, a short induction period is observed during which there is a negligible depletion of reactants and an exponential rise in the concentration of the chain carriers [e.g. $[\text{O}] = [\text{O}]_0 e^{at}$] at essentially constant temperature and pressure. Kondratiev¹ and others have shown that this exponential growth constant a is the positive root of the equation

$$a^3 + (K_1 + K_2 + K_3 + K_4[M])a^2 + (K_2K_3 + K_2K_4[M] + K_3K_4[M])a + (K_2K_3K_4[M] - 2K_1K_2K_3) = 0 \quad (I)$$

where $K_1 = k_1[\text{O}_2]$, $K_2 = k_2[\text{H}_2]$, $K_3 = k_3[\text{H}_2]$ and $K_4 = k_4[\text{O}_2]$. Using literature values for k_1, k_2, k_3 and the experimentally determined values for a and $[\text{M}]$, Equation (I) was solved for k_4 .

EXPERIMENTAL

In order to measure the exponential growth of the O-atom concentration during the induction period, H₂-O₂-CO-Ar mixtures were shock-heated and the chemiluminescent emission from the O + CO → CO₂ + hv was monitored. Since the emission intensity is proportional to [CO][O] and since the concentration of CO is constant during the induction period, the emission will exhibit the same exponential growth as the O-atoms. To obtain sufficient emission intensity for our induction period measurements, we used a special end-on technique, in which we studied the reaction behind the reflected shock wave by monitoring the total light emitted axially through a 7.6 cm diameter window mounted in the end flange of the shock tube. Under suitable conditions, the exponential growth constant of the integrated emission observed by this technique is identical to that for the free radical growth during the induction period.

The apparatus and experimental techniques were basically the same as those described earlier and therefore will only be summarized here.² The 10 cm diameter stainless steel shock tube used in this study has a 3.96 meter long test section and a 1.82 meter long driver section. Five thin film heat gauges used to measure the shock velocity are mounted 25.4 cm apart along the tube, the last one located 15.0 cm from the end of the shock tube. The end flange of the shock tube was fitted with a 10 cm diameter and 1.25 cm thick Pyrex glass disk, masked on the outside to provide a 7.6 cm diameter axial window. A plano-convex lens (focal length 57.1 cm, diam. 8.6 cm) located 3 cm behind the window focused the light, which is emitted parallel to the axis of the shock tube, onto a telecentric aperture 1.9 cm in diameter located at the focal point. The light intensity was recorded by an Amperex 150 AVP photomultiplier tube (S-11 response) located behind the aperture. The output of the cathode follower was directed to a Tektronix 545 oscilloscope (CA preamplifier) fitted with a Polaroid camera. A thin film heat gauge deposited on the window provided the signal that triggered a single sweep of the oscilloscope upon arrival of the shock wave at the end of the tube.

All experiments were performed in gas mixtures containing 0.50% H₂ - 0.50% O₂ - 3.0% CO - 96% Ar with the exception of three runs made with the same H₂-O₂ amounts but with 0.50% CO and 98.5% Ar. The gases were taken from commercial cylinders and were purified by passing them through a Drierite-filled trap cooled to dry-ice temperature. Two sets of experiments were performed - a high density set with densities in the range of 4.2 - 5.8 x 10⁻² moles/liter and a low density set having densities between 1.1 - 2.5 x 10⁻² moles/liter.

DATA REDUCTION

The shock velocity at the end of the tube was obtained from extrapolation of the data from the five thin film gauges mounted near the end of the shock tube. Hugoniot calculations for conditions of no chemical reaction behind both incident and reflected shock waves were used to determine the temperature and concentration conditions in each experiment. In all experiments, the vertical deflection was read from the oscillogram and plotted as a function of time on semi-log paper. A straight line was hand drawn through the data points and an experimental time constant $\alpha(\text{sec}^{-1})$ was calculated for each. The results are listed in Table I.

Solving Equation I for k_4 , we obtain

$$k_4 = \frac{-8\alpha'^3 - 4(k_1 + k_2n + k_3n)\alpha'^2 - 2k_2k_3n^2\alpha' + 2k_1k_2k_3n^2}{4[M]\alpha'^2 + 2(k_2n[M] + k_3n[M])\alpha' + k_2k_3n^2[M]} \quad (\text{II})$$

where $\alpha' = \alpha/2[O_2]$ and $n = [H_2]/[O_2]$.

By using Equation II and the experimentally determined growth constants α , we obtained a value for k_4 for each high density experiment. These values are given in the last column of Table I and are plotted in Figure II.

The calculated values for k_4 depend strongly on the value assumed for k_1 and only to a minor extent on the values used for k_2 and k_3 . This is because Reaction 1 is the slow step in the branching mechanism under our experimental conditions and is almost rate limiting. To obtain accurate and self-consistent values for k_1 for our calculations, we solved Equation I for α and varied k_1 until the experimental α values at high temperature and low density (where Reaction 4 is unimportant) corresponded to the calculated value. The best fit was with an expression $k_1 = 1.25 \times 10^{11} \exp(-14.97 \text{ kcal/RT})$ which yields values 30% higher than the expression reported by Gutman and Schott.² The Arrhenius expressions for k_2 and k_3 used for both the α and k_4 calculations were $k_2 = 3.25 \times 10^{10} \exp(-10.0 \text{ kcal/RT})$ liter/mole-sec³ and $k_3 = 6.15 \times 10^{10} \exp(-5.90 \text{ kcal/RT})$ liter/mole-sec.⁴ The lines drawn through the experimental points in Figure I are solutions to Equation I using: (1) the above values for k_1 , k_2 , and k_3 ; (2) a smoothed density function $[M] = M(T)$ obtained from the experimental densities (one for each line); and (3) the expression $k_4^{\text{Ar}} = 6.83 \times 10^{11}/T^{0.74}$ (liter²/mole²-sec) which is explained below. [Hereafter units of liter²/mole²-sec are implied for k_4 .]

To obtain a temperature dependent function of k_4 for use in the above calculations and also for use in comparing our results with others at different temperatures, we evaluated the parameters in the expression $k_4^{\text{Ar}} = A/T^n$ by joining the point $k_4^{\text{Ar}} = 3.75 \times 10^9$ at 1087°K at the low temperature end of our study with a value of $k_4^{\text{Ar}} = 12.5 \times 10^9$ at 225°K reported by Clyne and Thrush.⁵ The resulting expression is $k_4^{\text{Ar}} = 6.83 \times 10^{11}/T^{0.74}$.

The error limits for our k_4 values vary from $\pm 30\%$ at the low temperature end of our study to $\pm 100\%$ at the high temperature end. This change in accuracy is a result of the decreasing effect of Reaction 4 in the branching kinetics as the temperature increases and the density decreases. These limits were obtained from assigning a $\pm 20\%$ overall uncertainty to α' and are shown as error bars in Figure II.

Because of the rapidly increasing limits of error toward our higher temperature results, we have chosen the mean value $k_4^{\text{Ar}} = 3.75 \times 10^9$ liter²/mole²-sec at 1087° as our best value and assign it an accuracy of $\pm 30\%$.

DISCUSSION

The effects of adding CO to the H_2-O_2 system were discussed previously.² However, in this study an additional consideration is important due to the high densities used here. The reaction $O + CO + M \xrightarrow{k_6} CO_2 + M$, although slow,

was taken into account. It was added to the kinetic mechanism and a new cubic equation was obtained for α , which in turn was solved for k_4^{Ar} . Using a value of 1×10^8 liter²/mole²-sec,⁶ there was a negligible change in the calculated k_4 . We performed four experiments with 0.5% CO and obtained from these experiments calculated k_4 values in agreement with the others performed with mixtures containing 3% CO.

Our results are virtually in complete agreement with the value for k_4^{Ar} recently reported by Getzinger and Blair.⁷ They report a value of $k_4^{\text{Ar}} = 2.5 \times 10^9$ in the temperature range 1500-1700°K. Extrapolating our value to their temperature range, we calculate values 10-20% higher than theirs. Other values for k_4 , especially for $k_4^{\text{H}_2}$, have been reported near 800°K based on explosion-limit studies. These studies are in fair agreement with one another and report values for $k_4^{\text{H}_2}$ near 8×10^9 liter²/mole²-sec.⁸ Converting these to a value for k_4^{Ar} gives 1.4×10^9 (assuming the presently accepted ratio $k_4^{\text{H}_2}/k_4^{\text{Ar}} \approx 5$). At 800°K our k_4^{Ar} expression gives the value 6×10^9 . No explanation is offered at this time to account for this large discrepancy. A value for $k_4^{\text{H}_2\text{O}} = 100 \times 10^9$ has been reported by Fenimore and Jones from flame studies near 1350°K.⁹ If this value is adjusted to give a value for k_4^{Ar} using $k_4^{\text{H}_2\text{O}}/k_4^{\text{Ar}} = 20$, it yields a value somewhat higher but in good agreement with our k_4^{Ar} curve. The agreement might well be fortuitous, since their error limits are rather large and the correction for the relative efficiency of water is somewhat uncertain.

CONCLUSIONS

The end-on technique provides a means of making measurements during the induction period of chain-branching reactions. Since during this period radical concentrations are low, only those reactions which have a single radical reactant have an appreciable rate. Hence, this technique allows one to study combustion processes unperturbed by radical-radical reactions. In the case of $\text{H}_2 + \text{O}_2$ reaction, use of the end-on technique has resulted in values for k_1 , k_2 , and k_4 . In other systems where the mechanism is not clearly understood, measurements of the chain-branching coefficient under a variety of initial conditions could help to identify the important reactions.

ACKNOWLEDGEMENTS

We wish to thank Frank Dougherty, Robert W. Lutz, and Jacqueline Mutel for their help in performing the experiments and evaluating the data. This research was supported by the National Science Foundation and the Petroleum Research Foundation.

BIBLIOGRAPHY

1. V. N. Kondratiev, Chemical Kinetics of Gas Reactions, Pergamon Press, Inc., New York, 1964, Sec. 39.
2. D. Gutman and G. L. Schott, J. Chem. Phys., 46, in press.
3. The expression for k_2 is from Reference 2 and agrees closely with that recently reported by A. A. Westenberg and N. de Haas, J. Chem. Phys., 46, 490 (1967). Their expression $k_2 = 4.0 \times 10^{10} \exp(-10.2 \text{ kcal/RT})$ liter/mole-sec is derived from measurements made from 300-1000°K.

4. F. Kaufman and F. P. DelGreco, Symp. Combust. 9th, Cornell Univ., Ithaca, New York, 1962, 659 (1963).
5. M. A. A. Clyne and B. A. Thrush, Proc. Roy. Soc. (London), A275, 559 (1963).
6. This value for k_6 is taken from a line joining the room temperature results of V. N. Kondratiev and I. I. Prichkin (Kinetika i Kalatiz, 2, 292 (1961)) and those of T. A. Brabbs and F. E. Belles, (NASA TM X-52197) at 3000°K. The latter results were presented at the Eleventh Symp. Combust., Berkeley, California, 1966.
7. R. W. Getzinger and L. S. Blair, Paper presented at the Sixth International Shock-Tube Symposium, Freiburg, Germany, April, 1967. R. W. Getzinger and G. L. Schott, J. Chem. Phys., 43, 3237 (1965) reported a value for $k_4^{Ar} = 1.42 \times 10^9$ liter²/mole²-sec at 1500°K using almost the same experimental procedure as in the above paper.
8. For a review of these studies see B. A. Thrush in Progress in Reaction Kinetics, Vol III, Pergamon Press, New York, 1965, p. 63.
9. C. P. Fenimore and G. W. Jones, Symp. Combust. 10th, Cambridge, England, 1964, 489 (1965).

Table I

Experimental Results of induction period emission experiments

 $X_{H_2} = 0.0050$; $X_{O_2} = 0.0050$; $X_{CO} = 0.030$; $X_{Ar} = 0.960$ Low Density Experiments

$k \times 10^{-5}$ (sec ⁻¹)	[M] x 10 ² (mole/liter)	$a^1 \times 10^8$ (liter/mole-sec)	T (°K)	$k^{Ar} \times 10^{-10}$ (liter ² /mole ² -sec)
1.44	1.096	13.300	2040	
1.48	1.096	13.500	2040	
1.40	1.152	12.130	2000	
1.38	1.206	11.140	1943	
1.15	1.298	8.860	1793	
9.8	1.274	7.700	1750	
1.01	1.382	7.310	1705	
0.728	1.238	5.890	1655	
0.836	1.528	5.490	1613	
0.920	1.466	5.280	1608	
0.921	1.584	5.820	1600	
0.808	1.510	5.350	1577	
0.783	1.510	5.180	1576	
0.813	1.498	5.430	1555	
0.705	1.650	4.270	1515	
0.702	1.740	4.040	1465	
0.562	1.614	3.480	1455	
0.602	1.840	3.300	1440	
0.511	1.608	3.180	1437	
0.527	1.744	3.020	1395	
0.434	1.856	2.220	1355	
0.418	2.024	2.060	1325	
0.391	1.880	2.080	1296	

Low Density Experiments

$a \times 10^{-5}$ (sec ⁻¹)	[M] x 10 ² (mole/liter)	$a' \times 10^8$ (liter/mole-sec)	T (°K)	$K_{Ar} \times 10^{-10}$ (liter ² /mole ² -sec)
0.339	2.040	1.660	1296	
0.359	2.020	1.780	1280	
0.333	2.080	1.600	1270	
0.250	2.138	1.170	1220	
0.240	2.080	1.150	1192	
0.206	2.070	1.000	1182	
0.218	2.200	0.990	1173	
0.202	2.000	1.010	1160	
0.159	2.260	0.702	1130	
0.160	2.040	0.783	1110	
0.150	2.420	0.620	1105	
0.160	2.410	0.673	1100	
0.142	2.120	0.670	1100	
0.150	2.536	0.592	1060	

High Density Experiments

1.035	4.75	2.180	1370	0.419
1.065	4.59	2.320	1370	0.337
0.885	4.75	1.865	1295	0.173
0.561	5.30	1.060	1260	0.458
0.522	5.44	0.960	1220	0.334
0.338	5.52	0.610	1200	0.453
0.404	5.56	0.727	1180	0.307
0.268	5.80	0.462	1175	0.511
0.383	5.54	0.690	1175	0.309
0.279	5.59	0.529	1160	0.404
0.198	5.77	0.343	1155	0.423
0.163	5.83	0.279	1125	0.362
0.113	5.92	0.191	1130	0.422
*0.832	5.22	1.590	1285	0.270
*0.381	5.42	0.700	1185	0.346
*0.284	5.67	0.501	1166	0.380
*0.186	5.81	0.320	1135	0.371

* Experiments performed with:

$$X_{H_2} = 0.0050; X_{O_2} = 0.0050; X_{CO} = 0.005; X_{Ar} = 0.985$$

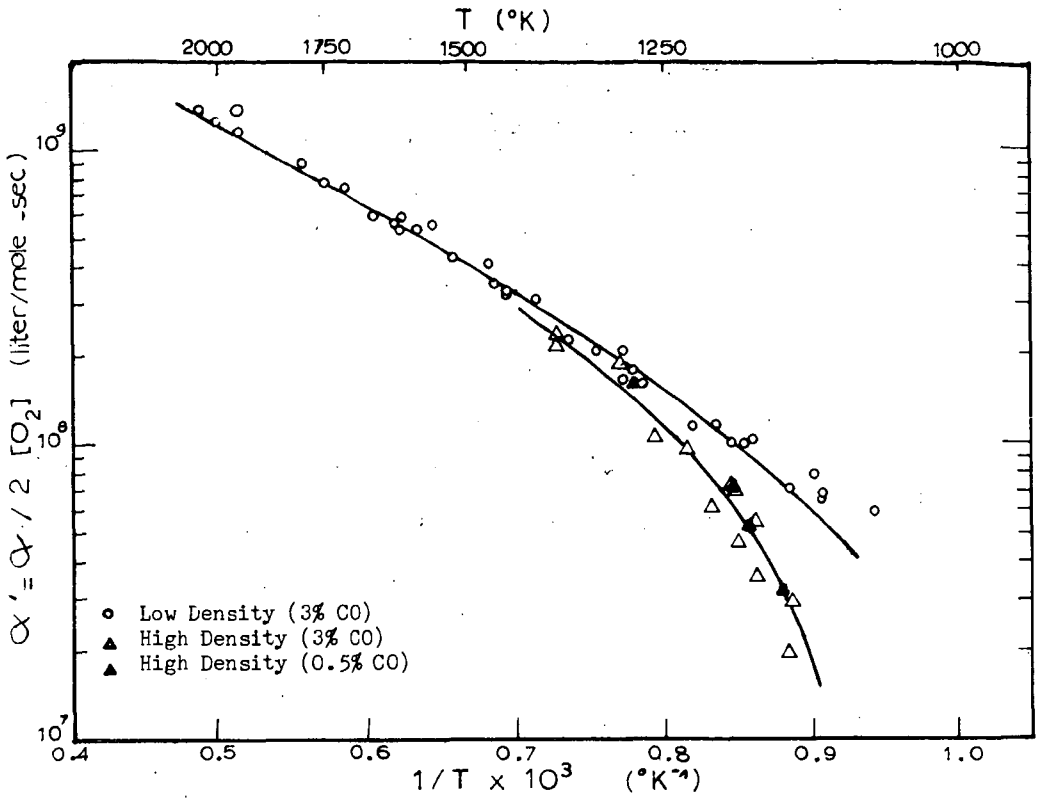


Figure I. plot of $\alpha / 2 [O_2]$ vs. $1/T$.

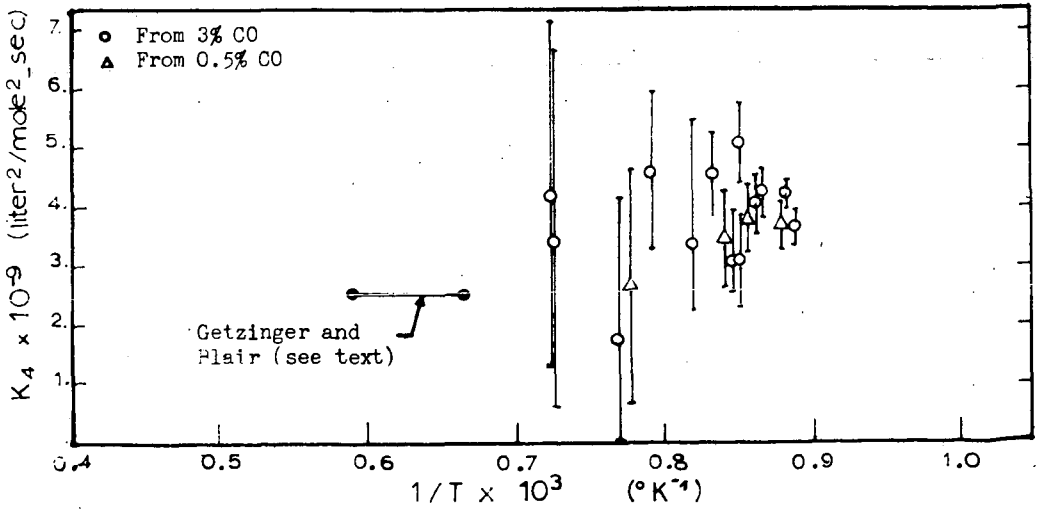


Figure II. Calculated values for k_4^{Ar} from corresponding points on high density curve in Figure I.

SHOCK FRONT STRUCTURE - A CHEMICAL KINETICS VIEW

S. H. Bauer

Department of Chemistry, Cornell University, Ithaca, New York 14850

INTRODUCTION

In the analysis of shock front structures in real gases, intermolecular processes which fall within the province of chemical kineticists play a dominant role. The determination of shock front profiles in density, temperature and in the concentrations of chemical species, provide kineticists with powerful techniques for exploring mechanisms for reactions which cannot be studied otherwise. This has been recognized for over a decade. Advances made in the state of the art through 1963 can be measured by the content of an 850-page treatise on shock tubes by H. Qertel⁽¹⁾, which covers theory, practice and applications in a detailed and thorough manner. More recent assessments may be obtained from the 94 abstracts of papers which were submitted for presentation at the 6th International Shock Tube Symposium,⁽²⁾ and the 37 reports given at the AGARD Colloquium on "Recent Advances in Aerothermochemistry."⁽³⁾

In this summary attention is called to several developments which have advanced the "state of the art" during the past year. A brief overall assessment shows that there is continued emphasis on the improvement of experimental techniques. These center around cleanliness of operation (good vacuum technique, insistence on low leak rates, etc.), the use of polished inner walls to reduce boundary layer perturbations, improved control of species concentrations, increased precision in shock speed measurements, refinement in sensitivity and reduction of response times for diagnostic devices used in recording the profiles of shock fronts, etc. In addition there is greater sophistication in the design of experiments. The improvements may be categorized into three groups: (1) use is being made of newly available devices, such as lasers; (2) it is now general practice to record in many channels concurrently, such as the mass spectra of several species, the concurrent recording of emission and absorption spectra at different wavelengths as a function of time; (3) combining shock tube techniques with other techniques for the preparation of samples to be studied; for example, preliminary flash photolysis or imposition of a glow discharge through the sample prior to its being exposed to the shock wave. Along with increased sophistication in the performance of experiments, extended computer programs are used routinely, both for equilibrium compositions and for obtaining kinetic profiles; also, to facilitate data reduction.

These trends will continue because they have already proved their worth, but they occur at the expense of increased complexity in equipment, leading inevitably to the need for collaboration among several persons in operating a facility. What remains for the lone experimenter? It appears to me that for some time to come the single-pulse shock tube technique will remain one of a few individualistic activities. The investigator will have to be ingenious in designing kinetic experiments in which knowledge of the concentrations of species after a specified reaction time permits an identification of a mechanism. Single-pulse shock tubes allow the exploration of complex systems in a qualitative manner, and provide the basis for selecting reactions which are critical steps in a complex reaction scheme for detailed study by other techniques.

TECHNIQUES AND DIAGNOSTIC DEVICES

A representative selection of interesting developments in technique is presented in Table 1. The use of narrow electron beams for exciting molecular spectra in a flowing medium merits an additional comment. The characteristic spectra excited permit identification of the species present, and an estimation of their densities (if proper calibrations are made). Vibrational and rotational temperatures can be obtained from band contours. In the hands of a careful experimentalist, this technique may give translational speeds as well (Doppler widths of spectral lines). For example, in a supersonic jet of nitrogen expanding from room temperature in an axi-symmetric nozzle, (8) the rotational temperature was observed to follow the isentropic curve initially, but at the lower temperatures the rotational population "froze" to a fixed distribution leading to a substantial degree of non-equilibrium.

Perhaps one of the most sensitive devices for measuring gradients at a shock front with high resolution is the laser-schlieren method described by Kieffer and Lutz. (11) Gradients as low as 10^{-5} gm/liter mm can be detected in argon, and characteristic times (lab scale) as short as 0.2μ sec. have been measured. Vibrational relaxation times for hydrogen and deuterium have thus been quantitatively determined for the first time. This technique has been effectively used to scan the heat release profile during the high temperature oxidation of acetylene. (12)

The best illustration of concurrent multichannel recording to provide a large amount of information for a single shock, and thus to correlate a variety of parameters, is the use of a rapid-scan mass spectrometer. A time-of-flight spectrometer coupled to a shock tube via a minute leak has been described by Kistiakowsky, (13) Dove, (14) Diesen (15) and Modica. (16) The successful application of a quadrupole mass filter for the analysis of products extracted from a back-reflected shock has been recently reported by Gutman. (17) As described this relatively low cost instrument could be set to record only one mass at a time; however, current developments in Gutman's laboratory indicate that it may be possible to set four mass filters for concurrent recording. The fidelity of sampling of back-reflected shocked gases through 0.002 inch apertures remains to be demonstrated. To avoid confusion of the desired sample with end-wall cooled gases and boundary layer perturbations, Marsters (18) extracts the sample from a rapidly quenched incident shock and by a sequence of large aperture nozzles converts the jet to a molecular beam for analysis by a time-of-flight spectrometer.

There is an intriguing possibility of using a small mass spectrometer to detect the onset of ionization (in particular, the onset of production of a particular species) and correlating this profile with spectroscopic data (chemiluminescence, or the appearance of a characteristic absorption). In this connection one should mention the successful application of a Nier-type mass spectrometer by Sturtevant (19) who demonstrated that the first ions to appear in shock-heated argon, at a threshold approximately four volts below the ionization potential of argon, were H^+ and O^+ , presumably from a very low level water impurity.

The technique of preparing equilibrium samples at elevated temperatures (as with reflected shocks) and quenching them so rapidly that one may study kinetic processes which occur during the cooling path has not attracted many devotees, although expansion through a small aperture in the end wall of a shock tube for sampling purposes is being used by mass spectrometrists. To avoid boundary layer problems and to achieve very rapid cooling, Wilson (20) inserted a pair of divergent airfoils in a shock tube, so that the incident shock passed through a double Prandtl-Meyer

expansion. This setup was used effectively for measuring the recombination rate of oxygen atoms at elevated temperatures, and is currently being developed in our laboratory for investigating condensation processes in metal vapors produced under supersaturated conditions by shock-heating metal carbonyls. The expansion generated by the interaction of the contact surface with the reflected shock was used for a kinetics study of the association of CN radicals prepared by shock-heating C_2N_2/Ar mixtures to about 2000° ,⁽²¹⁾ the CN concentration was followed spectrophotometrically. It was found that the rate of CN disappearance was first order in CN and first order in C_2N_2 (or C_mN_m polymers), and that the average polymer number under these conditions, $m \approx 10$. Finally, a rapid-quench sampling probe for non-equilibrium air flows has been described by Stoddard and Watt⁽²²⁾ in which a small sample scooped from the free stream region in a shock tunnel is rapidly cooled by contact with the walls of an explosively sealed probe.

An example of interesting results obtained from use of combined techniques is the glow tube described by Hartunian, *et al*⁽²³⁾ in which a steady-state concentration of reactive species is prepared in a glow-discharge flow system, and fully characterized (at room temperature). The plasma is then subjected to a shock, initiated by rupture of a diaphragm upstream from the rf source. Typically, the shock strength is less than that which causes further dissociation; the shock compresses, heats and accelerates those species which are already present in the glow tube. Thus, a means is provided for studying the temperature dependence of the gas phase recombination processes and of chemiluminescent reactions. This combination provides a considerable extension of atom fluxes for study of kinetic processes. In contrast to heating with shock waves, Petrella *et al*⁽²⁴⁾ describe a combination flash photolysis-flash pyrolysis system in which heating is accomplished by the comparatively slower process of allowing the gaseous sample to contact a flash-heated solid grid.

References to several current analyses on the non-ideal behavior of shock tube operation are listed in Table II, while Table III is a summary of papers in which the measurement of ionization cross-sections and of optical oscillator strengths are discussed.

MEASUREMENT AND CONTROL OF VIBRATIONAL STATE POPULATIONS

During the past two years much effort has been devoted to the study of the excitation of vibrational modes due to intra- and inter-molecular energy transfer processes. For many decades it has been accepted by kineticists that the measured reaction rate constants depend on the facility for energy transfer between the various parts of reacting molecules when in the transition state. The mere difficulty of properly estimating the density and symmetry character of the highly excited states even in simple systems, led to an attitude of futility, as expressed by the observation that there seems to be little relation between the states of interest to chemical kineticists and the transition probabilities measured for low-lying vibrational states. However, several examples are now known for which the measured rate constants may be calculated from measured vibrational relaxation times. The basis for the current activity is in part due to the recognition of the presence of strong coupling between vibrational modes and dissociation, and in part to the current explosive development in laser technology.

It has been known for several years that vibrational relaxation times for small molecules containing hydrogen atoms are much shorter than those predicted on the basis of the Slawsky-Schwartz-Herzfeld theory, and the observed relaxation times did not fit the correlation diagram proposed by Millikan and White. For example, the

vibrational relaxation times for HCl, DCI and HI measured by the spectrophone method⁽⁴³⁾ (at room temperature) are consistent with the high temperature data (infrared emission from shocked gases at 2000°)⁽⁴⁴⁾ in that the relaxation times were several orders of magnitude shorter than those predicted by the SSH theory. They are in better agreement with Cottrell's vibration-rotation theory⁽⁴⁵⁾. That rotational motion plays a role in exciting vibrational states was demonstrated by Millikan⁽⁴⁶⁾ who measured the relative rates of collisional deactivation of vibrationally excited CO by ortho and para hydrogen. Another example of the inadequacy of the SSH theory are the vibrational relaxation times for H₂-Ar, H₂-H₂, D₂-Ar, D₂-D₂ reported by Kiefer and Lutz⁽¹¹⁾. These data are better accounted for by Parker's semi-classical theory⁽⁴⁷⁾ with an angle-dependent potential used for calculating both rotational and vibrational relaxation times. Even though there is agreement for collision numbers with argon and krypton as collision partners, there remains an order of magnitude disagreement for self collisions of H₂ and D₂. A good summary of relaxation processes involving rotational-vibrational interactions and resonance collisions was given by R. C. Millikan;⁽⁴⁸⁾ a simple two-parameter model was developed by C. B. Moore.⁽⁴⁹⁾

The relaxation of NO X²Π (v = 1) in D₂S, H₂O, H₂S, D₂O and CH₄ was investigated by microwave-flash pulse-flash spectroscopy.⁽⁵⁰⁾ Deactivation by all the hydrides was very fast compared with the rate of self deactivation. The rate coefficient showed a systematic variation with the minimum energy which had to be converted to translation. The authors propose that the uniformly fast relaxation by the triatomic hydrides may arise from the formation of an intermediate complex between NO and the H₂S or H₂O. However, this does not account for the effect of isotopic substitution. For comparison, helium is ≈0.1 as effective as NO, which in turn is ≈0.01 as effective as H₂S.

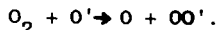
The vibrational relaxation of oxygen in the presence of small amounts of methane (0.5% to 1.6%) was measured at room temperature by ultrasonic techniques.⁽⁵¹⁾ The relaxation frequency did not vary linearly with the methane concentration. It appears that translation-vibration excitation occurs only for methane, but that oxygen molecules become excited only by vibration-vibration transfer from the methane. A similar mechanism for energy transfer was reported by Millikan in the quenching of carbon monoxide fluorescence by methane.⁽⁴⁸⁾ In contrast, for nitrogen-hydrogen mixtures (≈2% H₂) White⁽⁵²⁾ found that the vibrational relaxation time fitted their systematical correlation diagram.

The density profile at the shock front due to vibration relaxation in oxygen was explored with the laser-schlieren technique, in pure oxygen and in oxygen-ozone mixtures.^(53,54) Kiefer and Lutz report:

$$p\tau_{(O_2-O_2)} = (2.92 \pm 0.20) \times 10^{-10} \exp \left[\frac{(126.0 \pm 0.9)}{T} \right]^{1/3}, \text{ atm. sec.}$$

$$p\tau_{(O_2-O)} = (4.35 \pm 0.19) \times 10^{-8} - (7.75 \pm 0.81) \times 10^{-12} T, \text{ atm. sec.}$$

The latter is the deduced value for oxygen molecules dilute in an atmosphere of atoms. These clearly differing temperature dependencies indicate a strong chemical effect, possibly similar to those previously suggested for the CO₂-H₂O system and CO-CI₂ systems, but more likely due to atom exchange: ⁽⁵⁵⁾



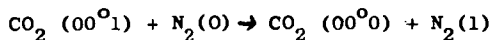
Measurement of the vibrational relaxation times in nitrogen presents an interesting case history. Sodium-spectrum line-reversal measurements for N₂ in

normal shocks gave vibrational relaxation times which checked well with interferometer-shock tube investigations. (Extrapolation to temperatures below 1500°K gives values which are orders of magnitude higher than sound dispersion and impact tube results.) However, when the line reversal technique was used to scan the vibrational non-equilibrium produced in supersonic expansions of undissociated nitrogen from reservoir temperatures 2800-4600°K (15° axi-symmetric nozzle, coupled to the end of a shock tube), the probability for de-excitation appeared to be ≈ 50 times greater.⁽⁵⁶⁾ This short relaxation time has now been confirmed by following the CO vibrational relaxation (introduced as a tracer in the expanding nitrogen stream), and by the electron beam technique in a low density non-steady expansion. For a while it was believed that the rapid relaxation was due to impurities present in the reservoir gas, but this was proven untenable.⁽⁵⁷⁾ A plausible explanation has now been proposed by Treanor and coworkers.⁽⁵⁸⁾ They point out that inadequate consideration has been given to effects of anharmonicity on vibrational relaxation for vibration-vibration exchange dominated regimes. When the translation temperature is quite low and the vibrational energy content is high (as in a rapidly expanding nozzle flow) vibration-vibration exchange introduces a slight but definite non-Boltzmannian vibrational population distribution. In such a case the population of the lowest vibrational level may be considerably lower than what it would be if the system were to relax through a sequence of Boltzmann distributions, thus indicating an apparent rapid relaxation time. Current experiments at CAL on the vibration relaxation in expanding nozzle flows for CO parallel the above observations reported for nitrogen. It is interesting to note that for the ascending path, i.e., the vibrational excitation of nitrogen, as followed by monitoring the $v''=9$ level (U.V. absorption at 1176Å), the recorded times⁽⁵⁹⁾ are consistent with the Shuler-Rubin-Montroll theory that the populations of vibrational levels relax via a continuous sequence of Boltzmann distributions (3000°-5500°K). For temperatures in excess of 5500°K, the local value for the characteristic relaxation time (τ_v) becomes increasingly dependent on the degree of vibrational excitation.

A large amount of attention is currently being devoted to studies of the vibrational relaxation processes that occur in carbon dioxide. One must consider not only intermolecular energy exchange (V-T) and (V-V) with various colliders for CO₂ molecules in its different vibrational states, but also vibrational energy redistribution in CO₂ molecules due to collisions with ambient gases. To date ultrasonic dispersion studies have uncovered only three gases which show two dispersion frequencies: SO₂, CH₂Cl₂, and C₂H₆. Many shock tube investigations have shown that the vibration-translation relaxation in CO₂ follows a single relaxation time. On the basis of careful measurements of the variation of density behind incident shock waves in carbon dioxide, up to temperatures 2500°K, Simpson, et al.⁽⁶⁰⁾ report that only a single relaxation time is discernable even though the density behind the shock front does not change strictly exponentially with distance; the departure is due to changes in the translational temperature which must accompany the relaxation process. A similar conclusion was reached by Weaner, et al.⁽⁶¹⁾ who made simultaneous measurements of the flow density with a Mach-Zehnder interferometer at the shock front and of the infrared emission at 4.3 μ . While the emission intensity monitored the population of the ν_3 level, the density provided a measure of the energy flow into all the vibrational modes. The single relaxation time was thus interpreted as evidence that equilibrium among all the vibrational modes was attained within the rise time of their detector (1.5 μ sec). However, the situation gets more complicated when one considers (V-V) energy transfer.

Moore and coworkers⁽⁶²⁾ measured decay curves of laser-excited vibrational fluorescence from the (00¹) level of CO₂ (asym. stretch), as dependent on the admixed gases. He

deduced (V-V) transfer rates at room temperature which ranged from 15.5 atm- μ sec for He as a collision partner, to 3.76 (self), to 0.34 (H_2) to 0.055 (H_2O). Ultrasonic data give relaxation times for the (01'0) level (V-T). Corresponding values, for self collision, CO_2 $6.8 \pm .3$ atm- μ sec; with He (0.39), H_2 (0.015) and H_2O (0.0030). They also deduced the energy transfer probability for the reaction.



to be $(2.0 \pm .4) \times 10^{-3}$. The significant catalytic role of water for CO_2 laser operation is now evident. At elevated temperatures over the range 800 to 3000°K shock tube measurements⁽⁶³⁾ with very short response time detectors show comparable differences between the several relaxation processes. Taylor and Bitterman⁽⁶⁴⁾ have prepared an exhaustive survey of vibrational relaxation data for processes important in the CO_2 - N_2 laser system. A brief review on (V-V) transfer efficiencies as deduced from ultrasonic measurements has been published by Lambert.⁽⁶⁵⁾

UNSOLVED PROBLEMS IN THE DISSOCIATION OF SMALL MOLECULES

One of the basic problems in chemical kinetics is the detailed analysis of the processes which occur when in diatomic molecules are dissociated thermally but homogeneously. Although a qualitative description has been given decades ago, it was not possible to perform the experiments nor to test details of the theory until the advent of shock tube techniques. One of the essential features required is the possibility to separate in time the vibrational excitation processes from the dissociation steps. It is now evident that conventional kinetic descriptions are not adequate. For example: The dissociation rate of very pure hydrogen at low concentrations in argon (0.01%-1.0%) has been measured by Watt and Myerson⁽⁶⁶⁾ using atomic absorption spectrophotometry (Lyman α line). An Arrhenius plot for the bimolecular rate constant gives an activation energy of 94.5 kcal over the temperature range 2200°K. These rates are approximately a factor of five lower than rates reported by previous investigators, presumably because their samples were contaminated with slight amounts of oxygen which accelerated the dissociation rate through the reaction $H + O_2 \rightarrow OH + O$, followed by $O + H_2 \rightarrow OH + H$. For contrast Hurler reported about a year ago⁽⁶⁷⁾ his studies of dissociation rates in hydrogen-argon mixtures (20% to 60% H_2) covering the temperature range 2500° to 7000°K, based on the Na-spectrum line-reversal technique for temperature measurement. He then deduced degrees of dissociation as a function of time (or distance behind the shock front), and was able to assign relative efficiencies to Ar, H_2 , and H atoms as colliders. When his results were converted to recombination rate constants it appears that H_2 is several times more efficient than argon as a chaperon for the $2H \rightarrow H_2$ recombination but both show an approximate T^{-1} dependence. However, the efficiency of H atoms as chaperons appears to be equal to that of H_2 for temperatures above 5500°K but as the temperature is lowered the efficiency rises sharply and at 3000° is about 30 times greater than that for H_2 . Furthermore, there are indications that for temperatures below 2500°K the efficiency drops again and the room temperature H atoms may be only three times as effective as H_2 .

The following observations are typical of most of the homoatomic diatom dissociation processes.⁽⁶⁸⁾ In all cases the self atom is much more efficient for the dissociation-association steps as a chaperon than is the molecule or an inert gas. That is not surprising since there are strong indications that the vibrational excitation efficiency of the self atom as a collider is greater than of any other molecular species.^(54,55) However, it is difficult to explain the observed temperature dependence of the atom-chaperon rate constants; they do not fit into the scheme proposed by Keck under the "variational theory of reaction

rates."⁽⁶⁹⁾ I believe it is essential for the experimentalists to provide boundary conditions for the theories which will be developed; in this instance, data on deuterium are needed to check the effect of mass (possible tunnelling).

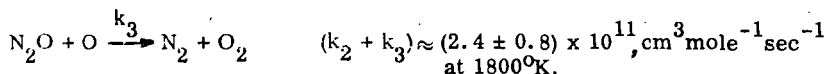
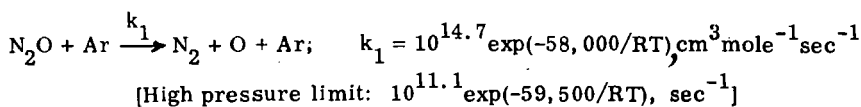
Recent publications describing dissociation rate studies of various diatoms are listed in Table IV. Inspection of such data shows that for the homatomic diatoms, simple Arrhenius plots gives lines with a slope for effective activation energies which are 7 to 10 kcal lower than the spectroscopic values. This is believed to be due to a statistical factor, i.e., the depletion of the upper vibrational states due to the slowness of the recombination reaction (3 body) such that their populations fall below the Boltzmann value calculated for the ambient translational temperature. This explanation is clearly not adequate to account for the much larger departures between the effective activation energies deduced from Arrhenius plots and the spectroscopic D_0 's for the hydrides HF, HCl, and DC ℓ . The dissociation rate of HF in shock waves has been studied in two laboratories. When the data published by Jacobs *et al*⁽⁷⁶⁾ were replotted and fitted by least squares, the bimolecular rate constant was well represented by $k_d = 10^{14.14} \exp(-108,600/RT)$, $\text{cm}^3 \text{mole}^{-1} \text{sec}^{-1}$. Independently Spinnler⁽⁷⁷⁾ found $k_d = 10^{14.16} \exp(-113,700/RT)$. The close agreement is striking, since Jacobs followed the rate of reaction by recording the IR emission intensity behind incident shocks while Spinnler looked at absorption behind reflected shocks. A larger discrepancy has been reported for HCl and DC ℓ by Jacobs and coworkers⁽⁷⁸⁾ and confirmed by Fishburne.⁽⁷⁹⁾ The observed apparent activation energy is 70 kcal for both gases while the spectroscopic values are 102 for HCl and 103 for DC ℓ . It does not make sense to try to force these data to a rate expression with a T^{-1} or T^{-2} pre-exponential factor, when the resulting coefficient has a magnitude of over 10^{21} in units of $\text{cm}^3 \text{mole}^{-1} \text{sec}^{-1}$.

In summary, considerable progress has been made in formulating an appropriate statistical mechanics for a dissociation reaction in a thermal bath, in which cognizance is taken of the departure from Boltzmann distribution in the upper vibrational levels.⁽⁸⁰⁾ Virtually no progress has been made in calculating transition probabilities for molecular encounters which produce dissociation. No explorations have been undertaken of the sensitivity of such probabilities to the shape of the interaction potentials but it is established experimentally that diatoms are specially sensitive to the self atoms as colliders.

THE HOMOGENEOUS PYROLYSIS OF POLYATOMIC MOLECULES

While the theoretical underpinnings of current collision theories for diatom dissociations are of dubious dependability, there are even more questions regarding the interpretation of rate data for triatomic fragmentations. The minimum activation energy anticipated for the first step is the thermochemical value minus some correction for the depletion effect due to depopulation of the upper vibrational levels. Shock tube data for one case (N_2O) gave an E_A value which was greater than the corresponding ΔE_T^0 , in full agreement with results obtained by conventional kinetics; there are several systems in which E_A was slightly less than ΔE_T^0 , as expected, but there are a disturbing number of studies which led to $E_A < \Delta E_T^0$ by 25-50 kcal/mole.

The molecule which has been subjected to the most intensive investigation has been nitrous oxide. The homogeneous unimolecular decomposition (high dilution in argon) was studied in both the low and high pressure regimes. Shock temperatures were 1300° to 2500°K , and pressures between 0.8 and 300 atm (concentration range 5×10^{-6} - 2×10^{-3} moles per liter).⁽⁸¹⁾ This pyrolysis was also studied in an adiabatic compression device,⁽⁸²⁾ and the overall results may be summarized in the following equations:



The pyrolysis of the N_2O was also studied with a shock tube leaking into a quadruple mass filter. (17)

At the AGARD Colloquium, Troe and Wagner⁽⁸³⁾ proposed a general treatment for the dissociation of small molecules, as a semi-quantum mechanical extension of unimolecular reaction rate theory. They considered both tri- and tetra-atomics and divided the former into two groups, those which follow spin-allowed dissociations and those which require a net change in spin. The latter include N_2O , CS_2 , and CO_2 . This analysis was amplified by Olschewski, Troe and Wagner.⁽⁸⁴⁾ The first step in the decomposition of 0.001% CS_2 in argon was observed, completely isolated from the consecutive reaction $\text{S} + \text{CS}_2 \rightarrow \text{CS} + \text{S}_2$, using a UV absorption technique. They also studied the rate of dissociation of SO_2 at concentrations below 0.3% in Ar, and of very dilute mixtures of water. The spin-forbidden dissociations approach their high pressure unimolecular limits at a few hundred atmospheres, but this condition cannot be reached for molecules which dissociate to the ground state atom species, as does H_2O . It is interesting to note that when one observes the rate of disappearance of water, say from its emission intensity in the infrared, at concentrations 0.02% to 0.2%, the rate constant is given by $k_{\text{uni}} = (\text{Ar}) 10^{14.2} \exp(-105000/\text{RT}), \text{cm}^3 \text{mole}^{-1} \text{sec}^{-1}$. Here, as in the case of SO_2 , over the temperature range 2700° to 4000°, the measured rate is twice the magnitude for the first step, because the initial dissociation of the water is followed by the very rapid reaction, $\text{H} + \text{H}_2\text{O} \rightarrow \text{OH} + \text{H}_2$. Above 4500°K only the first step is recorded, since all the subsequent steps are very rapid and the first step essentially controls the overall OH production. However, if the course of the reaction is followed by recording the amount of OH produced, (OH absorption at 3063A°)⁽⁸⁵⁾ the energy activation is about 50 kcal/mole. This was confirmed by the Göttingen investigators. Clearly, at the lower temperatures and higher concentrations the initial dissociation step is followed by a host of radical chains which involve OH; these are so rapid that they control the overall rate of its appearance.

One of the triatomic molecules which produces a product in an electronically excited state is CO_2 . Davies⁽⁸⁶⁾ reported that his shock tube study covered the temperature range 6000°-11000°K (1% in Ar). Dissociation was monitored by the infrared emission intensity at 2.7 and 4.3μ. His results were essentially confirmed by E. S. Fishburne and coworkers⁽⁸⁷⁾ (3000-5000°K; 1% to 10% in Ar or N_2). Their results are:

$$k_{\text{Ar}} = 7.11 \times 10^{11} T^{1/2} \exp(-84500/\text{RT}); \quad k_{\text{N}_2} = 5.33 \times 10^{11} T^{1/2} \exp(-79000/\text{RT}), \text{cm}^3 \text{mole}^{-1} \text{sec}^{-1}$$

The thermochemical dissociation energy is 125.3 kcal/mole. The Göttingen investigators also studied CO_2 but at low concentrations and very high pressures in Ar.

They report a preliminary rate constant, $k_{\text{u}} \approx 2 \times 10^{11} \exp(-111,000/RT)$, sec^{-1} , which they found to be practically independent of the argon concentration at levels of 5×10^{-4} moles/cm³. Thus, in this case also, the use of reagent concentrations of 1% or higher and modest Ar pressures permits steps subsequent to the first to confuse the dissociation process. Olschewski and coworkers⁽⁸⁸⁾ also found the bimolecular rate constant for CS₂ to be: $k_{\text{b}} = (\text{Ar}) 10^{15.56} \exp(-80,300/RT)$, $\text{cm}^3 \text{mole}^{-1} \text{sec}^{-1}$.

Other tri- and tetra-atomic species have been studied but not with the care devoted to the few molecules listed above. All of these show apparent activation energies considerably lower than the corresponding. These include HCN,⁽⁸⁹⁾ NH₃⁽⁹⁰⁾ NF₂⁽⁹¹⁾ C₂N₂⁽⁹²⁾ and others.

The following is a brief discussion of pyrolysis investigations of more complex species. Mass spectrometer and spectrophotometric detection ($\lambda 2536\text{\AA}$) of the decomposition of fluoroform on shock heating to 1600°-2200°K was reported by Modica and LaGraff.⁽⁹³⁾ As anticipated, the first step appears to be splitting of the molecules to HF and CF₂, for which the limiting high pressure rate constant is $k_{\text{u}} = 7.03 \times 10^{11} \exp(-58,400/RT)$, sec^{-1} . At pressures 0.29 atm they assumed that the reaction had attained the second order limit. The dissociation of C₂F₄ into difluorocarbenes has been previously studied using Ar as the diluent; Modica and LaGraff⁽⁹⁴⁾ repeated this work with N₂, in reflected shocks (1200°-1600°K). There is a difference in that during the course of the reaction the nitrogen was vibrationally unrelaxed. In turn, the CF₂ radicals generated facilitated vibrational relaxation such that in a 1% tetrafluoroethylene-nitrogen mixture the relaxation time was a factor (10-50) less than in pure nitrogen. Finally, on shocking mixtures of C₂F₄ and NO, Modica⁽⁹⁵⁾ concluded from mass spectra and UV absorptions that over the temperature interval 1600°-2500°K, there were the reversible reactions: $\text{C}_2\text{F}_4 \rightleftharpoons 2 \text{CF}_2$; $\text{CF}_3 + \text{NO} \rightleftharpoons \text{CF}_2\text{NO}$. Above 2500°K, $2 \text{CF}_2\text{NO} \rightarrow 2 \text{CF}_2\text{O} + \text{N}_2$. He does believe that the latter reaction occurs as a bimolecular event.

An extensive investigation of the interconversion of fluorocarbons in shock tubes has been reported by Bauer and coworkers.⁽⁹⁶⁾ Mixtures ranging from 0.5% to 3% in argon of perfluorinated ethylene, cyclopropane, cyclobutane, cyclohexane, propene and butadiene were investigated in a single-pulse shock tube. The reaction mixtures were maintained for about 1 millisecond at specified temperatures and rapidly quenched. Plots of product distribution as a function of reflected shock temperatures were prepared. For example, a product distribution plot for perfluoroethylene shows the initial production of cyclobutane, its rapid decline at 1000°K with a concurrent rise in the amount of propene and cyclopropane, followed by a slow rise in the production of butene-2. These products pass through a maximum between 1800 and 1900°K, and then decline. Above 2100°K, decomposition of perfluoroethylene leads to products which are not preserved in the gas phase. All the products observed may be accounted for by simple sets of fragmentation steps in which CF₂ is the dominant radical. The kinetic simplicity of the C/F system is in striking contrast with the still unresolved complexities of the kinetics of the C/H system; the crucial differences are (a) the relative ease of migration of hydrogen atoms and (b) the high stability of the CF₂ radical. Thus, C/F compounds pyrolyze by breaking C-C bonds, but there is little rearrangement in the free radicals due to F atom migration.

The pyrolysis of ethylene highly diluted in neon was investigated by Gay and coworkers.⁽⁹⁷⁾ The temperature range covered 1710°-2170°K in reflected shock with pressures of 225 to 1600 torr. Products of pyrolysis were analyzed by leaking into a mass spectrometer. The reported rate law shows unit order dependence on ethylene and half order dependence on neon.

$$-\frac{d[C_2H_4]}{dt} = k_{3/2} [C_2H_4] [Ne]^{1/2}; \log_{10} k_{3/2} = 0.01 - 50,500/2.303RT; \text{conc. in molecules cm}^{-3}$$

These results may be fitted equally well by a unimolecular process and by a free radical chain mechanism. However, the low activation energy is difficult to explain since it is only slightly larger than the difference between the enthalpies of acetylene plus hydrogen and of ethylene at the reaction temperatures.

Wing Tsang is continuing with his single-pulse shock tube studies of the thermal decomposition of low molecular weight alkanes and alkenes. (98,99) Many of the difficulties inherent in single-pulse shock tube techniques are minimized in this work, since he measures comparative rates, using the unimolecular decyclization of cyclohexene as an internal standard.

$$k_u (C_6H_{10} \rightarrow C_2H_4 + 1,3-C_4H_6) = 10^{15.02} \exp(-66,700/RT), \text{ sec}^{-1}.$$

His results are summarized in Table V (taken from Table II, ref. 99). The possibility of extending the comparative rate method to other types of reactions is intriguing, but it appears to be difficult to apply to other than unimolecular decompositions. It is essential that the reference reaction remain unaffected, and not participate in the reaction being studied. When free radicals abound, the possibility of maintaining parallel but independent paths for concurrent reactions is small indeed.

BRIEFLY ON HOMOGENEOUS ATOM EXCHANGE PROCESSES

There are very few clearly established gas phase reactions of the type $AB + X_2 \rightarrow AX + BX$; those which are known do not follow the simple rate expression

$$\frac{d[AX]}{dt} = \frac{d[BX]}{dt} = k [AB] [X_2].$$

It should be noted that to force this reaction to follow a molecular mechanism (4-center transition state) it must be carried out under strictly homogeneous conditions (no hot walls), at the lowest possible temperatures, to minimize contributions from $X_2 \xrightarrow{\text{wall}} 2X$; $X + AB \rightarrow AX + B$; $AB + X \rightarrow A + BX$. The results of a shock tube study of the homogeneous four-center reaction $H_2 + D_2$ have been reported over a year ago, as was the exchange reaction between CH_4 and D_2 . (100,101) Heuristic rate expressions for these systems are summarized in Table VI. These results, although unexpected, can be rationalized by assuming that exchange occurs with high probability only during the encounters between pairs of diatoms, one of which is vibrationally excited to a state approximately 0.4 of the way to dissociation. It appears that the probability for metathesis is low when molecules in low-lying vibrational states collide, even when the relative kinetic energy along the line of centers (plus vibrations) exceeds the activation energy. Support for this mechanism is provided by approximate calculations of the pre-exponential term for the exchange rate constant from vibrational relaxation data.

These simple reactions present a challenge to the theorist. The only calculation (106) which has been made of the transition probability for exchange as a function of vibrational excitation ($H_2 + H_2$) does show that the probability increases rapidly with vibrational excitation. However, it does not do so rapidly enough to overcome the lower population of the vibrationally excited states as controlled by the Boltzmann term. In this calculation, the representative point for the collision event moves in a classical trajectory, but the potential surface was obtained by a semi-empirical quantum mechanical procedure. We can only reach the conclusion that

apparently classical collision theory is not adequate. This is supported by the observation that in the vibrational excitation of homoatomic diatomic molecules the self atoms have a very high efficiency for vibrational excitation and for dissociation, but these effects have not yet been deduced theoretically.

SHOCK TUBE STUDIES OF COMBUSTION REACTIONS

Shock tube investigation of ignition delays is continuing at a modest level. The emission of visible light was used as a criterion for ignition in estimating delays as the function of temperature and composition for propane and methylcyclohexane.⁽¹⁰⁷⁾ Inhibition of the hydrogen-oxygen reaction by small amounts of methane, ethylene, trifluoromethylbromide, and 1,2-C₂F₄Br₂ was measured over the temperatures 970°-1300°K.⁽¹⁰⁸⁾ Ignition was detected photoelectrically from the light emitted at the 3090-3100Å band pass for OH, while the induction time was defined as that between the arrival of the reflected shock at the window and the time at which emission reached a maximum. The compounds listed inhibit ignition by reacting with the hydrogen atoms and other radicals which propagate the chain, but it is not essential that the additives first decompose. As for the initiation step of the branching chain for the H₂/O₂ reaction, Ripley and Gardiner⁽¹⁰⁹⁾ showed, by comparing experimental ignition delays with those calculated utilizing a full set of reactions, that initiation by a path other than diatom dissociation must occur. They proposed the exchange reaction $H_2 + O_2 \rightarrow 2 OH$ as one which would account for the data.

Gardiner and coworkers⁽¹²⁾ have effectively used the laser-schlieren technique for measuring density gradients and correlating the time profile for chemiluminescence with that for heat release in the oxidation of acetylene. They found that the OH absorption appeared at the end of the combustion, and that the OH profile was not directly related to the induction period chemistry. Apparently the OH profiles were related to the approach to partial equilibrium, including the reaction $OH + CO \rightleftharpoons CO_2 + H$. The formation of C-O bonds at partial equilibrium conditions indicates that the heat of reaction is liberated without recombination steps, in contrast to the thermal sequence which is followed in the H₂ + O₂ reaction. The C₂H₂/O₂ reaction has also been investigated by Homer and Kistiakowsky^(110,111) who recorded emissions by CO and CO₂ in the infrared, and compared them with the UV emission at the band head 433A (A²Δ - X²Π) transition for CH. They concluded on the basis of the observation that the time constants for CO and CO₂ were identical; that the reaction CO + OH → CO₂ + H does not apply to the initial stages of oxidation. They demonstrated that the time constant for CO emission was twice that for CH*, which supports those mechanisms wherein CH* is produced by second order processes in the chain, such as C₂ + OH → CO + CH*. These results are not in disagreement with the mechanism for C₂H₂ combustion proposed by Glass et al.⁽¹¹²⁾

A large amount of shock tube data has been assembled on the oxidation of ethylene.⁽¹¹³⁾ Chemiluminescence by CH* revealed induction periods, followed by exponential rise of the signals. Measurements of time-dependent species composition with a TOF mass spectrometer can be represented by a rather complex reaction scheme, based on branching chain oxidation steps. The most abundant chemi-ions were C₃H₃⁺ and H₃O⁺. The mechanism proposed for C₂H₄/O₂ is tentative. A similar technique was followed in the study of the pyrolysis and oxidation of formaldehyde in shock waves.⁽¹¹⁴⁾ The pyrolysis shows first order dependence on the formaldehyde and on the inert gas. There is a temperature-dependent induction period. Experiments with formaldehyde-d₂ show that the pyrolysis proceeds by a radical chain mechanism. The formation of the radical H₃CO has been detected. The observed activation energy (28 kcal/mole) is surprisingly low but is consistent with many other low values observed for initial stages of pyrolytic reactions as measured in shock tubes. The

first stage in the oxidation consists mainly of the decomposition of CH_2O into CO and H_2 , followed by a branching chain oxidation of the hydrogen as well as of the remaining formaldehyde.

The oxidation of ammonia under homogeneous conditions has been studied by Takeyama and Miyama.⁽¹¹⁵⁾ When mixtures of NH_3 , O_2 and Ar were shock-heated to temperatures $1550^\circ\text{--}2300^\circ\text{K}$, there was a delay in the appearance of OH, and as in the case of the H_2/O_2 reaction, $\log (\text{O}_2)\tau$ varied linearly with the reciprocal of the temperature. Following the induction period, the early stages of the reaction were monitored by recording the UV absorption by NH_3 at 2245\AA . They found

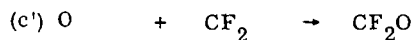
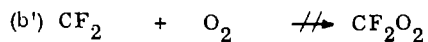
$$-d[\text{NH}_3]/dt = k_0 [\text{NH}_3]^{1.5} [\text{O}_2]^{0.5} [\text{Ar}]^{0.5}$$

The apparent activation energy is 38.8 ± 2.6 kcal/mole.

The oxidation of hydrogen sulfide in shock waves⁽¹¹⁶⁾ was observed by measuring the concentration of OH (in absorption) and of the generated SO_2 at 2909A and 2812A. The studies covered the temperature range 1350° to 2450°K . Two regimes were recognized; below 1560°K , OH and SO_2 appear concurrently after an induction period. Above 1700°K , SO_2 appears before OH. The authors proposed a branching chain mechanism, which at the higher temperatures includes the reaction $\text{O} + \text{H}_2\text{S} \rightarrow \text{SO} + \text{H}_2$. This provides an additional route for the formation of SO_2 and leads to a reduction in its induction period. They also found that the addition of hydrogen did not alter the basic features of the hydrogen sulfide oxidation. Additional hydrogen did reduce the induction period for the appearance of SO_2 and OH. The oxidation of H_2S is accelerated by hydrogen but the oxidation of hydrogen appears to be inhibited by H_2S .

A single-pulse shock tube study of the oxidation of perfluoroethylene was referred to above.⁽⁹⁶⁾ The mechanism of oxidation of fluorocarbons is characterized by comparative simplicity, in contrast to the many unresolved problems which remain in the area of hydrocarbon oxidations. The key feature is the rapid production of CF_2 , which reacts with the oxygen according to the following scheme:

				ΔH_{300}° (JANAF)
				kcal/mole
(a)	C_2F_4	\rightleftharpoons	2CF_2	+ 76.1
(b)	CF_2	+ O_2	$\rightarrow \text{CF}_2\text{O} + \text{O}$	- 52.4
(c)	O	+ C_2F_4	$\rightarrow \text{CF}_2\text{O} + \text{CF}_2$	- 95.5
(d)	CF_2	+ CF_2O	$\rightarrow \text{CF}_3 + \text{CFO}$	+ 38.4
(e)	CF_2	+ CFO	$\rightarrow \text{CF}_3 + \text{CO}$	- 58.5
(f)		2CF_3	$\rightleftharpoons \text{C}_2\text{F}_6$	- 92.8
(g)	CF_2	+ C_2F_4	$\rightleftharpoons \text{C}_3\text{F}_6$ (propene)	- 63.8
(h)	C_3F_6	+ O	$\rightarrow \text{CF}_2\text{O} + \text{C}_2\text{F}_4$	-107.8
(i)	CF_2	+ C_2F_6	$\rightarrow \text{CF}_4 + \text{C}_2\text{F}_4$	- 17.0
(j)	CF_3	+ CFO	$\rightarrow \text{CF}_4 + \text{CO}$	- 91.



~171.

This sequence accounts for the observed product distributions as functions of the temperature, for several compositions of ethylene and oxygen. The detailed confirmation of the individual steps and their reaction rate constants will have to be obtained from mass spectrometric diagnostics.

CONCLUSION

It is amusing to attempt to pinpoint the salient features of shock tube chemical kinetics. Among the many attractive ones, the most worthwhile in my opinion is the specificity in identification of transient species (and of states) on a time-resolved basis; the most troublesome is the lack of sufficiently precise temperature measurement; the most intriguing is the need to exploit sophisticated computer programs in order to unravel the coupling of reactions in a complex system.

ACKNOWLEDGMENT

This work was supported by the AFOSR under Grant No. AF49(638)-1448, to whom sincere thanks are due.

TABLE I. Instrumentation and Techniques

Description	Function	Author	Ref.
Heated shock tube; driven gas: pure Cs vapor (1 torr)	Plasma generation (16,000°K); study of magneto-fluid dynamics	H. G. Ahlstrom and P. A. Pincosy	STS #1
Heated shock tube (300° C) driven gas: Hg vapor	Plasma dynamics and spectroscopic studies	Y. W. Kim and O. Laport	STS #F10
Vaporization of aerosol in shock tube; metal wire exploded in controlled atm. prior to shock heating	0.05μ particles Al produced; spectra of vaporized ablation products	W. H. Wurster	STS #B3
Particles dispersed in test gas prior to shock heating (3-5μ teflon)-record emission and absorption spectra	Study of burn-up rates of small particles	R. Watson, <u>et al</u>	STS #F4
Alkali halide smoke in Ar - record absorption spectra	Study dissociation of MX into ions- time resolved spectra	M. Coplan, <u>et al</u>	STS #E8
Electric shock tube	Improvement in linear driver	R. G. Fowler	(4)
Spectroradiometric pyrometer; resolving time: 10μ sec	Measure temperatures of shock heated gases, and of self sustaining detonations	G. J. Penzias, <u>et al</u>	(5)
Relative emission intensities at two wavelengths in a molecular band system	Estimate temperature of shock heated gases	R. Watson	(6)
Induction flow meter (transverse Field)	Measure gas velocities in shock tubes- ionizing conditions	P. A. Croce	(7)
Electron beam probe: fluorescence stimulated by 17.5 KV electrons	Measure density in free jets and shock fronts; estimate rotational and vibrational temperatures	P. V. Marone	(8)
Laser light source	Diffusive separation of He, Ar in jets	D. E. Rothe	(9)
Single-pulse shock tube - double diaphragm design (exploding wire diaphragm opener)	For schlieren and interferometer systems - measure densities and gradients General pyrolysis studies	A. K. Oppenheim, <u>et al</u> S. Witting	(10) STS #48

TABLE II. On Non-Ideal Behavior of Shock Tubes

Topic	Coverage	Author	Ref.
Temperature variation behind attenuating shocks	2000-2700° K in O ₂ , N ₂ Used Na line reversal ²	T. A. Holbeche and D. A. Spence	(25)
Flow non-uniformity when shock front and contact surface have reached maximum separation	All fluid properties increase in value; non-uniformity greatest when γ is large and M is low; applies to turbulent and laminar boundary layers.	H. Mirels	(26)
Attenuation of shock due to non-equilibrium ionization and radiation	Attenuation calculated using linearized theory, with $\alpha \ll 1$.	J. Rosciszewski	(27)
Radiative cooling and self absorption--- effect on flow field and on heat transfer behind reflected shock waves in air	Numerical calculations for radiating reflected shock heated plasmas (air)	R. M. Nerem and R. A. Golobic	(28)
Brightness temperature of shock waves in xenon and air	Effect of self-absorption of radiation emitted by shock front on estimation of brightness temperature; theoretical analysis	A. E. Voitenko, <u>et al</u>	(29)

TABLE III. Ionization Cross-Sections and Oscillator Strengths

Substances	Measurement of --	Results	Author	Ref.
Kr and Xe	Identify ions in shock heated mixtures via mass spectra	Impurity ions present; no di-atomic ions appeared	R. Creswell, <u>et al</u>	(30)
Ar, Kr and Xe (5000-9000°K)	Ionization relaxation times from micro-wave attenuation; high purity system	Quadratic dependence on density; rate controlling step is excitation to lowest group of excited states	A. J. Kelly	(31)
Ar (monitor continuum emission at 4900°A)	Effect of impurities on time required to reach half of maximum intensity.	Pronounced effects due to H containing impurities	P. B. Coates	(32)
Ar	Ionization relaxation times (micro-waves)	Impurities blamed for very short times	S. Naki, <u>et al</u>	(33)
Air	Ionization rates behind strong shocks from IR emission at 6μ (free-free bremsstrahlung).	N + O → NO ⁺ + e ⁻ is pre-dominant mechanism for shock speeds less than 9.5 mm/μsec	J. Wilson	(34)
Cr(CO) ₆ in Ar	Ionization mechanism for Cr, from time resolved Cr(I) and Cr(II) emission spectra	Initial rate controlled by excitation to 3.1 ev lengths for Cr(I); rapid excitation to higher levels; ionization from excited states	W. L. Shackelford <u>et al</u>	(35)
Cr(CO) ₆ in Ar--reflected shocks	gf - values for Cr(II) from emission intensities at 8000°K	21 lines in region 3118-4559Å; these values are ≈0.1 of values obtained from arc spectra	W. L. Shackelford	(36)
Ar-CO (1/1)	C ₂ emission; matrix element for 3Π _g -3Π _u (Swan) bands	Calculated equi. C ₂ concentration; Report f = -.022 ± .008	A. G. Sviridov, <u>et al</u>	(37)
Ar-CO (1/1)	C ₂ absorption - Swan band system	Calculated equi. C ₂ ; estimated R _e ² = 0.44 ± 0.08 a.u.	A. G. Sviridov, <u>et al</u>	(38)
C ₂ H ₂ , C ₂ N ₂ , CO	Incident shocks - Swan band emission	f _{Swan} = -.033 ± 0.012	A. R. Fairbairn	(39)
C ₂ CF ₃ , CF ₄ , C ₂ F ₄	Emission intensities for C ₂ (A 3Π - X 3Π), and CF (A 2Σ - X 2Π)	f _{Swan} = -.028 ± .009 f _{CF} = 0.0051 ± .0015	J. A. Harrington <u>et al</u>	(40a, b)
Air	Various band systems for N ₂ , O ₂ , NO, H ₂ O	Oscillator strengths for intense bands; (ff) and (fb) continua	xxx	(41)
SO ₂ -Ar	Spectroscopically resolved emission intensities	Broad band due to three excited states (C, ¹ B ₂ , ³ B ₁)	B. P. Levitt and D. B. Shien	(42)

TABLE IV: Dissociation Rate Studies

Molecule	Medium	Experiment or Theory	Results	Author	Ref.
O ₂	Ar	Analysis of ladder climbing process	$k_d \propto [1 - \exp(-h_\omega/kT)] \times \exp(-D/RT)$	N. V. Kondratiev and E. E. Nikitin	70
2O → O ₂ + hν		Radiative recombination data; 2500° to 3800°K	Intensity $\propto (O)^2$ apparent $E_A = 28.9 \pm 2.2$	B. F. Myers and E. R. Bartle	STS #29
O	O ₂	Gladstone-Dale constant measured for O ₂ and O	O ₂ : G. D. = 1.93 cm ³ /gm O: G. D. = 2.04 cm ³ /gm	J. H. B. Anderson	STS #E4
N ₂	Ar	Dissociation rates; incident shocks (6000° - 9000°K)	Relative efficiencies N > N ₂ > Ar by 15:1:½	S. Byron	71
N ₂	Kr	Dissociation rates; incident shocks (5000° - 9000°K) 5% - 10% - 25% - 50%	Analysis incomplete (results agree with 71)	E. Wachsler	72
F ₂	Ne, Ar	TOF mass spec (1650° - 2700°K)	$E_A \approx 27$ kcal/mole; general agreement with previous work	R. W. Diesen	73
F ₂	Kr, Xe	Light absorption; dependence on F ₂ concentration	For Ar, $E_A = 27.3 \pm 2.5$ kcal/mole Kr essentially like Ar; Xe-F ₂ complex indicated (under shock conditions)	D. J. Seery and D. Britton	74
Cl ₂	Ar	Radiative recombination rates for 1:5 Cl ₂ -Ar mixtures; 1735° - 2582°K.	$k_r = 10^{13.94} \exp(-48,300/RT)$ cm ³ mole ⁻¹ sec ⁻¹	R. A. Carabetta and H. B. Palmer	75
Br ₂	Ar	Radiative recombination rates	Details not given - cite agreement with previous investigations	T. R. Lawrence and G. Burns	STS #B5

TABLE V. Rate Parameters for the Fission of Simple Hydrocarbons
 (from ref. 99)

Reaction Product	CH ₃		CH ₃ CHCH ₃		CH ₃ $\overset{\text{CH}_3}{\underset{ }{\text{C}}}$ -CH ₃		CH ₂ =CH-CH ₂	
	log ₁₀ A	E _A	log ₁₀ A	E _A	log ₁₀ A	E _A	log ₁₀ A	E _A
CH ₃	15.0	82.8	16.0	80.2	16.1	78.2	15.0	70.3
CH ₃ CHCH ₃			16.1	76.0	16.2	73.0	15.7	67.9
CH ₃ $\overset{\text{CH}_3}{\underset{ }{\text{C}}}$ -CH ₃					16.3	68.5	15.8	65.5
CH ₂ =CH-CH ₂							14.2	59.3

TABLE VI. Summary of Molecular Exchange Reactions, in Shock Tubes

$$d[AX]/dt = k[AB]^\alpha [X_2]^\beta [Ar]^\gamma$$

AB	X ₂	α	β	γ	E _A (kcal/mole)	A(T ^{3/2}) [moles/liter]	Ref.
H ₂	D ₂	0.38	0.66	0.98	42.26 ± 2.1	10 ^{9.84} T ^{1/2}	100
HSH	D ₂	0.47	0.98	0.61	52.3 ± 2	10 ^{10.43} T ^{1/2}	103
HNH ₂	D ₂	≈ 0	≈ 1	≈ 1	39 ± 3	10 ⁸ T ^{1/2}	102
HCH ₃	D ₂	0.3	1.1	0.6	52.00 ± 2.2	10 ^{9.04} T ^{1/2}	101
N ₂ (28)	N ₂ (30)	0.5	0.5	1.0	116 ± 3	10 ^{10.82}	104
O ₂ (32)	O ₂ (36)	0.5	0.5	≈ 1.0	37 ± 4	10 ⁹	105

REFERENCES

1. H. Oertel, STOSSROHRE, Springer-Verlag, Wien, 1966, 1030 pages; bibliography (p. 858-981), author and subject indices (p. 986-1030); 621 figures, 152 tables. Mss. completed in October 1963 but some publications which appeared in 1964 are included in the bibliography.
2. Abstracts, 6th International Shock Tube Symposium, Freiburg, Germany, April 12-14 (1967).
[References to these abstracts will be designated by STS # xx]
3. AGARD Colloquium (28th Propulsion and Energetics Panel Meeting) Oslo, Norway, May 16-20 (1966).
4. R. G. Fowler, Rev. Sci. Inst., 37, 545 (1966).
5. G. J. Penzias, S. A. Dolin and H. A. Kruegle, Applied Optics, 5, 225 (1966).
6. R. Watson, Applied Optics, 5, 215 (1966).
7. P. A. Croce, Rev. Sci. Inst., 36, 1561 (1965).
8. P. V. Marrone, Phys. of Fluids, 10, 521 (1967).
9. D. E. Rothe, Phys. of Fluids, 9, 1643 (1966).
10. A. K. Oppenheim, P. A. Urtiew and F. J. Weinberg, Proc. Roy. Soc. (London), 291, 279 (1966).
11. J. H. Kiefer and R. W. Lutz, J. Chem. Phys., 44, 658, 668 (1966); 45, 3889 (1966).
12. W. C. Gardiner, et al, J. Chem. Phys., 44, 4653 (1966).
13. G. B. Kistiakowsky and P. H. Kydd, J. Am. Chem. Soc., 79, 4825 (1957).
14. J. E. Dove and D. McL. Moulton, Proc. Roy. Soc., A283, 216 (1965).
15. R. W. Diesen and W. J. Felmler, J. Chem. Phys., 39, 2115 (1963).
16. A. P. Modica, J. Phys. Chem., 69, 2111 (1965).
17. D. Gutman, A. J. Hay and R. L. Bedford, J. Phys. Chem., 70, 1786 (1966).
18. G. F. Marsters, S. H. Bauer and E. L. Resler, Jr., Proc. 5th International Shock Tube Symposium, U. S. Naval Ord. Lab., May 1966, Ed. W. S. Filler (p. 155). See also: T. A. Milne and F. T. Greene, Summary Tech. Report to Power Branch, ONR, 8 May 1967 [Contract, Nonr-3599(00); Project No. 092-513].
19. B. Sturtevant, J. Fluid Mech., 25, 641 (1966).
See also: Dissertation submitted by C. P. Wang, May 1967 to Cal. Inst. Tech., Graduate Aeronautical Labs.
20. J. Wilson, J. Fluid Mech., 15, 497 (1963).
Also, see M. W. Slack, et al, STS #A4.
21. S. H. Bauer and W. S. Watt, J. Chem. Phys., 44, 1327 (1966).
22. F. J. Stoddard and W. S. Watt, Report to Arnold Engineering Development Center, distributed May, 1967 by Cornell Aero Lab, [AEDC-TR-67-65].
23. R. A. Hartunian, W. P. Thompson and E. W. Hewitt, J. Chem. Phys., 44, 1766 (1966). See also: R. W. F. Gross, STS #F1.
24. R. V. Petrella, T. L. Spink and L. T. Finlayson, Rev. Sci. Inst., 37, 1500 (1966).
25. T. A. Holbeche and D. A. Spence, Proc. Roy. Soc. (London), A279, 111 (1964).
26. H. Mirels, Physics of Fluids, 9, 1907 (1966).
27. J. Rosciszewski, Physics of Fluids, 10, 269 (1967).

28. R. M. Nerem and R. A. Golobic, STS #30.
29. A. E. Voitenko, I. Sh. Model' and I. S. Samodelov, *Soviet Physics (Doklady)* 11, 596 (1967).
30. R. Creswell, M. A. DiValentin and J. E. Dove, *Physics of Fluids*, 9, 2285 (1966).
- 31a. A. J. Kelly, *J. Chem. Phys.*, 45, 1723 (1966).
- 31b. A. J. Kelly, *J. Chem. Phys.*, 45, 1733 (1966).
32. P. B. Coates, *Nature*, 211, 300 (1966).
33. S. Nakai, K. Kasuya and C. Yamanaka, *J. Phys. Soc. Japan*, 21, 805 (1965).
34. J. Wilson, *Physics of Fluids*, 9, 1913 (1966).
35. W. L. Shackleford and S. S. Penner, *J. Chem. Phys.*, 45, 1816 (1966).
36. W. L. Shackleford, *J. Quant. Spectrosc. Radiat. Transfer*, 5, 303 (1965).
37. A. G. Sviridov, N. N. Sobolev and V. M. Sitovski, *J. Quant. Spectrosc. Radiat. Transfer*, 5, 525 (1965).
38. S. G. Sviridov, N. N. Sobolev and M. Z. Novgorodov, *J. Quant. Spectrosc. Radiat. Transfer*, 6, 337 (1966).
39. A. R. Fairbairn, *J. Quant. Spectrosc. Radiat. Transfer*, 6, 325 (1966).
- 40a. J. A. Harrington, A. P. Modica and D. R. Libby, *J. Chem. Phys.*, 44, 3380 (1966).
- 40b. However, note also, T. Wentink, Jr. and L. Isaacson, *J. Chem. Phys.*, 46, 603 (1967).
- 41a. D. R. Churchill and R. E. Meyerott, *J. Quant. Spectrosc. Radiat. Transfer*, 5, 69 (1965). [For remaining parts of ref. 41, see end of list.]
42. B. P. Levitt and D. B. Sheen, *Trans. Farad. Soc.*, 63, 540 (1967).
43. M. G. Ferguson and A. W. Read, *Trans. Farad. Soc.*, 63, 61 (1967).
44. P. Borrell, *Chem. Soc. Spec. Publication 20*, (Academic Press, 1966) p. 263.
45. T. L. Cottrell, *Int. Inst. Chem.*, 12th Conference, 1962 (Interscience N. Y. 1964).
46. R. C. Millikan, E. Switkes and L. A. Osburg, *Bull. Amer. Phys. Soc.*, 11, 201 (1966).
- 47a. J. G. Parker, *Phys. Fluids*, 2, 449 (1959).
- 47b. J. G. Parker, *J. Chem. Phys.*, 45, 3641 (1966).
48. R. C. Millikan, *Molecular Relaxation Processes*, Chemical Society Special Publication No. 20, pp. 219-233 (Burlington House, London, 1966).
49. C. B. Moore, *J. Chem. Phys.*, 43, 2979 (1965).
50. A. B. Callear and G. J. Williams, *Trans. Farad. Soc.*, 62, 2030 (1966).
51. J. G. Parker and R. H. Swope, *J. Chem. Phys.*, 43, 4427 (1965).
52. D. R. White, *J. Chem. Phys.*, 46, 2016 (1967).
53. R. W. Lutz and J. H. Kiefer, *Phys. of Fluids*, 9, 1638 (1966).
54. J. H. Kiefer and R. W. Lutz, private communication.
55. S. H. Bauer and S. C. Tsang, *Phys. Fluids*, 6, 182 (1963).
56. I. R. Hurle, A. L. Russo and J. G. Hall, *J. Chem. Phys.*, 40, 2076 (1964).
57. A. L. Russo, *J. Chem. Phys.*, 44, 1305 (1966).

58. C. E. Treanor, J. W. Rich, and R. G. Rehm, report to Mechanics Division of the AFOSR under Contract No AF49(638)-1488.
59. J. P. Appleton, STS #B7; see also, J. P. Appleton and M. Steinberg, *J. Chem. Phys.*, 46, 1521 (1967).
60. C. J. S. M. Simpson, K. B. Bridgman and T. R. D. Chandler, STS #B9.
61. D. Weaner, J. F. Roach and W. R. Smith, *Bull. Am. Phys. Soc.*, 12, 836 (1967).
62. C. B. Moore, R. E. Wood, B-L. Hu, and J. T. Yardley - pre-publication manuscript.
63. R. L. Taylor, M. Camac and R. M. Feinberg, AVCO Everett Research report #250, May 1966; To appear: Proceedings 11th Combustion Symposium.
64. R. L. Taylor and S. Bitterman, Pre-publication report.
65. J. D. Lambert, *Quart. Reviews*, 21, 67 (1967).
J. D. Lambert, D. G. Parks-Smith and J. L. Stretton, *Proc. Roy. Soc., A*, 282, 380 (1964).
66. W. S. Watt and A. L. Myerson, STS #E3.
67. I. R. Hurler, 11th Symposium (International) on Combustion, Berkely, California, August 1966.
68. S. H. Bauer, AGARD Colloquium, May 1966.
69. J. C. Keck, *Discussion Farad. Soc.*, 33, 173 (1962).
70. V. N. Kondratiev and E. E. Nikitin, *J. Chem. Phys.*, 45, 1078 (1966).
- 71a. S. Byron, *J. Chem. Phys.*, 44, 1378 (1966).
- 71b. K. L. Wray and S. Byron, *Phys. Fluids*, 9, 1046 (1966); and B. Cary, *Phys. Fluids*, 9, 1047 (1966).
72. E. Wachsler, Dissertation, Cornell University, 1967.
73. R. W. Diesen, *J. Chem. Phys.*, 44, 3662 (1966).
74. D. J. Seery and D. Britton, *J. Phys. Chem.* 70, 4074 (1966).
75. R. A. Carabetta and H. B. Palmer, *J. Chem. Phys.*, 46, 1325, 1333, 1538 (1967).
76. T. A. Jacobs, R. R. Giedt and N. Cohen, *J. Chem. Phys.*, 43, 3688 (1965).
77. J. F. Spinnler, Report No. S-127, Rohm and Haas Redstone Arsenal Research Labs., April 1967.
78. T. A. Jacobs, N. Cohen and R. R. Giedt, *J. Chem. Phys.*, 46, 1958 (1967).
79. E. S. Fishburne, *J. Chem. Phys.*, 45, 4053 (1966).
- 80a. H. J. Kolker, *J. Chem. Phys.*, 44, 582 (1966).
- 80b. C. A. Brau, J. C. Keck and G. F. Carrier, *Phys. Fluids*, 9, 1885 (1966).
- 80c. C. A. Brau, Avco Everett Research Laboratory, Report 261, December 1966.
- 80d. N. S. Snider, *J. Chem. Phys.*, 45, 3299 (1966).
81. H. A. Olschewski, J. Troe and H. Gg. Wagner, *Ber. Bunsengesellschaft. physik chem.*, 70, 450 (1966).
82. A. Martinengo, J. Troe, and H. Gg. Wagner, *Zeit. Phys. Chem.* 51, 104 (1966).
83. J. Troe and H. Gg. Wagner, AGARD Colloquium, Oslo, May 1966.

84. H. A. Olschewski, J. Troe and H. Gg. Wagner, 11th Symposium (International) on Combustion, Berkeley, August 1966.
85. S. H. Bauer, G. L. Schott, and R. E. Duff, *J. Chem. Phys.*, 28, 1089 (1958).
86. W. O. Davies, *J. Chem. Phys.*, 43, 2809 (1965).
87. E. S. Fishburne, K. R. Bilwakesh and R. Edse, *J. Chem. Phys.*, 45, 160 (1966).
88. H. A. Olschewski, J. Troe and H. Gg. Wagner, *Zeit. Physik. Chem.*, 45, 329 (1965).
89. D. Marshall and S. H. Bauer, unpublished data, Cornell University report to NASA, January 1966.
90. H. J. Henrici, Dissertation, Göttingen, 1966.
K. W. Michel and H. Gg. Wagner, 10th Symposium (International) on Combustion, The Combustion Inst., Pittsburgh, (1965), p. 353.
91. A. P. Modica and D. F. Hornig, *J. Chem. Phys.*, 43, 2739 (1965).
92. W. Tsang, S. H. Bauer, and M. Cowperthwaite, *J. Chem. Phys.*, 36, 1768 (1962);
See also: D. Schofield, W. Tsang and S. H. Bauer, *J. Chem. Phys.*, 42, 2132 (1965).
93. A. P. Modica and J. E. LaGraff, *J. Chem. Phys.*, 44, 3375 (1966).
94. A. P. Modica and J. E. LaGraff, *J. Chem. Phys.*, 45, 4729 (1966).
95. A. P. Modica, *J. Chem. Phys.* 46, 3663 (1967).
96. S. H. Bauer, K. C. Hou, and E. L. Resler, Jr., STS #E7.
97. I. D. Gay, R. D. Kern, G. B. Kistiakowsky, and H. Niki, *J. Chem. Phys.*, 45, 2371 (1966).
98. W. Tsang, *J. Chem. Phys.*, 44, 4283 (1966).
99. W. Tsang, *J. Chem. Phys.*, 46, 2817 (1967).
100. S. H. Bauer and E. Ossa, *J. Chem. Phys.*, 45, 434 (1966).
101. W. S. Watt, P. Borrell, D. Lewis, and S. H. Bauer, *J. Chem. Phys.*, 45, 444 (1966).
102. A. Lifshitz, C. Lifshitz, and S. H. Bauer, *J. Am. Chem. Soc.*, 87, 143 (1965).
103. D. Lewis, et al, Prepublication report
104. A. Bar-Nun and A. Lifshitz [Prepublication report].
105. H. Carroll, and S. H. Bauer, Prepublication report.
106. K. Morokuma, L. Pedersen and M. Karplus, In press.
107. R. D. Hawthorn and A. C. Nixon, *AIAA Journal*, 4, 513 (1966).
108. G. B. Skinner and G. H. Ringrose, *J. Chem. Phys.*, 43, 4129 (1965).
109. D. L. Ripley and W. C. Gardiner, Jr., *J. Chem. Phys.*, 44, 2285 (1966).
110. J. B. Homer and G. B. Kistiakowsky, *J. Chem. Phys.*, 45, 1359 (1966).
111. J. B. Homer and G. B. Kistiakowsky, Submitted to *Journal of Chemical Physics*.
112. G. P. Glass, et al. *J. Chem. Phys.*, 42, 608 (1965).
113. I. D. Gay, G. P. Glass, R. D. Kern and G. B. Kistiakowsky, Submitted to *The Journal of Chemical Physics*.

114. I. D. Gay, G. P. Glass, G. B. Kistiakowsky and H. Niki, *J. Chem. Phys.*, 43, 4017 (1965).
115. T. Takeyama and H. Miyama, *Bull. Chem. Soc., Japan*, 39, 2352 (1966); *Bull. Chem. Soc., Japan*, 38, 1670 (1965).
116. J. N. Bradley and D. C. Dobson, *J. Chem. Phys.*, 46, 2865, (1967); *J. Chem. Phys.*, 46, 2872 (1967).

NOTE

The complete set of references that comprise (41) are:

- 41a. D. R. Churchill and R. E. Meyerott, *J. Quant. Spectrosc. Radiat. Transfer*, 5, 69 (1965).
- 41b. K. L. Wray and T. J. Connolly, *J. Quant. Spectrosc. Radiat. Transfer*, 5, 111 (1965).
- 41c. R. A. Allen, A. Textoris and J. Wilson, *J. Quant. Spectrosc. Radiat. Transfer*, 5, 95 (1965).
- 41d. M. Jeunehomme, *J. Chem. Phys.*, 44, 4253 (1966).
- 41e. R. W. Patch, *J. Quant. Spectrosc. Radiat. Transfer*, 5, 137 (1965).

A SHOCK TUBE STUDY OF METHANE OXIDATION

Daniel J. Seery and Craig T. Bowman

United Aircraft Research Laboratories
East Hartford, Connecticut 06108

Although the oxidation of methane has been studied extensively there are still many unsolved problems related to the kinetics and mechanism of the reaction. The objective of the present investigation is to provide information on the reaction mechanism and chemiluminescence for the high temperature oxidation of methane. To this end an experimental study of methane oxidation behind reflected shock waves has been carried out. In this study pressure, OH, CH, CO, C₂ and H₂O emission and OH absorption were monitored during the reaction. In conjunction with the experimental work, an analytical study of methane oxidation was carried out. Using a proposed fifteen-step reaction mechanism, temperature, pressure and concentration profiles were calculated for the conditions of the experiment.

EXPERIMENTAL

The experimental study was carried out in a stainless steel cylindrical shock tube (shown in Fig. 1) having an internal diameter of 3.8 cm. The driver gas used in all experiments was room-temperature helium. To assure uniform diaphragm bursting pressures, a double diaphragm technique was employed (Ref. 1). Shock velocities were measured using four platinum heat transfer gauges mounted along the wall of the tube. The signals from these heat transfer gauges were displayed on a raster-sweep oscilloscope. The observation station was located 5.70 m from the diaphragm, and consisted of four observation ports. These ports were used to make various spectroscopic and pressure measurements. The reaction was studied behind reflected shock waves at a location 1 cm from the reflecting surface. This configuration gave a maximum test time of approximately 2 msec.

Pressure measurements were made using a piezoelectric pressure transducer (Kistler Model 605) with a 0.375 cm diameter pressure-sensitive diaphragm and a rise time of 3 μ sec. Two optical paths were available to monitor the emission and/or absorption of characteristic radiation during the reaction. The principal spectroscopic instrument was a 0.5 m Seya-Namioka vacuum monochromator equipped with an EMI/US 6255B photomultiplier. The entrance and exit slit widths were set to give a bandwidth of approximately 25 Å. The monochromator was used for both emission and absorption experiments. For the absorption experiments a Hg-Xe arc lamp (Hanovia 528B-1) was employed. Additional emission data were obtained from the other optical station using an EMI/US 9558BQ or a Philips 56CVP photomultiplier with various narrow-band pass interference filters. Sapphire windows were used for all optical stations. The output signals from the pressure transducers and photomultipliers were displayed on two dual-beam oscilloscopes which were triggered by one of the heat transfer gauges. The rise time of the photomultiplier/oscilloscope system was 2-3 μ sec.

The methane, oxygen and argon used in the experiments were Matheson Ultrapure Grade ($>99.9\%$), and the nitrogen was Linde High Purity Dry (99.9%).

Gas mixtures were prepared manometrically and stored in stainless steel or glass vessels. These vessels were evacuated to a pressure of less than 1μ Hg before preparing the mixture. Mixture total pressures varied from 300-3000 mm Hg. Composition of the gas mixtures was confirmed using a mass spectrograph. The mixtures were allowed to stand for at least 48 hours before use in an experiment.

Before a run, the experimental section of the shock tube was evacuated to less than 1μ Hg. The leak and outgassing rate was less than 2μ Hg/min. Initial pressures of the gas in the experimental section varied between 15-150 mm Hg.

In all the experiments the temperature behind the reflected wave was obtained from the ideal shock equations and the measured incident shock velocity at the reflecting surface with a suitable correction for "non-ideal" shock reflection (Refs. 2 and 3). In the present investigation a temperature correction of -35 deg K with an uncertainty of 35 deg K was employed. This correction was based on the results of a study of reflected shock temperature in argon. In this study reflected shock temperatures were obtained from measurements of incident and reflected shock velocities using an approach suggested by Skinner (Ref. 3). This approach could not be used with the fuel/oxidizer mixtures due to gas dynamic acceleration of the reflected shock wave in the vicinity of the reflecting plate. Hence a direct determination of a temperature correction was not possible for the fuel/oxidizer mixtures.

Due to boundary layer effects, the pressure behind the reflected shock wave decreased in time. It was assumed that pressure and temperature behind the reflected wave were related through the isentropic equations. This assumption is not strictly correct due to heat transfer and chemical reaction effects. It is felt, however, that the error introduced by this assumption is small.

The temperature for a given run was assumed to be a linear average of the temperature directly behind the reflected shock wave (corrected for "non-ideal" reflection) and the temperature directly before the increase in pressure accompanying the chemical reaction. A similar averaging technique was employed for the pressure. Since variations in temperature and pressure behind the reflected wave were small, a linear averaging is acceptable.

EXPERIMENTAL RESULTS

The oxidation reaction was studied using pressure measurements and spectroscopic observations. The spectroscopic measurements involved the emission and absorption of the OH radical (3067 Å) and the emission of CH (4315 Å), CO (2200 Å), C₂ (5165 Å) and H₂O (9300 Å). Typical oscilloscope traces are shown in Figures 2, 3 and 4. The bottom trace in Figures 2 and 3 is the output of the pressure transducer. The arrival of the incident and reflected shock waves at the observation station and the increase in pressure due to chemical reaction are indicated in the figures. The top trace in Fig. 2 is the photomultiplier output showing OH emission. From the pressure and OH emission traces of Fig. 2 it is seen that the reaction appears to pass through two phases - a first (induction) phase in which the pressure and OH emission increase slowly followed by a second phase in which the pressure and OH emission increase rapidly. As will be discussed later, these observations are consistent with the results of the analytical study. The top trace in Fig. 3 is the photomultiplier output showing CH emission. From this figure it is seen that excited CH(²Δ) is probably short-lived, undergoing a maximum in concentration just prior to the onset of fast reaction. In Fig. 4 the top trace is the photomultiplier output showing OH emission and the bottom trace shows OH absorption. It is apparent that the onset of emission and absorption occur simultaneously, indicating that the concentration of excited state (²Σ) and ground state (²Π) OH increase approximately at the same time.

For the purpose of comparing the experimental and analytical results it is convenient to characterize the oxidation of methane by an induction time. There is no generally accepted definition of induction time. In the present study the induction time was defined to be the time between the heating of the gas by the reflected shock wave and the rapid increase in pressure or characteristic emission or absorption. This definition permits a simple comparison between experimental and analytical results and is not dependent on the threshold of the instrumentation.

Induction time data for methane oxidation are presented in Figs. 5 through 8. In these figures the mole percent of methane, oxygen and argon or nitrogen in the mixture is given together with the fraction stoichiometric, Φ , where

$$\Phi = \frac{(X_{\text{CH}_4}/X_{\text{O}_2})}{(X_{\text{CH}_4}/X_{\text{O}_2})_{\text{stoichiometric}}}$$

and X is the mole fraction. The solid lines through the data points are a least-squares fit of the experimental data to an equation of the form

$$\tau = A \exp (E/RT)$$

where τ = induction time, T = temperature, and A and E = constants. The parameters A and E and the standard deviation in E are obtained from the least-squares reduction of the data, and are tabulated in Table 1.

Table 1. Least-Squares Parameters: Methane-Oxygen-Diluent

Φ	Diluent	$P(\text{atm})$	$A(\text{sec})$	$E\left(\frac{\text{kcal}}{\text{mole}}\right)$	σE
0.5	N_2	1.7	1.6×10^{-10}	44.7	3.7
0.5	Ar	1.7	2.3×10^{-10}	44.3	1.4
0.5	Ar	3.7	4.5×10^{-11}	46.6	4.3
0.5	Ar	6.0	2.1×10^{-12}	53.2	6.0
1.0	Ar	2.0	5.8×10^{-11}	49.0	2.1
2.0	Ar	1.7	2.1×10^{-10}	45.4	4.8

The induction time for oxidizer-rich ($\Phi = 0.5$) methane/oxygen/argon and methane/oxygen/nitrogen mixtures for an average pressure of 1.7 ± 0.3 atm is presented as a function of temperature in Fig. 5. In this figure the induction time is based on the rapid increase in pressure. It is noted that in the present study there was no observed difference between induction times based on rapid increase in pressure or those based on rapid increase in characteristic emission or absorption. The solid line is the least-squares fit of the methane/oxygen/argon data. From Fig. 5 and Table 1 it is seen that within the experimental uncertainty and for a given temperature the induction time is the same for the methane/oxygen/argon and the methane/oxygen/nitrogen mixtures. Hence for the conditions of the present investigation replacing nitrogen by argon in the oxidizer does not have a significant effect on the induction time.

The induction time for a stoichiometric methane/oxygen/argon mixture at an average pressure of 2.0 ± 0.3 atm is presented as a function of temperature in Fig. 6. From this figure it is seen that there is no significant difference between induction times based on OH emission or OH absorption.

The dependence of the induction time on the fraction stoichiometric ($\Phi = 0.5, 1.0, 2.0$) is presented in Fig. 7. The difference between the least-squares lines shown in this figure are within the experimental uncertainty presented in Table 1. Therefore there is no significant variation of the induction time with fraction stoichiometric in the range of $\Phi = 0.5$ to 2.0 (for induction times between $50 \mu\text{sec}$ and 1 msec).

A comparison of the induction times for an oxidizer-rich methane/oxygen/argon mixture ($\Phi = 0.5$) at average pressures of 1.7 ± 0.3 atm, 3.7 ± 0.4 atm and 6.0 ± 0.3 atm is presented in Fig. 8. It is apparent that for a given temperature as the pressure increases from 1.7 atm to 3.7 atm the induction time decreases. As the pressure increases to 6.0 atm no further decrease in induction time is observed. Also shown on Fig. 8 is a least squares fit of the ignition delay data of Snyder, et al (Ref. 4) for CH_4 -air, $P = 4$ atm and $\Phi = 0.5$. It is seen that there is good agreement between the two sets of data.

ANALYTICAL INVESTIGATION

In order to gain insight into the reaction mechanism for methane oxidation and to aid in understanding the experimental results a model calculation was performed using a fifteen-step reaction mechanism. The calculations were made using a computer program which numerically integrates the system of reaction kinetic and state equations to give the time rate of change of compositions and thermodynamic properties. In the present study the calculations were made assuming an adiabatic, constant volume reaction. Hence the model calculation closely approximates conditions behind a reflected shock wave.

The mechanism for methane oxidation at high temperature is probably different from the low-temperature, low-pressure mechanism of Enikolopyan (Ref. 5) which is used by many investigators. It is more probable that the same reactions that are important for methane flame propagation also are important in the high temperature oxidation of methane. The reaction mechanism and rate constants used for the calculations are presented in Table 2.

Table 2. Reaction Mechanism

Reaction	Rate Constant = $A \exp(-B/T)$		Ref.
	A*	B	
1. $\text{CH}_4 \rightarrow \text{CH}_3 + \text{H}$	3.8×10^{14}	51,900	6
2. $\text{CH}_4 + \text{H} \rightarrow \text{CH}_3 + \text{H}_2$	2.0×10^{14}	5,800	7
3. $\text{CH}_4 + \text{OH} \rightarrow \text{CH}_3 + \text{H}_2\text{O}$	2.85×10^{13}	2,500	8
4. $\text{CH}_4 + \text{O} \rightarrow \text{CH}_3 + \text{OH}$	1.0×10^{13}	4,030	7
5. $\text{CH}_3 + \text{O}_2 \rightarrow \text{CH}_2\text{O} + \text{OH}$	1.0×10^{11}	-0-	9
6. $\text{CH}_3 + \text{O} \rightarrow \text{CH}_2\text{O} + \text{H}$	1.9×10^{13}	-0-	7
7. $\text{CH}_2\text{O} + \text{OH} \rightarrow \text{HCO} + \text{H}_2\text{O}$	3.5×10^{14}	503	9
8. $\text{HCO} + \text{OH} \rightarrow \text{CO} + \text{H}_2\text{O}$	5.4×10^{12}	$T^{0.5}$ 252	9
9. $\text{CO} + \text{OH} \rightarrow \text{CO}_2 + \text{H}$	3.1×10^{11}	300	8

Table 2. Reaction Mechanism (Continued)

Reaction	Rate Constant = $A \exp(-B/T)$		Ref.
	A*	B	
10. $H + O_2 \rightarrow OH + O$	2.2×10^{14}	8,310	9
11. $O + H_2 \rightarrow OH + H$	1.1×10^{13}	4,730	9
12. $O + H_2O \rightarrow 2OH$	4.2×10^{13}	9,120	9
13. $H + H_2O \rightarrow H_2 + OH$	5.0×10^{13}	10,100	9
14. $H + H + M \rightarrow H_2 + M$	$5.0 \times 10^{18} T^{-1}$	-0-	9
15. $H + OH + M \rightarrow H_2O + M$	$4.5 \times 10^{21} T^{-1}$	-0-	9

* A is in $\text{cm}^3 \text{mole}^{-1} \text{sec}^{-1}$ except for (1) where the units are sec^{-1}

This mechanism is derived primarily from the flame studies of Fristrom and Westenberg (Ref. 7) and Fenimore and Jones (Ref. 9) plus the methane dissociation reaction to assist the initiation.

DISCUSSION

Before proceeding to a discussion of the experimental data it is of interest to consider some of the results of the analytical study (Figs. 9 and 10). Figure 9 shows the calculated temperature and pressure profiles for an initial temperature of 2000 deg K, an initial pressure of 3.4 atm and 0.5 fraction stoichiometric. The temperature and pressure increase slowly during the induction period and then increase rapidly. Calculated concentration profiles for several important species for the above conditions are presented in Fig. 10. The concentrations of the intermediates increase very rapidly during the early stages of the reaction and then maintain a nearly constant value through most of the induction period. The product species have different concentration profiles. CO and H₂O show a rapid increase early in the induction period and then increase almost linearly to their equilibrium concentrations. CO₂, on the other hand, increases almost linearly from the start and only at the very end of the induction period does it increase rapidly.

Calculations similar to those discussed above also have been made for initial temperatures of 1900 deg K and 1800 deg K (stoichiometry and initial pressure were identical with the 2000 deg K calculation). Qualitatively the temperature, pressure and concentration profiles are the same as for the 2000 deg K calculation except on a longer time scale. Since the calculated and observed pressure profiles are qualitatively the same, it is possible to compare calculated and observed induction times (based on rapid increase in pressure). The calculated induction times, presented in Fig. 8, exceed the experimental values by a factor of ten at 1800 deg K and by a factor of five at 2000 deg K. Considering the uncertainty in some of the

specific rate constants used in the reaction mechanism the difference between experiment and analysis is not unexpected. As an example, if the rate constant for reaction 10 is varied by a factor of ten there is a 30-40 percent variation in the calculated induction time at 2000 deg K. At lower temperatures variations in the rate constants of chain-branching reactions could have an even greater effect on the calculated induction times. In addition the neglect of certain chemical species in the analysis (e.g. HO_2 and H_2O_2) may contribute to the discrepancy especially at the lower temperatures.

At the present time the calculated concentration profiles only can be compared qualitatively with the experimental data. In particular it is noted that after the first few microseconds the calculated OH concentration increases approximately exponentially in time. Experimental results indicate that OH absorption (which is a measure of ground state OH concentration) also increases approximately exponentially in time.

It is of interest to compare the time variation of CH and OH emission and OH absorption in methane oxidation with similar observations in acetylene oxidation. Stubbeman and Gardiner (Ref. 10) have studied the oxidation of acetylene in a shock tube and observed OH emission and absorption (3067 Å) and visible chemiluminescence (4320 Å). It is probable that the 4320 Å emission is due to the ${}^2\Delta$ - ${}^2\Pi$ transition in CH. During the reaction a peaking of the 4320 Å emission (similar to that shown in Fig. 3) was observed. Coincident with the 4320 Å peak a pulse of OH emission at 3067 Å was observed. Following the tail-off of emission an increase in OH absorption was observed. In methane oxidation a peaking of CH emission is observed (Fig. 3); however OH emission and OH absorption are found to increase simultaneously during the reaction. If the lag between CH emission and OH absorption in acetylene oxidation is real then there must be different mechanisms for chemiluminescence in methane and acetylene oxidation. Indeed, Deckers (Ref. 11) has suggested that in acetylene oxidation there are two possible reactions for producing CH (${}^2\Delta$) but that only one of the reactions is important in methane oxidation.

ACKNOWLEDGEMENTS

The authors thank T. F. Zupnik, Pratt & Whitney Aircraft, for providing the computer program used for the reaction kinetic calculations. This work was sponsored, in part, by the Air Force Aero Propulsion Laboratory (Wright-Patterson) under Contract No. AF 33(615)-3179.

References

1. Wurster, W. H., *J. Chem. Phys.*, 36, 2112 (1962).
2. Strehlow, R. A. and C. T. Case, *J. Chem. Phys.*, 35, 1506 (1961)
Johnson, C. D. and D. Britton, *J. Chem. Phys.*, 38, 1455 (1963).
3. Skinner, G. B., *J. Chem. Phys.*, 31, 268 (1959).
4. Snyder, A. D., J. Robertson, D. L. Zanders and G. B. Skinner, Shock Tube Studies of Fuel-Air Ignition Characteristics, Monsanto Research Corporation Report AFAPL-TR-65-93. August 1965.
5. Enikolopyan, N. S., Seventh Symposium (International) on Combustion, London, Butterworths (1959), p. 157.
6. Palmer, H. B. and T. J. Hirt, *J. Phys. Chem.*, 67, 709 (1963).
7. Fenimore, C. P. and G. W. Jones, *J. Phys. Chem.*, 65, 1532 (1961), *ibid.*, p. 2200.
8. Wilson, W. E., paper presented at 1967 Spring Meeting, Western States Section The Combustion Institute, LaJolla, Calif., April 24-25, 1967.
9. Fristrom, R. M. and A. A. Westenberg, Flame Structure, New York, McGraw-Hill, 1965. See also Fristrom, R. M., Ninth Symposium (International) on Combustion, New York, Academic Press (1963), p. 560.
10. Stubbeman, R. F. and W. C. Gardiner, Jr., *J. Phys. Chem.* 68, 3169 (1964).
11. Deckers, J. M., Energy Distribution in Flames and Electric Discharges, Final Report Grant AF-AFOSR 375-65, Lash Miller Chemical Laboratories, University of Toronto, August 1966.

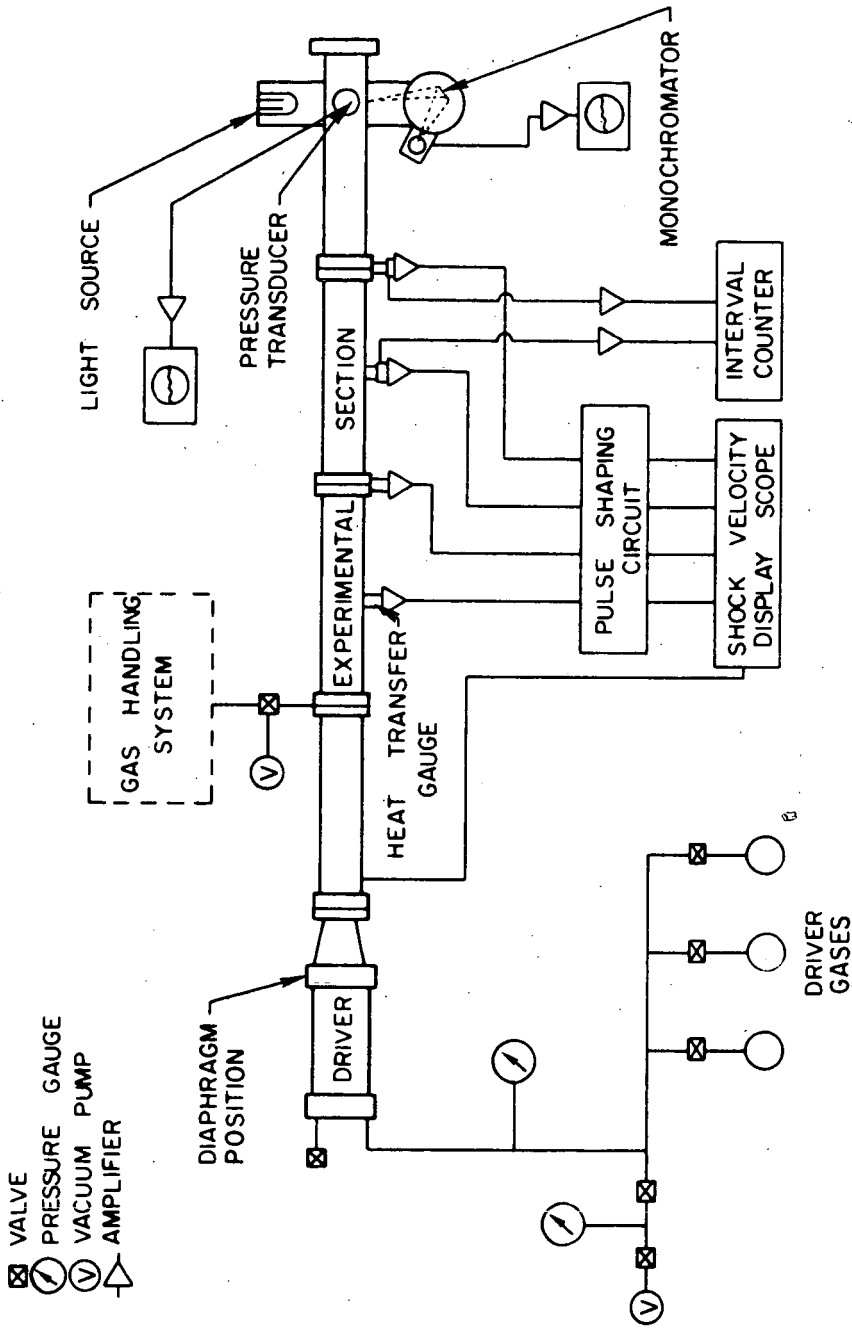


FIGURE 1. SCHEMATIC DIAGRAM OF EXPERIMENTAL APPARATUS

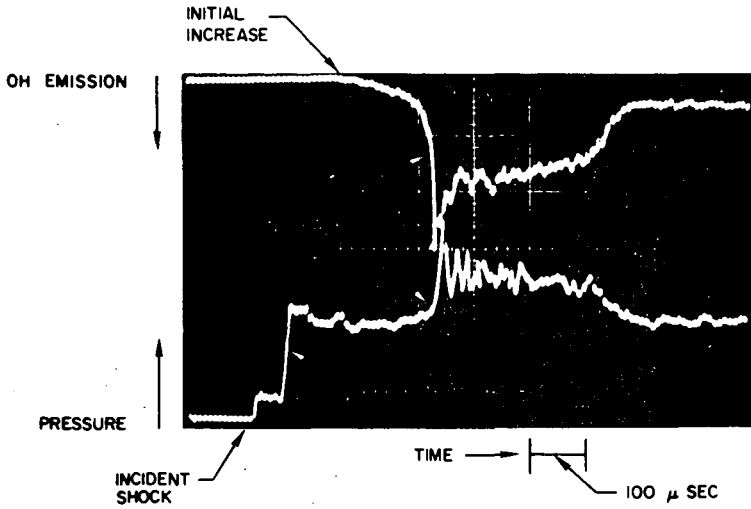


FIGURE 2. PRESSURE CHANGE AND OH EMISSION DURING INDUCTION PERIOD FOR METHANE IGNITION

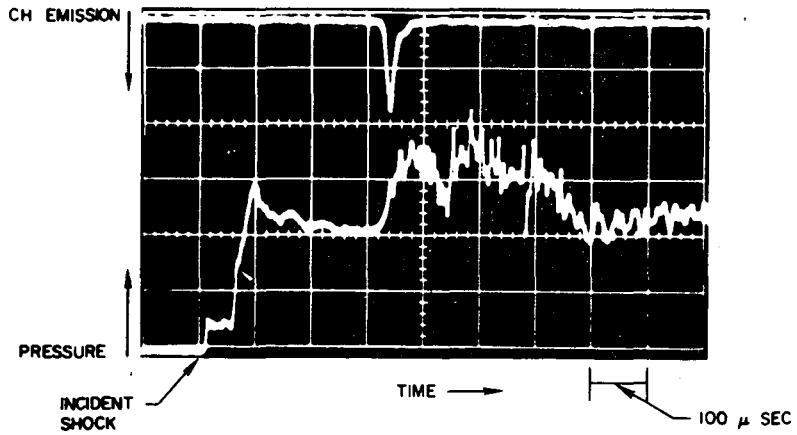


FIGURE 3. PRESSURE CHANGE AND CH EMISSION DURING INDUCTION PERIOD FOR METHANE IGNITION

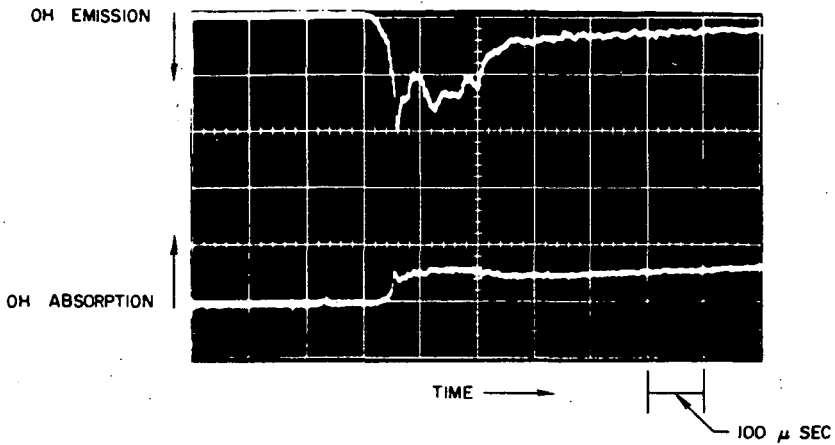


FIGURE 4. OH EMISSION AND ABSORPTION DURING INDUCTION PERIOD FOR METHANE IGNITION

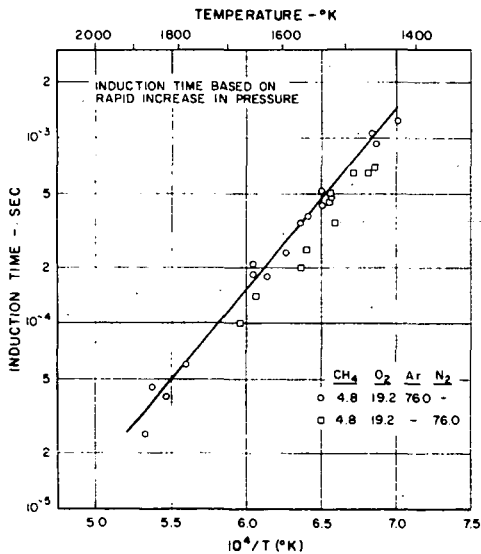


FIGURE 5. TEMPERATURE DEPENDENCE OF INDUCTION TIME FOR P=1.7 ATM AND $\phi = 0.5$

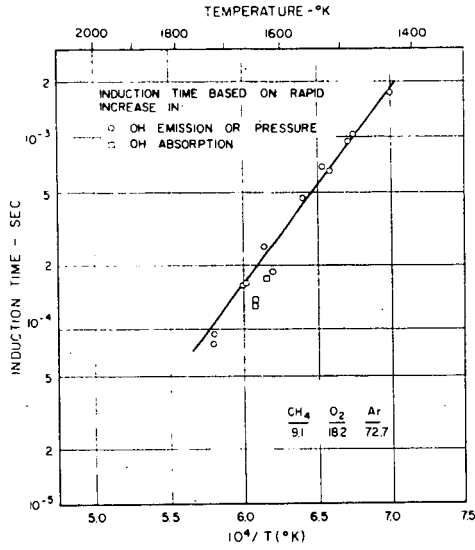


FIGURE 6. TEMPERATURE DEPENDENCE OF INDUCTION TIME FOR $P = 2.0$ ATM AND $\Phi = 1.0$

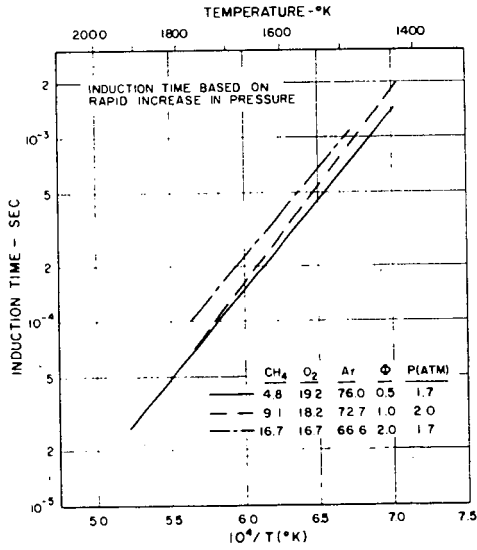


FIGURE 7. TEMPERATURE DEPENDENCE OF INDUCTION TIME FOR SEVERAL Φ

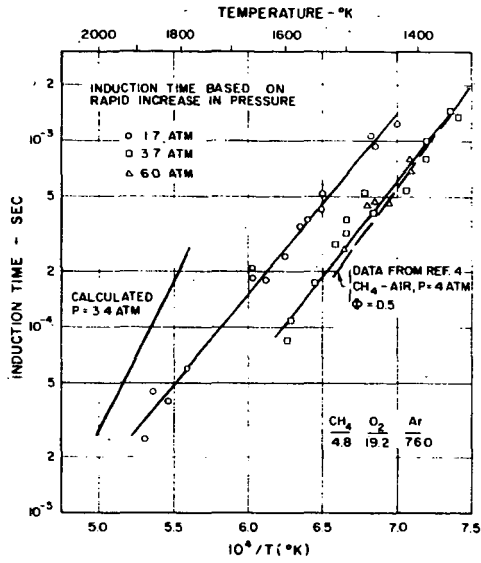


FIGURE 8. TEMPERATURE DEPENDENCE OF INDUCTION TIME FOR SEVERAL PRESSURES

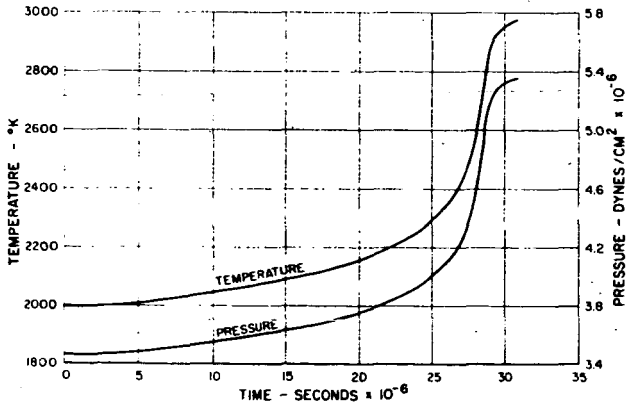


FIGURE 9. CALCULATED TEMPERATURE AND PRESSURE PROFILES FOR T = 2000°K, P = 3.4 ATM AND φ = 0.5

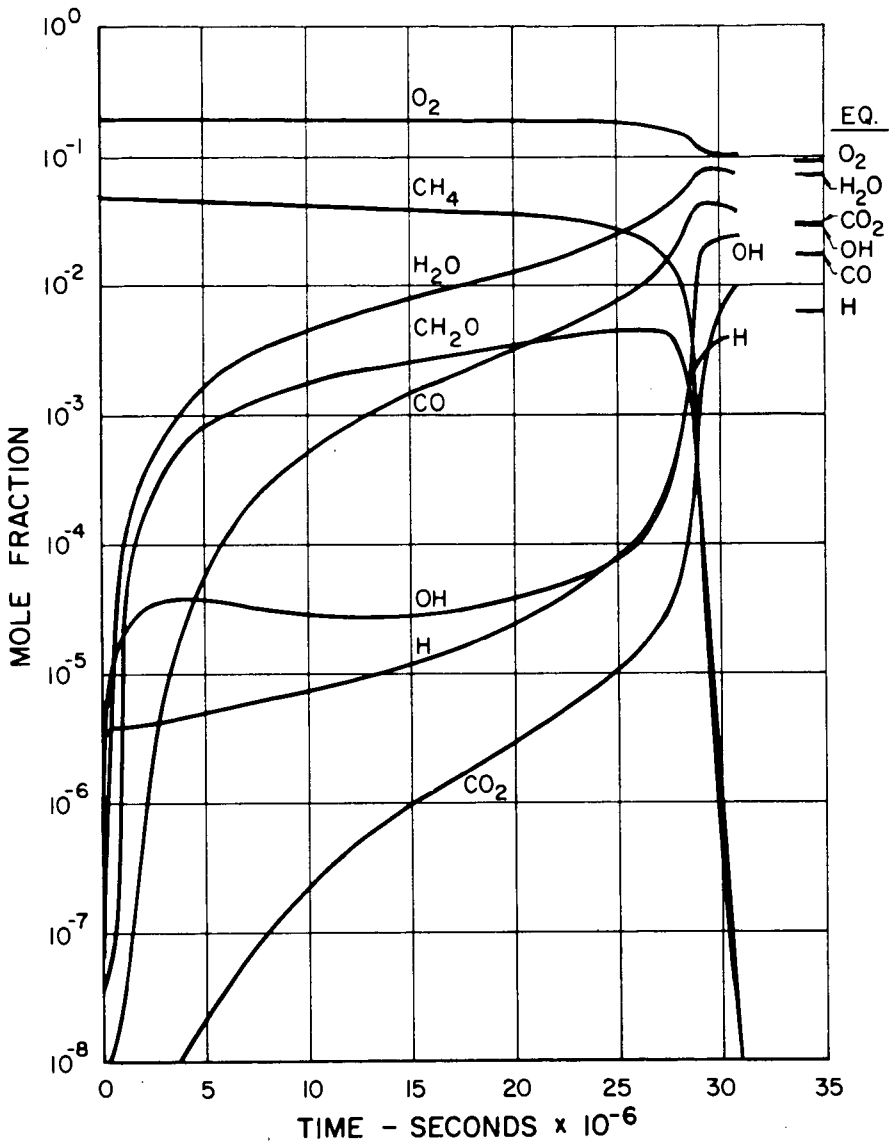


FIGURE 10. CALCULATED CONCENTRATION PROFILES FOR
 $T = 2000^\circ K$, $P = 3.4$ ATM AND $\Phi = 0.5$

KINETICS OF THE NITROUS OXIDE - HYDROGEN REACTION

Hans Henrici, Margaret Hunt, and S. H. Bauer

Department of Chemistry, Cornell University

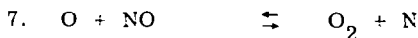
Ithaca, New York 14850

The reaction between nitrous oxide and hydrogen was investigated over the temperature range 1700^o-3000^oK in shock heated mixtures, diluted 1%-3% (for each reagent) in argon. Incident shock densities were (1-7) 10⁻⁶ moles cm⁻³. Most of the rate data were obtained by recording the absorption of characteristic OH radiation at 3094Å; additional spectrophotometric measurements were made at 2259Å (for NO) and at 2300 Å (for N₂O). The first objective was to determine whether the literature values for the rate constants of the elementary steps adequately account for the observed OH profiles, and the second, to deduce more reliable values for those constants the magnitudes of which are in doubt. Preliminary analysis of the data indicated that the OH concentration exceeded its equilibrium level particularly at the lower temperatures; this was also the case for NO. Detailed analyses using a shock kinetics program for 14 reactions (and their inverses) show that the "best" values generally accepted for the various rate constants lead to much faster rise times but lower maximum concentrations of OH than were observed. In view of the consensus currently being reached regarding the constants for the O/H reactions, our data place lower limits on the magnitudes for the (N₂O + O) steps and an upper limit for the (N₂O + H) step.

STATEMENT OF THE PROBLEM

The reaction between nitrous oxide and hydrogen at high temperatures is very rapid. While the main outlines of the mechanism may be formulated with reasonable certainty, the magnitudes of the kinetics parameters are not well established. In particular, several of the critical rate constants have been measured at lower temperatures only, and information which permits extrapolation to the higher temperature regime (up to 3000^oK) is not available. The entire sequence of steps may be divided into three groups.

I. The following involve oxygen and nitrogen only;

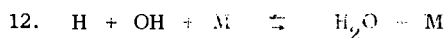
the initiation reactionthe depletion reactionsscrambling and recombination steps

II. This group involves oxygen and hydrogen only; all but the termolecular reactions are very rapid.

the primary step

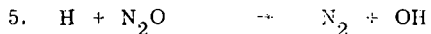


secondary steps



III Reactions which couple the N/O to the H/O system;

the primary step



secondary steps (of little consequence under shock conditions)



The reactions for which the rate constants are best established are the initiation step and some of the reactions in group (II). The rate constant for reaction (1) has been measured⁽¹⁾ over four powers of ten between 1500° and 2500°K. These experiments were conducted at a total density starting at 5×10^{-6} moles/cm³ and into the high pressure saturation region. The rate of N₂O decomposition was found to be proportional to the density up to 6×10^{-3} moles/cm³, a level which is much higher than the highest densities in our experiments. In group (II), the best known rate constants are those for reaction (9), which was determined to within 10% over the temperature range 1300° to 1700°K, and for reaction (4) which was determined in the same study combined with literature values available at lower temperatures. Reaction (5), the primary coupling step between groups (I) and (II) is the least well established of the controlling steps in the overall process. The thermochemical parameters for the above reactions are known with considerable precision, except possibly those involving HNO. The relevant data used in the following calculations were taken from the JANAF Tables.

The reaction rates between nitrous oxide and hydrogen were measured in shock heated mixtures (incident regime) over the temperature range 1700°-3000°K. The first objective was to determine whether the literature values for the rate constants of the elementary steps do adequately account for such data; the second, to deduce more reliable values for those constants the magnitudes of which are in doubt. The ($N_2O + H_2$) reaction is typical of complex oxidation systems and is particularly well suited for a shock tube study. Several spectroscopic probes are available as "handles" on the course of the reaction. Most of the data collected during this investigation were obtained by recording the absorption of characteristic OH radiation; additional spectrophotometric measurements were made in absorption for NO and for N_2O . When both of these gases were present, the net absorption at 2259Å was corrected for that due to N_2O . Other probes which are available for following this reaction are the intensities of emission in the infrared due to OH, H_2O and NO; these were not used in the present study. The mixtures of N_2O/H_2 used were, 1/1, 1/2, 1/3, 3/1, 3/3% in argon, with total densities from (1-7) 10^{-6} moles cm^{-3} . The levels of OH generated ranged 1.2×10^{-8} to 2.3×10^{-9} moles cm^{-3} .

EXPERIMENTAL PROGRAM

All our data were obtained in the incident shock regime, using a 6" I.D. stainless steel shock tube. It has an 8' driver section and a 30' test section. The observation windows are 26' downstream from the diaphragm. Prior to filling, the experimental section was pumped down to 10^{-4} torr; the apparent leak rate was 2.5×10^{-6} torr/min. Mylar diaphragms of 0.008" thickness were cross-cut to 0.005" and pressure broken. The speed of the incident shock wave was measured with a raster system, upon which calibrated markers were superposed at 10 μ sec. intervals. The raster was triggered by a piezoelectric pressure transducer. Further downstream were three platinum heat gauges with known separation. The error in the shock speed was estimated to be about 0.1%. The piezoelectric gauge also triggered the other electronic devices, including the discharge through the H_2O vapor lamp. We estimated the time constant of the recording system to be about 5 μ sec.

The N_2O used in these studies was doubly distilled in vacuum, mixed with hydrogen and argon in large glass vessels or in glass lined metal tanks and kept at least 10 hours before using, to insure complete mixing. Mass spectrometric checks revealed no oxygen impurity above the background level of the spectrometer.

The source of characteristic OH radiation was described previously⁽¹⁵⁾. The lamp emission was made parallel before entering the shock tube, and the exit light was focused onto the entrance slit of a Jarrell-Ash 500 mm focal length monochromator (JACO 8200), which has a 16Å/mm dispersion. In order to discriminate against the emission from the shock heated gas, the focusing lens was placed 70 cm from the exit window of the shock tube. Forty micron entrance and exit slits permitted selection of a portion ($\Delta\lambda = 0.64\text{Å}$) of the Q branch head (3094Å) of the $^2\Sigma^+ - ^2\Pi$ transition. The time rate of change in the concentration of N_2O and the final concentration of NO were measured using a deuterium arc*, as a source of continuum radiation.

For the NO absorption measurements, a wavelength region around 2259Å ($\pm 2.7\text{Å}$) was selected, this belongs to the γ band (0, 0 of $^2\Sigma^+ - ^2\Pi_{3/2, 1/2}$) transition. The average of 8 runs with 1% NO in argon, the absorption coefficient between 1800° and 2100°K was determined to be $8.55 (\pm 0.3) \times 10^{+4}$ $cm^2/mole$. For these measurements the NO was obtained from a commercial cylinder, and doubly distilled to remove N_2

* WHS 200 lamp, Dr. Kern, Göttingen.

and the higher oxides of nitrogen. Since N_2O absorbs only at shock temperatures, a reliable determination of the NO concentration in the reacting mixture was possible only after the N_2O had decomposed. The absorption of the generated NO remained constant for at least 1 msec, laboratory time, when the gas consisted initially of a mixture of pure N_2O in Ar, and also when hydrogen was added. The absorption coefficient of N_2O at 2300 Å as a function of temperature, has been determined by Troe⁽¹⁶⁾. The few preliminary measurements made in our laboratory do not disagree with that determination.

Test times ranged up to 500 μsec; however, most of the runs were taken up to 350 μsec only. Particle times were therefore of the order of 1500 μsec.

TYPICAL RESULTS AND PRELIMINARY ANALYSIS

Within the limits of the time constants of these measurements the OH concentration rises linearly with a finite slope for a period of 50 to 100 μsec, then slowly bends over and appears to approach a level value. In some cases there were clear indications that this passed through a maximum. The preliminary assumption that the maximum level of OH corresponded to the equilibrium concentration proved misleading. An equilibrium shock program not only gave values for the final reaction temperature (which ranged from 100-250° above shock temperatures calculated for no reaction) but also gave the equilibrium concentration of all the species. Comparison of the calculated with the observed values, based on the approximate absorption coefficient (for OH) of 2.2×10^6 cm²/mole is shown in Table I. It is clear that the overshoot is higher at the lower temperature. The cause for the overshoot is the same as in the H/O system, in that three body processes which reduce the atom and free radical concentrations are slow compared to the steps which produce OH, or bring it into local equilibrium with the other radicals. These preliminary studies also showed that the simplifying assumption regarding the OH production [i. e. that it is primarily controlled by reactions (1), (2), (3), and (4)] does not account for the data. Under the steady-state assumption for the oxygen atoms,

$$\frac{d(OH)}{dt} = k_1 [N_2O] [M] \left[1 + \frac{k_3 + k_4}{k_2} \frac{[N_2O]}{[H_2]} \right]^{-1} \quad ; \text{ see Fig. 1.}$$

A test of this equation can be made by assuming literature values for k_2 (1A), k_3 (2), and k_4 (3). This reduction is not acceptable in view of the fact that runs with different concentrations of N_2O and H_2 do not lie on the same line, nor does the dissociation rate constant for N_2O agree with the currently accepted value⁽¹⁾. However, the various curves are close to one another and fall below the previous data on the N_2O decomposition^(1A).

Not only does the OH concentration overshoot but the NO appears to behave likewise; this has been observed previously in studies of the N_2O decomposition^(1A). The proof requires measurement of the limiting value of the NO concentration, referred to the initial concentration of N_2O , which disappears completely by the time the test period is over. The ratio (in the absence of H_2),

$$\beta \equiv \frac{(NO)^\infty}{(N_2O)_1} = \frac{1}{1 + (a + b)} \approx 0.47; \quad (a + b) \approx 1.1$$

where a measures the fraction of oxygen atoms used in reaction (2), and b is the fraction of oxygen atom which follow reaction (14), compared with reaction (3) as a reference. Table II is a summary of magnitudes of β for several typical runs. The sum $(a + b) = 1.1$ indicates approximately comparable depletion of oxygen atoms by reactions (2), (3), and (4). In contrast, when hydrogen is present the observed value for β is

considerably less, also shown in Table II. The values for β in absence of hydrogen check with those obtained by Gutman^(1A), who reported $\beta = 0.56$ at 2515°K, with no detectable temperature dependence. Thus, in the presence of hydrogen a considerable fraction of the oxygen atoms are removed by the primary reaction (4), and the secondary step (9).

The partition of oxygen atoms among the various reactions, in the presence of hydrogen, cannot be directly estimated from the measured β , but this does provide an additional boundary condition on the correct assignment of reaction rate constants. One may now list the available experimental parameters:

- (a) the initial slope of the OH curve (absence of an induction period)
 - (b) the time required for the OH concentration to reach 63% of its final value
 - (c) the magnitude of the OH at the maximum
 - (d) the value of β
 - (e) the time required for the disappearance of N_2O to 1/2 of its initial value.
- The matching of the OH concentration-time profile, and the parameters listed above were used to test combinations of rate constants, as described in the next section.

EXTENDED CALCULATIONS AND CURRENT STATUS OF THE PROBLEM

Because of the coupling of a large number of reactions and their approximately comparable contributions, no simplifying assumptions permit an analytic solution of the coupled set of differential equations. Therefore a general kinetics program was introduced to obtain calculated values for the concentration profiles of all species. The program which was obtained from Cornell Aeronautical Laboratory⁽¹⁸⁾, permits the insertion of the enthalpy and free energy for each specie as a function of temperature. The thermodynamic functions are expressed as polynomials in the temperature. For the rate constants specific values must be inserted for the pre-exponential factor, the pre-exponential temperature dependence and the activation energy. This incident shock program computes the equilibrium constant for each reaction, obtains the rate constant for its reverse and gives the net rate of formation (Q_{ij}) for each species (j) from every reaction (i). It also gives the concentration of each species as a function of time and computes the temperature profile behind the shock. The printout of the Q_{ij} 's as a function of time is probably the most useful part of the output. It provides a measure of how dependent the net concentration profile for any species is on the contribution from each reaction. It helps to gauge how effectively coupled the system is, and whether some reactions which were introduced can be discarded because of their minor contributions. For example, this was found to be the case for OH derived from reactions (15, 16, 17 and 18).

In the tests which will be described below no change was made in the value for the dissociation rate constant for step (1). The study from which we took the rate constant⁽¹⁾ covered a wide range of total pressures and of temperatures for low concentrations of N_2O in Ar. The reported values show very little scatter from an Arrhenius line. In addition the same results were obtained behind incident and reflected shock waves, and they were crosschecked by experiments with an adiabatic piston⁽¹⁹⁾. Nevertheless, in our system, there still may be some uncertainty about the rate constant for this reaction due to the unknown collision efficiencies for activation by the species produced in the N_2O/H_2 reaction. These may be much larger than that for argon. The other rate constants were obtained from a survey of the literature and from discussions with several workers in the field; they are listed in Table III.

In a first group of tests the rate constants for reactions (2) and (3) were accepted, and only those of the H_2/O_2 system and that of reaction (5) were varied in an attempt to obtain a fit to the experimental OH profile at 2000°K. These tests showed that the computed rate of OH-formation, which was much faster than the observed, could be fitted only by

reducing the rate constants of reactions (5) and (10) by a factor of 30 to 40. In order to achieve a better fit for experiments at different concentrations, it was also necessary to reduce the rate constants for (9) by a factor of 10, and for (4) by 1/2. This is clearly an unacceptable combination. Figure 2a shows the contributions of the five critical reactions to the OH concentration profile (Q_{11}) for a typical run with 1% of N_2O and 1% H_2 in Argon; Fig. 2b shows the net OH profiles, calculated and observed as well as the calculated adiabatic temperature.

In view of the consensus now being reached as to the magnitudes of the rate constants for group II, the second exploration involved the rate constants for the depletion reaction (2) and (3), and the primary coupling reaction (5). At this stage it was demonstrated that reactions (15) to (18) have no discernable effect on the OH profile. Table IV is a summary of the various combinations tested, and Figures 3a and 3b show the Q_{11} and the net OH profile for one of the more successful combinations found to date.

As in the first series of tests for specified k_2 and k_3 , the OH profile depends most sensitively on the rates of reactions (5) and (10). A difficulty in all these attempts to fit the experimental data was that the computed OH profiles yielded maximum values for the OH concentrations which were at most half as large as those observed. Whether this is due to an uncertainty in the absorption coefficient of OH or to an incorrect combination of the rate constants will be tested in calibration measurements designed to determine the absolute OH concentrations under these conditions.

If the present set of rate constants is a reasonable approximation, the effect of the different reactions on each other and on the OH profile can be described as follows. The reaction is initiated by (1) which is rapidly followed by either (2) and (3) or by (4). If NO plays no further role, the only way in which reactions (2) and (3) contribute toward the building up of OH is through (9), the reaction of the O_2 generated in reaction (2) with hydrogen atoms. Between 1100° and 1700°K⁽¹³⁾ k_9 is by now known to within $\pm 10\%$. If the extrapolation to 2000°K is correct, reaction (9) makes only a minor contribution to the OH generation, at least when there is no large excess of N_2O over H_2 .

Apart from the current experiments there is other evidence for the stability of NO under conditions similar to those of the shock tube investigation. The decomposition of NO is a slow process as is also its rate of reaction with molecular hydrogen, reaction (16). The rate of production of HNO would have to be at least a 100 times faster than that determined by Bulewicz and Sugden⁽¹³⁾, in order to contribute measurably. Further, the decay of pure N_2O in argon is at least 100 times faster than the loss of N_2O through⁽²²⁾



The absorption by NO_2 at its band maximum (4200 Å) was not detectable in the Göttingen studies on the N_2O decomposition.

It follows that, apart from the contribution of reaction (9), oxygen atoms which react with N_2O via reactions (2) and (3) are lost for the production of OH. The net rate of OH production is therefore sensitive to the ratio: $k_4/(k_2 + k_3)$. The above preliminary experiments of the magnitude for β indicate that an increase in the rates of k_2 and k_3 is required to account for the observed ratio of $[NO]^\infty/[N_2O]^1$. Once the ratio $k_4/(k_2 + k_3)$ is fixed, the concentration profile of OH depends strongly on the coupled reactions (5) and (10). At the beginning, when little water is present, reaction (10) is faster than reaction (5), resulting in a net consumption of OH. As reaction (10) approaches local equilibrium, reaction (5) takes over until the N_2O is consumed. By

then, the buildup of OH is completed, and OH decays slowly via three body processes.

This relatively simple picture is complicated by the fact that reactions (9) and (11) also contribute to the OH profile but by an amount which is smaller than the contributions from reactions (4), (5), and (10). However, the significance of (9), (11) can be established only after the rate constants for (2), (3), and (5) have been measured. In order to achieve this, the experiments to determine β as a function of the H_2 concentration, and the profile for N_2O disappearance will be continued.

ACKNOWLEDGEMENTS

This work is being supported by the AFOSR, Contract AF49(638)-1448. We are particularly grateful to the Aerodynamics Research Group at the Cornell Aeronautical Laboratory for making available to us both the equilibrium and non-equilibrium shock programs used in this investigation. We wish to thank Dr. G. L. Schott for informative discussions of the "best" values for the rate constants for the hydrogen-oxygen reaction, and Professor J. E. Dove for sending us mass spectrometer data on the N_2O-H_2 reaction.

REFERENCES

1. H. A. Olschewski, J. Troe, and H. Gg. Wagner, Ber. Bunsenges. physik. Chem. 70, 450 (1966).
- 1A. D. Gutman, R. L. Belford, A. J. Hay, and R. Pancirow, J. Phys. Chem., 70, 1793 (1966).
2. C. P. Fenimore, and G. W. Jones, 8th (International) Symposium on Combustion, Williams and Wilkins, Baltimore 1962, p. 127.
3. D. Gutman, and G. L. Schott, in print.
4. C. P. Fenimore, "Chemistry in Premixed Flames", International Encyclopedia of Physical Chemistry and Chemical Physics, Topic 19, Vol. 5, MacMillan, New York, 1964.
5. A. L. Myerson, W. S. Watt, and P. J. Joseph, in print.
6. K. L. Wray, and J. D. Teare, J. Chem. Phys., 36, 2582 (1962).
7. H. G. Glick, J. J. Klein, and W. Squire, J. Chem. Phys., 27, 850 (1957).
8. D. L. Ripley and W. C. Gardiner, Jr., J. Chem. Phys., 44, 2285 (1966).
9. W. E. Kaskan and W. G. Browne, "Kinetics of the $H_2/CO/CO_2$ System", General Electric Reentry Systems Dept., Document 635D848 (1964).
10. H. A. Olschewski, J. Troe, and H. Gg. Wagner, Z. physik. Chem., NF, 47, 353 (1965).
11. G. L. Schott, private communication.
12. K. L. Wray, 10th (International) Symposium on Combustion, The Combustion Institute, Pittsburgh, Pa., 1965, p. 523.
13. E. M. Bulewicz and T. M. Sugden, Proc. Roy. Soc. (London), A277, 143 (1964).
14. K. A. Wilde, Report No. S-121, Rohm and Haas Company, Redstone Research Laboratories, Huntsville, Alabama 35807.
15. S. H. Bauer, G. L. Schott and R. E. Duff, J. Chem. Phys., 28, 1089 (1958).
16. J. Troe, Dissertation, Gottingen, 1965.
17. C. A. L. Equilibrium Normal Shock Program, Cornell Aeronautical Laboratory, Inc., Buffalo, New York 14221, September 1966.
18. L. J. Garr, P. V. Marrone, W. W. Joss, and M. Williams, Inviscid Non-equilibrium Flow Behind Bow and Normal Shock Waves, Cornell Aeronautical Laboratory, Inc., Buffalo, New York 14221,
CAL - Report No. QM - 1626 - A - 12 (I), May 1963
 QM - 1626 - A - 12 (II), May 1963
and revised QM - 1626 - A - 12 (III), October 1966.
19. A. Martinengo, J. Troe, and H. Gg. Wagner, Z. physik. Chem., NF, 51, 104 (1966).
20. E. Freedman and J. W. Daibler, J. Chem. Phys., 34, 1271 (1961).
21. K. L. Wray and J. D. Teare, J. Chem. Phys., 36, 2582 (1962).
22. F. Kaufman, and J. R. Kelso, J. Chem. Phys., 23, 602 (1955).

TABLE I

 $N_2O:H_2:Ar/3:3:94$

Run No.	p_O (total) torr.	$p_O \times 10^{-4}$ dynes/cm ²	U_{shock} mm/ μ s	$T_2^{O,K}$ equilibrium	obs. (OH) $\times 10^9$ plateau	calc. (OH) $\times 10^8$ equil.	$\frac{(OH)_{obs.}}{(OH)_{eq.}}$
82	43.2	5.7595	1.332	2078	9.965	0.194	5.12
83	37.7	5.0262	1.403	2235	12.224	0.398	3.08
79	16.5	2.2000	1.478	2386	10.292	0.438	2.35
85	13.2	1.7599	1.568	2551	9.179	0.695	1.32

 $N_2O:H_2:Ar/3:1:96$

64	27.0	3.5997	1.397	2110	8.424	0.244	3.45
54	21.0	2.7998	1.445	2222	9.900	0.317	3.12
92	12.5	1.6665	1.521	2394	7.642	0.384	1.99
93	10.3	1.3732	1.610	2586	7.620	0.540	1.41

 $N_2O:H_2:Ar/1:1:98$

31	27.0	3.3331	1.385	2064	5.558	0.0674	8.25
73	21.2	2.8261	1.446	2209	5.167	0.126	4.09
17	14.7	1.9598	1.515	2372	6.036	0.1939	3.12
16	13.3	1.7732	1.568	2494	5.905	0.249	2.37

 $N_2O:H_2:Ar/1:3:96$

48	13.0	1.733	1.548	2405	2.848	.0744	3.83
47	13.1	1.747	1.610	2554	2.310	.158	1.29

TABLE II

Determination of $\beta \equiv \frac{[\text{NO}]^\infty}{[\text{N}_2\text{O}]^2}$ in mixtures of $\text{N}_2\text{O}:\text{Ar} = 2:98$, and $\text{N}_2\text{O}:\text{H}_2:\text{Ar} = 2:1:98$

Total density: $(0.8 - 1.1 \times 10^{-5})$ moles/cm³

No.	T (°K)	β	
1	2009	0.42	$\text{N}_2\text{O}:\text{Ar} = 2:98$
3	2085	0.48	
4	2100	0.50	
5	2212	0.48	
17	1910	0.064	
18	1590	0.083	$\text{N}_2\text{O}:\text{H}_2:\text{Ar} = 2:1:97$
19	1965	0.063	
20	1995	0.072	

TABLE IV

Factors by which rate constants of Table III were varied in the second group of tests.

No.	Reaction	Test						
		1	2	3	4	5	6	7
2	$\text{O} + \text{N}_2\text{O} \rightleftharpoons \text{H}_2 + \text{O}_2$	10	10	10	10	10	30	30
3	$\text{O} + \text{N}_2\text{O} \rightleftharpoons 2\text{NO}$	10	10	10	10	10	30	30
4	$\text{O} + \text{H}_2 \rightleftharpoons \text{OH} + \text{H}$	1	1	1	1	1/2	1	1
5	$\text{H} + \text{N}_2\text{O} \rightleftharpoons \text{N}_2 + \text{OH}$	1	1/3	1/3	1/10	1/10	1/3	1/10
10	$\text{OH} + \text{H}_2 \rightleftharpoons \text{H}_2\text{O} + \text{H}$	1	1	2	1	1	1	1

TABLE III: "Best" literature values for k_1

No.	Reaction	ΔH_{2000}° kcal/mole	ΔS_{2000}° cal/mole deg.	K_{p2000} (atm)	k_f $\left[\frac{\text{moles}}{\text{cm}^3 \cdot \text{sec}} \right]$	Ref.
1	$\text{N}_2\text{O} + \text{M} \rightleftharpoons \text{N}_2 + \text{O} + \text{M}$	39.87	32.59	5.85×10^2	$10^{14.7} e^{-58/RT}$	1
2	$\text{O} + \text{N}_2\text{O} \rightleftharpoons \text{N}_2 + \text{O}_2$	-82.18	0.65	1.32×10^9	$10^{13.93} e^{-28.0/RT}$	1A
3	$\text{O} + \text{N}_2\text{O} \rightleftharpoons 2\text{NO}$	-38.92	6.73	5.29×10^5	$10^{14} e^{-28.0/RT}$	2
4	$\text{O} + \text{H}_2 \rightleftharpoons \text{OH} + \text{H}$	2.09	1.66	1.36×10^0	$10^{13.51} e^{-10.0/RT}$	3
5	$\text{H} + \text{N}_2\text{O} \rightleftharpoons \text{N}_2 + \text{OH}$	-66.50	5.56	3.02×10^8	$10^{14.48} e^{-16/RT}$	4
6	$\text{H}_2 + \text{M} \rightleftharpoons 2\text{H} + \text{M}$	108.46	28.69	2.63×10^{-6}	$1.18 \times 10^{12} T^{1/2} e^{-94.5/RT}$	5
7	$\text{O} + \text{NO} \rightleftharpoons \text{O}_2 + \text{N}$	32.07	-3.05	6.77×10^{-5}	$10^{9.5} T e^{-39.1/RT}$	6
8	$\text{N} + \text{NO} \rightleftharpoons \text{N}_2 + \text{O}$	-75.32	-3.03	3.69×10^7	$10^{13.18}$	7
9	$\text{H} + \text{O}_2 \rightleftharpoons \text{OH} + \text{O}$	15.67	4.91	2.28×10^{-1}	$10^{13.89} e^{-14.45/RT}$	3
10	$\text{OH} + \text{H}_2 \rightleftharpoons \text{H}_2\text{O} + \text{H}$	-14.80	-2.81	1.01×10^1	$10^{13.6} e^{-5.7/RT}$	8
11	$2\text{OH} \rightleftharpoons \text{H}_2\text{O} + \text{O}$	-16.89	-4.47	7.38×10^0	$10^{12.88} e^{-1/RT}$	9
12	$\text{H}_2\text{O} + \text{M} \rightleftharpoons \text{H} + \text{OH} + \text{M}$	126.26	31.51	2.61×10^{-7}	$10^{15.3} e^{-109/RT}$	10
13	$\text{H}_2 + \text{O}_2 \rightleftharpoons 2\text{OH}$	17.76	6.57	3.16×10^{-1}	$10^{12.4} e^{-39/RT}$	11
14	$\text{O}_2 + \text{M} \rightleftharpoons 2\text{O} + \text{M}$	122.04	31.94	4.40×10^{-7}	$10^{16.41} T^{1/2} e^{-118/RT}$	12
15	$\text{H} + \text{NO} + \text{M} \rightleftharpoons \text{HNO} + \text{M}$	-52.71	-29.11	3.99×10^0	$10^{18.99} T^{-1} \text{ (b)}$	13
16	$\text{H}_2 + \text{NO} \rightleftharpoons \text{HNO} + \text{H}$	55.75	-0.41	6.60×10^{-7}	$10^{14.48} e^{-57.9/RT}$	13(a)
17	$\text{OH} + \text{HNO} \rightleftharpoons \text{H}_2\text{O} + \text{NO}$	-70.55	-2.40	1.53×10^7	$10^{13.95}$	13
18	$\text{NO} + \text{HNO} \rightleftharpoons \text{N}_2\text{O} + \text{OH}$	-14.73	-4.65	3.92×10^0	$10^{12.79} e^{-34.1/RT}$	14

a. Calculated from reverse rate constants through K_{eq} .b. Units are mole⁻² cm⁶ sec⁻¹.

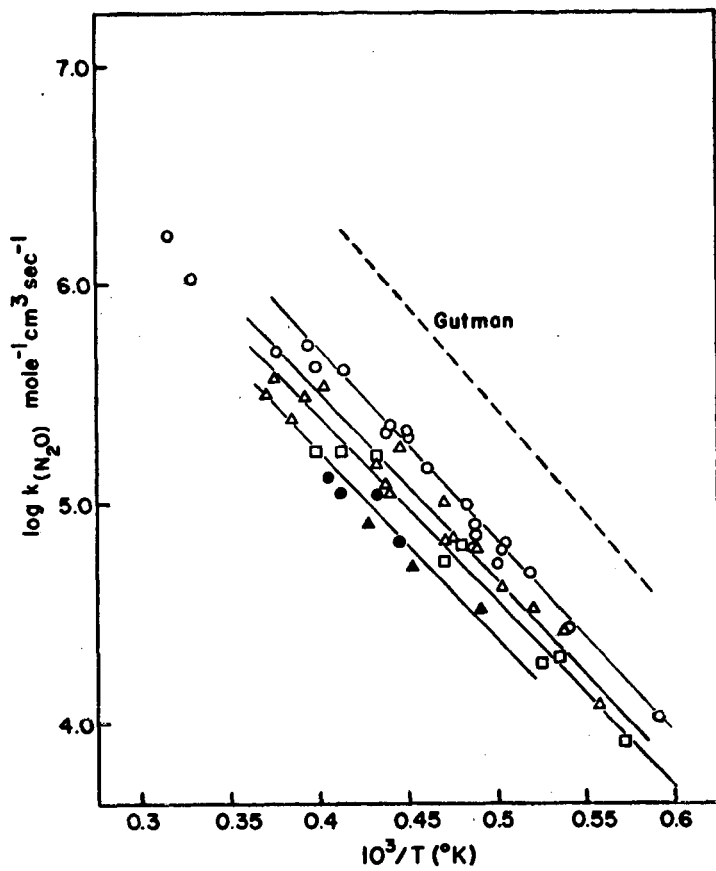


Figure 1. Bimolecular dissociation rate constant for N_2O , deduced from preliminary reduction of initial $[OH]$ slopes.
 $[N_2O]_0/[H_2]_0 = 1:1$ O; $3:1$ Δ ; $3:3$ \square ; $2:3$ \bullet and $2:4$ \blacksquare

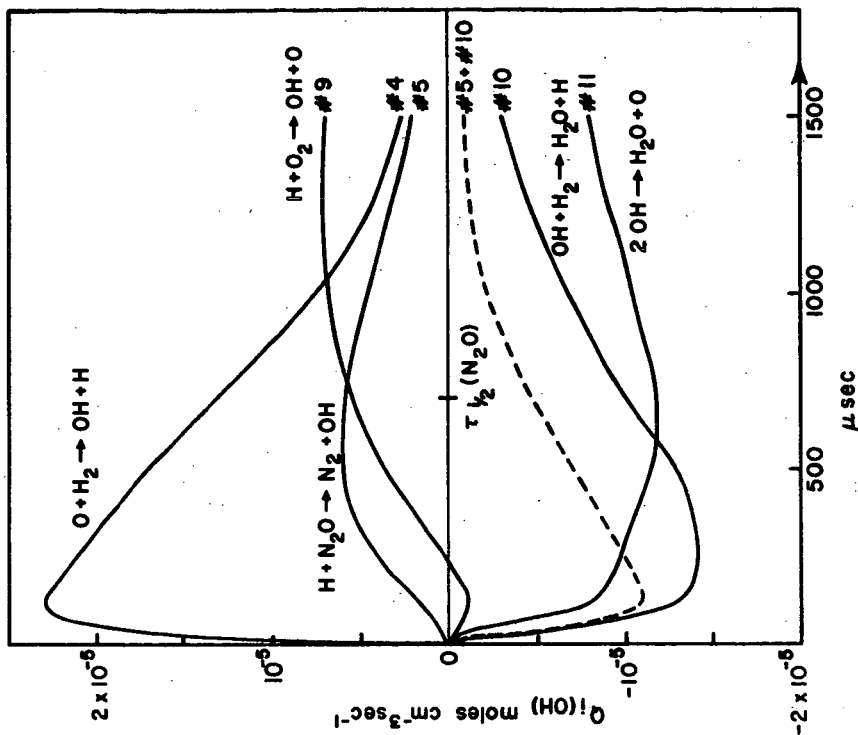


Figure 2a. Typical profiles for OH production rates from various reactions, 1st set on N₂/H₂ = 1:1.

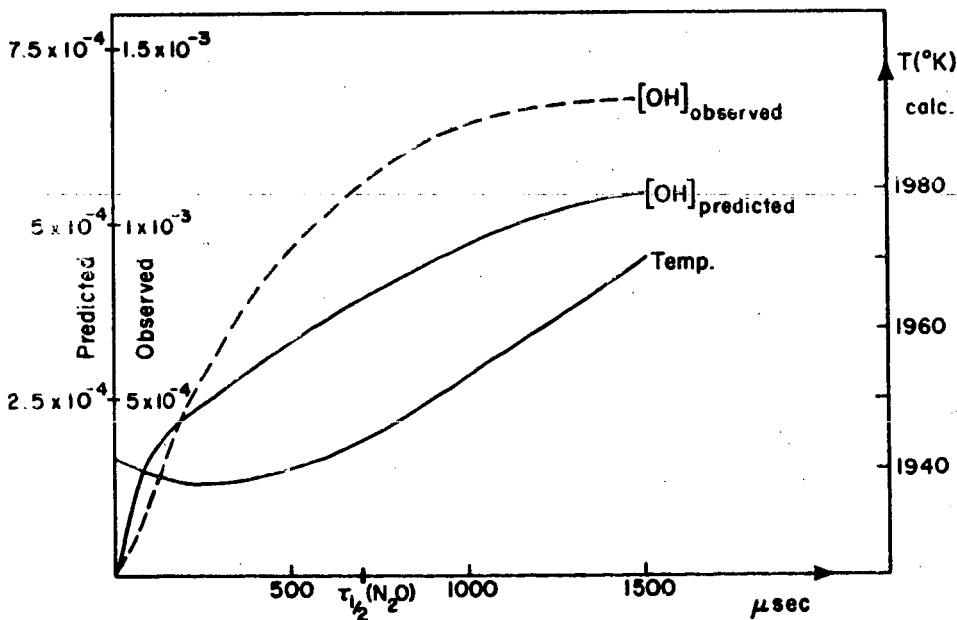


Figure 2b. Net [OH] produced, as a function of time.

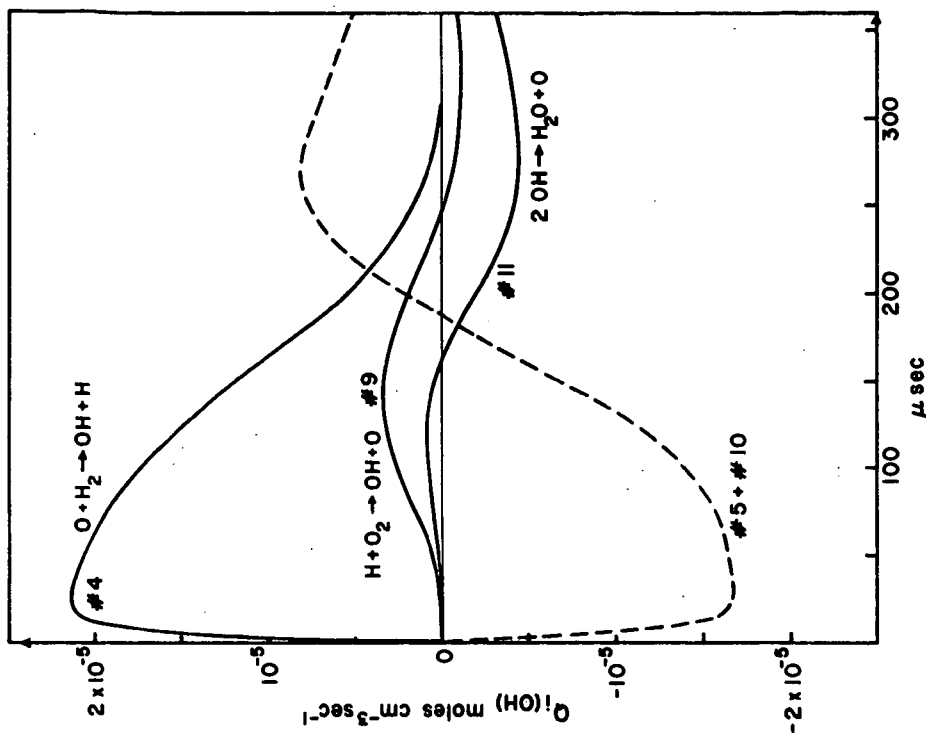


Figure 3a. Second test; OH production rates for $N_2O/H_2 = 1:1$ (same as 2a).

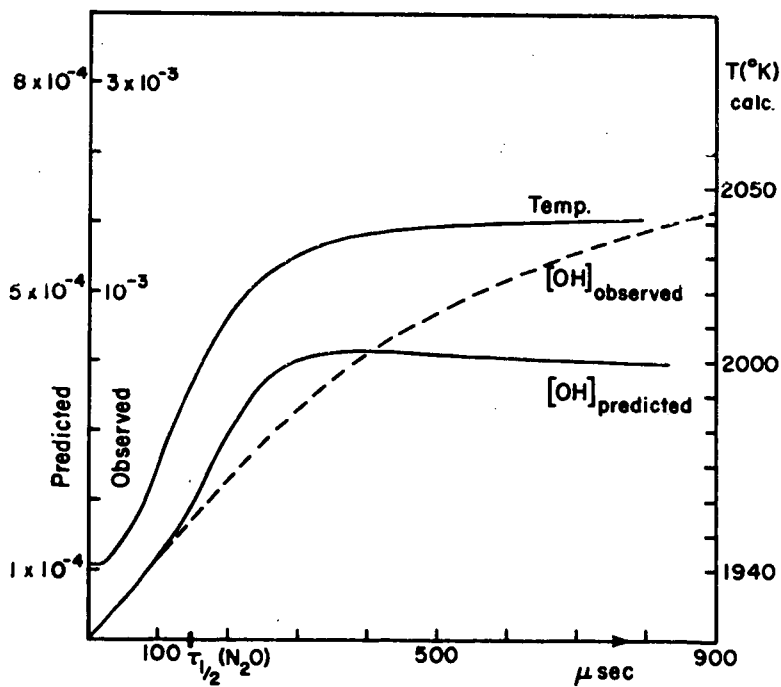


Figure 3b. Net [OH] produced, as a function of time.

SHOCK TUBE-MASS FILTER EXPERIMENTS ON LINEAR TRIATOMIC MOLECULES

R. Linn Belford

Department of Chemistry and Chemical Engineering
 Noyes Chemical Laboratory, University of Illinois, Urbana, Illinois

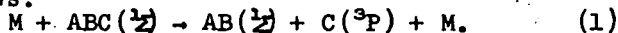
Introduction -- Use of fast mass spectrometry to follow high-temperature gas reactions in a shock tube was first introduced by Bradley and Kistiakowsky (1) and Diesen and Felmler (2) and has been exploited by several groups, all of whom have used a time-of-flight mass spectrometer. We have developed a combination of shock tube and Paul quadrupole mass filter and are using it to study reactions of linear triatomic molecules akin to CO_2 (3-7).

All the mass spectrometric shock sampling techniques have associated with them a number of common problems. These include the uncertainties in temperature caused by our partial ignorance of flow conditions through the sampling orifice into the region of the electron beam and of the rate of gas cooling by thermal transport to the end plate near the sampling leak.

In addition, there are special difficulties, but also special advantages accompanying each particular mass analyzer. The time-of-flight device operates on a cycle in which ionization occurs for only a small fraction of total reaction time (typically about 1/400). This feature limits sensitivity and interferes with noise recognition. However, one gets a full mass spectrum every cycle and can easily survey the species produced in a complex reaction. While a Paul mass filter could be built to operate essentially in the same fashion, it would offer no obvious advantage. It is best suited to the continuous ionization and study of the detailed time behavior of a single mass. Accordingly, mass filter detection is a valuable technique for the study of relatively uncomplicated systems, in which only a few species must be followed. It is also potentially useful for investigating the establishment of flow from the sampling orifice and the approach to steady state conditions in the ion source.

Here I shall outline the principal results of our studies of two related pyrolyses -- NNO and OCS -- and then consider together the existing shock tube data on all molecules of the same family. Of the several stable linear triatomic molecules having the same outer electron structure as that of CO_2 , only four -- CO_2 , N_2O , CS_2 , and OCS -- are common and have been studied under high-temperature shock conditions. Of these, only two -- CO_2 and N_2O -- have been studied extensively, and despite much progress in the past 4 years, there is still disagreement about some details of these decompositions.

Each reactant may be represented $\text{ABC}(\frac{1}{2})$, where C is a calcogen atom and AB is isoelectronic with carbon monoxide. At low pressure, high temperature, and high dilution in an inert gas (M), the first kinetic step is collisional excitation of the internal modes of ABC followed by rapid dissociation of every sufficiently energized reactant as follows:



Under some conditions of temperature and dilution, further steps can occur rapidly. The most important are (2) and (3):



With the mass spectral techniques it is easy to follow all of the possible species -- eg., ABC, C, M, CA, BC, AB, C₂ -- and so determine directly the role of steps such as (2) and (3).

Results -- In the nitrous oxide study (3-5) 4% and 2% mixtures of N₂O in Ar were shocked to temperatures between 1500 and 3500°K. All species found were accounted for by Reactions (1)-(3). All O⁺ signal could be ascribed to fragmentation. Formation of N₂, NO, and O₂ accompanied destruction of N₂O in the proportion of about 3:2:1.⁴ This suggests that Reaction (1) is immediately followed by (2) or (3), with equal probability. The chains and other reactions which we have looked into do not explain the observed distribution of species. That Reactions (2) and (3) keep up with (1) over most of the temperature range indicates that of the various reported expressions for k₂, the most reasonable is that of Fenimore and Jones (8) with an Arrhenius frequency factor of 10¹⁴ cc/mole sec and an activation energy of about 28 kcal. Essentially the same expression would hold for k₃. The general magnitude of these rates has been verified in a number of other shock experiments (9-11). They show an efficient atomic abstraction process with a high activation barrier which implies strong repulsion between triplet-state oxygen atom and N₂O.

Step (1) is of fundamental interest. In order to investigate it, one must know how Reactions (2) and (3) affect the rate. In this case the N₂O starting concentrations were sufficient to insure that the initial rate of N₂O destruction was 2k₁(M)(N₂O) at least up to 2500°K. At much higher dilutions, however, Steps (2) and (3) would be sufficiently slow to be negligible at small reaction times, and the initial rate would be k₁(M)(N₂O). If the experimental activation energy for Step (1) remains much higher than for Steps (2) and (3), at very high temperatures the near steady state concentration of O atom will not pertain, and the rate will drop from 2k₁(M)(N₂O) to k₁(M)(N₂O). It is not certain whether this situation applies in our experiments; therefore, we give the rate expression established for the points below 2500°K: $k_1 = A/\bar{T} (E/RT)^n \exp(-E/RT)$, with $A \approx 1.2 \times 10^7$ cc/mole sec $\sqrt{^\circ K}$, $E = 60$ kcal/mole, $n \approx 5.1$.

In the carbonyl sulfide study (6,7) 4%, 2%, and 0.5% mixtures of OCS in Ar were shocked to temperatures between 2000 and 3200°K. Typical ion current curves are shown in Fig. 1, and results for Step (1) are plotted in Fig. 2. Here the ions OCS⁺, CO⁺, CS⁺, S⁺, O⁺, SO⁺, S₂⁺ were seen. O⁺ is entirely accounted for by fragmentation, but the others are not, except that at low temperatures CS⁺ comes exclusively from fragmentation of OCS. Relative concentrations of S₂ and SO over a temperature range establish that the activation energy for (2) exceeds that for (3) by ca. 19 kcal/mole. In the 0.5% mixtures, the rise of S⁺ signal indicates that a steady state in S is not immediate and establishes the initial rate of OCS disappearance as k₁(M)(OCS). From this, $A \sim 1.1 \times 10^{11}$ cc/mole sec $\sqrt{^\circ K}$, and $n = 1.87$, if E is taken as $D_{O-C}^0 = 71.5$ kcal/mole. From the quantitative behavior of the S₂⁺, S⁺, and OCS⁺ ion currents, we estimate $k_2 \approx 6 \times 10^{11}$ cc/mole sec at 2600°K. If the steric factor for this reaction is "normal" (0.1 or greater), the activation energy is in the range 20-30 kcal/mole, and there is a barrier to reaction of triplet sulfur atom with OCS that is comparable to the corresponding O + N₂O barrier.

Given the magnitude of k_2 so deduced, one can calculate that at the higher (2% and 4%) percentages of OCS, a near steady-state concentration of S atom would be established almost immediately, and the measured rate would be $2k_1(\text{OCS})(M)$. Although the 2% and 4% measurements were less reliable because of troubles with solid sulfur, which deposited in the sampling orifice, the data indicated a rate about twice that yielded by the 0.5% mixtures, except at the upper end of the temperature range, where the values of k_1 from the 2% mixtures scattered about those from the 0.5% mixtures.

Theory -- The most interesting aspect of the high-temperature study of decomposition of triatomic molecules is the opportunity which it can afford to investigate some consequences of the details of collisional activation. The strong-collision assumption requires that in the steady state all bound quantum states of reactants are populated in Boltzmann fashion, and that the probability of exciting a molecule into an unbound state is proportional to the Boltzmann factor for the final state but independent of initial (bound) state. Thus, to get the reaction rate at low pressures, one need only divide all states into bound and unbound, apply the Boltzmann distribution to all, find the fraction of the Boltzmann population curve which covers unbound states, and multiply by collision rate. Thus, one has an a priori way of predicting reaction rate as a function of temperature (12). The rate should increase somewhat less rapidly with temperature than would be predicted by an Arrhenius extrapolation from low temperature. It is only at very high temperatures that one can expect the difference between the experimental and critical (low-temperature) activation energy to become significant. Thus, accurate data on the temperature dependence of these reaction rates under high-temperature shock conditions are potentially of great fundamental interest.

If the strong-collision assumption is seriously at fault, then reaction may proceed largely by collisional activation of the high-energy bound molecules. This process, in turn, may deplete the populations of the upper bound levels and act to limit the reaction rate. The effect would be expected to increase with temperature and yield a negative contribution to the experimental activation energy.

Accordingly, let us examine pertinent data so far collected on high-temperature activation energies for rupture of molecules of the CO_2 family.

In the case of OCS, the minimum possible critical activation energy is about 71.5 kcal/mole, the over-all dissociation energy D_0° . Our observed activation energy (7) over the range 1950-3150°K is 64.5 kcal/mole. Since at 2550°K the vibrational system of OCS is already excited by 15.5 kcal/mole and as the collision frequency involves an effective activation energy of $(1/2)RT = 2.5$ kcal/mole, the minimum expected over-all activation energy would be $71.5 - 13 = 58.5$ kcal/mole. On the basis of any strong-collision theory, which states that active molecules are formed in a Boltzmann distribution, about $1.2RT = 6$ kcal/mole is stored in vibrations of the average active molecule formed, putting the expected minimum experimental activation energy at 64.5 kcal/mole ($=58.5+6$), in agreement with that observed. Therefore, according to our current knowledge of the parameters involved in the OCS dissociation, the strong-collision

theory (such as the RRKM treatment) is not in conflict with the experiment. However, we lack independent information about the critical activation energy (which could be higher than the dissociation energy, as is apparently the case in N_2O (5)) or the activated complex (bottleneck) configuration (which tells us how to treat rotations in the strong-collision approach (7,12)). Therefore, predictions based on the strong-collision theory may not be shown to agree with the facts. Indeed, our calculations based on the RRKM theory (7) show that a low (~1%) collisional activation efficiency λ_D is required to fit the observed rates, and this may be considered reasonable grounds for suspecting the strong-collision model, as certainly not 99 of every 100 collisions are elastic. To make λ_D larger, one has to assume a larger critical activation energy, which in turn means that the experimental activation energy shows a negative term not provided by the strong-collision treatment.

In the case of SCS, the critical activation energy is sure to be essentially the dissociation energy, $D_0^0 = 96$ kcal/mole for $SCS(^1\Sigma) \rightarrow CS(^1\Sigma) + S(^3P)$; the reaction proceeds through the bent 3A_2 state of CS_2 , which is stable. The experimental activation energy has been reported (13) as 80.3 kcal/mole over the range 1800 to 3700°K. At 2850°K, 18.3 kcal/mole is stored in the vibrational modes of OCS, and correction for the temperature dependence of collision frequency brings the possible minimum expected activation energy to about $96. + 2.8 - 18.3 = 80.5$ kcal/mole. The strong-collision approximation adds about 6.5 kcal to this, bringing the expected strong-collision activation energy to about 87 kcal/mole. It is possible that a rotational correction is required (7,12), which might reduce this by as much as 2 kcal/mole; regardless, there is a discrepancy indicating the effective activation energy to be a bit too small to be explained within the strong-collision framework.

The large number of shock tube studies on N_2O rupture include at least one employing an infrared detection technique (14), two involving ultraviolet absorption measurements (11,14), three employing time-of-flight mass spectrometry, and ours using the quadrupole mass filter. The various investigators report experimental activation energies ranging from 30 to 49 kcal/mole, except for one study (11) which yielded 58 kcal/mole. There appears to be an activation barrier to recombination, giving a critical activation energy in the vicinity of 60 kcal/mole for $N_2O(^1\Sigma) \rightarrow N_2(^1\Sigma) + O(^3P)$. At the mean temperature of most of the experiments (~2250°K), there is roughly 12.5 kcal vibrational excitation; $60 - 12.5 + 2.2 \approx 50$ kcal/mole. With active molecules being formed with about 5 kcal average excess energy, in the strong-collision model we might expect an activation energy of about 55 kcal/mole; rotation would decrease it by 1-2 kcal (7). Fig. 3 shows data from various studies fitted to a least-squares Arrhenius line. It would be hard to reconcile the experiments with the strong-collision result. The discrepancy in activation energy is about $4RT$. The apparent collisional activation efficiency also is very small.

Several shock studies of OCO decomposition are on record; all have been done by spectroscopic techniques. The experimental activation energies from several of the studies are as follows:

Reference	T	$E_{\text{exp}} - \frac{1}{2} RT$	E_a (s.c.)	$D_0^0 - E_a$ (s.c.) $\langle RT \rangle$
(15)	2500-3000°K	86 kcal	95	5.5
(16)	2850-4200	95.5	110	2.2
(17)	3000-5000	84.5	99	3.2
(18)	3500-6000	74.5	92	3.7
(19)	6000-11000	62	93	2.1

Here, E_{exp} denotes experimental activation energy ($-\frac{d \ln k}{d(1/RT)}$) and E_a (s.c.) denotes the critical activation energy which, on a strong-collision model, would be computible with the given E_{exp} . Notice that the highest experimental activation energy obtained is still 30 kcal below the minimum dissociation energy, 126 kcal/mole.

In general, the preponderance of kinetic information so far obtained with shock experiments on low-pressure dissociations of linear triatomic molecules at high temperatures indicates a smaller temperature coefficient of rate than is predicted by the strong-collision theory of vibrational activation. However, more precise experimentation should be done. The effect is evidence of either some fairly widespread systematic error in shock measurements (such as a temperature error) or some serious breakdown of the (strong collision) theory.

Recently, Tardy and Rabinovitch(20) have reported a series of calculations on various stochastic weak-collision models for excitation. They found that the strong-collision rate expression requires a correction factor, β , which proved to be fairly insensitive to the details of the particular model chosen and principally dependent on $\langle \Delta E \rangle / \langle E^+ \rangle$, where $\langle \Delta E \rangle$ denotes the average energy transferred per down collision and $\langle E^+ \rangle$ denotes the mean energy of the active molecules in the strong-collision model. Ignoring any dependence of $\langle \Delta E \rangle$ on temperature, we find that for β between 0.2 and 0.01, $-\frac{d \ln \beta}{d(1/RT)} < -2 RT$. There is thus some theoretical justification for blaming an abnormally large high-temperature falloff of experimental activation energy on a weak-collisional energy transfer process.

Conclusion -- Measurements of temperature dependence in the rates of unimolecular reactions of small molecules in the second-order (low pressure) region offer exciting and heretofore unexploited opportunities to investigate certain aspects of the collisional activation process. However, precise data and particularly reliable temperature measurements are necessary. The considerable disagreement among various laboratories in the case of the reactions discussed here is prima facie evidence that accuracy sufficient to the purpose has not been routinely attained by most shock tube groups. Nevertheless, there is a general pattern of anomalously low activation energies at very high temperatures which suggests a weak-collision process with reactive depletion of the upper bound levels.

Acknowledgment -- This work is supported by the National Science Foundation, Professor David Gutman (now of Illinois Institute of Technology) and Dr. Arthur J. Hay (now of E. I. DuPont de Nemours and Co.) were responsible for much of the work, with considerable assistance from Dr. Roy Pancirov and Mr. George Sanzone.

References

- (1) J. N. Bradley and G. B. Kistiakowsky, *J. Chem. Phys.* 35, 256 and 264 (1961).
- (2) R. W. Diesen and W. J. Felmlee, *J. Chem. Phys.* 39, 2115 (1963).
- (3) D. Gutman, "High Temperature Gas Kinetic Study of Nitrous Oxide Decomposition Performed with a Shock Tube and Quadrupole Mass Filter," Ph.D. Dissertation, University of Illinois, Urbana, Illinois, May 1965.
- (4) D. Gutman, A. J. Hay, R. L. Belford, *J. Phys. Chem.* 70, 1786 (1966). (Describes the first version of the apparatus and performance tests.)
- (5) D. Gutman, R. L. Belford, A. J. Hay, and R. Pancirov, *J. Phys. Chem.* 70, 1792 (1966). (Describes an N₂O study performed with the apparatus of Ref. 4.)
- (6) A. J. Hay, "High-Temperature Gas Kinetic Study of Carbonyl Sulfide Decomposition Performed with a Shock Tube and Quadrupole Mass Filter," Ph.D. Dissertation, University of Illinois, Urbana, Illinois, Feb. 1966.
- (7) A. J. Hay and R. L. Belford, *J. Chem. Phys.*, (to appear). (Describes an improved apparatus and its use in an OCS study).
- (8) C. P. Fenimore and G. W. Jones, "8th International Symposium on Combustion," Williams and Wilkins Co., Baltimore (1962); *J. Phys. Chem.* 62, 178 (1958).
- (9) E. S. Fishburne and R. Edse, *J. Chem. Phys.* 44, 515 (1966).
- (10) J. E. Dove, Private Communication, and S. C. Barton, Ph.D. Thesis, University of Toronto, Canada, Feb. 1966.
- (11) H. A. Olschewski, J. Troe, and H. G. Wagner, *Ber. Buns. Ges.* 70, 450 (1966).
- (12) R. A. Marcus, *J. Chem. Phys.* 20, 359 (1952) and 43, 2658 (1965). Also G. M. Wieder and R. A. Marcus, *ibid.* 37, 1835 (1962).
- (13) H. A. Olschewski, J. Troe, and H. G. Wagner, *Z. fur phy. Chemie, Frankfurt*, 45, 329 (1965).
- (14) E. S. Fishburne and R. Edse, *J. Chem. Phys.* 41, 1297 (1964).
- (15) T. A. Brabbs, F. E. Belles, and S. A. Zlatarich, *J. Chem. Phys.* 38, 1939 (1963).
- (16) K. W. Michel, H. A. Olschewski, H. Richterig, and H. G. Wagner, *Z. fur phy. Chem., Frankfurt*, 44, 160 (1965). Also 39, 9 (1964).
- (17) E. S. Fishburne, K. R. Bilkawesh, and R. Edse, *J. Chem. Phys.* 45, 160 (1966).
- (18) W. O. Davies, *J. Chem. Phys.* 41, 1846 (1964).
- (19) W. O. Davies, *J. Chem. Phys.* 42, 2809 (1965).
- (20) D. C. Tardy and B. S. Rabinovitch, *J. Chem. Phys.* 45, 3720 (1966).

Figures

- Fig. 1a Sample, experimental oscilloscope traces of ion currents from shocks, OCS 0.5% in Ar, $\sim 2800^\circ\text{K}$. A: OCS^+ . B: CO^+ . C: S^+ . D: S_2^+ . E: CS^+ . F: SO^+ . The smooth line is a signal from a thin-film resistor in the shock tube end wall. Fine marks appear on the bottom line, 200 μsec . apart.
- Fig. 1b Typical adjustment of S^+ , CS^+ , and CO^+ dynamic in current curves to correct for OCS fragmentation.
- Fig. 2 Second-order rate constants (k_1) for the disappearance of OCS, 0.5% in Ar. Open circles correspond to initial pressure of 6 ton; shaded ones, 8 ton. The line is the result of a quantum RRKM calculation for an assumed critical activation energy of 71.5 kcal/mole, and $\lambda_D \approx 0.01$.
- Fig. 3 Arrhenius plot of second-order rate constants ($2k_1$) disappearance of N_2O , 1-4% in Ar. +: Our data. Other symbols denote other laboratories. Solid line: $k = 10^{12.4} \exp(-35.4 \text{ kcal/RT mole})$, from least-squares fit with half-weighting of our data. Dotted line: with equal weighting of all data.

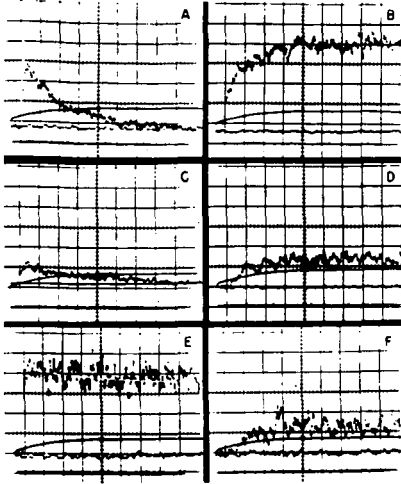


Fig. 1a Sample, experimental oscilloscope traces of ion currents from shocks, OCS 0.5% in Ar, $\sim 2800^\circ\text{K}$. A: OCS^+ . B: CO^+ . C: S^+ . D: S_2^+ . E: CS^+ . F: SO^+ . The smooth line is a signal from a thin-film resistor in the shock tube end wall. Fine marks appear on the bottom line, 200 μsec . apart.

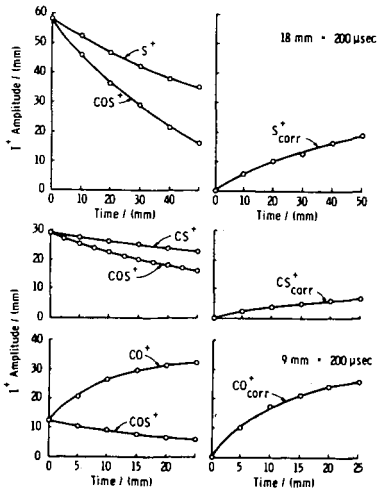


Fig. 1b Typical adjustment of S^+ , CS^+ , and CO^+ dynamic in current curves to correct for OCS fragmentation.

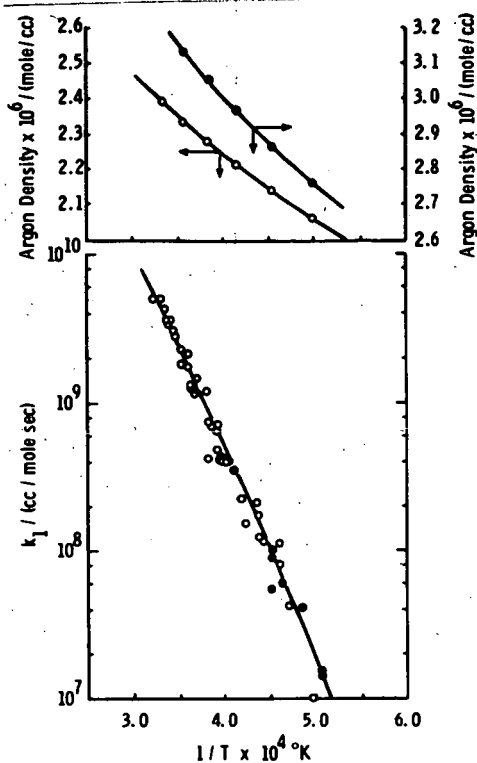


Fig. 2. Second-order rate constants (k_1) for the disappearance of OCS, 0.5% in Ar. Open circles correspond to initial pressure of 6 torr; shaded ones, 8 torr. The line is the result of a quantum RRKM calculations for an assumed critical activation energy of 71.5 kcal/mole, and $\lambda_D \approx 0.01$

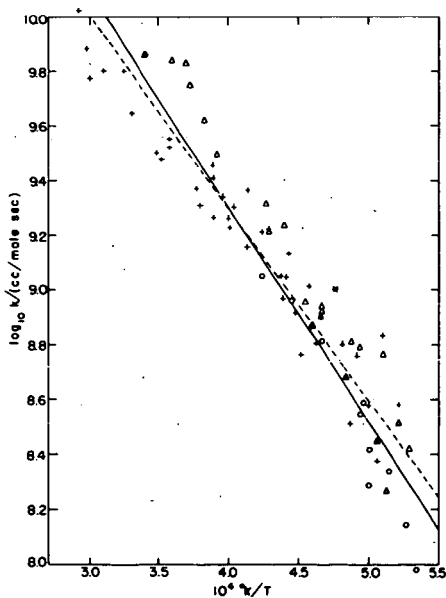


Fig. 3. Arrhenius plot of second-order rate constants for ($2k_1$) disappearance of N_2O , 1-4% in Ar. +: Our data. Other symbols denote other laboratories. Solid line: $k = 10^{12.4} \exp(-35.4 \text{ kcal/RT mole})$, from least-squares fit with half-weighting of our data. Dotted line: with equal weighting of all data.

A SHOCK TUBE STUDY OF THE RADIATIVE COMBINATION OF OXYGEN ATOMS
BY INVERSE PREDISSOCIATION

B. F. Myers and E. R. Bartle

Space Science Laboratory, General Dynamics/Convair
San Diego, California, 92112

ABSTRACT

Absolute emission intensity measurements of the radiative combination of oxygen atoms, $O(^3P)$, in the temperature range between 2500°K and 3800°K are presented. The emission intensity was recorded simultaneously in six spectral intervals in the wavelength range between 2300Å and 4511Å. The absolute emission intensity was found to be proportional to the square of the oxygen atom concentration and to be characterized by an activation energy of 28.9 ± 2.2 kcal mole⁻¹. These results are interpreted in terms of an inverse predissociation mechanism in which the oxygen atoms combine along a repulsive potential energy surface with a transition to the $B^3\Sigma_u^-$ state of molecular oxygen and a subsequent radiative transition to the ground electronic state of oxygen. The rate constant for the overall radiative combination of oxygen atoms was found to be $4.3 \times 10^6 \exp(-28900 \pm 2200/RT)$ cm³ mole⁻¹ sec⁻¹ for the wavelength range 2300Å to 5000Å.

I. INTRODUCTION

Measurements on the radiative combination of oxygen atoms, $O(^3P)$, in the temperature range between 2500°K and 3800°K are presented. This radiative process was first observed during an investigation¹ on the radiative combination of atomic oxygen and carbon monoxide. In the latter case, it was found that a contribution to the total emission intensity occurred at wavelengths below 4500Å in the presence of oxygen atoms only.

In the present experiments, absolute emission intensity measurements of the radiation resulting from the combination of oxygen atoms were made by shock heating $O_3 + Ar$ gas mixtures to temperatures in the range cited above and to pressures between 0.5 and 2.0 atm. The emission intensity was recorded simultaneously in six spectral intervals in the wavelength range between 2300Å and 4511Å. The emission intensity behind the shock front at the time of essentially complete ozone decomposition was correlated with the oxygen atom concentrations as determined by numerical calculations.

II. EXPERIMENTAL

The experiments were conducted with the 3 inch, internal diameter shock tube facility and the associated optical system and gas handling system previously employed.¹ For the measurement of the emission intensity of the radiative combination of oxygen atoms, the six slits in the image plane of the spectrograph had the center wavelengths and bandpasses given in Table I. The wavelength values listed have an error of less than 3Å. For detection of incident radiation in the spectral interval between 2300Å and 2500Å, two Dumont 7664 photomultipliers with S-13 spectral response and fused silica windows were employed, and in the spectral interval between 3000Å and 4511Å, four RCA type 1P28, photomultipliers with S-5 spectral response, two of which had quartz windows, were employed. The response of the detector system was linearly related to incident radiation¹ and output signal for each spectral channel was not affected by radiation transmitted in the other channels.¹ The output signals were calibrated in terms of the steradiancy of a calibrated tungsten ribbon filament lamp.¹ The entire optical system was

enclosed in a light tight box which could be flushed with Ar to avoid absorption of the emitted radiation by air.

The gas mixtures of O_3 and Ar were prepared from Matheson Co. supplies of Ar (ultra high purity grade) containing less than 12 ppm of contaminants and from Liquid Carbonic O_2 (electrolytic laboratory grade) containing less than 10 ppm of contaminants. The ozone was synthesized from the oxygen in a static ozone generator.² The gas mixtures prepared contained from 1% to 18% of O_3 . The quantitative analysis of the ozone in the prepared gas mixtures was made by a standard titration procedure.³ For each experiment the test gas mixture was shock heated within three minutes following addition to the shock tube, and a sample of the mixture was withdrawn from the shock tube for ozone analysis one minute before shock heating the mixture.

The $O_3 + Ar$ mixtures were shock heated to temperatures between 2500°K and 3800°K and pressures between 0.5 and 2.0 atm. At these temperatures and pressures, at least 99% of the ozone had decomposed within 0.1 μ sec (particle time) behind the incident shock wave to form atomic and molecular oxygen. The concentrations of oxygen atoms and molecules were determined for each experiment by a numerical calculation based on an assumed decomposition mechanism and corresponding elementary reaction rate constants as discussed below. The numerical calculations were made using the Cornell Aeronautical Laboratory normal shock wave computer program.^{4,5} The calculations were performed on an IBM 7090-7094 computer.

III. RESULTS

An oscillogram of the recorded emission intensities is shown in Figure 1. For this experiment, a mixture of 6% $O_3 + 94%$ Ar was shock heated to an initial temperature of 3048°K and a pressure of 1.41 atm; this temperature and pressure correspond to translational, rotational and vibrational equilibrium of the mixture with frozen chemical reactions. Opposite the beginning of each channel trace in Figure 1, the center wavelength and spectral interval are given in Angstrom units. The shock front arrival is indicated by the sudden rise in the upper trace of Figure 1b which shows the response of a heat resistor gauge mounted in the shock tube wall at the cross section of the radiation measurement. The response time of the detector system is $\leq 15 \mu$ sec (laboratory time) for all channels except that channel with a center wavelength of 3002Å for which the response time is 20 μ sec (laboratory time). To obtain the emission intensity immediately after essentially complete ozone decomposition which occurs within 0.1 μ sec (particle time) of shock front arrival at the observation station, the emission-time profiles are extrapolated practically to zero time. Numerical calculations demonstrate that after the ozone decomposes, the concentrations of atomic and molecular oxygen and the temperature change slowly under the present experimental conditions toward an equilibrium state. For that portion of the emission intensity-time profile following the initial rise in signal, the signal was either constant or linearly increasing or decreasing slowly for 50 to 150 μ sec (laboratory time), allowing for the noise in the signal; the extrapolation was based on this portion of the trace.

The extrapolated values of the signals near zero time were converted to intensity values for each spectral channel (i) by using the following relation:

$$I_i = \frac{S_i C_i}{[1+R_i]d} \frac{\text{watts}}{\text{str-}\dot{\text{A}}\text{-cm}^2} \quad (1)$$

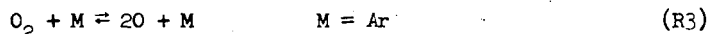
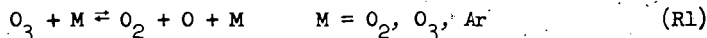
where S_i is the extrapolated oscillogram signal in volts, C_i , the calibration factor in watts $\text{str}^{-1} \dot{\text{A}}^{-1} \text{cm}^{-2} \text{v}^{-1}$, determined from the measured oscilloscope signal corresponding to the known steradiancy of the standardized, tungsten ribbon filament lamp in each wavelength interval of the spectral channels, $d (= 7.70 \text{ cm})$

the diameter of the shock tube and R_1 , the reflectivity at the center wavelength of channel 1 of the shock tube wall opposite the observation station window which serves as a bounding plane to the optical field. The dependence of the reflectivity on the wavelength which was determined in two independent experiments⁶ and the normalization of the intensity with respect to the diameter of the shock tube, d , have been discussed previously.¹

The values of I_1 computed as described above, are shown in Table II; also given are the initial conditions, the shock velocity and the calibration factors for each spectral channel.

Contributions to the observed emission intensity from molecular oxygen, argon or impurities in the test gases were examined by shock heating argon and oxygen-argon mixtures to temperatures up to 3600°K. No signal was observed with shock-heated oxygen-argon mixtures until significant decomposition of the molecular oxygen to form oxygen atoms occurred; with shock-heated argon, a signal was observed only in the spectral channel with a center wavelength of 4511Å. This signal was a transient lasting about 50 μ sec (laboratory time) and was apparently caused by an impurity in the argon or by residual gases in the shock tube. In applying the extrapolation procedure to the data for this channel, the oscillogram trace for $t(\text{laboratory time}) < 50 \mu\text{sec}$ was disregarded. However, when the extrapolation was made using that portion of the trace for which $t(\text{laboratory time}) \geq 150 \mu\text{sec}$, a lower, but not significantly different value of the signal was obtained. The intensities corresponding to the latter signal values are only considered below in connection with Figure 7. This difference could indicate a contribution to the oscillogram trace by the transient signal for $t(\text{laboratory time}) > 50 \mu\text{sec}$, although this is difficult to establish because of the signal noise.

For each experiment, the oxygen atom concentration immediately behind the shock front was determined by a numerical calculation based on the following reaction mechanism:



The forward rate constants for these reactions were part of the input data for the computer program⁴ while the reverse reaction rate constants were calculated from thermodynamic data and the forward reaction rate constants as part of the computer program. The rate constants for reactions R1 and R2 have been deduced from experiments on the thermal decomposition of ozone at temperatures between 343°K and 383°K in static experiments^{7,8} and at temperatures between 689°K and 910°K in shock tube experiments.⁹ The relative efficiencies of Ar, O₂ and O₃ in reaction R1 were determined in the low temperature experiments.^{7,8} The use of these rate constants at temperatures above 2500°K involves a large extrapolation and recent experiments¹⁰ indicate that the ratio k_1/k_2 is as much as five times smaller than the extrapolated value in the approximate range of temperatures between 1500°K and 2800°K. This conclusion is based on rate constant expressions given in the Arrhenius form.^{7,8,9} It will be shown below, however, that this discrepancy is practically resolved for the present experiments by using the rate constant for reaction R1 in the form corresponding to the Hinshelwood-Rice-Ramsperger-Kassel theory of uni-molecular reactions as given by Jones and Davidson⁹ and the rate constant for reaction R2 in the collision theory form, i.e., $k = AT^{1/2} e^{-E/RT}$, based on the data of Benson and Axworthy.^{7,8} The values of the parameters in these rate constant expressions for reactions R1 and R2 are given in Table III in the group labelled set II; in the group labelled set I, the values of the parameters for the rate constants expressed in the Arrhenius form are given for reactions R1

and R2. The rate constant parameters for the forward direction of R3 are also given in Table III; however, exclusion of the data for R3 from the numerical calculations did not significantly alter the calculated oxygen atom concentration at the time of essentially complete ozone decomposition. To reduce the machine computing time, the calculations were stopped after greater than 99% ozone decomposition and the final oxygen atom concentration was determined by a linear extrapolation based on the concentration of the ozone remaining and on the rate of oxygen atom production per unit ozone concentration in the last machine integration step. Also in making the numerical calculations, the assumption was adopted that the vibrationally excited oxygen, formed in reaction R2,¹¹ had no effect on the decomposition of ozone. (The chemical relaxation time for ozone decomposition was about 0.1 μ sec while the vibrational relaxation time for oxygen in the present,^{10,12} experiments was between 0.1 and 1.0 μ sec as estimated from the available data.)

In Table IV, the computed oxygen atom concentrations and the temperatures after ozone decomposition are given. From data in Tables II and IV, it was found that:

$$I_1 = \Gamma_1 (O)^2 \quad (2)$$

where I_1 is the emission intensity in watts $\text{str}^{-1} \text{\AA}^{-1} \text{cm}^{-3}$ obtained by extrapolating the emission-time profiles on the oscillograms of shock heated $O_3 + \text{Ar}$ mixtures to the time immediately following shock front arrival at the observation station, Γ_1 , a constant for each spectral channel and (O) , the atomic oxygen concentration in moles cm^{-3} . Three examples of data plotted according to equation 2 are shown in Figure 2. The concentration-normalized, absolute emission intensities, Γ_1 are functions of the temperature only and the logarithms of Γ_1 are found to be linearly related to the reciprocal of the absolute temperature. This is illustrated in Figures 3 and 4 for the six spectral channels employed (see Table I). The lines drawn through the data points are the least squares fits to the data and the vertical bars indicate the standard deviation at the 90% confidence level. The values of Γ_1 plotted in these figures were calculated according to equation 2 with oxygen atom concentrations determined from numerical calculations using the rate constants for R1, R2 and R3 given in set II of Table III. When the oxygen atom concentrations were calculated using the rate constants in the Arrhenius form as given in the literature^{8,9} and in Table III as set I, the values of Γ_1 were found to depend on the initial ozone concentration as shown in Figure 5. In this figure, the lines drawn through the data points are the least squares fits for each initial ozone concentration, $(O_3)_0$. In Figure 5, equation 2 is valid for each set of data corresponding to a particular initial ozone concentration. However, as shown in Figures 3 and 4, the dependence of Γ_1 on $(O_3)_0$ can be made insignificant by introducing a reasonable pre-exponential temperature dependence into the rate constant expressions for reactions R1 and R2. For each initial ozone concentration, the data for each spectral channel as shown in Figures 3 and 4 are found not to be significantly different at the 90% confidence level based on the standard deviations determined for the least squares fits to the data at constant $(O_3)_0$ and λ_c .

From the temperature dependence of Γ_1 , as shown in Figures 3 and 4, values of the activation energy E_1 , in the relation

$$\Gamma_1 = A_1 e^{-E_1/RT} \quad (3)$$

were determined for each spectral interval employed; the results are shown in Table V. There is no significant dependence at the 90% confidence level of the activation energy on the wavelength. The average of these activation energies and the corresponding standard deviation are 28.6 and 2.2 kcal mole⁻¹, respectively.

Rate constants corresponding to the overall radiative combination of oxygen atoms, i.e., for the process



were calculated at five temperatures and then combined in an Arrhenius expression to obtain the value $k = 4.3 \times 10^6 \exp(-28900 \pm 2200/RT)$ cm³ mole⁻¹ sec⁻¹ for the wavelength range 2300Å to 5000Å.

IV. SUMMARY AND DISCUSSION

Absolute intensity measurements were made of the emitted radiation in the wavelength region between 2300Å and 4511Å; this radiation was observed by shock heating mixtures of ozone and argon to temperatures between 2500°K and 3800°K. The presence of oxygen atoms was necessary to observe this radiation and the absolute emission intensity was found to be proportional only to the square of the oxygen atom concentration at a given temperature. Furthermore, the temperature dependence of the absolute emission intensity normalized with respect to the square of the oxygen atom concentration could be characterized by an activation energy of 28.9 ± 2.2 kcal mole⁻¹.

These observations can be rationalized in terms of the potential energy curves for oxygen as shown in Figure 6; the curves presented here were selected from the diagrams of Gilmore.¹³ The thermal decomposition of ozone produces ground state oxygen atoms, O(³P), which may then combine along several potential energy surfaces. Such a process would be proportional to the square of the oxygen atom concentration, at least. The fact that the radiative process observed has an activation energy of 28.9 ± 2.2 kcal mole⁻¹ leads to the following suggested mechanism. The ground state oxygen atoms combine along a repulsive potential surface with a subsequent transition to the B³Σ_u⁻ state of molecular oxygen; the radiative transition from the latter state to the ground state, X³Σ_g⁻, then occurs. The vibrational levels of the B³Σ_u⁻ state from which the transitions originate lie at $v' \leq 4$. This conclusion is based on the fact that the energy difference between the $v' = 4$, $J = 0$ level of the B³Σ_u⁻ state and the ground state of the oxygen atoms is 30.68 kcal mole⁻¹ while the upper limit to the experimental activation energy is 31.1 kcal mole⁻¹ at the 67% confidence level.

The mechanism described is the reverse of a predissociation mechanism suggested¹⁴ to account for observations made during the photolysis of O₂ at 1849Å. In this case, molecular oxygen is excited to the B³Σ_u⁻ state and predissociates along a repulsive potential curve to yield two oxygen atoms, O(³P). Additional photochemical¹⁵ and spectroscopic¹⁶ evidence has been obtained to support this predissociation mechanism.

There are two other mechanisms for the radiative combination of oxygen atoms which are not significant for the shock tube experiments. In one of these, ground electronic state oxygen atoms combine along the potential surfaces leading to the A³Σ_u⁺, c¹Σ_u⁻ or C³Δ_u state of O₂ with subsequent radiative transitions to the states, X³Σ_g⁻ or to b¹Σ_g⁺. One transition (A³Σ_u⁺ → X³Σ_g⁻, in the wavelength range between 2563Å and 4880Å)⁶ and also perhaps several of the other possible transitions have been observed^{17,18,19} in flow systems containing atomic oxygen at low pressures and near room temperature. However, this mechanism is inconsistent with the present experimental observations since (a) a near zero activation energy is predicted in contrast to the observed activation energy of 28.9 kcal mole⁻¹, and (b) the contribution of the O₂ Herzberg bands to the measured emission intensity is estimated to be less than 3% of the total intensity. The latter conclusion may be demonstrated in two ways. If the value of the room temperature rate constant¹⁸ for the radiative combination of oxygen atoms to give the O₂ Herzberg bands is extrapolated to temperatures greater than 2700°K by assuming a T^{-1/2} dependence, this rate constant becomes at least 30 times smaller than the rate constant derived from the present experimental data. Alternatively, the ratio of the emission intensity, I(Schumann-Runge)/I(Herzberg), may be estimated to be greater than 130 on

the basis of a simplified mechanism as shown in Appendix A. In the second mechanism, the oxygen atoms combine along the potential surface of the $B^3\Sigma_u^-$ state of O_2 after collisional excitation of one of the atoms, $O(^3P) \rightarrow O(^1D)$; the radiative transition $B^3\Sigma_u^- \rightarrow X^3\Sigma_g^-$ subsequently occurs. This mechanism is also inconsistent with the present experimental observations since (a) an activation energy of about $45 \text{ kcal mole}^{-1}$ is predicted and this is significantly greater than the observed activation energy, and (b) the spectral intensity distribution resulting from this mechanism is unlikely to result in transitions originating only from $v' \leq 4$ of the $B^3\Sigma_u^-$ state of O_2 .

On the assumption that the observed transition is $B^3\Sigma_u^- \rightarrow X^3\Sigma_g^-$, a comparison of the experimental and theoretical relative spectral distribution curves indicates that the observed radiative transitions originate primarily from the $v' = 0$ and 1 levels of the $B^3\Sigma_u^-$ state. The comparison is shown in Figure 7 for temperatures of 2632°K , 3030°K and 3571°K ; the experimental data are represented by discrete symbols and the theoretical data are represented, for the sake of clarity, by curves which pass through the data calculated for the experimental spectral intervals which the horizontal bars span. The vertical bars through the symbols represent the standard deviation at the 90% confidence level. In making this graphical comparison, the theoretical relative spectral distribution curves were vertically adjusted so as to coincide with the experimental absolute spectral distribution curve at $\lambda_c = 3002\text{\AA}$. The three curves are calculated for transitions originating from $v' = 0$ and 1, 0, 1 and 2 and 0, 1, 2 and 3 and in this order demonstrate an increasing deviation of the theoretical calculations from the experimental data at wavelengths below 3000\AA . (The double points at $\lambda_c = 4511\text{\AA}$ are calculated as described above; the error in these data are too large to permit a comparison with the various theoretical relative spectral distribution curves.) However, the comparison is imprecise and is only employed here to introduce the possibility that the observed radiative transitions may originate primarily from the $v' = 0$ and 1 levels of the $B^3\Sigma_u^-$ state. In making the calculations,²¹ the assumptions of thermodynamic equilibrium,^{20,22,23} of the smeared rotational line model^{22,23} and of $\Delta J = 0$ for all vibration-rotation transitions^{20,24} were employed. These assumptions are not strictly valid for use in a comparison with the present experimental data. At the least, the inverse predissociation mechanism predicts a truncation of the population distributions in the vibrational and rotational levels near the crossing level (i.e., near an intersection of the potential curves in a certain low approximation, see ref. 25) which would introduce a perturbation in these distributions. In the converse case of a predissociation mechanism, such a perturbation has been observed²⁶ and corresponds to that predicted²⁷ in dissociation processes.

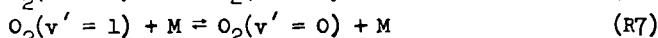
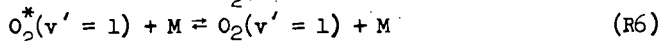
Qualitatively, the statement may be made that calculations which include significant contributions by transitions originating in vibrational levels with $v' \geq 2$ will result in a predicted intensity greater than observed at wavelengths less than 3000\AA . This is corroborated by noting that, at $T = 3030^\circ\text{K}$, for example, 94% of the observed radiation occurs in the wavelength range between 2640\AA and 4400\AA ; this is expected for transitions solely from $v' = 0$ and 1 to the approximation that the transitions occur only at the classical turning points of the potential curve for the $B^3\Sigma_u^-$ state. Also, for transitions from the various vibrational levels which contribute to the emission intensity observed in a given spectral interval, the strong influence of transitions from $v' \geq 2$ on the intensity is indicated, for example, in the wavelength interval between 2269\AA and 2331\AA (Channel 1 in Table I) by the relative increase in the Franck-Condon factors; for the levels $v' = 0, 1, 2, 3$ and 4 , the relative magnitudes of the Franck-Condon factors are roughly in the ratios²⁸ $1:10:10^2:10^3:5 \times 10^3$, respectively.

From the experimental absolute spectral distribution curves and the comparison with theoretical relative spectral distribution curves, the tentative conclusion was

reached that radiative transitions originate primarily from the vibrational levels $v' = 0$ and 1. On the other hand, from the experimental activation energy of 28.9 ± 2.2 kcal mole⁻¹, the conclusion is reached that vibrational levels as high as $v' = 4$ may possibly be occupied by newly formed oxygen molecules in the $B^3\Sigma_u^-$ state. The relation between these conclusions can be qualitatively understood on the basis of two factors. According to the first factor, there is a preferential transition from one to another potential surface into states with large values of J (or N) and small values of v (< 4), i.e., molecules of O_2 are formed with considerable angular momentum.²⁹ The second factor accounts for the temperature dependence associated with the vibrational deactivation of the newly formed oxygen molecules; inclusion of this factor in the analysis would result in a value of the energy required to reach the crossing point smaller than the experimental activation energy. These factors will be discussed briefly.

The preferential formation of O_2 in states of large J and small v may be understood in terms of the effective potential curves³⁰ as shown schematically in Figure 8 rather than in terms of the potential curves for a non-rotating molecule such as those shown in Figure 6. The effective potential curves illustrate that for given v values ($v = 0$ in Figure 8) the potential curves cross at higher energy values for larger values of J when the selection rule $\Delta J = 0$ is taken into consideration.³⁰ Therefore it is possible to observe an activation energy for molecule formation which is greater than the energy corresponding to the vibrational level occupied ($v = v'$, $J = 0$) as was implied in the conclusions stated above.

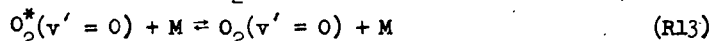
The contribution to the temperature dependence of the absolute emission intensity by the vibrational deactivation of newly formed O_2 molecules can be shown with the aid of the following mechanism:



where $O_2^*(v' = 1)$ is a newly formed molecule in the $v' = 1$ level of the $B^3\Sigma_u^-$ state with the rotational energy corresponding to the crossing level, $O_2(v' = 0$ or $1)$, a molecule with less rotational energy than $O_2^*(v' = 1)$, and O_2 , a molecule in the ground electronic state, $X^3\Sigma_g^-$. For this mechanism, the following expression for the emission intensity can be derived

$$I = \frac{k_5 k_6}{k_{-5} k_{-6}} k_{10}(0)^2 \left\{ 1 + \frac{k_7}{k_{-7} + k_9 + k_{11} M^{-1}} \right\} \quad (4)$$

when k_{-5} represents an allowed transition ($k_{-5} \sim 10^{11}$ sec⁻¹),³⁵ and other rate constants have the values as estimated (see Appendix B). When account is taken of the temperature variation of the bracketed term, the activation energy assigned to k_5 becomes ~ 1.5 kcal mole⁻¹ smaller than otherwise in accordance with the estimated values of the rate constants. Thus the energy level of the crossing is found on this basis also to be lower than that corresponding to the experimental activation energy. It may be noted that the variation of the bracketed term of Eq. (4) is primarily a result of the temperature coefficient of the vibrational deactivation process represented by k_7 . If, however, the oxygen may be formed in several vibrational levels directly, the effect of vibrational deactivation becomes negligible in the approximations used here. For example, if the following two reactions are added to the above mechanism



then the emission intensity expression becomes

$$I = \left\{ \frac{k_5 k_6}{k_{-5} k_{-6}} + \frac{k_{12} k_{13}}{k_{-12} k_{-13}} \right\} k_{10} (0)^2 \quad (5)$$

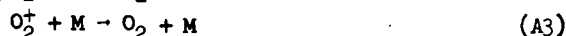
and the dependence of I on k_7 can be neglected.³¹ The reverse of this case occurs in predissociation when a breaking-off in successive vibrational levels is observed.³⁰ In potential curves of the form of those in Figure 8 but including the several vibrational levels of interest, the energy difference of the breaking-off points is found to be large in predissociation. If the reverse of this process were observed in the inverse predissociation mechanism, considered above, it would imply that the observed activation energy is an average over the energy levels corresponding to the several crossing points.

If the radiative transitions observed in the present experiments originate primarily from vibrational levels $v' = 0$ and 1 of the $B^3\Sigma_u^-$ state, then predissociation ought to be observed at least in the $v' = 2$ level. Several spectroscopic experiments^{16,32} have led to the observation of predissociation in the $B^3\Sigma_u^-$ state of oxygen. While interpretation of these experiments does not include predissociation from the $v' = 2$ level, there is not general agreement³³ that predissociation from the $v' = 2$ level is excluded. The spectroscopic studies were conducted in absorption and demonstrated predissociation in levels from $v' = 3$ to $v' = 12$ with maxima at $v' = 4$ and 11 and a minimum at $v' = 9$ in the probability for predissociation. Furthermore, from the investigation¹⁶ of the predissociation at $v' = 3, 4$ and 5, the transition was found to be allowed and therefore^{14,16,32} could be represented as $B^3\Sigma_u^- \rightarrow ^3\Pi_u$. On the basis of calculations, Vanderglice, Mason and Maisch³³ believe the $^3\Pi_u$ curve crosses at the bottom of the $B^3\Sigma_u^-$ curve and then rises along the left hand branch of the latter curve; the interpretation of the present experiments is in best agreement with this. In postulating this potential curve shape, these authors reject the explanation¹⁶ that the abnormal widths found in absorption for the rotational lines in the 2-0 and 1-0 bands of the Schumann-Runge bands result from a blending of fine structure and imply that predissociation occurs in the $v' = 0, 1$ and 2 levels. Other potential curve shapes that have been suggested^{14,16,32} require a predissociation at $v' > 3$; the above experimental results could only be strictly in agreement with this requirement if a systematic error exists in the relative spectral intensity measurements for $\lambda \leq 3000\text{\AA}$. At the present, no such error has been identified. Furthermore, this disagreement would be reduced where the potential curve shape is such that tunneling is important.³²

The spectral resolution in the present experiments was too small to permit spectroscopic identification of the radiating species. In the oxygen system of potential curves (Figure 6) there are two allowed transitions, $B^3\Sigma_u^- \rightarrow X^3\Sigma_g^-$ ¹³ and $^3\Pi_u \rightarrow X^3\Sigma_g^-$.³² The latter transition would result in an emission continuum which would shift to lower wavelengths at higher temperatures. Since this is not observed (see Figure 7), the transition $B^3\Sigma_u^- \rightarrow X^3\Sigma_g^-$ was assumed to be that one detected in the present experiments.

APPENDIX A

To estimate the ratio of the emission intensity, I (Schumann-Runge)/ I (Herzberg), the following simplified mechanism is assumed to apply to both radiative processes:



where O_2^* is a newly formed molecule in either the $B^3\Sigma_u^-$ or the $A^3\Sigma_u^+$, $c^1\Sigma_u^-$ or $C^3\Delta_u$ states, O_2^+ , a stabilized molecule in one of these states and O_2 , a molecule in the $X^3\Sigma_g^-$ state. If k_2 , k_{-2} , and k_3 are assumed to be identical and larger than $k_{11} M^{-1}$ for each of the four electronic states, then the ratio of the emission intensities will be:

$$\frac{I_{SR}}{I_H} \approx \left(\frac{k_{4,SR}}{k_{4,H}} \right) \left(\frac{k_{1,SR}}{k_{1,H}} \right) \left(\frac{k_{-1,H}}{k_{-1,SR}} \right) > 130 \quad (A5)$$

where $k_{4,SR}/k_{4,H} > 10^{5,18,20}$; $(k_{-1,H}/k_{-1,SR}) \sim 10^{13}/10^{11,34,35}$ assuming k_{-1} to represent an allowed radiationless decomposition³⁵; and $(k_{1,SR}/k_{1,H}) \sim 3 Z_1 10^{-2} e^{-28900/RT/7Z_1}$, with Z_1 , the collision number, $3/7$ the ratio of the statistical weights for formation of O_2 in the respective electronic states from which the Schumann-Runge or Herzberg O_2 band transitions originate, and 10^{-2} , the probability of the radiationless transition from the repulsive to the bound state assumed to be equal to the transition probability for the reverse process.³⁵

APPENDIX B

Estimates of the rate constants for reactions R6 to R11 were made as follows. For k_6 and k_{-6} , rotational deactivation and activation were assumed to occur at least once in every four collisions so that at 2500°K and 3500°K, the rate constants were $\geq 1 \times 10^{14}$ and $1.3 \times 10^{14} \text{ cm}^3 \text{ mole}^{-1} \text{ sec}^{-1}$, respectively. The rate constant for vibrational deactivation was estimated using the empirical relation of Millikan and White¹² in the following form

$$\log(\rho\tau)^* = (\theta^*/\theta)^{4/3} \log \rho\tau + 8[(\theta^*/\theta)^{4/3} - 1] \quad (B1)$$

where the starred quantities refer to the excited state, $B^3\Sigma_u^-$ and the unstarred quantities to the ground state, $X^3\Sigma_g^-$; θ is the characteristic oscillator temperature and $\rho\tau$, the pressure-relaxation time product. The values of τ were estimated from data on T-V process for $O_2-O_2^{12}$ and O_2-Ar^{12} and from the vibrational relaxation of O_2 by O^{10} with the following expression:

$$\tau^{-1} = X_{O_2} \tau_{O_2-O_2}^{-1} + X_{O} \tau_{O_2-O}^{-1} + X_{Ar} \tau_{O_2-Ar}^{-1} \quad (B2)$$

where X_i is the mole fraction of i and τ_{x-y} , the relaxation time of x in the presence of y . For the mixtures employed, the average of the estimated values of $k_7 (= \tau^{-1} M^{-1})$ were 3×10^{12} and $6 \times 10^{12} \text{ cm}^3 \text{ mole}^{-1} \text{ sec}^{-1}$ at 2500°K and 3500°K, respectively. The activation rate constant, k_7 was estimated from $k_7 \exp(-1970 \text{ cal mole}^{-1}/RT)$. The rate constants for electronic deactivation, k_8 and k_9 , were found to be 4.3×10^{12} and $5.1 \times 10^{12} \text{ cm}^3 \text{ mole}^{-1} \text{ sec}^{-1}$ at 2500°K and 3500°K, respectively on the assumption that one in one hundred collisions was effective for this process. Finally, the radiative rate constants, k_{10} and k_{11} , were estimated using the relation

$$k = \tau_R^{-1} = 1.013 \times 10^{-6} \sum q(v', v'') \nu^3(v', v'') \quad (B3)$$

where q is the Franck-Condon factor for the transition $v' \rightarrow v''$ and ν is the wave number, evaluated at the band head in the approximation employed. For both k_{10} and k_{11} , τ_R^{-1} was $2.7 \times 10^7 \text{ sec}^{-1}$; the data of reference 20 were used in this evaluation.

VI. ACKNOWLEDGEMENT

The authors are indebted to E. A. Meckstroth for maintaining the operational standard of the shock tube facility and for help in conducting the experiments and to M. R. Schoonover for his assistance in the computer-code preparation and numerical calculations. We thank Mr. K. G. P. Salzman for a critical reading of the manuscript. We gratefully acknowledge support of this work under Contract No. DA-01-021-AMC-12050(Z), ARPA Order 393, Amendment No. 4 through the U. S. Army Missile Command, Redstone, Arsenal, Alabama.

VII. REFERENCES

1. B. F. Myers and E. R. Bartle, *J. Chem. Phys.*, in press.
2. B. F. Myers, E. R. Bartle, P. R. Erickson and E. A. Meckstroth, *Anal. Chem.* 39, 415 (1967).
3. D. H. Byers and B. E. Saltzman, "Ozone Chemistry and Technology," *Advances in Chemistry Series No. 21*, American Chemical Society, Washington, D. C., 1959, p. 93.
4. L. J. Garr and P. V. Marrone, "Inviscid, Nonequilibrium Flow Behind Bow and Normal Shock Waves, Part II. The IBM 704 Computer Programs," CAL Report No. QM-1626-A-12(II), May 1963.
5. Received by this laboratory through the courtesy of Dr. W. Wurster, Cornell Aeronautical Laboratory, Inc., Buffalo, New York.
6. We are indebted to Dr. J. T. Neu, Space Science Laboratory, General Dynamics/Convair for conducting these experiments.
7. S. W. Benson and A. E. Axworthy, *J. Chem. Phys.* 26, 1718 (1957).
8. S. W. Benson and A. E. Axworthy, *ibid*, 42, 2614 (1965).
9. W. M. Jones and N. Davidson, *J. Amer. Chem. Soc.* 84, 2868 (1962).
10. J. H. Kiefer and R. W. Lutz, *Symp. Combust. 11th*, Berkeley, 1966, to be published.
11. W. G. McGrath and R. G. W. Norrish, *Proc. Roy. Soc.* A242, 265 (1957).
12. R. C. Millikan and D. R. White, *J. Chem. Phys.* 39, 3209 (1963).
13. F. R. Gilmore, "Potential Energy Curves for N₂, NO, O₂ and Corresponding Ions," Memorandum RM-4034-1-PR, The Rand Corporation, April 1966. Also published in *J. Quant. Spectry. Radiative Transfer* 5, 369 (1965).
14. P. J. Flory, *J. Chem. Phys.* 4, 23 (1936).
15. D. H. Volman, *ibid*, 24, 122 (1956).
16. P. K. Carroll, *Astrophysical J.* 129, 794 (1959).
17. H. P. Broida and A. G. Gaydon, *Proc. Roy. Soc.* A222, 181 (1954).
18. R. A. Young and R. L. Sharpless, *J. Chem. Phys.* 39, 1071 (1963).
19. C. A. Barth and M. Patapoff, *Astrophysical J.* 136, 1144 (1962).
20. R. A. Allen, *Avco-Everett Research Report* 236, April, 1966.
21. The method of calculation follows approximately that of reference 20. To obtain the relative spectral distribution curves, the ratios $(\int_{\Delta\lambda_1} \phi^b d\lambda) / (\int_{\Delta\lambda_3} \phi^b d\lambda)$ were calculated for transitions originating from the levels $v' = 0$ and 1, 0, 1 and 2 and 0, 1, 2 and 3 which contributed to the emission in the spectral interval $\Delta\lambda_i$; $\Delta\lambda_i$ represents the wavelength interval corresponding to channel i ($i = 1, \dots, 6$) in Table I; ϕ is the spectral distribution function.
22. J. C. Keck, J. C. Camm, B. Kivel and T. Wentink, Jr., *Ann. Phys.* 7, 1 (1959).
23. R. W. Patch, W. L. Shackelford and S. S. Penner, *J. Quant. Spectry. Radiative Transfer* 2, 263 (1962).
24. R. A. Allen, *J. Quant. Spectry. Radiative Transfer* 5, 511 (1965).
25. G. Herzberg, "Spectral of Diatomic Molecules," D. Van Nostrand, 1950, p. 424.
26. B. P. Levitt, *Trans. Faraday Soc.* 59, 59 (1963).
27. E. E. Nikitin, "Theory of Thermally Induced Gas Phase Reactions," Indiana University Press, 1966.
28. These ratios are based on the Franck-Condon factors given in Reference 20.
29. We are indebted to Mr. K. G. P. Sulzmann for bringing this possibility to our attention.
30. G. Herzberg, *op. cit.*, p. 426, 430f.
31. The observed dependence of the absolute emission intensity on $(0)^2$ (see Figure 2, for example) is, within the experimental error, in accordance with the prediction of the mechanisms represented by either Eq. (5) or (6).
32. P. G. Wilkinson and R. S. Mulliken, *Astrophysical J.* 125, 594 (1947).

33. J. T. Vanderslice, E. A. Mason and W. G. Maisch, *J. Chem. Phys.* **32**, 515 (1960).
 34. V. N. Kondrat'ev, "Chemical Kinetics of Gas Reactions," Pergamon Press, 1964, p. 229.
 35. G. Herzberg, *op. cit.*, p. 419.

TABLE I: SPECTRAL CHANNEL CENTER WAVELENGTHS AND BANDPASSES

Channel	1	2	3	4	5	6
$\lambda_c, \text{\AA}$	2300	2500	3002	3506	4010	4511
$\Delta\lambda, \text{\AA}$	62	102	200	206	208	202

TABLE III: FORWARD RATE CONSTANTS, $k^{(a)}$

Reaction	Set I			Set II		
	A	n	E_a	A	n	E_a
1a $O_3 + O_3 \rightarrow O_2 + O + O_3$	1.4×10^{15}	0	23.15	10.91×10^{18}	-1.25	24.35
1b $O_3 + O_2 \rightarrow 2O_2 + O$	5.80×10^{14}	0	23.15	5.15×10^{18}	-1.25	24.35
1c $O_3 + Ar \rightarrow O_2 + O + Ar$	3.76×10^{14}	0	23.15	3.12×10^{18}	-1.25	24.35
2 $O + O_3 \rightarrow 2O_2$	3.0×10^{13}	0	5.60	1.04×10^{12}	0.50	5.288
3 $O_2 + M \rightarrow 2O + M$	1.19×10^{21}	-1.5	118.0	1.19×10^{21}	-1.5	118.0

(a) $k = A T^n e^{-E_a/RT}$; units for A, $\text{cm}^3 \text{mole}^{-1} \text{sec}^{-1}$ or $\text{cm}^6 \text{mole}^{-2} \text{sec}^{-1}$, for E_a , kcal mole^{-1} .

TABLE IV: OXYGEN ATOM CONCENTRATIONS AND TEMPERATURES

Run	$(O) \times 10^7$ mole cm^{-3}	$T, ^\circ K$	Run	$(O) \times 10^7$ mole cm^{-3}	$T, ^\circ K$	Run	$(O) \times 10^7$ mole cm^{-3}	$T, ^\circ K$
1014	1.620	2976	1026	0.9073	3130	1041	1.084	3390
1015	1.640	2976	1027	2.218	3097	1042	2.101	3835
1016	2.192	2969	1028	3.360	3164	1043	1.067	3767
1017	2.449	2990	1029	1.500	3259	1044	2.776	3335
1018	0.8171	2939	1030	0.7501	3232	1045	1.422	3728
1019	1.626	2691	1031	2.238	3266	1046	1.365	3530
1020	2.482	2738	1034	1.415	3709	1081	0.3471	3309
1021	0.8370	2718	1035	0.7102	3719	1082	0.5163	3205
1022	1.131	2824	1036	2.119	3698	1083	0.7712	2755
1023	2.186	2841	1039	2.197	3519	1085	0.7963	2494
1024	3.349	2883	1040	1.086	3413	1086	0.6354	2965

TABLE V: THE TEMPERATURE DEPENDENCE OF I_0

$\lambda_c, \text{\AA}$	$A_1 \times 10^{-6}, \text{watt str}^{-1} \text{\AA}^{-1} \text{cm}^3 \text{mole}^{-2}$	$E_1, \text{kcal, mole}^{-1}$
2300	1.14	29.8
2500	7.42	27.4
3002	119.2	27.8
3506	89.1	30.4
4010	47.1	31.1
4511	7.38	25.1

TABLE II: SUMMARY OF EXPERIMENTAL DATA

Run	Initial Conditions and Shock Velocity				$I_1 \times 10^9$, watt str $^{-1}$ Å $^{-1}$ cm $^{-3}$						
	T, °C	P, mm Hg	X ₃	U, mm μsec $^{-1}$	λ _c =2300Å	λ _c =2500Å	λ _c =3002Å	λ _c =3506Å	λ _c =4010Å	λ _c =4511Å	
1014	25.6	18.92	0.060	1.822	---	---	---	12.7	5.39	2.49	
1015	25.0	19.11	0.060	1.822	0.191	1.83	28.0	12.7	6.36	2.92	
1016	24.8	25.54	0.060	1.820	0.313	3.18	48.0	23.0	12.3	4.30	
1017	25.0	28.46	0.060	1.827	0.515	4.32	66.4	31.4	14.0	5.51	
1018	24.7	9.46	0.060	1.811	0.0441	0.442	6.06	3.32	1.47	---	
1019	24.7	20.34	0.060	1.719	0.149	1.285	20.3	8.64	3.85	1.895	
1020	24.5	30.62	0.060	1.736	0.307	3.03	46.5	22.4	10.76	0.516	
1021	24.4	10.16	0.060	1.731	0.0284	0.321	4.94	2.19	0.960	---	
1022	24.7	8.51	0.120	1.799	0.0641	0.735	10.5	5.25	2.88	---	
1023	24.7	16.92	0.120	1.797	0.302	2.91	36.8	17.04	10.2	4.56	
1024	24.6	25.51	0.120	1.813	0.695	6.80	110.2	47.5	25.0	8.94	
1026	24.6	6.17	0.120	1.910	0.066	0.683	9.65	5.03	2.27	1.20	
1027	24.5	15.45	0.120	1.900	0.362	4.46	59.5	27.8	13.04	5.85	
1028	24.5	23.31	0.120	1.924	1.235	11.05	157.0	69.6	33.5	13.76	
1029	24.4	16.60	0.060	1.919	0.277	2.49	36.6	19.4	9.26	3.26	
1030	24.7	8.27	0.060	1.910	0.0594	0.564	8.89	4.9	2.06	4.14	
1031	24.8	24.80	0.060	1.921	0.632	5.43	86.0	41.5	18.8	7.91	
1034	24.6	14.91	0.060	2.060	0.429	3.70	30.8	30.8	13.85	4.81	
1035	24.5	7.44	0.060	2.063	0.117	0.905	14.6	7.90	36.8	---	
1036	24.5	22.34	0.060	2.057	0.855	8.15	129.0	69.8	33.3	11.2	
1039	24.8	14.08	0.120	2.052	0.606	6.43	102.1	51.4	33.7	---	
1040	24.5	7.02	0.120	2.018	0.165	1.65	26.1	12.0	5.55	2.06	
1041	25.1	7.05	0.120	2.010	1.64	1.64	23.3	12.3	5.49	2.24	
1042	25.7	12.93	0.120	2.156	1.01	10.0	161.0	75.0	37.6	---	
1043	24.8	6.56	0.120	2.136	0.273	2.34	33.4	18.4	8.51	3.78	
1044	24.4	14.40	0.180	2.010	0.944	8.55	128.8	65.9	26.6	---	
1045	24.5	6.64	0.180	2.159	0.378	3.47	57.2	29.6	14.1	---	
1046	24.9	6.67	0.180	2.088	0.296	2.65	39.5	21.4	9.64	4.30	
1081	24.3	17.67	0.0105	1.864	---	---	1.96	1.05	---	---	
1082	24.2	26.42	0.0105	1.833	---	---	3.83	2.00	---	---	
1083	24.1	40.79	0.0105	1.688	---	---	4.54	2.14	---	---	
1085	23.7	45.93	0.0100	1.597	---	---	3.05	1.36	---	---	
1086	23.4	34.55	0.0100	1.756	---	---	4.29	2.25	---	---	

Calibration factors, $C \times 10^7$, watts str $^{-1}$ Å $^{-1}$ cm $^{-3}$ v $^{-1}$

15.82

6.81

0.3485

0.0185

0.00303

1.97

0.3485

0.0185

0.00303

1.97

0.3485

0.0185

15.82

6.81

0.3485

0.0185

0.00303

1.97

0.3485

0.0185

0.00303

1.97

0.3485

0.0185

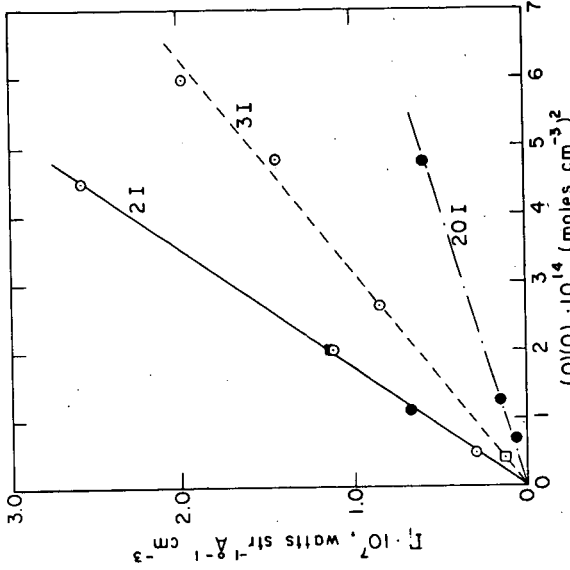


FIGURE 21 ABSOLUTE EMISSION INTENSITY VS. $(O)^2$. For $\lambda = 35064$, $3086 = 7.6 \times 10^4$; for $\lambda = 3726$, $\lambda = 30024$, $2965 = 7.9 \times 10^4$; for $\lambda = 2990$, $3086 = 7.6 \times 10^4$; for $\lambda = 2718$, $2718 = 7.7 \times 10^4$; for $\lambda = 2641$. For all curves, (O) is represented by \square for 1%, \circ for 5%, \bullet for 12% and \blacksquare for 15%. Each datum on the figure is selected from the results of a different shock tube experiment.

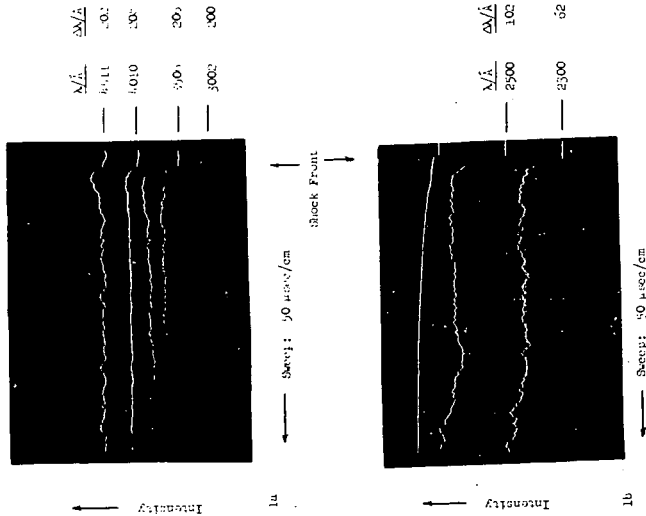


FIGURE 1: INTENSITY TIME OSCILLOGRAM. Oscillogram of the emission behind an incident shock wave traveling through a mixture of 5% O_2 + 95% Ar . Run 1015.

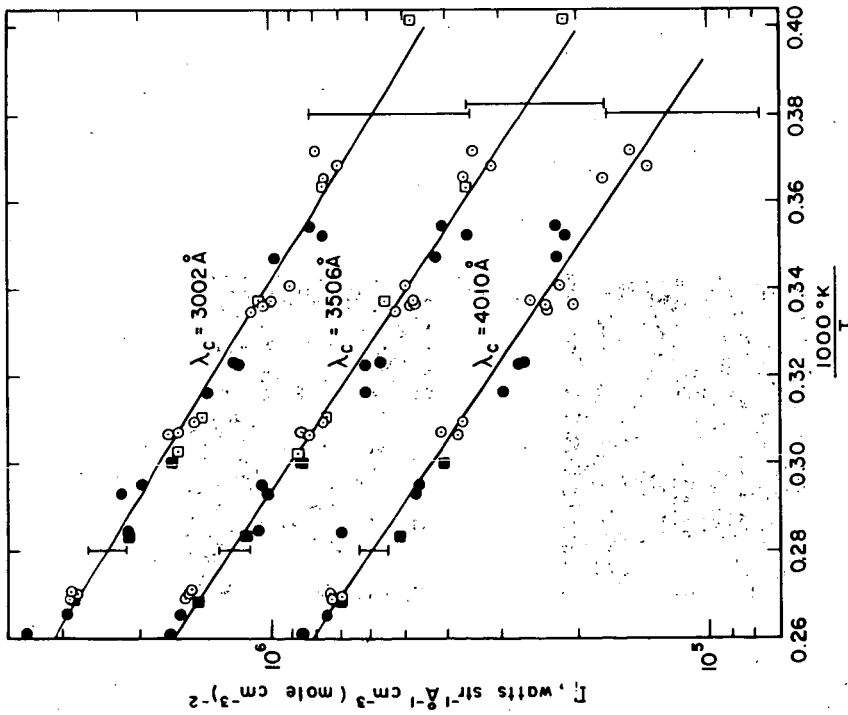


FIGURE 3: $\log I$, vs. $1000^\circ K/T$. For $(O_2) = 1\%$, the data are represented by \square for $(O_2) = 6\%$, by \circ for $(O_2) = 12\%$ by \bullet and for $(O_2) = 18\%$ by \circ . The solid lines are least squares fits to the data and the vertical bars indicate the standard deviation at the 90% confidence level.

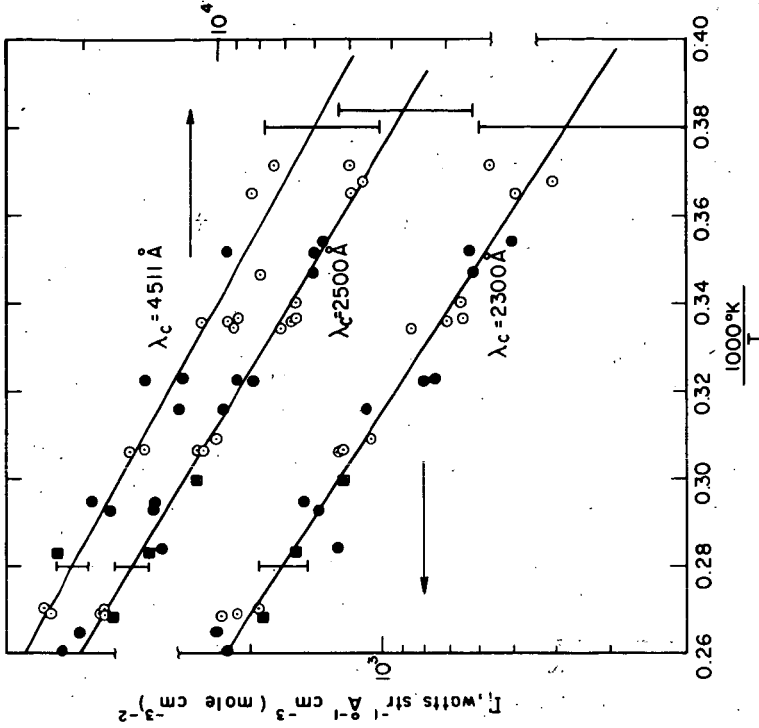


FIGURE 4: $\log I$, vs. $1000^\circ K/T$. For $(O_2) = 1\%$, the data are represented by \square for $(O_2) = 6\%$, by \circ for $(O_2) = 12\%$ by \bullet and for $(O_2) = 18\%$ by \circ . The solid lines are least squares fits to the data and the vertical bars indicate the standard deviation at the 90% confidence level.

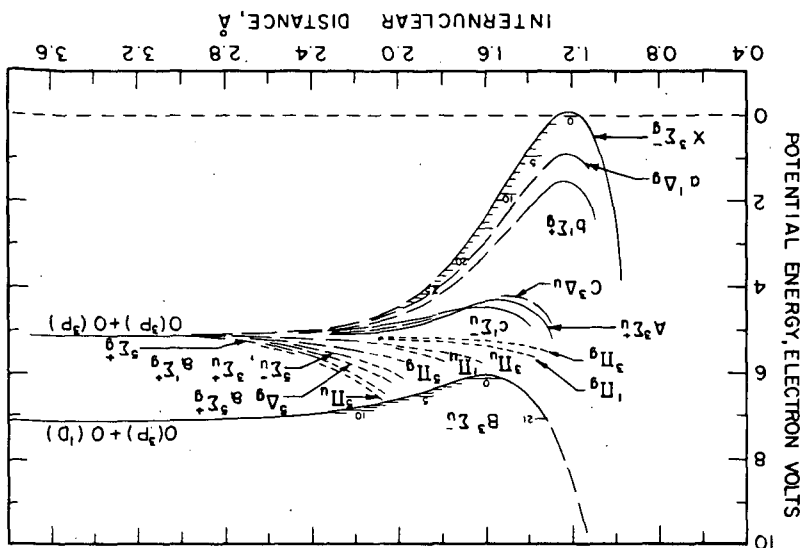


FIGURE 6: POTENTIAL ENERGY CURVES FOR O₂ AFTER GILMORE.¹³

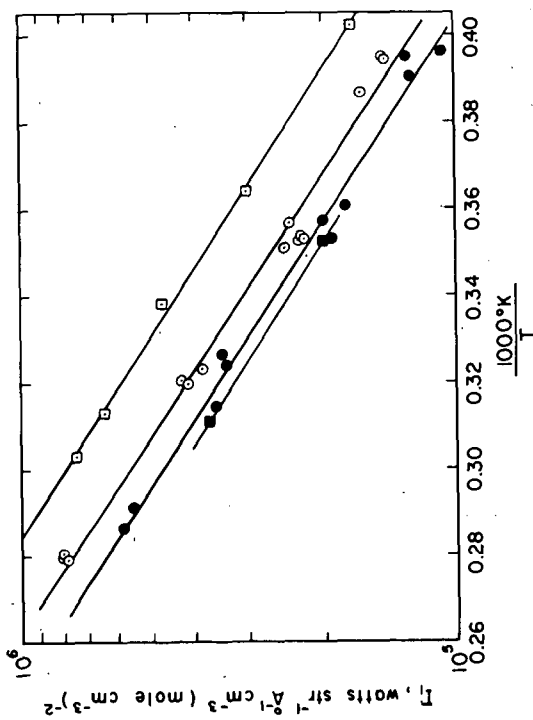


FIGURE 5: $\log I_1$ VS $1000/T$. For $\lambda_c = 3500\text{\AA}$: curve $\square - 1\%$; curve $\circ - (0.3)\%$; curve $\triangle - (0.1)\%$; curve $\bullet - 12\%$. The solid curves are least-squares fits to the data points for each initial ozone concentration.

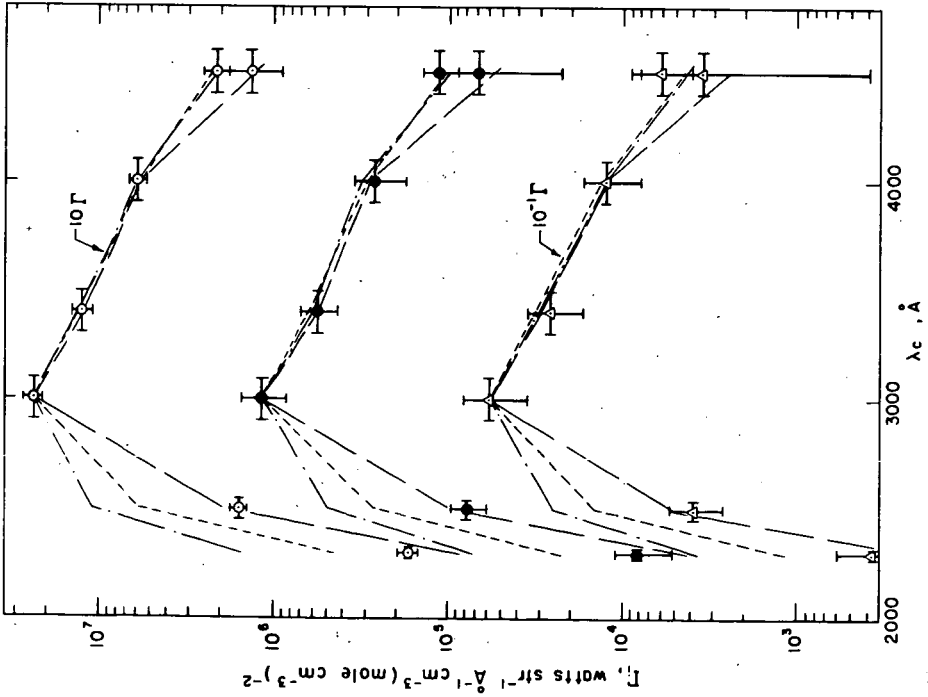


FIGURE 7: ABSOLUTE EMISSION INTENSITY SPECTRAL DISTRIBUTION CURVES.

The experimental data points are represented by \odot for 3571°K, by \bullet for 3030°K and by Δ for 2532°K. The vertical bar represent the standard deviation at the 90% confidence level and the horizontal bar represent the spectral interval over which the data are average values. The theoretical relative intensity distribution is represented for each temperature by three curves drawn through the points calculated for the $J=0, 1, 2$ states and the $v=0, 1, 2$ vibrational levels. Each set of points has been vertically displaced for clarity with the experimental absolute emission intensity values. $\lambda_c = 3002\text{\AA}$ for each temperature. Contributions to the calculated relative intensity from various vibrational levels of the $B^2\Sigma_u^+$ state have been included as indicated by the legend --- , $v=0, 1, 2$; --- , $v=0, 1, 2$; --- , $v=0, 1, 2, 3$. Note that the data sets at the three temperatures have been artificially separated by the factors indicated to improve the clarity of presentation.

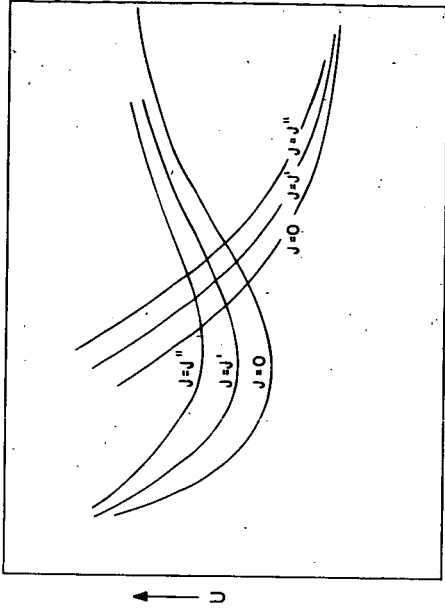


FIGURE 8: EFFECTIVE POTENTIAL CURVES (schematic diagram). The potential energy U is plotted versus the internuclear distance r for $v=0$ and for several rotational levels with $J' > J'' > J$ and spin splitting neglected.

POTENTIAL DESTRUCTIVENESS OF GAS DETONATIONS

J. N. Murphy, N. E. Hanna, D. S. Burgess, and R. W. Van Dolah

Explosives Research Center
Bureau of Mines
U. S. Department of the Interior
Pittsburgh, Pennsylvania 15213

Background

The potential destructiveness of gas detonations was evaluated in terms of the depth of earth that could be heaved when various gas mixtures were detonated in long underground excavations. A number of years ago, a spectacular destruction of 26.8 miles of underground pipeline in Texas was ascribed to the occurrence of a detonation. The pipeline had carried crude oil and was being cleaned by forcing a scraper plug along its length with compressed air. It is not known whether the event was a gas detonation or a heterogeneous detonation of a film on the wall.^{1/} The intermittent cratering that occurred seemed curious but now may be explained in terms of the impulse needed to heave the earth cover. No explanation can be offered for the apparent low velocity of propagation indicated by the total elapsed time. An average velocity of only 296 feet per second was reported.

This investigation primarily covered propane-air, acetylene-air and MAPP^{2/}-air mixtures. In some cases a partial pressure of oxygen greater than in air was employed. Limits of detonability were obtained from plots of propagation velocity versus fuel concentration in a 7-inch diameter by 12-foot long pipe which was closed at both ends. Impulse, which determines the momentum that can be imparted to a load, was measured from pressure versus time transients in a 24-inch diameter by 163-foot long steel pipe that could be closed at one end. The soil mechanical problems related to earth movement were studied in hand-dug tunnels of 3 foot x 5 foot cross-section and 150 feet length incorporating right angle turns and side entries.

Detonation Velocities and Limits of Detonability

Fuel/air mixtures were admitted to the 7-inch apparatus of figure 1 by the partial pressure method, recirculated via the sideline for 10 minutes, and sampled for gas chromatographic analysis. A solid explosive initiator ranging from 1.1 grams PETN to 100 grams tetryl was detonated and the velocity of the resulting ionization wave was measured between velocity stations with electronic time-interval meters.

A plot of this wave velocity versus fuel concentration is given in figure 2 for MAPP/air mixtures. Velocities in excess of 1400 meters/sec indicate detonation while velocities of about 1000 meters/sec or less are obtained from shocks accompanying deflagration. The difference is clearly shown by the pressure traces of figure 3, wherein trace A indicates deflagration with pressure rising over a period of about 25 milliseconds while in trace B the first pressure pulse is the strongest.

Limits of detonability as defined by this method are somewhat sensitive to the strength of the initiator. Thus, the detonable range for MAPP/air widens appreciably as the initiator is increased from 1 to 10 grams PETN (table 1). Both propane/air and acetylene/air detonate over the full reported range of flammability when initiated with 10 grams PETN.

Pressure-time Transients and Impulses

The major part of the experimental program was carried out using the 24-inch steel tube shown in figure 4. Fuel was metered through calibrated spray nozzles into the 260 cfm output stream of a gasoline-powered blower, which stream was passed through the tube to give three changes of atmosphere. Gas sampling and detonation pressure measurements were accomplished at five stations spaced evenly along the length of the pipe. Initiation was typically effected with 100 grams tetryl, usually at the upstream end of the pipe near the end closure.

Pressure transients at the five stations were compared with predictions derived from standard references^{3,4} dealing with one-dimensional gas detonations. Figure 5 shows the predicted transient for stoichiometric acetylene/air at a point 60 feet from an initiation source at the closed end of a 150-foot long pipe. The peak (C-J) pressure was assumed to be twice the constant volume explosion pressure and this proved to be a fairly accurate assumption for measurements within 2 stations (53 feet) of the initiation. For example, with 7.2 percent MAPP in air, the predicted peak was 281 psig while nine measurements averaged 278 ± 6 psig. At greater distance from the initiator, peak pressures became progressively more erratic as though the detonation were departing from its one-dimensional character.

The gas expansion behind the C-J plane was calculated by Taylor's equations using an equilibrium gamma which was typically about 1.17. This gave excellent agreement with experimental pressures in the static gas zone, however, the duration of the gas expansion (from D to E in figure 5) was typically underestimated by about 20 percent. Neither this deviation from prediction nor the erratic peak pressures were of any practical consequence to the impulse of the explosion.

The duration of the pressure plateau, EH in figure 5, was about 20 percent overestimated because no account had been taken of the three-dimensional expansion of the wave as it emerged from the open end of the pipe; that is, the interval FG in the figure should actually be shorter than indicated and the rarefaction starts back through the pipe at an earlier time than G. Since the dominant factor in the time interval EH is the velocity of sound in the burned gases, off-stoichiometric mixtures with lower burned gas temperatures had relatively long pressure histories and high impulses. This trend is shown in table 2; note that 4.9 percent MAPP in air is close to stoichiometric while 3.4 percent MAPP is the reported lean limit of flammability.

For the same reason, propane/air and gasoline/air mixtures had impulses comparable to those of acetylene/air and MAPP/air even though their pressure peaks were lower. Thus, the average of impulses at the 5 pressure stations in 6 MAPP/air detonations was 7.7 psi sec, in 6 propane/air detonations 7.4 psi sec and in 3 gasoline/air detonations 7.5 psi sec.

When both ends of the pipe were open, the pressure plateau was nearly eliminated. This is shown by the transients of figure 6 (compare curves C and D with curves A and B). In 7 MAPP/air detonations the average impulse was only 3.2 psi sec and in 5 acetylene/air detonations 3.1 psi sec. Even a partial temporary closure, as exemplified by loose-fitting sandbags in the ends of the pipe, brought the average impulse (for 7.2 percent MAPP/air) back to about 6.3 psi sec.

No particular difference in average impulse could be detected as a result of initiating the detonation at the longitudinal midpoint of the tube or simultaneously at the two ends.

In the dry-walled steel tube, suspended aluminum powder (even though much of it was deposited on the walls) could participate in the post-detonative reactions to give about 50 percent greater impulse. Comparative values are given in table 3. But in dirt tunnels, the powder was collected on the damp walls and played no apparent part in the explosion.

Destructiveness of Gas Detonations to Earthen Structures

In field tests, a surprising fraction, usually 50-100 percent, of the impulse of the explosion was converted into momentum of the overburden. This means that soil mechanical factors such as plasticity and shear strength were unimportant so that the overburden was behaving essentially as a frictionless piston. When the earth velocity was made to exceed 20 ft/sec, as measured at ground level by Fastax photography, the tunnel usually failed. Because of the weakness of end closures, as compared with an end plate on a steel pipe, the largest impulse attained in the field was about 6 psi sec and the greatest depth of burden defeated by a single gas detonation was 8 feet.

REFERENCES

- 1/ Armistead, George, Jr. Safety in Petroleum Refining and Related Industries, 2nd Edition, Simmonds, N. Y., 1959, p. 43.
- 2/ MAPP is a commercial mixture of methylacetylene, propadiene and propylene.
- 3/ Zeldovich, Ya. B., and A. S. Kompaneets, "Theory of Detonation," Academic Press, New York, N. Y., 1960.
- 4/ Taylor, G. I., "The Dynamics of the Combustion Products behind Plane and Spherical Detonation Fronts in Explosives," Proc. Roy. Soc., v. 200, 1950, p. 285.

TABLE 1. - Limits of Flammability and of Detonability

Mixture	Initiator	Flammable Range	Detonable Range
Propane/air	Spark	2.1 - 9.5%	--
	10 g PETN	--	2.2 - 9.2%
Acetylene/air	Spark	2.5 - 100%	--
	10 g PETN	--	2.0 - 100%
MAPP/air	Spark	3.4 - 10.8%*	--
	1 g PETN	--	4.1 - 7.6%
	10 g PETN	--	2.4 - 13.7%

*Hembree, J. O., et al, Welding Journal, May 1963.

TABLE 2. - Plateau Durations, Plateau Pressures, and Impulses of MAPP/Air Detonations in 24" Diameter by 163' Long Steel Tube with Initiation End Closed

MAPP Concentration (%)	Plateau Duration (milliseconds) at Instrument Stations					Averaged	
	#1	#2	#3	#4	#5	Plateau Pressure (psig)	Impulse (psi sec)
3.4	71	54	35	12	2	85	6.8
4.9	58	46	32	15	--	103	8.9
6.1	64	49	35	14	--	98	8.3
8.7	64	52	33	14	--	99	7.8

TABLE 3. - Impulses Obtained in Detonations in the Steel Tunnel with and without Added Aluminum Powder

Gaseous Fuel	Closure of Initiation End	Aluminum (#422)	Impulse (psi sec)*
Acetylene	Open	None	3.0, 3.9
Acetylene	Open	2 lbs on floor	4.5
Acetylene	Closed	None	3.9
Acetylene	Closed	2 lbs on floor	6.5
MAPP	Open	None	3.4
MAPP	Open	2 lbs suspended	5.6
MAPP	Closed	None	4.3
MAPP	Closed	2 lbs on floor	6.6

*As measured at a station close to the open downstream end of the tunnel.

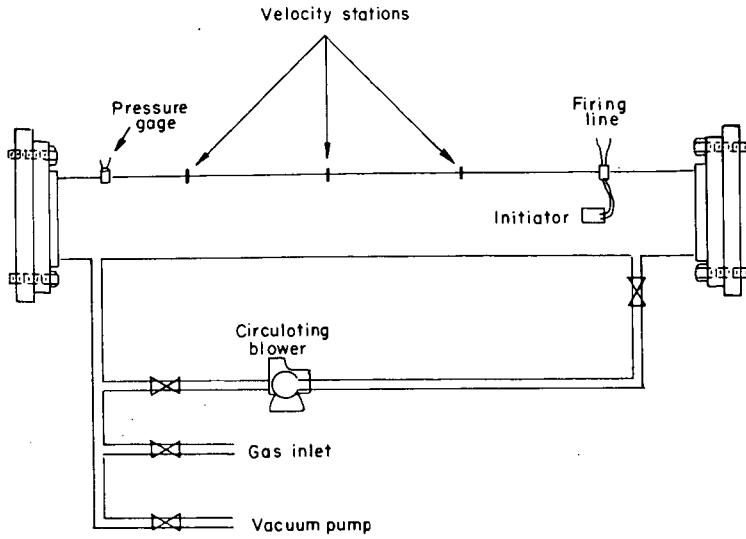


FIGURE 1. - LABORATORY DETONATION TUBE.

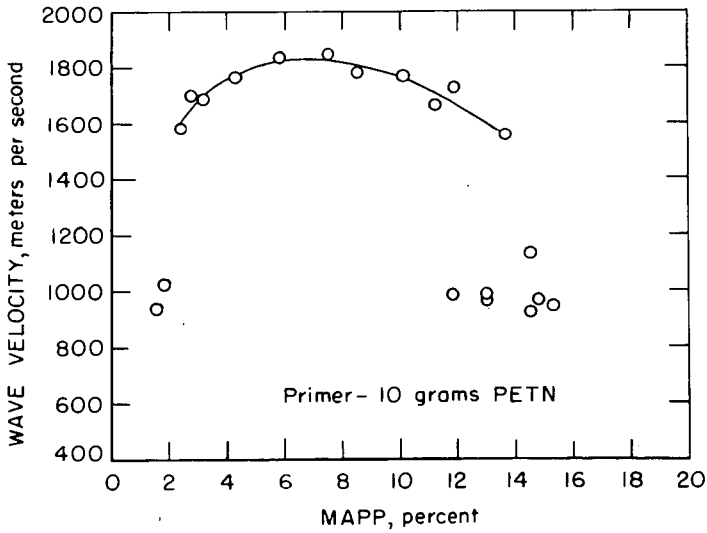


FIGURE 2. - DETONABLE LIMITS OF MAPP/AIR.

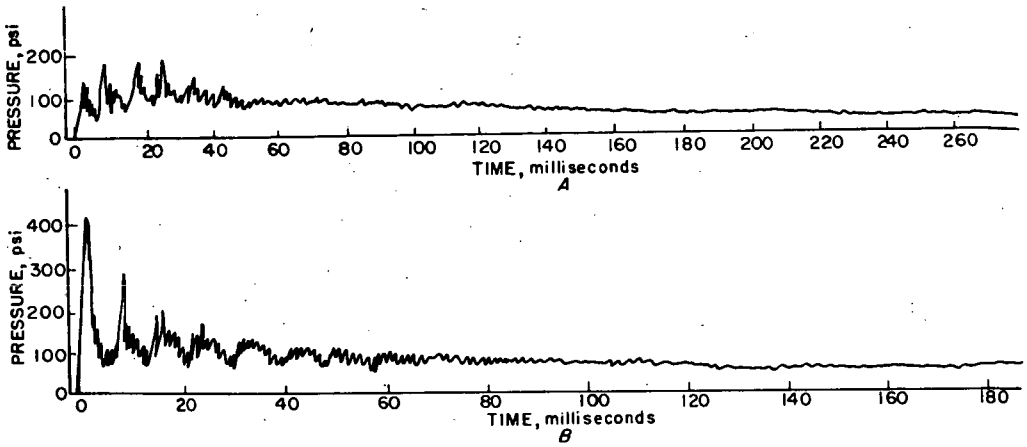


FIGURE 3. - PRESSURE TRANSIENTS IN CLOSED CHAMBER
A. Deflagration
B. Detonation

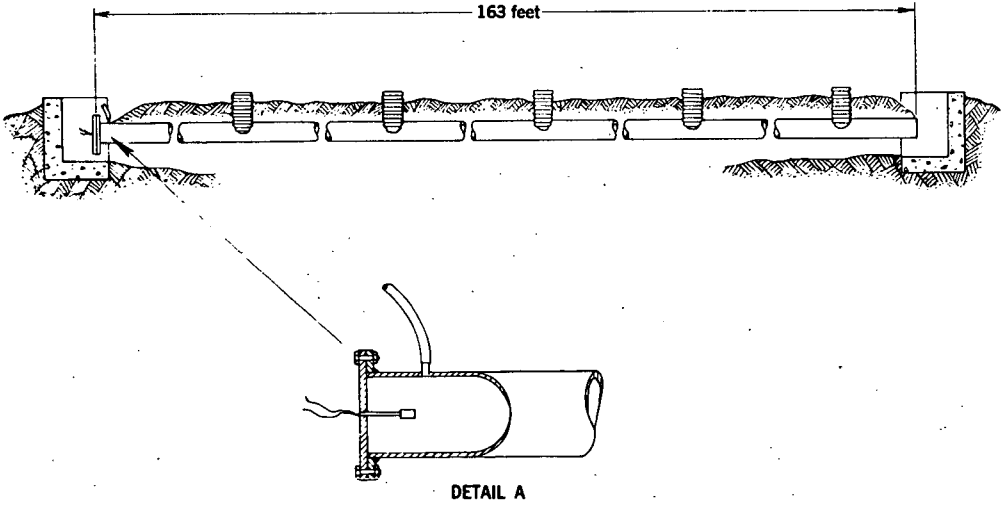


FIGURE 4. - LARGE DETONATION TUBE (2 x 163 FEET).

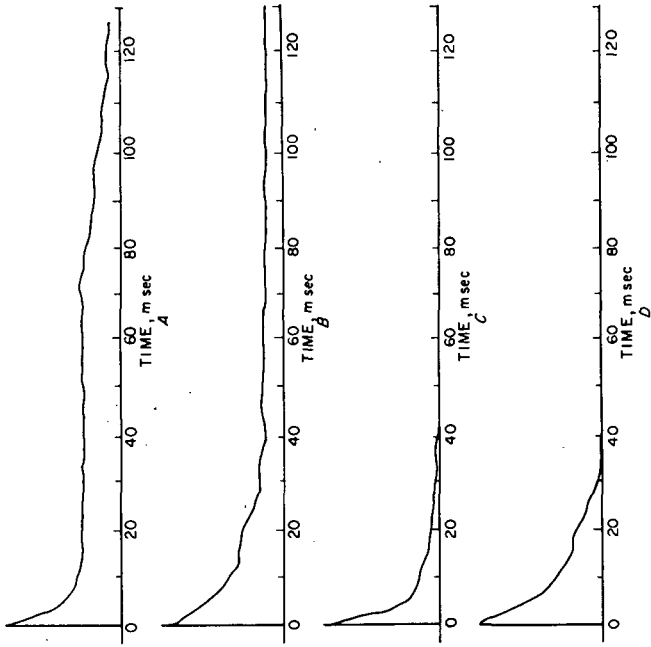
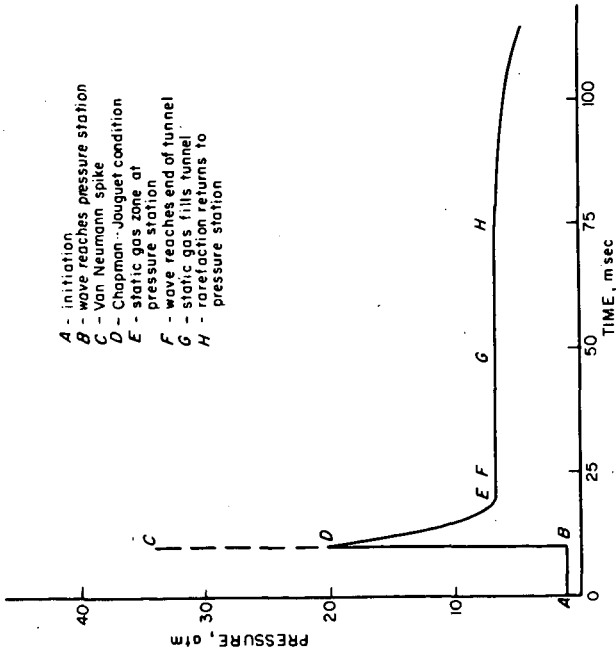


FIGURE 6. - OBSERVED PRESSURE TRANSIENTS
 A,B - Initiation end closed; C,D - both ends open
 A,C - Transducer near initiation; B,D - transducer downstream



- A - initiation
- B - wave reaches pressure station
- C - Van Neumann spike
- D - Chapman-Jouquet condition
- E - static gas zone at pressure station
- F - wave reaches end of tunnel
- G - static gas fills tunnel
- H - rarefaction returns to pressure station

FIGURE 5. - PREDICTED PRESSURE TRANSIENT.

INITIATION OF CONDENSED EXPLOSIVES BY GAS DETONATION

M. L. Weiss, T. J. Schellinger, and E. L. Litchfield

Explosives Research Center
Bureau of Mines
U. S. Department of the Interior
Pittsburgh, Pennsylvania 15213

Introduction

There are two ways in which stimuli may induce detonation in secondary explosives. A strong shock may cause detonation with an induction time of a few microseconds, i.e., time intervals of a few microseconds between application of the stimulus and the appearance of detonation. A weaker shock or a purely thermal stimulus may initiate reactions that begin as a deflagration and accelerate to detonation. The acceleration of the reaction occurs as a consequence of increasing pressure, or self-pressurization, produced by the hot, gaseous decomposition products. Maintenance of pressure for periods of 10's to 100's of microseconds, as may be required to obtain detonation from weak initiation stimuli, is achieved by confinement of the explosive sample.

Although such confinement is usually provided by high-strength metallic containers, for short periods of time it can also be a consequence of inertial effects. If low-strength confinement surrounds the explosive sample the acceleration of the confinement material is directly proportional to the pressure seen by the explosive sample and inversely proportional to the confinement mass per unit area of explosive sample. At early times, the expansion and escape of product gases are limited by the low velocity of expansion of the container and self-pressurization of an explosive sample may be maintained for considerable periods. Inertial confinement, or self-confinement might be provided by a large pile of explosive to a reaction initiated within the interior of the pile.

Examples of the first type of stimulus are initiation by other condensed phase explosives and by projectile impact. Initiation of detonation in condensed explosives has been studied using strong shocks across air gaps¹ or through inert barriers^{2,3} and by determining projectile impact initiation parameters.^{4,5,6} Threshold initiation shock pressures for condensed explosives range from 1 to 100 kbar. An example of the second type of stimulus is that of thermal ignition transforming to detonation in the confined explosive.^{7,8}

This paper describes results obtained with an initiation source producing a stimulus that is continuously variable from less than that required to ignite explosive flours to more than that required to detonate pressed pellets. The initiation source is the detonation wave produced in gaseous mixtures of stoichiometric ethylene-oxygen ($C_2H_4 + 3 O_2$).

Until recently, gas detonation waves free from incandescent solid debris had to be obtained by run-up in a detonation tube.^{9,10,11,12} Such tubes were economically unattractive, inconvenient in use, or restricted in use by the run-up characteristics of the gaseous mixture. In Bureau of Mines' studies, gas detonations have been obtained without run-up in a detonation tube and without explosive detonators.¹³

One possible difference between the shock from a projectile and the gas detonation shock is the difference between a "cold" and a "hot" shock. In the first case, temperature increase in the condensed explosive sample is entirely a consequence of mechanical interactions and conversion of translational energy into heat. In the second case, there is additional thermal energy in the hot ethylene-oxygen combustion

products. Phenomenological analysis and experimental results indicate that the transport from the hot gases is negligible when the explosive is initiated within 1μ sec.

Experimental Procedures

The test container was a 17.8 cm length of 1-inch schedule 80 pipe, reamed to an inside diameter of 2.54 cm. Explosive samples were positioned at one end of the tube and the wires to initiate the gas detonation were positioned near the other end.

The detonable gas mixture was 25 percent ethylene and 75 percent oxygen as determined by partial pressures. Gases were injected into the evacuated chamber through 1/16-inch orifice fittings for mechanical mixing and 20 minutes was allowed for additional diffusional mixing. Gases were from commercial cylinders and were used without further treatment. Initial pressures of the prepared gas mixture were from 3 to 85 atm gage. Initial pressures less than 3 atm were obtained by reducing a 3-atm mixture to the desired pressure.

To initiate the gas, a 0.15 mm (No. 35 B&S) copper wire, 2 cm long, was exploded with the discharge from a 1.5 μ f condenser charged to 5.5 kv or more (25 joules energy, or more) using a hydrogen thyratron switch. Control trials in which the wire was exploded with inert gas plus condensed explosive gave no evidence of debris impingement or reaction of the explosive.

Representative particle size analyses of the floured or granulated materials are given in table 1. Particle sizes and distributions under the test conditions may have been slightly different. Gas was injected through orifices to produce turbulent, circulatory gas mixing. This injection must have disturbed the surfaces of the unpressed samples with some increase of "fines" occurring at the top of the sample.

The unpressed flour or granulated samples were prepared by pouring a standard weight of material into the test vessel and tapping lightly to level the sample surface. Standard weights were: 10 gm PETN,* 10 gm RDX,** 13.2 gm tetryl,*** or 14 gm Composition A5.**** Direct determinations of possible densities in the tested charges of floured or granulated explosive have given: for PETN - 0.40 to 0.69 gm/cc; for neat RDX - 0.67 to 0.91 gm/cc; for Composition A5 - 0.93 to 1.02 gm/cc; and for tetryl - 0.93 to 1.14 gm/cc. As initially prepared in the test vessel, densities were near the larger figure in all cases and these are the numbers quoted in the tables. The particle size distributions of table 1 imply adequate porosity to permit pressure equilibration within the floured or granulated sample by gas flow during loading of the detonable gas mixture. Thus, the gas charging pressure would not affect, per se, the density of the charges. As was the case with particle size data, the effect of the gas jet mixing action upon the charge density is not known.

Pellets of Composition A5 and of tetryl were prepared and tested at pellet densities of 1.6 gm/cc and 1.4 gm/cc. Pellets of PETN + 1 percent graphite were tested at densities of 1.6 gm/cc. All pellets were 1 inch long. Comparative tests of PETN and PETN + 1 percent graphite, both in flour form, did not reveal any noticeable difference in sensitivity resulting from the graphite addition.

* Pentaerythritol tetranitrate.

** Cyclotrimethylenetrinitramine (hexahydro-1,3,5 trinitro-s-triazine).

*** 2,4,6-trinitrophenylmethyl nitramine.

**** RDX + 1% stearic acid coating material.

Measurements were made of the pressure-time history at the initial explosive surface until detonation, location of first appearance of significant reaction, and the propagation velocity on the axis. These data were obtained from resistive pressure transducers¹⁴ and continuous wire probes.¹⁵

The resistive transducer was a composition resistor of 0.1 watt rating. The variation of resistance with loading pressure has been established in Bureau of Mines investigations.¹⁴ The approximate constancy of the calibration over periods of about 100 μ sec after application of the gas detonation shock stimulus has been established in one instance by direct comparison with strain gage measurements. This result provides justification for reading a "pressure at detonation" at the time that detonation is shown by the velocity probe.

The wire probe consisted of a fine, nichrome axial wire helically wound with a nylon filament for insulation from the surrounding, collapsible aluminum tube. Collapse of the aluminum tube altered the probe resistance and gave a direct indication of the physical location of the shorting point. Rates of change of the probe resistance were proportional to the velocities of the pressure front. For trials at charging pressures greater than 14 atm gage, the probe record displayed the time-position loci in both the gaseous and the solid phases.

Results

The explosive flours or granules were observed to react in three different ways depending upon the explosive and the gas charging pressure. At higher gas charging pressures, supersonic reaction was induced with a time delay ≤ 1 microsecond. At lower pressures, significant chemical reaction was evident only after a delay of several microseconds and detonation commenced at some distance below the original surface of the explosive sample. At still lower pressures, granular tetryl or Composition A5 was not initiated to self-sustaining chemical reactions even though a portion of the sample might have been consumed in the test.

Test results are summarized in table 2 where charging pressures are given for the reaction modes of the several samples. PETN flour samples at a density of 0.7 gm/cc required detonable gas mixture charging pressures of 20 atm, gage, to initiate detonation with induction times ≤ 1 μ sec. At charging pressures of 0 atm gage the flour was initiated to lower order reaction and transitioned to detonation after considerable delay (≥ 200 μ sec). When pressed to a density of 1.6 gm/cc, PETN required charging pressures of 85 atm gage to produce detonation within 1 μ sec of the impact of the detonation wave. At charging pressures less than about 9 atm gage, the 1.6 gm/cc PETN pellet was not initiated to self-sustaining reaction.

The initiation sensitivity for RDX and tetryl also reduced with increasing density as would be expected. In the unpressed, flour or granule form the ordering of the sensitivities, S , is

$$S_{\text{PETN}} [\rho = 0.7 \text{ gm/cc}] > S_{\text{RDX}} [\rho = 0.9 \text{ gm/cc}] > S_{\text{tetryl}} [\rho = 1.0 \text{ gm/cc}];$$

this ordering appears applicable to both the production of detonation with ≤ 1 μ sec delay and to the failure to produce a self-sustained reaction. The same ordering of sensitivities appears to apply when pressed pellets of nearly equal density are compared; and is the same ordering as found by drop-weight impact¹⁶ and by projectile impact.⁶

The detonation velocities observed in the present tests were similar to those reported by Hampdon and Stresau¹⁷ with the qualifications noted by Jones and Mitchell.¹⁸ With a gas charging pressure of 2 atm gage, PETN flour was initiated to a velocity of 3.5 mm/ μ sec after a delay of 4 μ sec; 8 μ sec later this velocity accelerated to the stable value, 4.8 mm/ μ sec. When RDX flour was initiated to

detonation with 12 atm gage gas charging pressure, the initial velocity was about 2.6 mm/ μ sec; after 4 μ sec, acceleration to the stable velocity, 5.4 mm/ μ sec, occurred. With 2 atm gage charging pressure, a subsonic reaction rate of 0.3 mm/ μ sec in the RDX accelerated to the stable value, 5.4 mm/ μ sec, after 30 μ sec. With 16 atm gage, tetryl flour was initiated at a velocity of 2.8 mm/ μ sec, and with 6 atm gage, 1.55 mm/ μ sec was observed. Acceleration to the stable, high rate of 5.3 mm/ μ sec did not occur. This result is presumed to be a consequence of the dimensions of the explosive sample.¹⁸

When detonation occurs after induction times of several microseconds, it is to be expected that details of the hot gas-solid explosive-confinement interactions are important in determination of the course of the reaction. It was observed that after the initial pressure pulse impingement, the pressure remained nearly constant for several microseconds and then increased at a high rate. The high rate of pressure increase is seen first as a series of spikes probably due to individual pressure wave interactions followed by an approximately exponential rise to quite high values of pressure. The high values of pressure in the container following the exponential rise are of the same order as detonation wave pressures to be expected in the condensed sample.

Associated with incidence of the approximately exponential rate of increase in pressure, was an increased rate of propagation as shown by the velocity probe. Comparison of records obtained with various initial gas charging pressures showed that the pressure at appearance of the high rate could be correlated with the explosive density and with the explosive type. As an example, with PETN flour and a charging pressure of 0.7 atm gage, the induction time was 24 μ sec and the vessel pressure at appearance of detonation was about 2 kbar. With the same type of explosive sample but a charging pressure of 20 atm gage, the induction time was about 1 μ sec and the pressure in the vessel at appearance of detonation was again about 2 kbar. This type of observation of a critical pressure for the occurrence of detonation is supported by the results of Price, Wehner, and Roberson.⁷

Table 3 compares pressures for the appearance of detonation as determined in this study, to the shock pressure required to initiate unconfined charges as given by, or derived from, the results of other investigations.^{2,4,5,6,19} The reasonable conformity of measured values from such diverse techniques strongly suggests that the tabulated pressures are indeed critical pressures for the occurrence of detonation. The individual values of table 3 and of table 4 are offered as representative data. Additional experience with the sensors and additional experimental data are required before the results are considered to be more than semiquantitative.

Application of Results to a Large Pile of Explosives Under Conflagration Conditions

A. Assumed Stimulus is a Gas Detonation External to the Pile

The stoichiometric mixture of ethylene and oxygen must be charged to pressures of 20, 26, or 26 atmospheres respectively in order that the gas detonation be able to induce detonation in PETN, RDX, or tetryl flours with delay times of about 1 μ sec. Buildings, bins, or containers capable of withstanding more than 275 psig are economically and architecturally incompatible with the storage of tons of explosives.

Concern, then, is entirely with pressures of approximately zero psig for such a detonable gas mixture. Table 4 summarizes induction times as functions of detonable mixture charging pressure for PETN and RDX. (According to table 1, tetryl was not initiated to detonation at charging pressures below 3 atm gage.) Induction times of PETN and RDX, at 1 atm charging pressure, are ≥ 200 and 250 μ sec respectively. Detonations produced in sufficiently large external volumes of gas could

maintain the gas stimulus at the explosive surface for these, or longer, periods of time²⁰ but such "gas detonation confinement" would not support the relatively slow buildup of pressure to values in excess of the critical pressure for appearance of detonation (more than 28,000 psi). One test with 1.1 gm/cc, Composition A5 explosive showed transition directly from a level of about 2000 psig in the container without observable pressure run-up in the gas phase close to the explosive surface. However, 2000 psig is beyond the range of sustained pressures available from an unconfined gas detonation.

It is thus improbable that an external, unconfined, gas detonation would cause direct initiation of a large pile of flour explosives of the types tested. If the gas detonation were to produce fragments having velocities of 300 m/sec or more⁶ such fragments might produce detonation in the large pile. Existing data on projectile initiation are not sufficiently complete to permit numerical prediction of gas volume versus projectile size and velocity relationships.

B. Assumed Stimulus is Internal to the Large Pile of Explosives

Peak pressure in the reflected gas detonation wave, of these studies, at 0 psig is believed to be less than 0.2 kbar; the Chapman-Jouguet pressure is even lower, of course. In view of the appreciable difference between these pressures and the critical pressure required for appearance of detonation in the condensed phase, it is probable that the initiation sequence is that of ignition of the explosive particles and then self-pressurization of the test vessel by the decomposition products. The exact mechanism by which deflagration of the explosive particles is initiated, whether by an enthalpy wave, by an internal autoignition of "cook off" gases, or by an external flame, is not of particular importance. The important question is whether or not adequate confinement is provided to permit the pressurization to occur. Two circumstances can be postulated to provide the necessary confinement by an explosive pile--collapse of a cavity formed by erosion, or enfoldment of burning particles by a sliding pile. Because of lack of knowledge about ullage space--induction time relationships and because of the complicated dynamics of the mechanical collapse or enfoldment, it is not presently possible to discuss these circumstances in detail. It may be of academic interest to note that rigid collapse of a 5-meter-high pile of material having a sonic velocity of 2000 m/sec would provide nearly rigid confinement for a time of 200 μ sec.

Summary and Conclusions

Gas detonations generated in stoichiometric ethylene-oxygen mixtures have been used to produce detonations in PETN, RDX, and tetryl explosive. The explosive has been tested both as a flour and as pressed pellets. The experimental results suggest the existence of a critical pressure for the appearance of detonation in the condensed explosive. Induction time does not have a strong effect upon the induction pressure--the pressure to which the explosive is subject at the time of appearance of detonation. These induction pressures were sensitive to explosive type, density, and particle size. From these results, it has been deduced that a gas detonation cannot produce detonation of a large pile of these materials without the interposition of some action producing confinement of the ignited explosive grains. The requisite confinement cannot be provided by an unconfined gas detonation.

Induction pressures for the tested flours or granules of PETN, RDX, and tetryl were 2, 3, and 3 kbar respectively. In pressed pellets, pressures for appearance of detonation were: 13 kbar for 1.6 gm/cc PETN; 12 kbar for 1.4 gm/cc Composition A5; 16 kbar for 1.6 gm/cc Composition A5; 16 kbar for 1.4 gm/cc tetryl; and 20 kbar for 1.6 gm/cc tetryl.

References

1. Sultanoff, M., V. M. Boyle, and J. Paszek. Shock Induced Sympathetic Detonation In Solid Explosive Charges. Third Symposium on Detonation, September 1960, Princeton, New Jersey, Office of Naval Research Symposium Report ACR-52, v. 2, pp. 520-533.
2. Seay, G. E., and L. B. Seely, Jr. Initiation of a Low-Density PETN Pressing by a Plane Shock Wave. J. Appl. Phys., v. 32, 1961, pp. 1092-1097.
3. Campbell, A. W., W. C. Davis, J. B. Ramsey, and J. R. Travis. Shock Initiation of Solid Explosives. Phys. of Fluids, No. 4, 1961, pp. 511-521.
4. LeRoux, A. Detonation of Explosives Through the Shock of a Solid Body Launched at High Velocity. Mem. Poudres, v. 33, 1951, pp. 283-321.
5. Eldh, D., P. A. Persson, B. Ohlin, C. H. Johansson, S. Ljungberg, and T. Sjolín. Shooting Test with Plane Impact Surface for Determining the Sensitivity of Explosives. Explosivstoffe, v. 5, May 1963, pp. 97-103.
6. Weiss, M. L., and E. L. Litchfield. Projectile Impact Initiation of Condensed Explosives. Bur. Mines Rept. Investigations 6986, 1967, 17 pp.
7. Price, Donna, J. F. Wehner, and G. E. Roberson. Transition from Slow Burning to Detonation. Further Studies of the Free Volume and the Low Velocity Regime in Cast Pentolite. Naval Ordnance Laboratory Tech. Rept. 63-18, February 1963, 33 pp.
8. Price, Donna, and F. J. Petrone. Detonation Initiated by High Pressure Gas Loading of a Solid Explosive. Naval Ordnance Laboratory Tech. Rept. 63-103, April 1963, 18 pp.
9. Andreev, K. K., and V. P. Maslov. Action of Gas Explosion on Solid Explosives. Comptes Rendus (Doklady) de l'Acad. Sci. (URSS), XXV, v. 195, 1939, pp. 195-197.
10. Gordeev, V. E., A. I. Serbinov, Ya. K. Troshin, G. I. Filatov. Initiation of the Explosive Conversion of Condensed Explosives by Gaseous Detonation. Combustion, Explosion, and Shock Waves, v. 1, No. 2, 1965, pp. 7-13.
11. Makomaski, A. H. Preliminary One-Dimensional Investigation of the Initiation of Low-Density PETN by Hydrogen-Oxygen Detonation Waves. Univ. of Toronto Inst. of Aerospace Studies Tech. Note 83, February 1965, 24 pp.
12. Cook, M. A., and F. A. Olson. Chemical Reactions in Propellant Ignition. AIChE Jour., v. 1, 1955, pp. 391-400.
13. Litchfield, E. L., M. H. Hay, and D. R. Forshey. Direct Electrical Initiation of Freely Expanding Gaseous Detonation Waves. Ninth Symposium (International) on Combustion. Academic Press, Inc., New York, N. Y., 1963, pp. 282-286.
14. Watson, R. Gage for Measuring Shock Pressure. Rev. Sci. Instruments, in press.
15. Gibson, F. C., M. L. Boswer, and C. M. Mason. Method for the Study of Deflagration to Detonation. Rev. Sci. Instruments, v. 30, 1959, pp. 916-919.

16. Copp, J. L., S. F. Napier, T. Nash, W. J. Powell, H. Shelby, A. R. Ubbelohde, and P. Woodhead. The Sensitiveness of Explosives. Phil. Trans. Roy. Soc., v. A-241, 1949, pp. 197-296.
17. Hampdon, L. E., and R. H. Stresau. Small Scale Technique for Measurement of Detonation Velocities. NAVORD Report 2282, December 27, 1951.
18. Jones, E., and D. Mitchell. Spread of Detonation in High Explosives. Nature, v. 161, 1948, pp. 98-99.
19. Coleburn, N. L., and T. P. Liddiard, Jr. Hugoniot Equations of State of Several Unreacted Explosives. Jour. of Chem. Phys., v. 44, March 1966, pp. 1929-1936.
20. Kufer, John H. Air Blast Predictions for Operation Distant Plain. Ballistics Research Laboratory Tech. Note 1612, Aberdeen Proving Ground, Maryland, June 1966.

TABLE 1. - Particle size distributions of explosive flours or granules

Particle size range R, microns	Percent of sample in range			
	PETN	RDX ^{1/}	RDX ^{2/}	Tetryl
710 < R	7	2	1	14
350 < R < 710	81	20	85	79
105 < R < 350	7	63	13	6
74 < R < 105	0	2	1	0
R < 74	0	15	0	2

^{1/}Neat RDX.

^{2/}RDX + 1% stearic acid (Composition A5).

TABLE 2. - Threshold charging pressures of stoichiometric ethylene-oxygen mixtures to produce gas detonation initiation of detonation in PETN, RDX, and tetryl

Explosive	Density, gm/cc	Detonation with	
		$\leq 1 \mu$ sec delay, atm gage	No detonation atm gage
PETN	0.7	20	< 0
PETN ^{1/}	1.60	85	<u>3/</u> 9
RDX	.9	26	< 0
RDX ^{2/}	1.1	80	8
RDX ^{2/}	1.40	84	<u>3/</u> 15
RDX ^{2/}	1.64	> 84	<u>3/</u> 39
Tetryl	1.0	26	<u>3/</u> 3
Tetryl	1.39	> 85	<u>3/</u> 39
Tetryl	1.57	> 85	<u>3/</u> 67

^{1/} 1% graphite added.

^{2/} 1% stearic acid added.

^{3/} Average from lowest value for detonation and highest value for no detonation.

TABLE 3. - Comparison of minimum shock pressures for initiation of explosive compounds by gas detonation or for initiation with the indicated stimulus

Source	Density, gm/cc	Type of Stimulus	Shock Pressure, kbar
<u>PETN</u>			
This work	0.7	Gas detonation	<u>1/</u> 2.1 ± 0.3
LeRoux	0.7	Projectile impact	<u>2/</u> 2.0
Seay and Seely	1.0	Plane shock wave	2.5
Weiss and Litchfield	1.48	Projectile impact	11.0
Eldh and coworkers	1.53	Projectile impact	<u>2/</u> 11.0
This work	1.60	Gas detonation	<u>1/</u> 13.3 ± 0.5
<u>RDX</u>			
Weiss and Litchfield	0.8	Projectile impact	3.0
This work	.9	Gas detonation	<u>1/</u> 3.1 ± 0.4
LeRoux	1.0	Projectile impact	<u>2/</u> 3.0
This work	1.1	Gas detonation	3.4 ± 0.5
This work	1.40	Gas detonation	12.
This work	1.64	Gas detonation	<u>1/</u> 16. ± 1
Weiss and Litchfield	1.62	Projectile impact	21.0
Eldh and coworkers	1.65	Projectile impact	<u>2/</u> 22.0
<u>Tetryl</u>			
This work	1.0	Gas detonation	<u>3/</u> 3.
Weiss and Litchfield	1.00	Projectile impact	3.5
LeRoux	1.00	Projectile impact	<u>2/</u> 3.5
This work	1.39	Gas detonation	<u>3/</u> 11.
Weiss and Litchfield	1.57	Projectile impact	19.0
This work	1.57	Gas detonation	13.
Eldh and coworkers	1.65	Projectile impact	<u>2/</u> 22.0

1/ Mean and estimated standard deviation per observation.

2/ These values calculated by the authors from projectile velocity data of other investigators.

3/ For low-velocity detonation.

TABLE 4. - Summary of parameters for initiation of flour and pelletized explosive compounds by gas detonation

Explosive	Density gm/cc	Charging pressure, atm gage	Container pressure at detonation, kbar	Induction time, μsec
PETN	0.7	0.0	--	≥200
PETN	.7	0.7	2.2	28
PETN	.7	1.0	--	8
PETN	.7	1.7	--	5
PETN	.7	2.1	--	4
PETN	.7	3.1	1.9	6
PETN	.7	20.0	--	1
PETN	1.60	54.0	13.0	4
PETN	1.60	85.0	13.5	1
RDX	0.9	0.0	--	≥270
RDX	.9	1.0	--	50
RDX	.9	1.4	--	56
RDX	.9	1.7	--	28
RDX	.9	3.1	--	12
RDX	.9	5.9	--	5.7
RDX	.9	20.0	3.3	4
RDX	.9	26.0	2.9	1
RDX ₁ /	1.1	11.2	6.0	70
RDX ₁ /	1.1	11.2	4.0	72
RDX ₁ /	1.1	27.2	3.1	36
RDX ₁ /	1.1	40.4	3.0	16
RDX ₁ /	1.1	58.0	3.4	7
RDX ₁ /	1.1	80.0	--	1
RDX ₁ /	1.40	50.0	--	7
RDX ₁ /	1.40	84.0	12.5	1
RDX ₁ /	1.64	57.0	17.0	14
RDX ₁ /	1.64	82.0	15.0	4

1/ RDX + 1% stearic acid (Composition A5).

EXPLOSIVE BEHAVIOR OF AMMONIUM PERCHLORATE

Donna Price, A. R. Clairmont, Jr., and I. Jaffe

U. S. NAVAL ORDNANCE LABORATORY
White Oak, Silver Spring, Maryland

The inorganic oxidizer, ammonium perchlorate (AP), is widely used as a major propellant ingredient. It is, in addition, a very interesting high explosive because its behavior differs markedly from that of conventional explosives such as TNT. AP is a member of a group of explosives which exhibit more ideal detonation behavior at high than at low porosity.¹ No member of this group has been studied very systematically; only a careful investigation of typical members will enable us to understand these materials at least as well as we understand more conventional explosives. Because AP seems a representative group member, because it is frequently used as a propellant component, and because it has been extensively studied in the related fields of thermal decomposition and combustion, we have started a systematic study of its explosive behavior. The purpose of this paper is to report the results obtained from our recent work.

The detonation of AP has been studied before, chiefly by Andersen and Pesante.² But their data had too much scatter, and did not extend sufficiently far into the high charge density region to demonstrate the distinctive explosive behavior defined by the present results. That behavior is typified by a detonability limit curve along which critical density increases with critical diameter, and a finite diameter detonation velocity which is not uniquely defined by loading density, i.e., which exhibits a non-linear curve with a maximum in the detonation velocity.

EXPERIMENTAL

All ammonium perchlorate used was propellant grade; it contained 0.2 to 1% tricalcium phosphate. The three lots of perchlorate had weight-median particle sizes of 10, 25, and 200 μ , respectively. For charge preparation, the material was dried at 50°C for four hours or longer and packed in cellulose acetate envelopes to form 20.32 cm-long cylinders of 1.90 to 7.62 cm diameter. Compacting was by hand, by hydraulic press, or by isostatic press (followed by machining to size), according to the charge density desired and the grain size of the perchlorate. All low density charges were fired almost immediately after preparation to avoid the formation of small cracks and column separation, phenomena which occur with aging.

The best quality charges were, of course, those prepared in the isostatic press from the 10 μ material. As the grain size of the perchlorate increased or as the charge density (ρ_0) decreased, charge quality became poorer. At $\rho_0 < 1$ g/cc, the charges were of such poor quality that only a few small diameter charges prepared from the 10 μ material were accepted for firing.

The charges were fired in the experimental setup of Fig. 1 with either tetryl or pentolite boosters. A 70 mm smear camera was used to record the flasher enhanced luminosity of the reaction front. The camera was used at a writing speed of between 1 and 3 mm/ μ sec to obtain a

smear trace of the disturbance at 45° to the base of the film.

The smear camera photographs were of excellent quality, and detonation velocity was determined from the slope of the trace, i.e., by a least square fit of the linear distance - time data. For the lowest resolution, the maximum error estimated from error in reading these records is 1.5%. In over a dozen replications the maximum deviation was also 1.5%; the mean precision was 0.7%.

RESULTS AND DISCUSSION

Failing Reactions

The first interesting result of this work is that charges of ammonium perchlorate (of any grain size) when subcritical are nevertheless capable of showing fading but vigorous reaction. Such charges of the $10\ \mu$ and $25\ \mu$ materials, under shock from the booster, produced curved luminous traces persisting to distances as large as 8 - 9 diameters down the charge. As the charge diameter was increased toward its critical value, the curvature of the trace decreased. It was, therefore, almost impossible to determine the exact critical limits for the perchlorate; instead, they were bracketted by two densities at which failure and detonation occurred at a given diameter.

The coarsest material ($200\ \mu$) failed to detonate at its pour-density of 1.29 g/cc in a 7.62 cm diameter charge. (Larger charges cannot be used in the available firing facilities.) However, it too showed vigorous reaction persisting for two diameters down the charge.

Detonability Limits

The limit or failure curve for the $10\ \mu$ perchlorate in the charge diameter (d) vs ρ_0 plane is approximated in Fig. 2. The critical values are d_c , the diameter at and above which detonation propagates, and ρ_c , the density above which detonation cannot occur. The trend of increasing critical density with increasing critical diameter and the consequent definition of ρ_c are both opposite to those for TNT-like explosives.¹ Figure 2 also shows measurements made by two other investigators on fine AP's. The agreement is very good in view of approximating the particle size distribution by the median size and of the difficulty of determining that median.

The limit curve for the $25\ \mu$ AP was not as well defined as that for the finer material. The relevant data are:

<u>d(cm)</u>	<u>ρ_0(g/cc)</u>	
	<u>Deton.</u>	<u>Failure</u>
3.81	1.02	1.11
5.08	1.36	1.41
7.62	1.47	1.56

This limit curve will therefore lie above and to the left of that for the finer perchlorate. The limit curve for the $200\ \mu$ material is beyond the experimental range of the present work. The trend of particle size effect is the expected one for all explosives, that of increasing d .

with increasing particle size. The shift in ρ_0 is, however, toward lower values for ammonium perchlorate, toward higher for TNT-like explosives.

Detonation Behavior Pattern

The detonation velocity (D) vs ρ_0 curves at various diameters of the finest perchlorate are shown in Fig. 3. Typically the D vs ρ_0 curve at fixed d shows detonation velocity increasing with increasing density to a maximum value. Beyond this maximum, D decreases as ρ_0 increases until it reaches its critical value at the failure limit.

The curve for each diameter has been terminated at the critical density given by the smoothed curve of Fig. 2. The limit line of Fig. 3, which divides the detonation from the failure area, is shown as the dashed line through these terminal points. The curve seems slightly concave upward and gives the critical detonation velocity (D_c) as a function of ρ_0 at different diameters, but at fixed particle size.

Fig. 4 shows the analogous pattern, analogously derived, for the 25 μ material. This pattern is very like that of Fig. 3; it is, however, compressed into the smaller diameter range which results from the particle size shift of the limit curve, d vs ρ_0 . At any given values of d and ρ_0 , the detonation velocity of the finer perchlorate is greater than that of the coarser. This point is further illustrated in Fig. 5 where the particle size effect on the D vs ρ_0 curves at $d = 5.08$ cm is shown. The terminal points of the two curves are on a limit curve (indicated by the dashed line) which gives D_c vs ρ_0 at constant diameter but at different particle sizes.

Infinite Diameter Values

Since most of our D vs ρ_0 curves are non-linear, our experimental range is one in which diameter effect on D is large. At $\rho_0 = 1.0$ g/cc all data are on the low density side of the maximum D or, in one case, at the maximum. Under these circumstances, the usual D vs d^{-1} curve is linear (Fig. 6) and gives the ideal value D_1 of 3.78 mm/ μ sec at $\rho_0 = 1.01$ g/cc in good agreement with the comparable value of 3.75 determined by Evans et al.

For an analogous selection of data at $\rho_0 = 1.26$ g/cc the solid symbols of Fig. 6 are from the high density side of the maximum D and must be neglected; they would lead to values of D_1 which are too high. The remaining data give $D_1 = 4.79$ mm/ μ sec at $\rho_0 = 1.25$ g/cc in very poor agreement with the Ref. (2) value. However, if the Ref. (2) data are extrapolated as in the present work, the analogous D_1 is 4.85 instead of the reported 4.37 mm/ μ sec.

Even so, it is quite likely that the D_1 value obtained in this manner at the higher density (where detonation behavior is less ideal) is too high. Measurements at larger diameters are necessary to decide this. Meanwhile the present values have been used in Figs. 3 and 4 to indicate a portion of the D_1 vs ρ_0 curve. The data for the 25 μ material also extrapolate to the same curve.

Reaction Zone Lengths, Reaction Times

Of the available diameter effect theories, the curved front theory^{7a}

seems to fit our data best. Ref. (7) gives the detonation reaction zone length by

$$a = d (1 - D/D_1) \quad (1)$$

The modified theory^a gives a zone length

$$z = (s/3.5) (1 - D/D_1) \quad (2)$$

where s is the radius of curvature of the reaction front. For the reasonable assumption that s is directly proportional to d , Eqs. (1) and (2) are identical except for a constant factor and will lead to the same relative reaction zone lengths.

The reaction time (τ) is defined and related to the reaction zone length by

$$a = (D - \bar{u}) \tau \quad (3)$$

where \bar{u} is the average particle velocity between the leading von Neumann shock and the C-J plane of the detonation front. Moreover, according to the grain burning theory⁷,

$$\tau = R/\lambda k \quad (4)$$

where R is the average particle radius, λ the molecular diameter, and k the specific reaction rate of a single molecule.

For each ideal value $D_1(\rho_0)$, there is a corresponding detonation temperature $T_1(\rho_0)$. Moreover, these infinite diameter values are independent of the grain size. Hence Eqs. (1) or (2) and (3) can be used to obtain the ratio of the reaction times of the 10 μ and 25 μ perchlorate at T_1 . If in addition we assume that this material detonates by a grain burning mechanism, we can incorporate Eq. (4) into the relations to obtain

$$(a_1/a_2) = (z_1/z_2) = (\tau_{11}/\tau_{21}) = (R_1/R_2) \quad (5)$$

where the subscripts 1 and 2 denote 10 μ and 25 μ ammonium perchlorate, respectively. Calculation of the ratio of the reaction times by Eq. (5) gives $(\tau_{11}/\tau_{21}) = 0.40 \pm 0.04$ over the range of $0.90 \leq \rho_0 \leq 1.20$ g/cc. This is in good agreement with the ratio $(R_1/R_2) = 10/25 = 0.40$, a result consistent with the grain burning mechanism for the detonation of this material; such a mechanism is also consistent with its more ideal behavior at greater porosities.

REFERENCES

- (1) D. Price, "Contrasting Patterns in the Behavior of High Explosives," Eleventh Symposium (International) on Combustion (1967) pp 19-28, in press.
- (2) W. H. Andersen and R. E. Pesante, "Reaction Rate and Characteristics of Ammonium Perchlorate in Detonation," Eighth Symposium (International) on Combustion, Williams and Wilkins Co., Baltimore (1962) pp 705-10.
- (3) R. L. Jameson, S. J. Lukasik, and B. J. Pernick, J. Appl. Physics 35, 714-720 (1964).
- (4) M. W. Evans, C. M. Ablow, B. O. Reese, and A. B. Amster, "Shock Sensitivity of Low Density Granular Explosives," Proceedings of the International Conference on Sensitivity and Hazards of Explosives, Ministry of Aviation, U. K. (1963).
- (5) M. W. Evans, B. O. Reese, L. B. Seely, and E. L. Lee, "Shock Initiation of Low-Density Pressings of Ammonium Perchlorate," Proceedings of the Fourth Symposium on Detonation, October 1965, in press.
- (6) M. L. Pandow, K. F. Ockert, and H. M. Shuey, "Studies of the Diameter-Dependence of Detonation Velocity in Solid Composite Propellants I, Proc. of the 4th Symposium on Detonation, October 1965, in press.
- (7) H. Eyring, R. E. Powell, G. H. Duffy, and R. B. Parlin, Chem. Revs. 45, 69 (1949).
- (8) W. W. Wood and J. G. Kirkwood, J. Chem. Phys. 22, 1920 (1954).

FIG. 1 EXPERIMENTAL ASSEMBLY

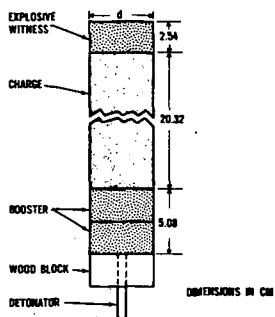


FIG. 2 DETONABILITY LIMIT CURVE FOR AP (10 μ)

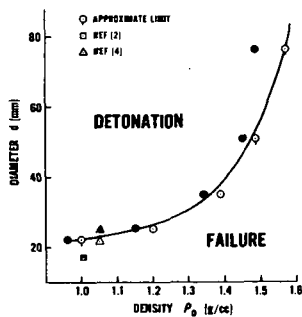


FIG. 3 DETONATION BEHAVIOR OF AP (10 μ)

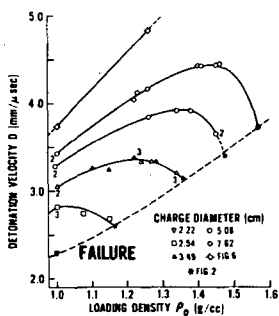


FIG. 4 DETONATION BEHAVIOR OF AP (25 μ)

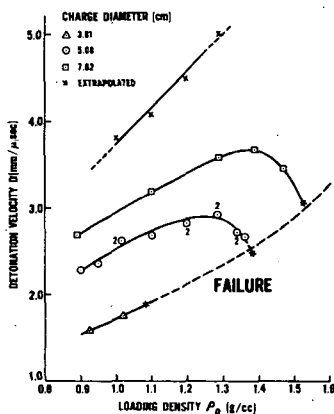


FIG. 5 EFFECT OF PARTICLE SIZE ON DETONATION VELOCITY OF AP (d=5.08 cm)

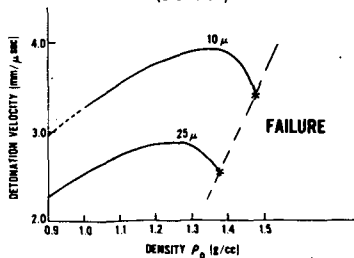
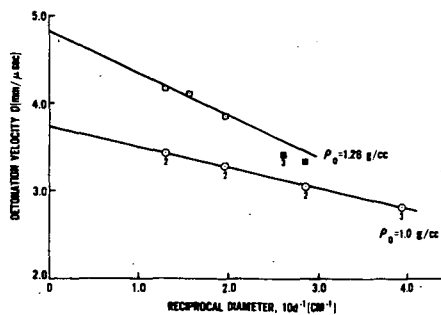


FIG. 6 EXTRAPOLATION TO INFINITE DIAMETER VALUES



ACCELERATING DETONATIONS IN COMPOSITION B-3 EXPLOSIVE

Robert Sewell, Lawrence Cosner, James Sinclair

U. S. Naval Ordnance Test Station, China Lake, California 93555

INTRODUCTION

The problem of predicting what will happen when a fragment or projectile strikes cased high explosive munitions is complicated not only by the complexity of the projectile-munition geometry but also by the number of different reactions which can and do occur.

Recourse to the literature on the subject exposes one to such terms as no reaction, burning, deflagration, low order, mild low order, large low order, partial detonation, high order and deflagration to detonation transition.

Examining the literature on explosive sensitivity is about as helpful and introduces a series of tests which regularly produce confused ranking of the "sensitivity" of high explosive systems. (The theory or theories of detonation are not a great deal of help either.)

The major problem is actually one of continual attempts to link all the various modes of chemical reaction and all the means of physical excitation into one simple model which would be useful in explosive applications. The probability of success in such a venture is small at best, but an attempt must be made since studies are going to be made with or without adequate models.

In any attempt to tackle this problem the explosive system should first be examined from a chemical as well as a physical viewpoint, the adiabatic auto ignition temperature and its connotations, the shock sensitivity spectrum, experimental results, effects of geometry, and an attempt to create a limited analytic model.

THE EXPLOSIVE

GENERAL COMMENTS

Explosives in general use vary over a wide range of chemical compositions, but do have several similar characteristics.

They consist of chemical compositions which contain both the fuel and the oxidizer in an "unstable" molecular configuration which when broken allows the various atoms to combine into such products as H_2O , CO , CO_2 , N_2 , etc., with a rapid net production of energy.

The stability of the explosive molecule should and apparently does play an important part in the sensitivity of the explosive.

Analysis of the statistical nature of chemical kinetics shows that some of the molecules are decomposing at any temperature above absolute zero but that the number of molecules decomposing or reacting per second remains "insignificant" up to some critical temperature dependent on the ability of the explosive to dissipate the energy generated by the reacting molecules. Above this temperature the number of molecules involved increases exponentially leading to significant evolution of energy. The dissipative factors involve the heat capacity, the thermal conductivity, the geometry of the explosive, the nature of the confining media, and the temperature of the environment.

(In the presence of air, surface reactions involving the oxygen in the air are, of course, possible.)

In an investigation of the problem of explosive storage and handling, Longwell (ref. 1) measured the adiabatic auto-ignition temperatures of various explosives and developed relations for safe storage times and temperature for various charge geometries.

SHOCK MOLECULAR EFFECTS

When a shock wave strikes a molecule, the molecule absorbs energy and if the energy is high enough, bond rupture occurs. As long as the energy is absorbed into the molecule with no effect from other molecules or their decomposition fragments, the weakest part of the molecule will undergo rupture first. This will be regardless of other factors and certainly is the first effect of the shock wave.

However, once the molecule is disrupted, reactive fragments such as ions and free radicals can collide with the unreacted molecule to cause further bond rupture. Since this latter effect will depend on the spatial features of the molecule, steric factors are important and the bonds disrupted may not necessarily be the weakest in the molecule. In fact they may well be the strongest if the atoms involved are easier to reach by being on the outside of the molecule.

This being the case it is easy to select the bonds that are broken first, i.e., the N-NO₂ and the C-NO₂ (Table I). However, after the initial phase it is probable that the C-H bonds are next ruptured since they occur in both molecules and the hydrogen atoms are on the outside of the molecule.

SHOCK SENSITIVITY SPECTRUM

Energy levels calculated as associated with shock waves in explosives show that for shocks of the order of a few kilobars some chemical reaction is quite probable, but the extent and rate of propagation of the reaction would be strongly dependent on the duration of the pressure pulse as well as its amplitude and thus strongly dependent on the nature of the confinement. Studies by Liddiard et al. (ref. 2) have shown that with proper confinement sustained chemical reaction can be produced in Comp B at pressure amplitudes of the order of 5 to 7 kbars.

This sustained chemical reaction is not to be confused with detonation, which is a chemically supported shock wave, but it can produce burning or deflagration which has often, improperly, been called low order detonation.

Low order detonation--a nonideal detonation--is generally unstable (it is either accelerating or decaying) and is produced when a shock wave with intensity above a given level (dependent on the curvature of the shock front) enters the explosive and either accelerates to full high order detonation or decays to no reaction. The curvature of the wave front during acceleration is strongly dependent on the confinement, the size and shape of the shock producing system, and the physical properties of the explosive.

It has been shown (ref. 3) that for pressures greater than 21 kbars the growth to detonation is dependent upon peak pressure and is relatively independent of impulse. It is interesting to note that the factor of 3 between the values of critical pressures obtained by Liddiard et al. (ref. 4) and Cosner and Burford (ref. 4) correspond to the factor of 3 between the average bond strengths of the N-NO₂ and the C-H bonds.

The initiation of explosive by shock impact is characterized by several zones or thresholds. At very low shock levels no significant chemical reaction occurs, as the shock level is increased surface reactions will be triggered, and as the shock level is increased still further other effects will begin to predominate.

If the input shock level is above 202 kbars (ref. 3), an almost instantaneous jump to stable detonation is observed with a CJ pressure of 272 kbars. Studies have shown that in the region from 21 to 202 kbars the growth of pressure with distance can be represented by

$$\frac{dP}{dx} = k(P - P_c) \quad (\text{ref. 3}) \quad (1)$$

where $P_c = 21$ kbars and $k = 0.132 \text{ mm}^{-1}$ with P in kilobars and x in millimeters.

Using an assumption based on Adams' (ref. 5) investigation of nonideal detonation, the pressure is directly proportional to the square of the propagation velocity

$$P = \gamma U^2 \quad (\text{ref. 5}) \quad (2)$$

The constant γ in this expression is found to be 3.38 with P in kilobars and U in millimeters/microseconds.

Integration of eq. (1) yields solutions for pressure as a function of distance and these combined with eq. (2) yield shock velocity as a function of distance and input pressure. A table of parameters of interest associated with these solutions is shown in Table II.

Wedge experiments of the type performed by Boyle, Jameson, and Allison (ref. 6) measure directly the shock velocity as a function of distance. Their determination of the pressure is dependent on the assumption that the explosive will return to its initial density upon release of the pressure. This assumption seems highly unjustified in view of the accelerating reaction which is observed. Their velocity-position data are free of these assumptions and could be used for direct comparison. Unfortunately, "for ease of plotting," Boyle, Jameson, and Allison divided their actual distance by the initiation distance to "normalize" the measurements and failed to publish the actual distances. Working from what they have published, the initiation distance is found to be 15 mm with a variation of about 1 mm. A plot of their data compared to our calculated values is shown in Fig. 1.

If a spherically divergent system is presumed, eq. (1) is modified by substituting r for x and introducing a spherical loss term

$$\frac{dP}{dr} = k(P - P_c) - \frac{P}{r} \quad (3a)$$

or

$$\frac{dP}{dr} = P(k - \frac{1}{r}) - kP_c \quad (3b)$$

If eq. (3b) is correct and if the constant k is correct a minimum radius of curvature for any stable detonation becomes

$$r = \frac{1}{k} \quad (4)$$

For Comp B-3 this would be $r = \frac{1}{0.133} = 7.52 \text{ mm}$.

This value is not the limiting radius of a cylinder which would propagate detonation but would be the radius of curvature of the central portion of the detonation wave in the limiting cylinder. Actually since the pressure would not be much above 202 kbar at the limit situation the limiting radius of curvature would be about 8.4 mm. If a hemispherical front is postulated the limiting diameter for full detonation velocity would be 16.8 mm which is equivalent to the d_m^* of ref. 7.

A graph of the pressure required to produce an accelerating detonation as a function of the radius of curvature of the front is shown in Fig. 2. Converging wave fronts (negative radius of curvature) require less pressure than the critical pressure to produce an accelerating front which tends to invert rapidly to a divergent wave front. If during the period of convergence the pressure increases enough over a large enough zone, continued acceleration should occur.

Below and to the left of the positive radius of curvature curve the reaction produced is a decaying detonation. Near the curve, a slight change in radius of curvature through a density change or a void in the explosive could have a large effect on the occurrence of growth to detonation.

REFERENCES

- (1) P. A. Longwell, NAVWEPS Report 7646, NOTS TP 2663, China Lake, Calif., Mar 1961.
- (2) T. P. Liddiard, Jr. and S. J. Jacobs, NOLTR 64-53, White Oak, Md., 1965.
- (3) L. N. Cosner, R. G. S. Sewell, and J. E. Sinclair, NOTS TP 3984, China Lake, Calif., June 1966, pp. 150-64.
- (4) M. K. Burford and L. N. Cosner, NOTS TP 3301, China Lake, Calif., Aug 1963, pp. 251-68.
- (5) G. K. Adams, "Theory of Initiation to Detonation in Solid and Liquid Explosives," Ninth Symposium (International) on Combustion, Academic Press, New York, N. Y., 1963, pp. 545-53.
- (6) V. M. Boyle, R. L. Jameson, and F. E. Allison, BRL Report No. 1250, Aberdeen Proving Grounds, Md., 1964.
- (7) M. A. Cook, "The Science of High Explosives," Reinhold Publishing Company, New York, N. Y., 1958.
- (8) L. Pauling, "The Nature of the Chemical Bond," 3rd ed., Cornell University Press, Ithaca, N. Y., 1960.
- (9) A. D. Little Company, Navy Contract No. W-19-020-ORD 6433, Cambridge, Mass., 1946.

Table I

Average Bond Dissociation Energies

C=C	146 kcal/mole	(ref. 8)
C-H	98.7 kcal/mole	(ref. 8)
C-C	86.6 kcal/mole	(ref. 8)
C-N	72.8 kcal/mole	(ref. 8)
C-NO ₂	48 kcal/mole	(calcd. from ref. 9)
N-NO ₂	32 kcal/mole	(calcd. from ref. 9)

Table II

Pressure Distribution and Propagating Velocity for Accelerating Shock

mm x	kbars $\Delta P = (P_o - P_c)e^{kx}$	kbars $P = \Delta P + P_c$	mm/ μ sec $U = \sqrt{P/\gamma}$	Distance to go to detonation, mm 70 - x
70	181	202	7.78	0
65	93.5	114	5.86	5
60	48.3	69.3	4.56	10
55	25.0	46.0	3.71	15
50	12.9	33.9	3.19	20
45	6.68	27.7	2.88	25
40	3.45	24.5	2.71	30
35	1.78	22.8	2.61	35
30	0.92	21.9	2.56	40
25	0.48	21.5	2.54	45
20	0.25	21.3	2.52	50
15	0.13	21.1	2.52	55
10	0.07	21.1	2.51	60
5	0.03	21.0	2.51	65
0	0.02	21.0	2.51	70

$k = 0.132$

$\gamma = 3.34$

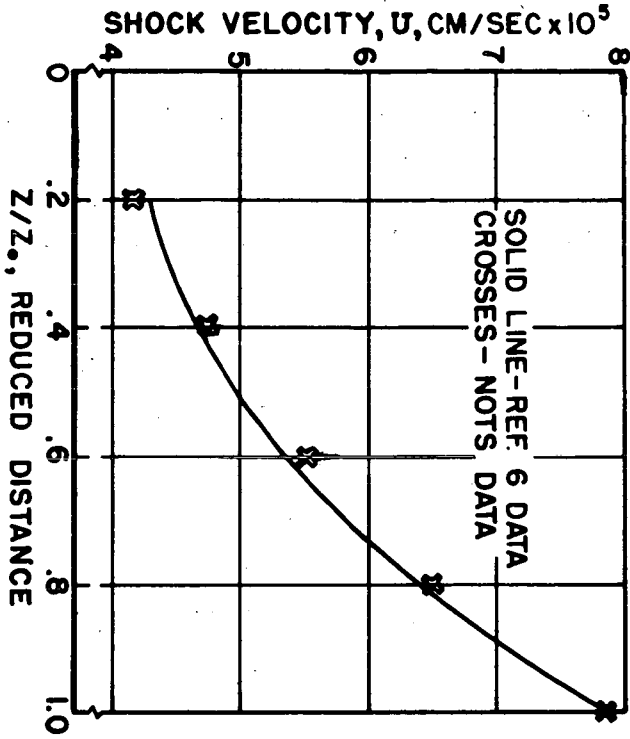


Fig. 1. Shock velocity, U, versus reduced distance Z/Z₀.

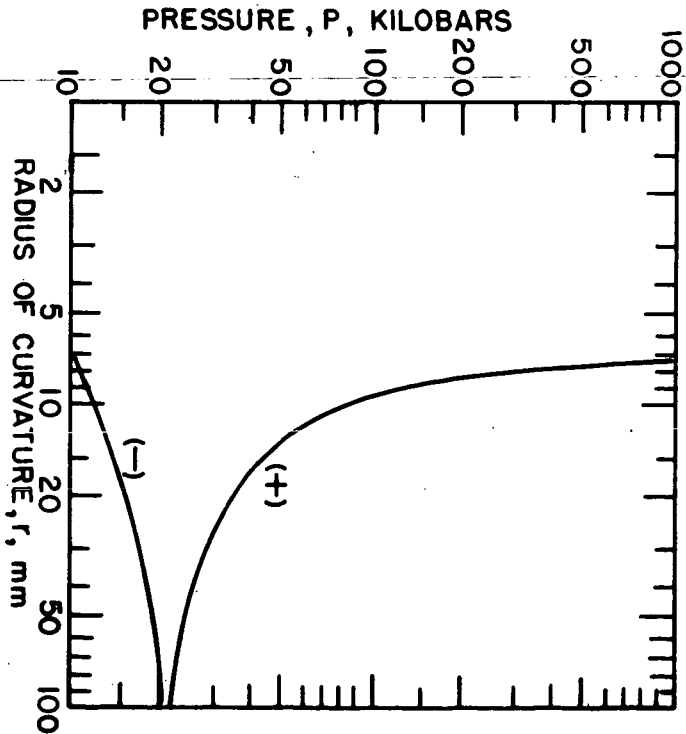


Fig. 2. Shock pressure required to produce an accelerating detonation in Composition B-3 as a function of radius of curvature.

165
The Heat and Products of Detonation of Cyclotetramethylene
tetranitramine (HMX), 2, 4, 6-trinitrotoluene (TNT), Nitromethane (NM),
and Bis [2, 2-dinitro-2-fluoro-ethyl] -formal (FEFO)*

Donald L. Ornellas

Lawrence Radiation Laboratory, University of California
Livermore, California

1. INTRODUCTION

Calorimetric measurements combined with product analysis offer a precise method for obtaining fundamental information about the detonation process. This information can then be used to provide normalization and boundary conditions for thermodynamic-hydrodynamic codes that predict explosive performance.

Three pure CHNO explosives and one fluorine containing explosive were investigated. This work is an extension of the work reported¹ for PETN. Jointly, these studies span the range of oxygen balance in explosives that is of greatest interest.

Previous detonation calorimetric work with TNT²⁻⁵ and HMX⁶ is not amenable to theoretical interpretation because of the geometries used or the lack of reliable product information. No information concerning the experimental determination of the heat and products of detonation of NM and FEFO has been found in the literature.

2. EXPERIMENTAL

2.1 Apparatus and Operation

The apparatus and its operation have been described; however, some changes have been made.

The thermometric system is a quartz thermometer which has a sensitivity of 1×10^{-4} °C for differential measurements, is easily calibrated, and has direct digital readout.

The heat equivalent of the standard instrument, taken as the average of six calibration runs, was $15, 193 \pm 2$ cal/°C. The error is the standard deviation of the mean.

Charges are now completely confined by a 1.27-cm thickness of gold. Formerly the ends of the confining cylinder were left open. Since the bottom of the interior of the bomb was most damaged by flying fragments, it was protected by a 0.64-cm-thick, 6.4-cm-diameter stainless steel disc which we replaced after each experiment.

In order to contain NM under vacuum conditions, we sealed the gold cylinder 1.27 cm from each end with a translucent film which is a laminate of 0.025-mm polyethylene and 0.013-mm Mylar. A vacuum-tight seal was obtained by compressing the film between appropriately machined gold surfaces. The weight of film averaged 0.017 g per experiment.

NM was initiated through this film with a 0.75-g PETN booster at a density of 1.71 g/cc. HMX and FEFO were initiated with a 0.3-g booster. No booster was required for the TNT experiments since initiation was effected by means of the detonator alone.

2.2 Explosive Materials

Military specification, grade II HMX was used. Analyses by thin layer

*Work performed under the auspices of the U.S. Atomic Energy Commission.

chromatography showed about 0.5% cyclotrimethylene-trinitramine (RDX) and less than 1% each of an incompletely characterized linear nitramine (compound C) and 1(N) acetal - 3, 5, 7 trinitrocyclotetranitramine (SEX). The melting point was 278-282°C. Charges were machined from billets which had been prepared with a special solvent-pressing technique.

Granular TNT, military specification, grade III was used. Analysis by thin-layer chromatography showed less than 2% impurities. These were identified as 2, 4, 5 TNT, 2, 4 dinitrotoluene and trinitrobenzoic acid. Elemental analyses for carbon, hydrogen, and nitrogen were in agreement with theory for pure TNT within the limits of the analyses. The melting point was 82.0°C. Charges were pressed in increments to a density at which TNT detonates reliably in small diameters.

Commercial grade NM was used. Chromatographic analysis showed a purity of 96.7%. Impurities were nitroethane 0.94%, 2-nitropropane 2.5%, 1-nitropropane 0.03%, and water 0.1% maximum. The empirical formula on which results are based was calculated from the above analyses and adjusted to carbon equals 1.00.

We de-aerated NM to avoid the formation of an air bubble between the booster and liquid when the bomb was evacuated. This was accomplished by subjecting frozen NM to vacuum, sealing the container, and then thawing the NM. This procedure was repeated several times.

FEFO, bis[2, 2-dinitro-2-fluoro-ethyl] -formal was available only in research quantities. It is a liquid with a vapor pressure of about 40 μ at 90°C. The sample was determined to be 94.4% pure by chromatographic analyses. The principle impurity is bis[2, 2-dinitro-2-fluoro-ethyl] -diformal and it contains 0.1% water as received.

Water was removed by vacuum distillation in order to avoid loss of FEFO from the confining cylinder when the calorimeter was evacuated. The empirical formula on which results are based was calculated from elemental analyses and adjusted to carbon equals 5.00.

3. RESULTS and DISCUSSION

3.1 Products from Heavily Confined Charges

Studies^{1,2,7} indicate that the products from heavily confined charges represent those found on the Chapman-Jouguet (C-J) isentrope at temperatures in the range of 1500 to 1800°K. Table 1 lists these products and the heats of detonation for HMX, TNT, NM and FEFO.

As one proceeds down the scale of oxygen balance - FEFO, HMX, TNT - the proportion of carbon which appears as solid carbon increases, and which appears as carbon dioxide decreases. Also, the proportion of hydrogen appearing as hydrogen gas increases, and which appears as water decreases. NM, a low-density explosive with a high hydrogen-to-carbon ratio, is the exception to these trends. It has the same oxygen balance as TNT, yet proportionally more carbon appears as carbon monoxide and less as solid carbon than one might expect from the TNT results. In addition, greater amounts of methane are present in the NM products than for any of the other explosives.

It is noteworthy that all of the fluorine in FEFO appears as hydrofluoric acid. Carbon tetrafluoride or other compounds containing the C-F structure were not observed.

The products from heavily confined charges attain equilibrium under non-ideal gas conditions since the pressure at 1500 to 1800°K is of the order of 5,000 to 50,000 atm. In order to calculate the product composition along the C-J isentrope, one must therefore use complex thermodynamic-hydrodynamic calculations. Calculations

were made by using the two best equations of state available, the Becker-Kistiakowsky-Wilson⁸ (BKW) equation in the RUBY⁹ code, and the LJD¹⁰ equation. The comparisons of observed products with calculated products for the four explosives studied (Tables 2, 3, 4, and 5) are fair. Data of this type will be used to improve equations of state for detonation products.

The ideal experiment to allow isentropic expansion of detonation products is an infinitely long, heavily confined, open-ended charge. For such a configuration end effects would be negligible. However, charge length is limited by the calorimeter dimensions, and end effects are such that some of the detonation products are sufficiently shock heated on colliding with the calorimeter wall to cause re-equilibration. Because of this the ends of the charges were also confined in gold. For oxygen-deficient explosives such as TNT, doing this increases the observed heat of detonation by almost 6%. The change is less for higher oxygen-balanced explosives.

3.2 Products from Unconfined Charges

It has been shown¹ that the temperature at which equilibrium becomes frozen can be found by comparing observed detonation products from unconfined charges with products calculated with ideal gas laws. Work with PETN¹ and the calculations of Jones and Miller⁷ indicated a freeze-out temperature of 1500 to 1800°C. Unconfined charges of HMX and TNT were fired and products were compared (Tables 6 and 7) to those calculated. The agreement is good, confirming the earlier work.

The TNT data indicate that solid carbon equilibrates rapidly during the reshocking of products that occurs with unconfined charges. The value for solid carbon, frozen out in the initial isentropic expansion, is 3.65 moles/mole TNT (from Table 1). If it were not equilibrating, the amount found in the products from unconfined charges (1.01 moles/mole TNT, Table 8) should be at least as large as that found in the products from heavily confined charges.

ACKNOWLEDGEMENTS

The author wishes to thank Dr. John W. Kury for his assistance and guidance in the interpretation of results; Dr. Edward L. Lee and Mr. Milton Finger for providing calculations using the BKW equation of state, and Dr. Wildon Fickett (Los Alamos Scientific Laboratory) for providing calculations using the LJD equation of state.

REFERENCES

1. D. L. Ornellas, J. H. Carpenter & S. R. Gunn, Rev. Sci. Instr. 37, 907 (1966).
2. A. Y. Apin, N. F. Velina & Y. A. Lebedev, 2 L. Prik. Mekhan. i. Tkhn. Fiz. 5, 96 (1962).
3. Ministry of Supply, ARE Memo No. 1/51, April 1951.
4. R. Robertson & W. E. Garner, Proc. Roy. Soc. (London) 103A, 539 (1923).
5. ARDE Report (S) 4/56 as quoted by D. Price, Chem. Rev. 59, 801 (1959).
6. H. W. Sexton, ARDE, private communication.
7. H. Jones & A. R. Miller, Proc. Roy. Soc. (London) 194A, 480 (1948).
8. C. L. Mader, Los Alamos Scientific Laboratory, Report LA-2900 (1963).
9. H. B. Levine & R. E. Sharples, Lawrence Radiation Laboratory (Livermore) Report UCRL-6815 (1962).
10. W. Fickett, Los Alamos Scientific Laboratory, Report LA-2712 (1962).

Table 1

The Heat and Products of Detonation of Heavily Confined Charges of Explosives^{a,b}

Explosive	HMX	TNT	NM ^c	FEFO ^d
Density (g/cc)	1.89	1.53	1.13	1.60
Charge weight (g)	25	22	15	25
ΔH detonation, 298°K, $H_2O_{(l)}$, (cal/g)	1479 \pm 5	1093 \pm 5	1227 \pm 5	1227 \pm 5
Products (moles/mole explosive)				
CO ₂	1.92	1.25	0.261	3.16
CO	1.06	1.98	0.550	1.88
C(s) ^e	0.97	3.65	0.095	not detected
N ₂	3.68	1.32	0.394	1.99
H ₂ O	3.18	1.60	0.882	2.14
H ₂	0.30	0.46	0.294	0.046
HF	0	0	0	1.87 ^f
NH ₃	0.40	0.16	0.118	0.023
CH ₄	0.039	0.099	0.083	0.009
HCN	0.0081	0.020	0.0081	not detected
C ₂ H ₆	0.001	0.004	0.001	not detected

^aCylindrical charges, 1.27 cm diameter, confined in 1.27 cm gold.^bCorrected for PETN in the initiation system.^cNM = C_{1.00} H_{2.96} N_{0.96} O_{1.92} by analysis and adjusted to C = 1.00. Trace amounts of acetylene were observed.^dFEFO = C_{5.00} H_{5.74} N_{4.09} O_{10.06} F_{1.87} by analysis and adjusted to C = 5.00.

Results are corrected for reaction of HF with stainless steel. Charge not confined on the ends.

^eDetermined-by-difference.^fFrom total fluorine contained in FEFO.

Table 2

Comparison of Calculated C-J Isentrope Products with Observed Products from Heavily Confined Charges of HMX

Products	Observed, Heavily Confined	Moles/mole HMX			
		Calculated			
		BKW C-J Isentrope		LJD C-J Isentrope	
		1520°K	1800°K	1490°K	1760°K
N ₂	3.68	3.97	3.97	3.98	3.97
H ₂ O	3.18	3.11	3.67	2.90	3.06
CO ₂	1.92	2.39	2.13	2.16	2.01
CO	1.06	0.10	0.071	0.77	0.93
C(s)	0.97	1.13	1.68	0.73	0.81
NH ₃	0.40	0.076	0.073	0.047	0.063
H ₂	0.30	0.005	0.001	0.36	0.34
CH ₄	0.039	0.38	0.11	0.34	0.26
HCN	0.0081	0	0	not allowed	

Table 3

Comparison of Calculated C-J Isentrope Products with Observed Products from Heavily Confined Charges of TNT

Products	Moles/mole TNT				
	Observed, Heavily Confined	Calculated			
		BKW		LJD	
		C-J Isentrope		C-J Isentrope	
	1505°K	1835°K	1500°K	1870°K	
C(s)	3.65	3.57	4.50	3.52	3.80
CO	1.98	0.56	0.32	1.60	1.58
H ₂ O	1.60	1.06	1.87	1.33	1.64
N ₂	1.32	1.49	1.48	1.50	1.50
CO ₂	1.25	2.19	1.91	1.53	1.39
H ₂	0.46	0.043	0.017	0.48	0.40
NH ₃	0.16	0.026	0.047	not allowed	
CH ₄	0.099	0.68	0.27	0.34	0.23
HCN	0.020	3.6×10^{-6}	1.3×10^{-6}	not allowed	
C ₂ H ₆	0.004	not allowed		not allowed	

Table 4

Comparison of Calculated C-J Isentrope Products with Observed Products from Heavily Confined Charges of NM

Products	Moles/mole NM				
	Observed, Heavily Confined	Calculated			
		BKW		LJD	
		C-J Isentrope		C-J Isentrope	
	1520°K	1835°K	1500°K	1800°K	
H ₂ O	0.88	0.75	0.77	0.81	0.85
CO	0.55	0.18	0.21	0.43	0.48
N ₂	0.39	0.47	0.47	0.5	0.5
H ₂	0.29	0.049	0.027	0.32	0.29
CO ₂	0.26	0.49	0.47	0.38	0.33
NH ₃	0.12	0.017	0.027	not included	
C(s)	0.095	0	0	0	0
CH ₄	0.083	0.33	0.32	0.19	0.18
HCN	0.0081	0	0	not included	

Table 5

Comparison of Calculated C-J Isentrope Products with Observed Products from Heavily Confined Charges of FEFO

Products	Moles/mole FEFO		
	Observed, Heavily Confined	Calculated BKW C-J Isentrope	
		1520°K	1820°K
CO ₂	3.16	3.92	3.82
H ₂ O	2.14	1.38	1.57
N ₂	1.99	2.04	2.03
CO	1.88	0.83	0.85
HF	1.87	1.87	1.85
H ₂	0.046	0.045	0.025
NH ₃	0.023	0.018	0.026
CH ₄	0.0009	0.24	0.16
CF ₄	0	0	0.005
C(s)	0	0	0.17

Table 6

Comparison of Calculated Equilibrium Products at Constant Volume with Observed Products from Unconfined Charges of HMX^a

Products	Moles/mole HMX		
	Observed Unconfined	Calculated for Ideal Gas	
		1500°K	1800°K
N ₂	4.01	4.00	4.00
CO	2.65	2.36	2.52
H ₂ O	2.50	2.36	2.52
H ₂	1.53	1.64	1.48
CO ₂	1.45	1.65	1.49
HCN	0.0006	0.00002	0.00002
NH ₃	not detected	0.0006	0.0002
CH ₄	not detected	0.0004	0

^a25-g charges at density 1.89 g/cc and 2.54 cm diameter.

Table 7

Comparison of Calculated Equilibrium Products at Constant Volume with Observed Products from Unconfined Charges of TNT^a

Products	Moles/mole TNT		
	Observed Unconfined ^a	Calculated for Ideal Gas	
		1500°K	1800°K
CO	5.89	5.97	6.00
H ₂	2.31	2.10	2.36
N ₂	1.36	1.49	1.47
C(s)	1.01	0.81	0.90
H ₂ O	0.17	0.007	0.003
CO ₂	0.063	0.009	0.003
HCN	0.024	0.018	0.056
NH ₃	0.022	0.0005	0.0003
CH ₄	0.0092	0.192	0.053

^a25-g charges at density 1.53 g/cc and 1.27 and 2.54 cm diameter.